Investigating the biological effects of (nano)particles in Alzheimer's disease pathologies

A thesis submitted in fulfilment of the requirements for the degree of
Doctor of Philosophy

Charlotte Fleming

September 2022

School of Life Sciences
Faculty of Science
University of Technology Sydney

Certificate of Original Authorship

I, Charlotte Fleming declare that this thesis, is submitted in fulfilment of the requirements for the award of Doctor of Philosophy, in the School of Life Science, Faculty of Science at the University of Technology Sydney.

This thesis is wholly my own work unless otherwise referenced or acknowledged. In addition, I certify that all information sources and literature used are indicated in the thesis.

This document has not been submitted for qualifications at any other academic institution. This research is supported by the Australian Government Research Training Program.

Signature Production Note:
Signature removed prior to publication.

Date 22/09/2022

Statements

In accordance with the University of Technology Sydney thesis committee 'Graduate Research Candidature Management, Thesis Preparation and Submission Procedures (Version 1.10, 2021)', this PhD thesis is presented by compilation. It is comprised of two original Systematic and Bibliometric studies and two original Research studies submitted in peer reviewed journals of which I am the first author. I hereby declare that I have contributed significantly to these studies.

For the Systematic and Bibliometric studies, I procured all the data, performed systematic analysis of the papers identified and drafted the first copy of the two review papers.

For the Research studies, I carried out all experimental procedures, data analysis and drafted the first copy of the two research papers.

Production Note:
Signature removed prior to publication.

Charlotte Fleming

22nd September 2022

Acknowledgments

First and foremost, I would like to acknowledge my principal supervisor, Dr Kristine McGrath, and co-supervisors Dr Cindy Gunawan and Dr Mojtaba Golzan for their continuous support and encouragement throughout my PhD. I am so thankful to have been their student and without their constant advice and expertise, I would not have produced the quality of work I have for this dissertation. Particularly Dr Kristine McGrath, who I have now been working with for the past 6 years. I truly admire you, and I would not have started or finished this without you. Thank you so much.

I want to express my sincere appreciation to Lal Overlunde and particularly Fiona Ryan, for taking care of my animals and their continuous encouragement and care while working in the Ernst Facility both for my experiments but also personally, you are both the best. I would like to thank Dr Catherine Gorrie for answering all my questions regardless of how silly they are and to all the help Associate Professor Louise Cole who always very patient in was assisting me with the Clarity clearing method. I would like to extend my gratitude to our collaborators – Professor Fraser Torpy and Dr Peter Irga, without which my project would not have been possible.

This study would not have been completed without the vast support from many research students and support staffs. I would like to thank the members of The Inflammation Team, Claire Rennie, Michael Chhor and Gihani Manadora for always being available to go for a coffee break, to discuss the most recent failed experiment, as well as their high-quality banter in the lab. In addition, I would like to thank my research friends Gerard Li, Daniel Turkewitz, Tara Nyugen and Alison Ricafrente for their support throughout my entire PhD. Thank you for your constant banter during our lunch breaks. I would like to also thank my housemates who have lived with me throughout my candidature who have always been there to hear me rant and complain and just for being there.

Finally, I would like to thank my family and friends. Lastly, and most importantly thank you Mum, Dad and Annabel for your unconditional love and support always. Words cannot describe how much I appreciate the hard work and dedication you have given to me; I would not have been able to do this without you.

Thank you everyone!

Publications

The following publications have arisen directly from work contained within this thesis.

Systematic and Bibliometric Analysis of Magnetite Nanoparticles and Their Applications in (Biomedical) Research.

Authors: Fleming, C.; Golzan, M.; Gunawan, C.; McGrath, K.

Accepted to Global Challenges. Manuscript no. gch2.202200009.

The Biological Roles of Air Pollutant Particulate Matters in the Early Onset Pathologies of Alzheimer disease.

Authors: Fleming, C.; Golzan, M.; Amal, R.; Wong, R.J.; Torpy, F.; Irga, P.; Gunawan, C.; McGrath, K.

Intend to submit to *ACS Nano*

Insights from a bibliometrics-based analysis of publishing and research trends on cerium oxide during 1990 – 2020

Authors: Fleming, C.; Wong, J.; Golzan, M.; Gunawan, C.; McGrath, K.

Intend to submit to *Dovepress*

Effects of cerium oxide nanoparticles in a mouse model of Alzheimer's disease exposed to magnetite pollution particles

Authors: Fleming, C.; Golzan, M.; Amal, R.; Esmailpour, A.; Gunawan, C.; McGrath, K.

Intend to submit to *ACS Nano*

Conference proceedings

New Horizons 2019

Charlotte Fleming, Peter Irga, Fraser Torpy, Cindy Gunawan, Mojtaba Golzan, Kristine McGrath. Investigating the Effects of Air Pollutant Nanoparticles in Alzheimer's Disease. 2019, Sydney, Australia.

FoSTER 2019

Charlotte Fleming, Peter Irga, Fraser Torpy, Cindy Gunawan, Mojtaba Golzan, Kristine McGrath. Investigating the Effects of Air Pollutant Nanoparticles on the Onset or Progression of Alzheimer's Disease. 2019; Sydney; Australia.

International Brain Research Organization 2019

Charlotte Fleming, Peter Irga, Fraser Torpy, Cindy Gunawan, Mojtaba Golzan, Kristine McGrath. Effects of Air Pollutant Particles in the Pathogenesis of Alzheimer's Disease. 2019, Daegu, Republic of Korea.

Graduate Research Symposium, 2021

Charlotte Fleming, Peter Irga, Fraser Torpy, Cindy Gunawan, Mojtaba Golzan, Kristine McGrath. Effects of Air Pollutant Particles in the Pathogenesis of Alzheimer's Disease. 2021, Malaysia.

Funding and Scholarships

This research was funded by the:

Australian Postgraduate Awards (APA) funded by the Australian Government, Department of Education and Training Scholarships

Table of Contents

List of Figures

List of Tables

Abbreviations

%	Percentage
µg	Micro gram
µl	Micro litre
µm	Micrometre
Aβ	Amyloid-Beta
ACEC	Animal Care & Ethics Committee
AD	Alzheimer's disease
AKI	Acute kidney injury
ATCC	Mouse embryonic stem cells
ANCOVA	Analysis of covariance
ANOVA	Analysis of variance
APP	Amyloid precursor protein
APP/PS1	Human amyloid precursor protein (Mo/HuA695swe)/Presenilin 1 transgenic mouse model
BACE1	Beta-Secretase 1
BALB-C	Bagg Albino mouse model
BBB	Blood brain barrier
BDNF	Brain derived neurotrophic factor
BV2	Murine microglial cells
β-actin	Beta-actin
β-secretase	Beta-secretase
Ca	Cornu ammonis
CAT	Catalase
cDNA	complementary deoxyribonucleic acid
CeO_2	Cerium oxide

Ce^{3+}	Cerium (oxidised)
Ce^{4+}	Cerium (reduced)
CO	Carbon monoxide
CNS	Central nervous system
CREB	cAMP-response element binding protein
C57BL/6	C57 black 6 mouse model
DE	Diesel
DCF	2'7'-Dichlorofluorescein
DG	Dentate gyrus
DMEM	Dublbecco's Modified Eagle Medium
DNA	Deoxyribonucleic acid
DPX	Dibutylphthalate polystyrene xylene
EDS	Ehlers-Danlos syndrome
EDTA	Ethylenediamine tetraacetic acid
EPM	Elevated plus maze
FBS	Foetal bovine serum
FCR	Field citation ratio
Fe_2O_3	Iron oxide
Fe^{2+}	Ferrous ion
Fe^{3+}	Ferric ion
Fe_3O_4	Magnetite
GAPDH	Glyceraldyde-3-phosphate dehydrogenase
GFAP	Glial fibrillary acidic protein
H_2O_2	Hydrogen peroxide
HEPES	(4-(2-hydroxyethyl)-1-piperazineethanesulfonic acid
HUVECs	Human umbilical vascular endothelial cells

HRP	Horseradish peroxidase
Iba-1	Ionized calcium binding adaptor molecule 1
ICAM-1	Intercellular adhesion molecule 1
IgG	Immunoglobulin G
IκB	Inhibitor of kappa B
IKKB	IκB kinase
IL-	Interleukin
iNOS	Inducible nitric oxide synthase
IRON	Iron and iron oxide air pollutant particles
JNK	c-Jun N-terminal kinase
LPS	Lipopolysaccharide
MAG	Magnetite nanoparticles
MAPK	Mitogen-activated protein kinase
MCP-1	Macrophage chemoattractant protein-1
MDPI	Molecular diversity preservation international
MNPs	Magnetite nanoparticles
MRI	Magnetic resonance imaging
mRNA	Messenger RNA
MS	Multiple Sclerosis
MTT	3-(4,5-dimethylthiazol-2-yl)-2,5-diphenyltetrazolium bromide
NAC	N-acetylcysteine
NFκB	Nuclear factor-κB
NFTs	Neurofibrillary tangles
NIRF	Near infrared fluorescence
NMDA	N-methyl-D-aspartic acid
NO	Nitric oxide

NOR	Novel object recognition
NPs	Nanoparticles
OH^-	Hydroxide
OS	Oxidative stress
PD	Parkinson's disease
PM	Particulate matter
pMAPK	Phosphorylated MAPK
pmol	Picomole
pNFκB	Phosphorylated NFκB
pJNK	Phosphorylated JNK
pTau	Phosphorylated tau protein
qPCR	quantitative polymerase chain reaction
RIPA	Radioimmunoprecipitation assay buffer
ROI	Region of interest
ROS	Reactive oxygen species
RNA	Ribonucleic acid
RNS	Reactive nitrogen species
SEM	Standard error mean
SOD	Superoxide dismutase
SPION	Superparamagnetic iron oxide nanoparticles
TBST	Tris buffered saline with tween
TEM	Transmission electron microscopy
TGX	Tris-glycine extended
TLR	Toll-like receptor
TNF	Tumour necrosis factor
TST	Tail suspension test

TTau	Total tau protein
UV	Ultraviolet
WGS	Water-gas shift
WoS	Web of Science
W/T	Wild type
XRD	X-ray diffractometer
XPS	X-ray photoemission spectroscopy

Abstract

Alzheimer's disease (AD) is the most common form of dementia, with sporadic AD accounting for over 95% of cases and thought to be influenced by lifestyle and environmental factors. Magnetite pollutant particles have been found in abundance in brains of people with AD in densely populated cities. This observation highlighted the need for increased understanding of the potential impact on human health. Therefore, chapter 3 commenced an extensive systematic and bibliometric analytical review of the characteristics and applications of magnetite from 1990-2020, identifying the formation and broad applications in environmental, industrial, and biomedical fields, also highlighting the cytotoxic effects from overuse as a biomedicine and its potential implication in neurodegeneration and AD as an air pollutant. Subsequently, chapter 4 explored the biological effects that air pollutants (iron, diesel and magnetite) have on AD pathologies. This study showed air pollutants, particularly magnetite, increased anxiety, stress, and cognitive impairment, and increased neuronal cell loss in the hippocampus of the double transgenic APP/PS1 and W/T mice. Air pollutants also increased amyloid plaques and inflammation, in both the *in vivo* and *in vitro models*, neuroblastoma SH-SY5Y cells, with oxidative stress found to be induced via NFκB pathway, suggesting a global inflammatory response that occurs through activated microglial and astrocytes.

The current therapies for AD, while effective in managing symptoms do not delay or reverse disease progression. Oxidative stress is a central process in AD pathogenesis therefore the antioxidant, cerium oxide has emerged as a potential therapy. Cerium oxide has been used as a biomedicine for cancer therapy and ischemic stroke, however not for AD. This inspired the systematic and bibliometric review on cerium oxide from 1990-2020 (chapter 5), bringing to light the catalytic and redox properties used for innumerable environmental/industrial and biomedical applications. The advanced nanotechnology engineering was a focus in increasing nanoparticle efficiency for a wide range of applications, including AD. Consequently, because air pollutant magnetite induces AD pathologies, chapter 6 explored if cerium oxide nanoparticles could delay or reverse this. Cerium oxide nanoparticles decreased cognitive impairment, neuronal death, amyloid-beta species formation and inflammation in the APP/PS1 and W/T mice, and decreased inflammation and oxidative stress in SH-SH5Y and microglial BV-2 cells.

In summary, air pollutants induce neurological changes associated with AD, and after exposure to cerium oxide nanoparticles these changes are delayed or reversed. Overall, this study concludes that cerium oxide nanoparticles are promising potential therapeutics for air pollutant induced AD pathologies.

Chapter 1: Introduction

Chapter Summary

Background information on the pathogenesis of sporadic Alzheimer's disease is presented in this chapter, as well as the potential role that air pollutant iron, diesel and magnetite particles may play in the progression of the disease. A potential therapy for Alzheimer's disease, cerium oxide, is also introduced in this chapter highlighting its advantages in delaying or reversing Alzheimer disease pathologies.

1.1 Alzheimer's disease

Dementia is the second leading cause of death in Australia with approximately 420, 000 Australians currently living with the disease. Alzheimer's disease (AD) is the most common form of dementia and is the underlying cause of death in the aging population (>65 years of age) (1, 2). AD symptoms include the inability to retain new information, memory loss, difficulty in completing familiar tasks, changes in mood, poor judgement, increased anxiety and the failure to undertake basic bodily functions such as walking or swallowing (3, 4). AD is a very complex disease arising from either genetic mutation, accounting for less than 1% of cases or sporadic Alzheimer's, accounting for over 95% of all cases (5). The exact cause for development of sporadic AD is unknown but is suspected to occur due to lifestyle and environmental factors (5-9).

1.2 Alzheimer's disease pathogenesis

AD is pathologically defined by the extensive neuronal loss, accumulation of extracellular amyloid-beta (Aβ) plaque deposits and intracellular neurofibrillary tangles (NFTs) (10, 11). There are many theories regarding its initiation, including the Aβ cascade, Tau, cholinergic, oxidative stress and neuroinflammation hypotheses (12). While the pathogenesis and progression of AD does involve and indeed closely links all hypothesis listed, pinpointing the initial trigger of AD is still under investigation.

The amyloid cascade hypothesis is the most researched and has the greatest influence for AD initiation, which refers to Aβ plaque deposition once initiated leads to NFTs and neurodegeneration (13). Under normal conditions Aβ peptides are cleaved from the amyloid precursor protein (APP; a transmembrane protein associated with neuronal development and axonal growth and transport) by α- (cleaving 90%), γ- and β-secretase enzymes releasing the peptide outside of the cell, where they are rapidly degraded or removed (14, 15). However, when there is a homeostatic imbalance the metabolic activity changes, and the ability to degrade Aβ peptide is reduced leading to its accumulation (14). Aβ plaque deposits are large accumulations of Aβ peptide aggregates which occurs as a result of differential cleavage of the APP producing Aβ fibrils which then oligomerize and further polymerize forming the Aβ40 (soluble) and more favourable and neurotoxic, Aβ42 (insoluble) peptide aggregates. These structures then migrate into synaptic clefts causing synaptic signalling disruption. The

accumulation of Aβ42 peptides, induces Aβ fibril formation in turn forming Aβ plaque deposits (16). In AD pathogenesis Aβ plaques are found in hippocampus, neocortex, amygdala, basal ganglia and diencephalon (11). The presence of Aβ plaques induces an immune response, activating glial cells (microglial and astrocytes) leading to local inflammatory response which contributes to neurotoxicity, which can induce tau pathology and eventually neurodegeneration (5, 17-19). This hypothesis is supported by the genetically predisposed AD or familial AD, consistent with pathogenic mutations of APP increasing the cleavage of Aβ42 production and in turn Aβ plaque deposits, known to cause early onset AD (14, 20). There are many genetically modified *in vivo* murine model that have been genetically modified having mutations of APP (e.g., APP/PS1, PDAPP, Tg2576, APP23, TgCRND8, PSAPP, APPSwe, BRI2-AB etc.) to induce the development of Aβ plaque deposits, without the coinciding NFT pathologies (21). Which indicates that Aβ plaques may not induce NFTs formation (14). Studies have also found that extensive Aβ plaque deposits in the brains of non-demented people, suggesting that Aβ plaques also are not the only sign for AD development (14). While Aβ plaques are the central pathogenic cause of AD, there are other significant contributing factors which also play a role in AD pathogenesis.

NFTs are another hallmark of feature of AD pathogenesis, with the "tau hypothesis" proposed as the fundamental pathogenic initiator of the pathological events which result in the onset of AD. NFT's are composed of hyperphosphorylated microtubule-associated protein tau, independently of Aβ plaque deposition (14, 22). Tau is a microtubule-associated protein is localized mainly in the axons of neuronal cells in adult neurons under normal conditions, directly binding microtubules, promoting scaffold structure and stability (12, 22). Tau protein has also been found in dendrites, plasma membrane, Golgi complex, rough endoplasmic reticulum, nucleus and nucleolus and has been found to play important roles in regulating synaptic function and RNA and DNA protective properties during an early stress response (22, 23). Neuronal cells are the fundamental units of the brain and nervous system, responsible for receiving sensory input and sending motor commands to our muscles (24). The mechanism by which tau becomes phosphorylated and therefore dysfunctional is unknown, however is thought to be triggered by homeostatic imbalance, where the tau microtubule proteins become destabilized, rendering it prone to extensive phosphorylation, in turn leading to aggregates forming in bundles and eventually NFTs, resulting in enhanced cellular stress and eventually neuronal apoptosis (11, 25). Hyperphosphorylated tau is more closely associated with the

development of cognitive decline in AD pathogenesis and is thought to be closely associated with increased neurogenesis, which is consistent with studies using a transgenic *in vivo* murine model with tau mutations (e.g., human tau four-repeat domain with aggregation-promoting FDTY-17 mutation ΔK280) (26). Opposingly, tau dysfunction has been found to be associated with reduced neurogenesis in various *in vivo* murine models (27). Tau dysfunction and pathology has also been found to be associated with neuroinflammatory and oxidative stress response in the development of AD, depending on the extent of the response (28). Like Aβ plaque deposits, NFTs appear to be insufficient as the primary initiator for AD and therefore other modulators or mediators of AD need to be investigated.

Neuroinflammation is another hallmark feature of AD development and is another theory in the pathogenesis of AD. Microglial and astrocytes (glial cells) are macrophagic cells that play a significant role in the innate immune response in the brain (29). Microglia are phagocytic cells and can ingest the Aβ plaques, therefore the inability of microglia to digest Aβ plaques may be a contributing factor to its accumulation, further signified by the close proximity of Aβ plaques to microglia (29). Astrocytes under pathological conditions, exhibit morphological changes, including hypertrophy and upregulation of glial fibrillary acidic protein (GFAP) (29). They can detect aggregated proteins, like Aβ and can polarize its processes around Aβ plaques, leading to its degradation (30). This polarized M2 state of glial cells becomes activated, exhibiting neuroprotective mechanisms, releasing anti-inflammatory mediators and cytokines (e.g., interleukin 4; IL-4, IL-10, transforming growth factor beta; TGF-β, insulin-like growth factor 1; IGF-1 and brain derived neurotrophic factor; BDNF etc.) (30). Alternatively, microglial and astrocyte cells can be M1 polarized, releasing pro-inflammatory mediators and cytokines (e.g., tumour necrosis factor; TNF, interferon-γ; IFN-γ, IL-6, IL-1β, IL-8, GFAP and intercellular adhesion molecule-1; ICAM-1) (12, 30). This M1 polarized state is activated and associated with the presence of Aβ plaques in and around neuronal cells, which plays an integral role in the pathogenesis of AD and contributes to the low-grade chronic inflammation (31-35). Low-grade chronic inflammation is neurotoxic, leading to immune cell infiltration and neuronal dysfunction and death. This neuronal cell dysfunction results in protein misfolding and mutated processes further contributing to Aβ plaque deposition and NFT formation (12, 30).

There has been increased interest in the role of oxidative stress and an increase in free radicals as a significant factor in the development of AD pathologies (36). Oxidative stress is a state of redox imbalance resulting from the generation and detoxification of free radical (reactive oxygen species; ROS, and reactive nitrogen species; RNS) formation exceeding the capacity of antioxidant defence mechanisms (36). Free radicals are molecules with unpaired electrons with high reactivity which react with another electron or hydrogen atom to become more stable (37). Oxidative phosphorylation is important in respiratory pathway of mitochondrial cells, producing water (H_2O), whilst producing superoxide (O_2^-), hydroxide (OH^-), hydroxyl (OH) and hydrogen peroxide (H_2O_2), volatile ROS (37). Neurons are highly reliant on oxidative phosphorylation reactions to generate adenosine triphosphate (ATP) as an energy source, therefore, susceptible to oxidative damage due to its high oxygen content compared to other organs in the body (38, 39). The response of neurons to oxidative stress is not uniform and while many neurons can cope with the imbalance, certain populations (i.e., hippocampal neurons) are vulnerable, leading to cell death and neurodegeneration (40). Neurodegeneration is known to correlated with iron overload, which is commonly formed via the Fenton reaction (i.e., formation of OH^- and OH from the interaction between Fe^{2+} and H_2O_2), along with various enzymatic, non-enzymatic and glial cellular mechanisms the formation of ROS and RNS is increased (16, 37, 38, 41). The increased generation of ROS like superoxide (O_2^-) leads to interactions with nitric oxide (NO) producing peroxynitrite ($ONOO^-$), a volatile RNS thereby further mounting the OS in the brain (40). An increase in oxidative stress has been associated in various neurodegenerative diseases, coinciding with persistent neuroinflammation they both act to progress both Aβ plaques and NFTs in AD development (37, 42).

While the amyloid and tau hypothesis do offer rational basis for the development of AD, they do not take into account the underlying homeostatic changes which influence and perhaps induce these pathologies that may be occurring simultaneously. Therefore, investigating further the intimate and perhaps causal relationship between neuroinflammatory signalling and oxidative stress, might suggest that appropriate antioxidant strategies that could also antagonize negative CNS immune reactions (38). Investigating these broad pathological pathways is relevant to my dissertation.

1.3 Air pollutant particulate matter and neurodegeneration

Air pollution has surfaced as being implicated in neurodegeneration and AD development in recent years, with a study by *Calderon-Garciduenas et al*. (2016) (43) suggesting that there is a correlation of people living in cities or in close proximity to highways having a higher risk of neurodegeneration compared to those people living in less air polluted cities (43-45). Air pollution is any chemical biological pollutant that can form from natural or manmade sources that alter the atmosphere and become part of our ambient air. Both natural pollutants (e.g., dust, wildfires and volcanoes) and manmade sources (e.g., power plants, industries and transportation) of air pollution are human health hazards, however manmade air pollution has been recognized as the main source affecting human health (46).

Manmade air pollutant particular matter (PM) includes carbonaceous aerosol particles, presenting a broad range of chemically and physically diverse mixture of compounds comprised of solid particles or liquid droplets suspended in the air. Primary PM, which is of particular interest for this thesis, are PM directly emitted into the atmosphere by combustion sources. These consist of electrical power plants, vehicle emissions or any industrial source which uses the burning of fossils fuels (e.g., coal, petrol, natural gas, oil shales, and diesel exhaust) for energy (47, 48). Urbanization and industrialisation in the past two centuries have led to increased and uncontrolled production of hazardous air pollutant PM. Manmade air pollutant PM is one of the biggest health hazards worldwide, accounting for up to 9 million deaths per year (49).

Short-term exposure to air pollutants is closely related to coughing, shortness of breath, wheezing, asthma, chest tightness, cause headaches, nausea, dizziness and irritation of eyes, nose, skin and throat (50). These can be aggravated and extend into long-term exposure to pollutants, like chronic asthma, pulmonary insufficiency, cardiovascular diseases, cardiovascular mortality, diabetes and neurological diseases (51, 52). Air pollutant PM has also been linked to DNA damage causing diseases like lung, breast and pancreatic cancer (53). Furthermore, long-term exposure to air pollutants have been founds to effect mental health and perinatal effects resulting in infant mortality or chronic diseases (52). In developing countries, due social disparities, lack of education and poor management of the environment, urbanization and industrialization has led to poor air quality that is continuing to increase (54). China is

facing a serious health concern from exposure to air pollutant PM due to the industrial development and overpopulation, similar to that of India and Nepal (54-58). Extremely high levels of air pollution have also reported in Mexico City, Rio de Janeiro, Milan, Ankara, Melbourne, Tokyo, and Moscow (59). Epidemiology studies in the 1950's and 1960's in London and New York respectively found that air pollutant PM, consisting of fine sulphur dioxide and smoke particles was lethal and led to approx. 4000 deaths in London and 400 in New York (59). The mortality rate in this study was associated with the fine particle size of sulphate PM compared to the other components of air pollutant PM (e.g., various aerosols and nitrogen dioxide) (60).This suggests that the small size of PM is directly associated with the extent of their penetration into the lungs (50) PM ranging from 1-10 μm in diameter (PM_1-PM_{10}), with ultrafine particles, generally defined as 0.1 μm ($PM_{0.1}$) or smaller, sanctioning them to be easily inhaled in the respiratory system where they can translocate across the alveolar-capillary barrier into systemic circulation and subsequently extrapulmonary organs, including the brain (47, 61, 62).

Air pollutants have also been implicated in neurodegenerative diseases like AD and Parkinson's disease as PM can also pass directly through the nasal canal and olfactory bulb, and also inhaled into the lungs and translocate into the circulatory where the enter the brain via the blood brain barrier (BBB), as seen in Figure 1.1 (61). Various studies have found that ambient air is neurotoxic, contributing to various CNS disease like neurodegeneration (63). A study by *Anderson et al.* (2018) (64) found that $PM_{2.5}$ consisting of nitrogen oxide affects the CNS causing systemic inflammation, neuroinflammation and oxidative stress (64). Fine dust PM ($PM_{2.5}$) has been found to trigger cognitive impairment and neurodegeneration through changes in mitochondrial structure and function, particularly affecting oxidative phosphorylation leading to the formation of NFTs in cortex of middle-age C57BL/6 female mice (65). Another study found that PM contributes to oxidative stress and inflammation in the brain and also implicated in NFT increase in the frontal cortex of the brain (18, 66). The cortex (outermost region) and frontal cortex (most anterior part) brain regions in these *in vivo* murine models studied are responsible for high cognitive functions like memory, emotions, impulse control, social interaction and motor function (18, 66). Furthermore, it has been found that continual exposure to $PM_{2.5}$ causes neurotoxicity, metabolic abnormalities, oxidative damage and atrophy of the grey matter resulting in cognitive decline (65, 67). These studies show that various forms of air pollutant PM play a role in increasing oxidative stress and

neuroinflammation, and therefore PM could be a causative factor to the growth and manifestation of AD (46, 68).

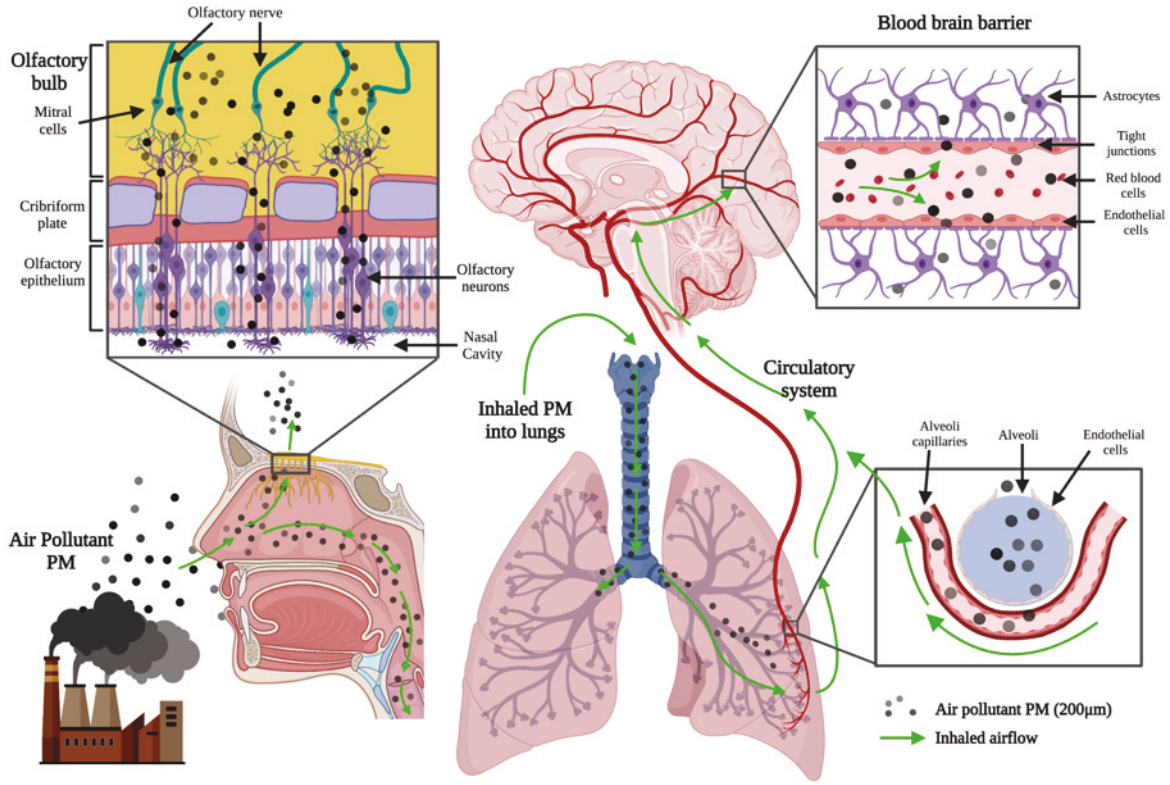

Figure 1.1. Schematic diagram of air pollutant PM entering the brain through the nasal canal via the olfactory bulb, alternatively inhaled into the lungs then translocating into the circulatory system into the brain via the BBB. Created with BioRender.com.

1.3.1 Diesel exhaust air pollutant PM

In populated urban environments, diesel engine emissions make up a large majority of the PM in ambient air (62, 69). There are many forms of diesel PM that have proven harmful to humans, including compounds like sulphates, nitrates, carbon, ammonium, hydrogen ions, and graphite (70). Diesel exhaust PM are formed through the burning of fuels through a combustion reaction at high temperatures and very quickly allowing for the mass production of ultrafine nanoparticles (70, 71). The size of diesel exhaust PM varies greatly, however have been found to permeate the BBB and therefore can be as small as 50-200 nm in diameter (72). Previous studies have found that diesel exhaust PM promote inflammation through the increase in interleukin 6 (IL-6), tumour necrosis factor (TNF) and interleukin 1β (IL-1β) expression causing DNA and RNA damage, eventually cell death and promoting Aβ deposition (72-75).

Recent studies have found that there is a clear correlation of residential proximity to highways and the development of sporadic AD (69).

1.3.2 Iron air pollutant PM

Magnetic particles including iron (Fe^{2+} and Fe^{3+}) are known to be present and form naturally in human brains as they are necessary to sustain normal brain function of the central nervous system (CNS) including neurotransmitter synthesis, myelination of neurons, and mitochondrial function (76, 77). Iron in the brain is present in three main forms; iron-bound haemoglobin, ferritin for iron storage and magnetite and iron oxide, relying on a careful balance of Fe^{2+} and Fe^{3+} (77). While iron is an important feature in the CNS function, excess amounts of free iron have been found to increase as age increases, consistent with the development of AD (78, 79). Research has found that the tau protein, a component of NFTs, binds to iron, providing an explanation as to why excess iron is found in NFTs (80). An accumulation of excess iron has also been found to trigger the formation of ROS, which increases oxidative stress affecting numerous pathways, progressing the pathogenesis of AD (81, 82). Further, iron species accumulation (reduced; Fe^{2+} and oxidised; Fe^{3+}) has been found to participate in Fenton and Fenton-like (a heterogenous process generating both hydroxyl radicals and higher oxidative states of iron) reactions leading to the generation of ROS and higher oxidation states of iron (reduced; Fe^{2+}) inducing oxidative stress (76, 78). Externally derived iron nanoparticles are formed from combustion reactions, similarly to diesel emission PM and therefore are also produced in abundance. High levels of externally derived iron have been found in the brain tissue of people with neurodegeneration, suggesting that these particles can also penetrate the BBB (80, 81, 83).

1.3.3 Magnetite air pollutant PM

Magnetite (Fe_3O_4), an iron oxide mineral forms biogenically (i.e., forming naturally) in bacteria, protists and a variety of animals, including humans. Like excessive quantities of iron in the brain, large amounts of magnetite can also have detrimental impacts due to its potent redox activity and highly magnetic behaviour (84). Magnetite can alternate its lattice structure from $Fe_{2+}O_{4-}$ (reduced) to $Fe_{3+}O_{4-}$ (oxidised) enhancing its redox activity due this unique structural property (84-86). Magnetite, like iron is a highly efficient catalyst for ROS production, due to its oxygen component making it more reactive than iron, and therefore more

damaging in the brain (41, 85). This is supported by evidence of severe brain tissue damage found at the sites of magnetite accumulation surrounding both NFTs and Aβ plaques (41, 87). Air pollutant magnetite nanoparticles (MNPs) are produced in copious amounts from combustion sources (84). *Maher et al.* (2016) and colleagues found MNPs in excessive quantities in the brain tissue of people suffering from AD (85, 88). Biogenic magnetite is formed naturally in the brain from normal metabolic processes, either of the tetrahedral or octahedral shape with blurred edges, quite different to combustion derived MNPs with smooth surfaces in a cuboidal shape with a diameter of ~200 nm, small enough to permeate the BBB (88). While the exact mechanism of magnetite or MNPs in the brain is not well understood, it is evident that it can form in unfavourable conditions and therefore there is an association present between MNPs and the progression of AD (87).

1.4 Current treatment options for Alzheimer's disease

The management of AD has always been a challenging area of interest (89). There are a number of drugs currently on the market as symptomatic therapeutics for AD; cholinesterase inhibitors, donepezil, rivastigmine, galantamine, and tacrine, and N-methyl-D-aspartate (NMDA)-receptor modulator memantine. Despite being unable to prevent or reverse the disease progression, they have been extremely effective (90). These treatments aim at replacing mediators that become damaged or dysfunctional, rather than targeting the underlying drivers of the disease. There are many proposed pathogenic mechanisms that have been theorised for AD, including the amyloid cascade, hyperphosphorylated tau, inflammation and oxidative stress (89). As such, disease-modifying with various studies focusing on the amyloid hypothesis and associated targets by blocking its aggregation into Aβ plaques and dissembling the existing Aβ plaques, therefore may delay or reverse the progression of AD (90, 91).

Immunotherapies using an active immunisation AN-1792 (synthetic Aβ42 plus adjuvant) seemed to show some ability to clear Aβ plaques associated tau lesions through plaque removal, however, did not continue due to the limited tau removal seen in phase II of the trial and also the continuing cognitive decline seen regardless of the treatment (92, 93). Various studies have also focused on tau-inhibitors, like methylene blue as it has been found to block the polymerization of tau monomers, however when this was given over extended period of times it showed no notable difference between any treatment groups (94, 95). Another study

used leuco-methylthionium bis (hydromethanesufnate; LMTM), which acts as a selective inhibitor of tau protein aggregation, finding gastrointestinal and urinary side effects and therefore was discontinued (96). While some studies show promising results, targeting the wholistic pathogenic mechanisms of AD proves difficult, and therefore research focus has shifted to oxidative stress and inflammation, the underlying instigators of AD progression. Various studies have looked into anti-inflammatory inhibitors, like prostaglandin H synthase (97) inhibitors, IL-1 receptor agonists, somatostatin receptor-2, vitamin D receptor, endothelial cell protein C receptor and adenosine 2A receptors, which aim to down regulate the pro-inflammatory response (98-101). While all of these targets have been characterized as inflammatory paradigms, they have yet to be used as potential AD therapeutic targets (102). Oxidative stress is a central pathogenic process implicated with AD and therefore antioxidants have surfaced as potential therapies to slow the progression of senile plaques and NFTs (103). The brain is the most active organ in the body, highly susceptible to oxidative stress due to the high oxygen content and utilization. Antioxidant therapies like acetylcholinesterase inhibitors (e.g., Reminyl, Aricept and Exelon) have been researched as AD therapies along with vitamin E and C (102, 104). These studies show contradictory results, with many limited in their ability to cross the BBB, therefore development into smaller antioxidant molecules that would more readily pass the BBB would offer much promise (105).

1.5 Cerium oxide nanoparticles as a therapy for Alzheimer's disease

Cerium oxide (CeO_2) is a rare Earth metal, with CeO_2 nanoparticles used in industrial and environmental applications as a strong catalyst in renewable energy (105-107). CeO_2 nanoparticles have also been extensively used as a biomedicine for cancer therapies, diabetes, inflammatory diseases and neuro-associated diseases (e.g., ischemic stroke and brain tumours) (105, 106). Due to its enzymatic activity and potent ROS scavenging abilities, CeO_2 nanoparticles have surfaced as promising oxidative stress and neuroinflammatory mediators (106). The scavenging of free radicals is controlled and reduced through the action of endogenous enzymatic antioxidants like superoxide dismutase (SOD), catalase (CAT) and glutathione peroxidase mimetic enzymes, either inside or outside the mitochondria. SOD, CAT and glutathione peroxidase are all in the first line of defence category and can break down ROS and RNS (107). CeO_2 nanoparticles are able to efficiently breakdown hydroxyl radicals (OH; the strongest and most biologically free ROS) and also peroxynitrite ($ONOO^-$; the most volatile RNS) using its enzymatic mimicking abilities of SOD and CAT (106, 108). CeO_2 nanoparticles

can effectively switch valence states from the Ce^{3+} (reduced form) to the Ce^{4+} (oxidised form) donating an electron, allowing it to act as an efficient free radical agent, while enabling its own neutralization by other antioxidants and also allows its regeneration (106, 109).

Studies have also found that CeO_2 nanoparticles have excellent cancer targeting abilities, generating ROS to be cytotoxic towards cancer cells, whilst having little effect to surrounding healthy cells (110). In acidic conditions the antioxidant ability of CeO_2 nanoparticles is lost, behaving instead much like a strong oxidant, which may influence the oxidation of intracellular and extracellular components to induce apoptosis (111). This ability to become cytotoxic has been found to induce oxidative stress, could be attributed to cancer cells being more acidic than normal cells (112, 113). The bifunctional characteristic of CeONPs allows it to exhibit both ROS scavenging and cytotoxic effects is possible due to its ability to change structural composition in valency depending on the environment (106, 114). This makes it an extremely versatile and remarkable compound for various biomedical applications including neurodegeneration and AD, as oxidative stress plays a significant role in the progression of neurodegenerative diseases (106).

The advancements in nanoparticle technology have allowed a greater understanding into characterizing nanoparticles, which is essential for toxicity studies as the size, shape, surface reactivity, solubility are all significant factors when in a biological system (115, 116). Bare CeO_2 nanoparticles have been found to agglomerate more so than coated CeO2 nanoparticles, therefore increasing their diameter size to ~ 40 nm in diameter. This reduces cellular uptake resulting in cytoplasmic accumulation and an increase in ROS production, thereby reducing overall efficiency (29). Doping of CeO_2 nanoparticles with polymer, starch, silica have been found to reduce agglomeration and increase the oxygen vacancies on the nanomaterials surface (enhancing its catalytic and redox properties). This development has enhanced the ROS scavenging abilities, in turn improving its antioxidant and anti-inflammatory capabilities (117). Silica coated CeO_2 ($SiCeO_2$) nanoparticles have been studied previously demonstrated to decrease $CeO_{2\ \text{induced}}$ lung fluid inflammatory responses, in the male Sprague-Dawley rats (118). Silica coating also has found to improve biocompatibility, through increased dispersibility, increased retention rates and thereby evading the immune response, however there is little evidence about its potential benefits for neurodegenerative diseases (118, 119).

1.6 Significance

Though a link is present, the influence that iron, diesel and most interestingly, magnetite has regarding the development of AD is still unknown. There are many properties of magnetite not yet understood and therefore the size, composition, morphology, and surface texture could influence their characteristics and their effect on the brain (88). Understanding the mechanisms of these air pollutant particles in the brain could lead the development of potential therapies for air pollutant induced AD, and other neurodegenerative disorders that may be caused by air pollutant PM.

CeO_2 has emerged as a fascinating and versatile biomedicine, found to be effective anti-cancer and drug delivery agents due to their remarkable ROS scavenging properties, and therefore show potential as an antioxidant therapy for neurodegeneration and AD (108). CeO_2 nanoparticles have also proven to be effective anti-cancer and drug delivery agents (107). Silica doped CeO_2 nanoparticles, in an amorphous structure (silicon dioxide structure that does not have a crystalline structure) have been used for this study enhancing the antioxidant abilities, improving biocompatibility through increased retention time, and reduced toxicity. Understanding the exact antioxidant mechanisms of CeO_2 nanoparticles on the brain is important and necessary, while also investigating any other underlying effects that may be taking place. These are important factors to establish whether CeO_2 nanoparticles have potential as an AD therapy in a clinical setting.

1.7 Aims and Hypothesis

The proposed project will therefore test the hypotheses (i) that air pollutant iron, diesel and magnetite particles induce the onset of AD and (ii) that CeO_2 nanoparticles can delay or reverse the onset of AD.

Specific Aims

Study 1 aims to investigate the properties and mechanisms of magnetite formation, as well as identify the gaps in knowledge about the long-term exposure impacts as an air pollutant particle. **Chapter 3** of this thesis consists of a systematic and bibliometric analysis of magnetite and MNPs over the past three decades and their applications in (Biomedical) research.

Study 2 aims to investigate the potential role that air pollutant iron, diesel and magnetite particles play in the development of neurodegenerative diseases like AD. **Chapter 4** examines the biological effects of air pollutant particles (iron + iron oxide; IRON, diesel exhaust emission; DE, and magnetite particles; MAG) in the pathologies of AD, using both an *in vitro* human neuroblastoma SH-SY5Y cell and an *in vivo* double transgenic murine model (APP/PS1) for AD.

Study 3 aims to provide an analysis of the research on cerium oxide from 1990 - 2020 and identify the gaps in knowledge to permit a relevant assessment on its emerging application(s) in the scientific field. **Chapter 5** examines the literature on CeO_2 from 1990 - 2020 in a bibliometric analysis determining research trends.

Study 4 aims to explore the antioxidant, anti-inflammatory properties of CeO_2 nanoparticles mechanisms in counteracting the air pollutant induced AD pathologies. This study also investigated the biological of effects of bare CeO_2 nanoparticles and amorphous blue silica doped CeO_2 nanoparticles. **Chapter 6** examines the effects of CeO_2 nanoparticles on the delay/alleviation of AD pathologies after exposure to magnetite particles on both an *in vitro* human neuroblastoma SH-SY5Y cell and murine microglial BV-2 cell models, and an *in vivo* double transgenic murine model (APP/PS1) for Alzheimer's disease.

Chapter 2: Materials and Methods

Chapter Summary

There are two key research focuses presented in this thesis. The first was to investigate the effects of air pollutant particles (iron oxide, diesel and magnetite) in an AD mouse model and their mechanism of action in key cells that play a role in the development of AD. The second was to assess the potential of CeO_2 nanoparticles as an antioxidant therapy for AD. Most methods have been included in the papers submitted for publication, methods that referred to previous publications in the papers have been presented in detail in the following chapter.

2.1 Synthesis of particles

2.1.1 Synthesis of air pollutant particles

The diesel emission nanoparticles (DE) and iron oxide (IRON) sample were synthesised by A/Prof Fraser Torpy and Dr Peter Irga. Briefly, the iron and iron oxide (IRON) sample was produced by grinding hardened cast iron (rail track) with a fibreglass-reinforced grinding wheel, 25 mm in diameter, at 37, 000 rpm. The sample contained a broad range of particle sizes and a range of iron oxides (Fe_3O_4) along with un-oxidised iron (Fe^{2+}). The diesel emission nanoparticles (DE) were produced by burning retail grade diesel fuel in a spirit burner collecting the effluent in an inverted conical flask, then immersing it in hexane which then evaporated off overnight, leaving the particles to be collected. The sample contained remnant high boiling hydrocarbons along with a range of sulphur and nitrogen compounds. The magnetite particles (MAG) were purchased from Sigma Aldrich (MO, USA) to pure 97 % sample (molecular weight 231.53) and approximately 100 - 400 nm in diameter.

2.1.2 Synthesis of cerium oxide nanoparticles

The cerium oxide (CeO_2) and blue silica oxide CeO_2 ($SiCeO_2$) nanoparticles were synthesized by Dr Ali Asghar Esmailpour and Dr Rose Amal (UNSW) using flame spray pyrolysis (FSP), described previously (120, 121). For CeO_2 nanoparticles, cerium (Ce) 2-ethylhexanoate (Alfa Aesar, 49 % in 2-ethylhexanoic acid) was dissolved in xylene with a final Ce concentration of 0.5 M, fed to the centre of the flame by a syringe pump at 1-10 mL/min, then dispersed with 5 L/min oxygen to control to rate of combustion and manipulate nanoparticle size. A constant pressure drop of 1.5 bar was maintained by adjusting the orifice gap. The spray flame was surrounded and ignited by a premixed methane/oxygen (1.5/3.2 L/min, respectively) flame from an annular gap (0.15 mm spacing, at a radius of 6 mm from the centre of nozzle). A sintered metal plate ring (8 mm wide, at inner radius of 9 mm from the centre of nozzle) provided an additional 5 L/min O_2 as a sheath for the supporting flame. Additionally, a modified set up was used where the flame was enclosed in a quartz tube to maintain the sheath gas at 20 L/min O_2 and preserve heat. This temperature gradient causes the metal vapour to supersaturate to form nuclei as the flame temperature reduces downstream. The nuclei coalesce, sinters and agglomerates before leaving the flame as nanoparticles, and is then collected on glass fibre filter. The average nanoparticle diameter was 7 nm. Two separate

precursors (Si:Ce) in a 20:80 ratio, were combined by adding hexamethyldisilane, (HMDSO, Sigma Aldrich) and cerium 2-ethylhexanoate (Alfa Aesar, 49 % in 2-ethylhexanoic acid) dissolved in xylene, with a final Si:Ce concentration of 0.5 M, which was fed to the centre of the flame by a syringe pump at a rate of 3 mL/min. "Blue" $SiCeO_2$ was prepared by hydrogenation of these nanoparticles, by heating 1200 mg of the sample in a carbonite tube furnace. A constant flow of 50 mL/min of 10% H_2 in N_2 was implemented and the furnace was heated at a rate of 5°C/min to 500°C and then held for 180 mins. The average diameter of 7.5 nm.

2.2 Transmission electron microscopy (TEM)

High resolution (HR)-TEM analysis was performed by Dr Roong Jien Wong and Dr Rose Amal (UNSW) for the assessment of primary particle size and morphology of IRON, DE, MAG, CeO_2 and blue $SiCeO_2$ nanoparticles. Samples were dispersed in 95 % (w/v) ethanol and sonicated for 30 mins at room temperature. A drop of suspension was added to the copper grid and air dried before each measurement took place. TEM measurements were performed using a Phillips CM200 operating at 200 kV with an SIS CCD camera.

2.3 Double Transgenic APP/PS1 *in vivo* models

The effects of the air pollutant particles and CeO_2 nanoparticles were assessed in APP/PS1 transgenic mice and C57BL/6 wild-type (W/T) littermates for comparison (purchased from Professor Anna King, University of Tasmania, Tasmania Australia). The APP/PS1 model is a double transgenic mouse that expresses a chimeric mouse/human amyloid precursor protein (Mo/HuAPP695swe) and a mutant human presenilin 1 (PS1) on C57BL/6 (B6. Cg-Tg (APP6953DboTg (PSEN1dE9) S9Dbo) background (APP/PS1) (122). This model exhibits amyloid pathology that closely resembles the Aβ deposits in the initial stages of AD and has been extensively used to study mechanisms of AD neuropathology (123). This model exhibits Aβ deposition as young as 6 weeks of age in the cortex and 3 - 4 months in the hippocampus (124, 125). Reactive glial cells appear around Aβ deposits at about 6 weeks of age, coinciding with a pro-inflammatory response (126). While global neuronal loss is not observed in the APP/PS1 model, modest neuronal loss in the dendate gyrus granule cells (127). Synaptic loss and cognitive impairment are also observed in this animal model at approximately 3 and 7 months of age (128). This animal model was chosen as the relevant AD pathological

biomarkers are expressed at 5 - 7 months of age which coincides with the experimental time period of both animal study 1 and 2. The mice were house according to sex, with 2 - 5 mice per cage, and kept on a 12-hour light/dark cycle at room temperature 22/5 ± 2°C. Before commencing the *in vivo* experiments, the mice were allowed to acclimatize for 1 week.

2.4 Preparation and administration of particles and nanoparticles for the *in vivo* models

The IRON, DE and MAG particles used for this study were prepared at a concentration of 3.3 mg/mL, in sterile saline solution. The CeO_2 and blue $SiCeO_2$ nanoparticles were prepared at a concentration of 1.65 mg/mL, in sterile saline solution. Samples were sonicated using the Q500 Sonicator (Q500 Sonica Sonicators, CT, USA) for 5 mins at 50 % amplitude to disperse particles. Once sonicated, all particles were ready for intranasal administration to the mice in their designated treatment groups. Sonication of air pollutant particles and CeO_2 and blue $SiCeO_2$ nanoparticles is essential to prevent agglomeration. Intranasal administration was completed by inducting the mice with 4 % isofluorane and 2 L/min oxygen in a chamber until no movement was observed, then immediately administering particle solution.

2.4.1 Animal study 1 - Exposure to air pollutant particles (Chapter 4)

In week 1 of the animal experiment (13 weeks of age; W/T; n = 37, APP/PS1; n = 38), the mice were grouped according to genotype and gender (male; n = 55 and female; n = 20), as shown in Table 2.1, to receive intranasal administration every third day of (i) saline (ii) IRON (47) DE or (iv) MAG (66 µg/20 µL) for 4 months. The concentration of iron, diesel and magnetite particles for this model (66 µg/20 µL) was established based on previous air pollutant studies which have found that the average ambient $PM_{2.5}$ is between 12-35 $\mu g/m^3$ with an intake of approximately 6-17.5 µg/day/person (based on urban environments in India, Portugal, Italy, Spain, Belgium, England and Poland etc.) (129, 130). This administration was completed every third day from week 1 through to week 16 of the animal experiment. The mice were monitored daily, and their weight was recorded weekly (Figure 2.1). All animal experiments were conducted with the approval from the University of Technology Sydney Animal Care and Ethics Committee (ACEC ETH17-1418) and in accordance with the guidelines described by the Australian National Health and Medical Research council code of conduct for animals.

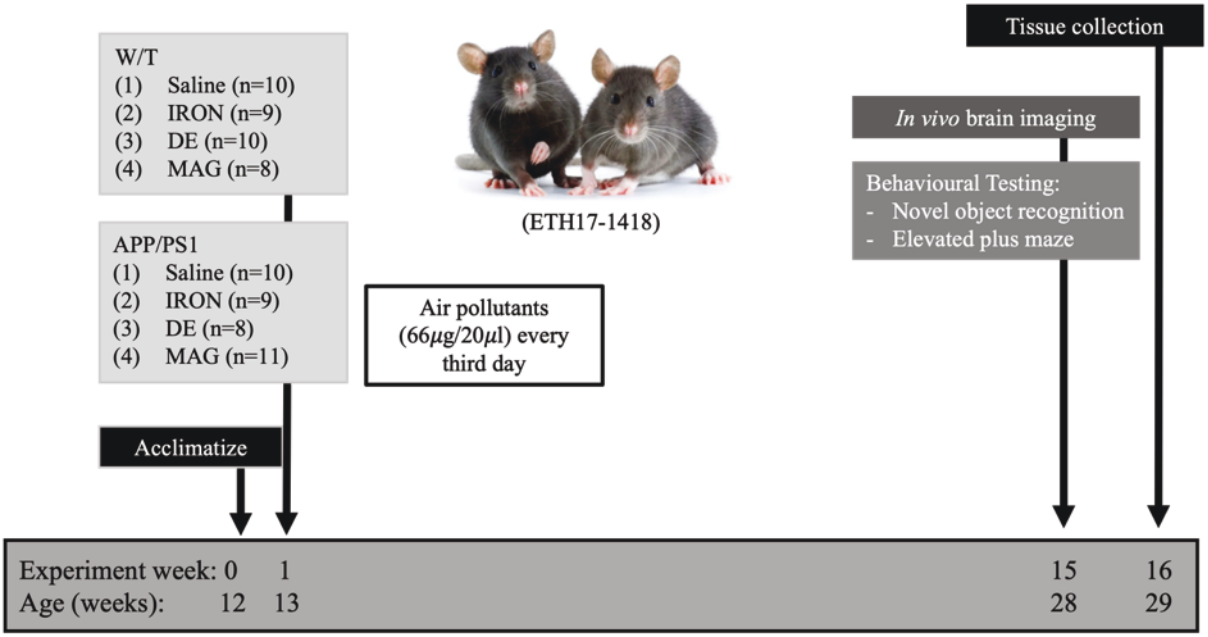

Figure 2.1. A timeline summary of animal study 1. After 1 week of acclimatizing the mice were divided into eight groups to receive either saline, IRON, DE or MAG (66 μg/20 μL) every third day. In week 15 the mice underwent behavioural testing and *in vivo* brain imaging, and in week 16 the tissue was collected.

Table 2.1. Summary of treatment and genders grouped for animal study 1

Genotype	Treatment	Male	Female
W/T	Saline	6	4
	IRON	7	2
	DE	9	1
	MAG	7	1
APP/PS1	Saline	7	3
	IRON	7	2
	DE	6	2
	MAG	6	5

Total		55	20

2.4.2 Animal study 2 - Treatment with cerium oxide nanoparticles (Chapter 6)

In week 1 of the animal experiment (11 weeks of age; W/T; n = 37, APP/PS1; n = 28) the mice were grouped according to genotype and gender (male; n = 41 and female; n = 24), as shown in Table 2.2, to receive intranasal administration every third day of either (i) saline or (ii) MAG (66 µg/20 µL of saline). This administration continued every third day from week 1 to week 32 of the animal experiment. In week 16, the mice were further subdivided to receive either (i) saline, (ii) MAG, (47) MAG + CeO_2 or (iv) MAG + blue $SiCeO_2$ nanoparticles (CeO_2 concentration 33 µg/20 µL of saline) every third day for the remainder of the experiment. Previous *in vivo* studies assessing C57BL/6, 5xFAD, $ApoE^{-/-}$ mice in one study and Sprague-Dawley rats in another, after subacute inhalation exposure to high amounts of CeO_2 nanoparticles (4 mg/m^3 for 3 hours/day, 5 days/week for 4 weeks and 2.7 mg/ m^3 2 hours/day, 4 days respectively) (131, 132). Another study used CD-1 (133) mice that were administered CeO_2 nanoparticles intranasally at a daily dose of 40 mg/kg for 2 weeks (134). Due to the long treatment period required for this experiment including *in vitro* studies determining that CeO_2 nanoparticles were effective against decreased cell viability and increased ROS and NO levels induced by magnetite exposure, half the concentration CeO_2 nanoparticles to magnetite particles was to be used as the treatment dose. All mice were monitored daily, and their weight recorded on a weekly basis (Figure 2.2). All animal experiments were conducted with the approval from the University of Technology Sydney Animal Care and Ethics Committee (ETH19-4326) and in accordance with the guidelines described by the Australian National Health and Medical Research council code of conduct for animals.

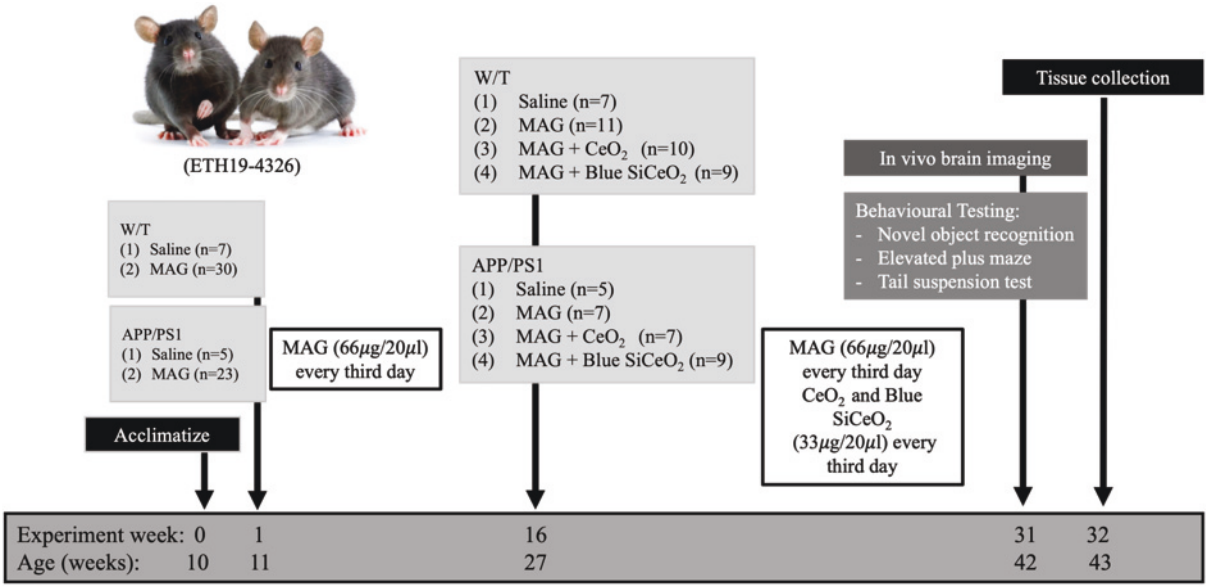

Figure 2.2. A timeline summary of animal study 2. After 1 week of acclimatizing the mice were divided into four groups to receive saline or magnetite particles (66 μg/20 μL) every third day. At week 16 the mice were further subdivided into eight groups, with continued magnetite particles administration (66 μg/20 μL) every third day, with the addition of CeO_2 or blue $SiCeO_2$ nanoparticle (33 μg/20 μL) administration to the specified groups every other third day for remainder of the experiment. In week 31 the mice underwent behavioural testing and *in vivo* brain imaging, and in week 32 the tissue was collected.

Table 2.2. Summary of treatment and genders grouped for animal study 2

Genotype	Treatment		Male	Female
W/T	Saline		4	3
	MAG		6	5
	MAG	CeO_2	7	3
	MAG	$SiCeO_2$	5	4
APP/PS1	Saline		3	2
	MAG		5	2
	MAG	CeO_2	5	2
	MAG	$SiCeO_2$	6	3
Total			41	24

2.5 Behavioural testing

Behavioural testing was performed as indicated in Figures 2.6.1-3. At week 15 and 31 of the *in vivo* studies (animal study 1 and 2 respectively) the mice were subjected to behavioural tasks. The mice were acclimatized to the testing room for 1 hour prior to testing. All testing sessions were conducted between 10:00 - 16:00 hours and were video recorded. The APP/PS1 animal model is known to exhibit cognitive deficits and spatial learning and memory defects as young as 6-7 months of age (128) which is relevant to the behavioural testing time points in both animal study 1 and 2.

2.5.1 Novel object recognition test

The novel object recognition (NOR) test was used to assess short-term memory, a key symptom in AD development (135, 136). This test is a commonly used behavioural assay for testing cognitive deficits in learning and memory in murine models (135, 136). The mice were acclimatized to the testing room for 1 hour prior to testing. This test consists of two phases (Figure 2.3), the first phase is the familiarisation phase where the animal was placed in the apparatus with two identical objects for 5 mins. The animals were removed for an interval of

1 hour, before the test phase was completed, which consisted of the mice being placed back into the same apparatus for 5 mins, however exchanging one “familiar” object for a “novel” object. The total time spent investigating each object was recorded. Between each test the apparatus and objects were cleaned with 80 % ethanol.

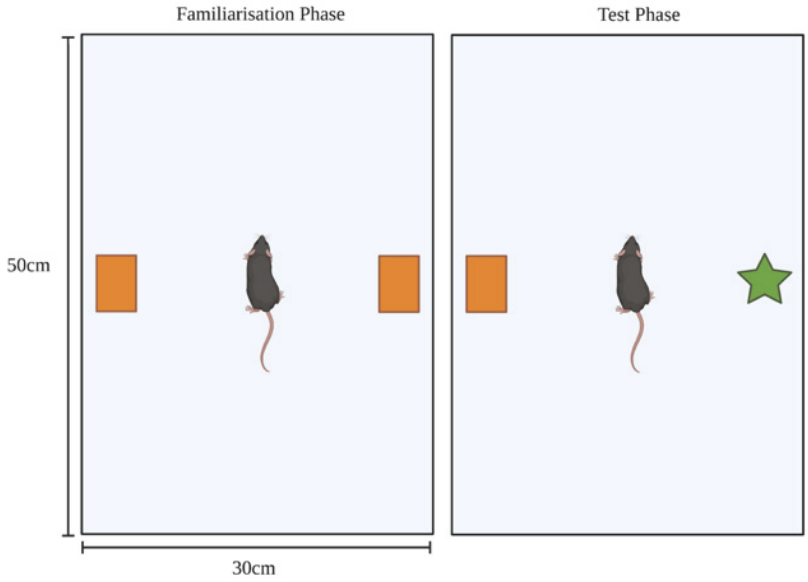

Figure 2.3. Schematic representation of the NOR experiment. This test consists of two phases, the first is a familiarisation phase with two familiar objects and the test phase with one familiar and one novel object. The interaction with each object is recorded. Created with BioRender.com.

All data from the NOR test was calculated using the recognition index as a score of short-term memory retention. The recognition index was calculated using the time spent exploring the novel object (Tn) divided by the total time spent on both objects (Tn + Tf), shown in the equation below.

$$Recognition\ Index = \frac{Tn}{(Tn + Tf)}$$

It was expected that a normal animal would spend equal amounts of time on the identical object in the familiarisation phase but more time on the novel object in the test phase. This would indicate that the animal recognises an object that it has seen previously and therefore does not explore the object as often compared to the novel object.

2.5.2 Elevated plus maze

The elevated plus maze (EPM) is widely used assessment of anxiety and stress, which are significant symptoms in AD pathogenesis (137, 138). C57BL/6 (WT) mice are not expected to exhibit age-related anxiety changes, however APP/PS1 model is expected to exhibit age-related anxiety behavioural changes at approximately 9 months old (139). The EPM test is a (+) shaped apparatus that consists of four arms. The east and west arms consist of "closed/walled" arms and the north and south arms are "open/exposed" with only the platform (Figure 2.4). No acclimatization was necessary as this would affect the anxiety and stress response of the mice. Each animal was placed in the centre of the maze facing the same orientation and allowed to move freely for 3 mins whilst being video recorded. The time spent investigating the open and closed arms were recorded along with the number of head dips, whole body stretches in the open arm and closed arm (protected arm). An "open arm" or "closed arm" was when the mouse had 3 or more limbs in and open (exposed) or closed arm of the maze respectively. Head dips were defined when the mouse had 3 or more limbs in a specified region (i.e., open arm or closed) and it dips its head over the edge of the maze. An "arm stretch" is when the mouse had 3 or more limbs in a specified region outstretched in that designated area. The number of times each animal crossed the centre of the EPM was also recorded. Video recording was analysed and to keep consistent arm entries were defined as when the animal had more limbs in the newly chosen arm on the apparatus. Between each test the apparatus and object were cleaned with 80 % ethanol.

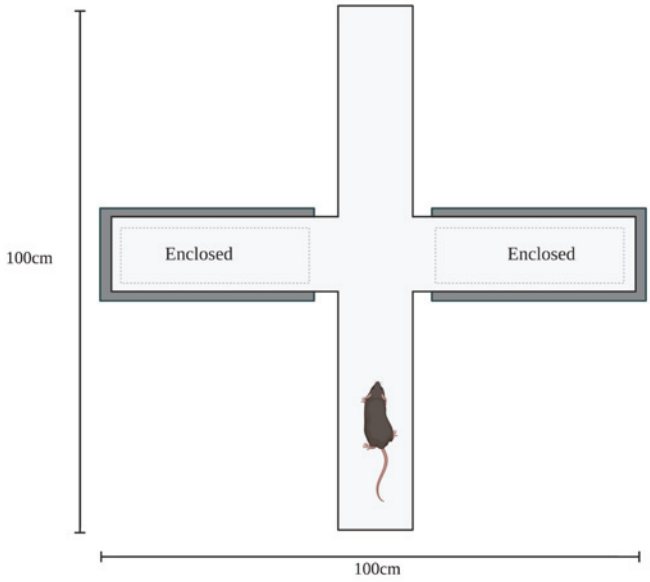

Figure 2.4. Schematic representation of the EPM test – bird's eye view. The mice were placed in the centre of the maze facing the same orientation and their movement recorded. Created with BioRender.com.

2.5.3 Tail suspension test

The tail suspension test (TST) is widely used method for measuring depressive-like symptoms, as people with depression have a higher risk of developing AD, therefore it is a common symptom coinciding with AD development (140). After acclimatization each animal was placed upside down hanging from the centre of the apparatus as indicated in Figure 2.5. A plastic tube was placed around the base of the tail to prevent the mouse from climbing up its tail whilst its tail was taped to the bar. The mice were then hung for a total of 3 mins which was video recorded. For consistency, when analysing the video recording, mobility was defined as when they were trying to reach for walls of the apparatus, suspension bar, strong shaking of the body, and movement of the limbs akin to running (140). The mobility of the animal was then video recorded for a total of 3 mins. Decreased mobility time (secs) indicates depressive-like symptoms. Between each test the apparatus and object were cleaned with 80 % ethanol.

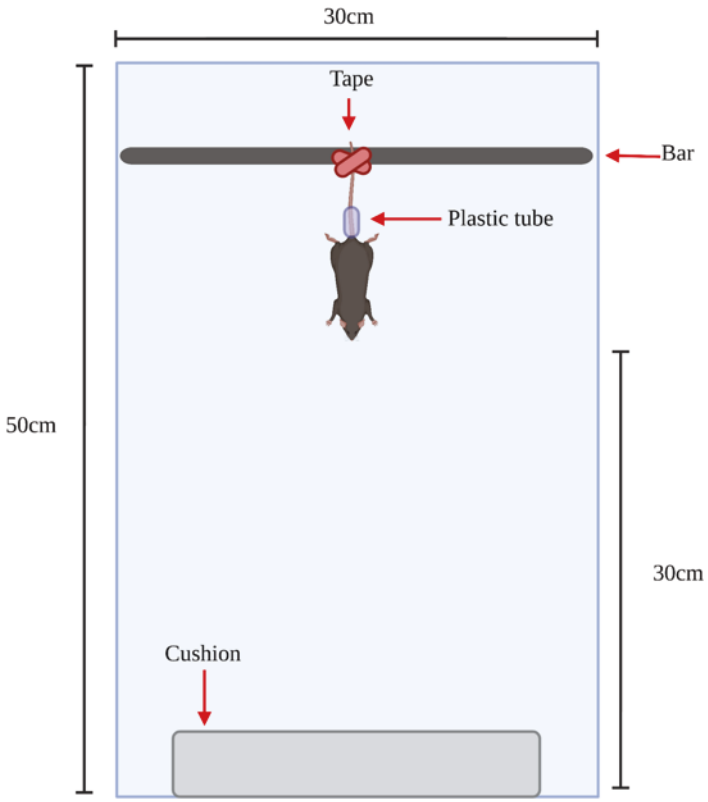

Figure 2.5. Schematic representation of the TST experiment. The mice were placed upside with their tails taped to the bar, and the mobility time was recorded. Created with BioRender.com.

2.6 Near-infrared (NIRF) *in vivo* brain imaging

At week 15 and 31 of the animal experiments (animal study 1 and 2 respectively) the development of Aβ species formation, detecting both the soluble (Aβ40) and insoluble (Aβ42) peptide aggregates, was assessed in the mice brains using a NIRF molecular imaging probe, CRANAD-2 (Abcam, Cambridge, UK) (141). The *in vivo* CRANAD probe detects for presence of the insoluble Aβ42 peptide. The CRANAD-2 probe was prepared in a mixture of 15 % DMSO, 15 % cremaphor and 70 % PBS at a concentration of 5 x 10^3 mg/mL. The mice heads were shaved and inducted in a chamber using 4 % isofluorane and 2 L/min oxygen. Baseline fluorescence of the brain was obtained using the IVIS fluorescent scanning machine (IVIS Lumina II; Caliper Life Sciences, MA, USA). The mice were then intravenously injected with the CRANAD-2 (5 mg/kg) before they were inducted again and fluorescence signals from the brain was recorded 5 mins after injection. A small circular region of interest (ROI), in the

centre of the fluorescence region was established to be consistent, between mice measurements. The average radiance (p/s/cm^2/sr) in the region of interest was recorded.

2.7 Tissue harvest and blood collection

At experimental endpoint the mice were euthanized with isofluorane in an induction chamber and then placed on a nose cone until no reflex to pedal or ocular stimulation was observed. Cardiac puncture was performed via the left ventricle to collect approximately 1 mL of blood using an 18-gauge syringe pre-coated with heparin (100 I.U/mL DBL Heparin Sodium Injection, Hospira, Vic, Australia). Following collection, the whole blood sample was immediately centrifuged (13, 500 RCF, 5 mins). The plasma layer was removed and stored at -80°C. To ensure the mouse was deceased before any further procedures, cervical dislocation was performed. For this study many different techniques were of interest, therefore the brains were halved; the right hemisphere was fixed in 4 % paraformaldehyde (PFA), while the left was dissected and the hippocampus and cerebral cortex were snap frozen in liquid nitrogen, then stored at -80°C until required.

2.8 Biochemical analysis of plasma

2.8.2 Beta-secretase assay

β-secretase plasma levels have been shown to be increased in both the peripheral blood and cerebrospinal fluid of AD patients and therefore has been identified as a suitable early diagnostic biomarker (142, 143). To assess β-secretase levels in the plasma samples collected at experimental endpoint, the β-secretase fluorometric assay activity kit (BioVision, CA, USA, cat. K360) was completed following the manufacturer's protocol. Briefly, plasma samples were prepared in duplicate in a 96-well plate (50 µL) per well, along with appropriate controls, with 50 µL of reaction buffer added to all wells and incubated at 37°C for 20 mins. β-Secretase substrate (2 µL) was then added to all wells, which was then covered and incubated at 37°C for 20 mins. The plate was read on the infinite M1000 PRO microplate reader (Tecan Sunrise, Grödig, Austria) at 335 Ex/ 495 Em (excitation/emission). The results are expressed as percentage increase from control.

2.9 Tissue fixation, processing, embedding, and cutting

The right hemisphere was fixed in 4 % PFA (Sigma-Aldrich, MO, USA) overnight, then rinsed with phosphate buffered saline (PBS) before being stored in 70 % ethanol for one week. Brain tissues were then placed in cassettes and processed using the ExcelsiorTM AS Tissue Processor (Thermo Fisher Scientific, MA, USA) for an overnight process involving two changes of formalin, increasing grades of ethanol and two changes of paraffin wax. After processing, brain tissues were embedded in paraffin wax and cut in sagittal sections using microtome (Epredia, MICH, USA). Brain sections were cut at a thickness of 10 µm, through the entire right hemisphere, resulting in approximately 25-30 slides (e.g., slide labelled #1 is closest to the midline) per tissue. Three brain tissue sections were mounted on every Platinum PRO adhesive glass slides (Trajan, VIC, AU), left to dry at 37°C overnight and stored at room temperature until required.

2.10 Histological analysis of the hippocampus

2.10.1 Cresyl Violet staining for the identification of neurons

Three slides (slides #1, #3, #5) for all brain tissue samples were stained with cresyl violet to differentiate neurons from other cells within the hippocampus and somatosensory cortex. Briefly, paraffin was removed from tissue sections by soaking in two changes of xylene for 3 mins each. Sections were then rehydrated through decreasing concentrations of ethanol (100 %, 95 %, 70 %) for 3 mins each before being immersed completely in water for at least 6 mins. After rehydration, sections were stained with cresyl violet (0.1% cresyl violet powder (wt/vo); Sigma-Aldrich, MO, USA) for 3.5 mins. Sections were then rinsed in water (5 mins) and dehydrated in two changes of 100% ethanol and two changes of xylene (3 mins each). Sections were then cover-slipped using dibutyl phthalate polystyrene xylene (DPX) and left to air dry overnight. To quantify neurons stained in regions of interest, images of the stained slides were visualised on the ZEISS AxioScan Digital Slide Scanner (Carl Zeiss Microscopy, Germany). The sagittal section for all tissue sections on each slide were imaged at 20 x magnification. The hippocampal region is associated with memory and spatial recognition, and the somatosensory region in the cortex is responsible for receiving and processing sensory information (e.g., touch, temperature and pain etc.) (144, 145). The number of neuronal cell bodies were counted (10-400 μm^2) using the QuPath Software Quantitative Pathology & Bioimage Analysis (QuPath) Software 0.2.3 (Edinburgh, UK) in regions of interest (ROI) in the hippocampus:

cornu ammonis (Ca) 1, Ca3 and dentate gyrus (DG), and the somatosensory cortex (SS 2, 3, 4, 5, 6a) (146). Every brain tissue sample (n = 5-11 biological replicates) that was analysed had 9 technical replicates accounting for staining, imaging and analysis bias.

2.10.2 Thioflavin S staining for the identification of Aβ plaques

Three slides (slides #2, #4, #6) for all brain tissue sample were stained with thioflavin S for quantification of Aβ plaque formation. Slides were re-hydrated as described above (section 2.10.1). Rehydrated sections were then stained with thioflavin S (1 % thioflavin S stain (wt / filtered aqueous solution); Sigma-Aldrich, MO, USA) for 10 mins. Slides were washed well with water for 5 mins, followed by dehydration in two changes of 100 % ethanol and two changes of xylene (3 mins each). Finally, slides were cover-slipped using DPX and left to air dry overnight. Slides were visualised on the ZEISS AxioScan Digital Slide Scanner (Carl Zeiss Microscopy, Germany) and the entire sagittal section fields of view were imaged at 20 x magnification. The number of fluorescent Aβ plaque formations were counted using Image J (IJ1.46r Revised Edition), by implementing a fluorescent threshold highlighting the Aβ plaque formations in each brain tissue. W/T (C57BL/6) mice do not develop Aβ plaques, however APP/PS1 mice that are 6-12 months of age develop round dense Aβ plaque formations that are approximately 50-150 µm in diameter that form throughout the entire neocortex region (147, 148). The number of fluorescent Aβ plaque formations were automatically counted in a region of interest (ROI) in the neocortex above the hippocampus, using Image J (IJ1.46r Revised Edition), by implementing a fluorescent and size (50-150 μm^2) threshold, highlighting the Aβ plaque formations in the brain tissue. Every brain tissue sample (n = 5-11 biological replicates) that was analysed had 9 technical replicates accounting for staining, imaging and analysis bias.

2.11 Cell culture *in vitro* models

To determine the effects of an immune response in the brain, two key cell types have been used that are important in CNS function. Human neuroblastoma (SH-SY5Y) cells (Chapter 4 and 6) were used to represent neuronal cells and murine microglial (BV-2) cells (Chapter 6) were used for microglia representation. The SH-SY5Y cells (provided by Dr Cathy Gorrie, University of Technology Sydney) are a subline of the neuroblastoma SK-N-SH line derived from a metastatic bone tumour. These cells were grown in Falcon® T75 flasks and maintained in DMEM/F12 GlutaMAX™ medium (Gibco, MA, USA) supplemented with 5% FBS and 5 mM

HEPES. Growth media was changed every 3-4 days and the cells were passaged when they reached confluency (80-90 %). To prevent cell senescence the passage was kept under 40. The cells were cultured at 37°C in a humified atmosphere containing 95 % air and 5 % CO_2.

The BV-2 cells (kindly donated by Dr Alessander Cassorina, University of Technology Sydney) were grown in Falcon® T75 flasks and maintained in DMEM F12 GlutaMAX™ media supplemented with 5 % FBS and 5 mM of HEPES. Growth media was changed every 3-4 days and the cells were passaged when they reached confluency (80-90 %). To prevent cell senescence the passage was kept under 30. The cells were cultured at 37°C in a humified atmosphere containing 95 % air and 5 % CO_2.

For each biochemical assay that was performed with both cell lines, cells were seeded in a 96-well plate with 8 technical replicates per plate and per assay. Each assay was repeated 4 times (n = 4 biological replicates), at different passages to account for reproducibility issues (149) which is stated in the results.

2.11.1 Cell study 1 – Air pollutant particle preparation and exposure (Chapter 4)

Iron, diesel and magnetite air pollutant particles were prepared in filtered Dulbecco Modified Eagle Medium (DMEM) F12 GlutaMAX™ media supplemented with 5 % foetal bovine serum (FBS) and 5 mM of HEPES at a concentration of 100 µg/ml. Samples were sonicated, using the Q500 Sonicator (Q500 Sonica Sonicators, CT, USA) for 5 mins at 50 % amplitude, to disperse particles. Sonication of air pollutant particles after sonication is essential to prevent agglomeration. The SH-SY5Y cells were seeded onto 6-well plates (80, 000 cells/well) for RNA/protein extraction or 96-well plates (30, 000 cells/well) for biochemical assays and allowed to settle overnight. The cells were then serum starved for 24 hours before exposure to 100 µL IRON, DE, MAG particles (100 µg/mL) in DMEM/F12 containing 5 % FBS for a further 24 hours. By which point the cells were ready for further testing. Cells not exposed to nanoparticles acted as controls. This concentration was established based on *in vitro* studies (e.g., human lung epithelial A549 and murine macrophage RAW 264.7) testing air pollutant induced toxicity for the same exposure time and concentration (150, 151).

2.11.2 Cell study 2- Treatment with cerium oxide nanoparticles (Chapter 6)

The SH-SY5Y cells and BV-2 cells were seeded onto 6-well plates (80, 000 cells/well) for protein extraction or 96-well plates (30, 000 cells/well) for biochemical assays and allowed to settle overnight. The cells were then serum starved for 24 hours before exposure to 100 µL magnetite particles (100 µg/mL) in DMEM/F12 containing 5 % FBS for a further 24 hours. To assess the effects of magnetite particles, the cells were left to incubate for a further 24 hours – 48 hours exposure in total. To assess the effects of CeO_2, following exposure to magnetite particles for 24 hours, the cells were treated with either CeO_2 or blue $SiCeO_2$ nanoparticles (50 µg/mL) and incubated for another 24 hours. The magnetite particles used for this study were prepared as previously described (section 2.12.1). The CeO_2 and blue $SiCeO_2$ nanoparticles were prepared in the same medium, at 50 µg/mL, then sonicated and administered as previously described (section 2.12.1). The concentration of both CeO_2 and blue $SiCeO_2$ nanoparticles was established based on preliminary in vitro studies investigating the effects of CeO_2 nanoparticles in various concentrations on both SH-SY5Y and B-V2 cells (Chapter 6, Figure S4A-D), where the concentration of 50 µg/mL for 24 hours was chosen (152, 153). The cell viability, ROS and NO production was further tested on both cell types with LPS being used as the inflammatory stimuli (Chapter 6, Figure S4E-J). By which point the cells were ready for further testing. Cells not exposed to nanoparticles acted as controls.

2.12 Biochemical assays

2.12.1 Methylthiazolydiphenyl-tetrazolium bromide (MTT) assay

The MTT assay is a widely used method for cell viability and cytotoxicity (154). A stock solution of MTT dye (Sigma Aldrich, MO, USA) was prepared at a concentration of 5 mg/mL with PBS. After the cells had been starved and treated an aliquot of the MTT dye (10 µL) was added to each well (96-well plate) and then incubated in dark sterile conditions at 37°C for 3-4 hours. The MTT dye is utilised by cell mitochondria, converting the dye to formazan, forming insoluble purple granules. Once the purple-coloured formazan crystals were observed visually, the media and dye are then removed followed by adding 100 µL of DMSO (Sigma Aldrich, MO, USA) each well to solubilize formazan and turn the solution purple. The absorbance at 570 nm was obtained on the infinite M1000 PRO microplate reader (Tecan Sunrise, Grödig, Austria). The results are expressed as percentage increase from control.

2.12.2 2'7'-Dichlorofluoerscein (DCF) assay

The DCF assay is a measure of ROS (Sigma Aldrich, MO, USA). The DCF assay uses the 2' 7'-dichlorofluorescein diacetate, a cell-permeable non- fluorescent probe that becomes highly fluorescent upon oxidation. Fluorescence was used as a measure of ROS production in the cells. The DCF powder is dissolved in DMSO at a concentration of 10 µM and stored in the dark -20°C. After the cells had been starved and treated the DCF stain (100 µL) was added to each well in a 96-well plate and incubated at 37°C for 12 mins. Excess stain was removed from the cells by washing twice with PBS (2 x 100 µL). The plate was then measured at 485 nm excitation and 535 nm emission using the infinite M1000 PRO microplate reader (Tecan Sunrise, Grödig, Austria). The results are expressed as percentage increase form control.

2.12.3 Griess assay

The Griess assay detects nitric oxide (NO) production in a variety of mediums (Sigma Aldrich, MO, USA). The Griess reagent is based on a chemical reaction that uses naphthyl ethylenediamine dihydrochloride suspended in water and sulphanilamide in phosphoric acid. This reaction reacts with nitrite in samples to form a purple azo product. To prepare the solution Griess powder is dissolved in milliQ water at a concentration of 40 mg/mL. Following cell treatments, the media was collected and aliquoted (100 µL) in duplicates into wells on a 96 well plate. The Griess reagent was then added to each well (100 µL). The reaction mix was then incubated at room temperature for 15 mins followed by 30 mins in the dark at 37°C. An absorbance reading was obtained at 540 nm on the infinite M1000 PRO microplate reader (Tecan Sunrise, Grödig, Austria). The results are expressed as percentage increase from control.

2.13 Quantification of gene expression by RT-qPCR

2.13.1 Total RNA extraction

The Total RNA was extracted from the SH-SH5Y cells (Chapter 4) by the addition of TRIsure™ (Bioline, MA, USA) to each well on a 6 well plate. Cells were lysed by repeatedly washing the cell monolayer with the added TRIsure™ before transferring to a clean Eppendorf

tube containing 100 µL of 1-bromo-chloropropane in each sample. The samples were vortexed and centrifuged at 12, 000 RCF for 15 mins at 4°C. The aqueous phase was transferred to a clean tube and 500 µL of isopropanol was added. The samples were briefly vortexed and incubated at room temp for 10 mins to precipitate the RNA. Following the incubation, the samples were centrifuged (12, 000 RCF for 15 mins, 4°C). The supernatant was removed, and the RNA pellet washed with 1ml of ice-cold ethanol, followed by another centrifugation (12, 000 RCF for 10 mins, 4°C). After removing the ethanol wash, the RNA pellet was air dried for at least 5 mins before resuspending in approximately 30 µL of nuclease free PCR water (Bioline, UK). The RNA samples were stored at -80°C until required.

Total RNA was extracted from the hippocampal regions (Chapter 4) of the brains using the Isolate II RNA/DNA/Protein Kit (Phenol free) (Bioline, UK). All components were extracted the from tissue following the manufacturer's instructions. Briefly, for RNA extraction, the entire left hemisphere hippocampus was lysed, and the lysate loaded into a column for DNA extraction. The flow-through containing the RNA was washed with ethanol and loaded onto the RNA/protein column. RNA bound to the column was washed and eluted in RNA elution buffer. RNA was stored at -80°C until used.

2.13.2 RNA quality check

The integrity of the extracted RNA was assessed using an Experion™ RNA standard Sensitivity Analysis Kit (Bio-Rad, CA, USA) and the Experion™ Automated Electrophoresis Station (Bio-Rad, CA, USA), as per manufacturer's instructions, to ensure that the RNA was of satisfactory quality and purity for downstream qPCR analysis. An electropherogram and virtual gel (Figure 2.6) was produced displaying distinct peaks/bands corresponding to 18S and 28S ribosomal RNA respectively, when aligned with the ladder provided in the sample preparation kit. An RNA Quality Indicator (RQI) was also generated which indicates the quality of sample tested. An RQI of 10 indicates intact RNA and an RQI of 1 indicates completely degraded RNA, with samples with an RQI above 7 deemed acceptable for further analysis.

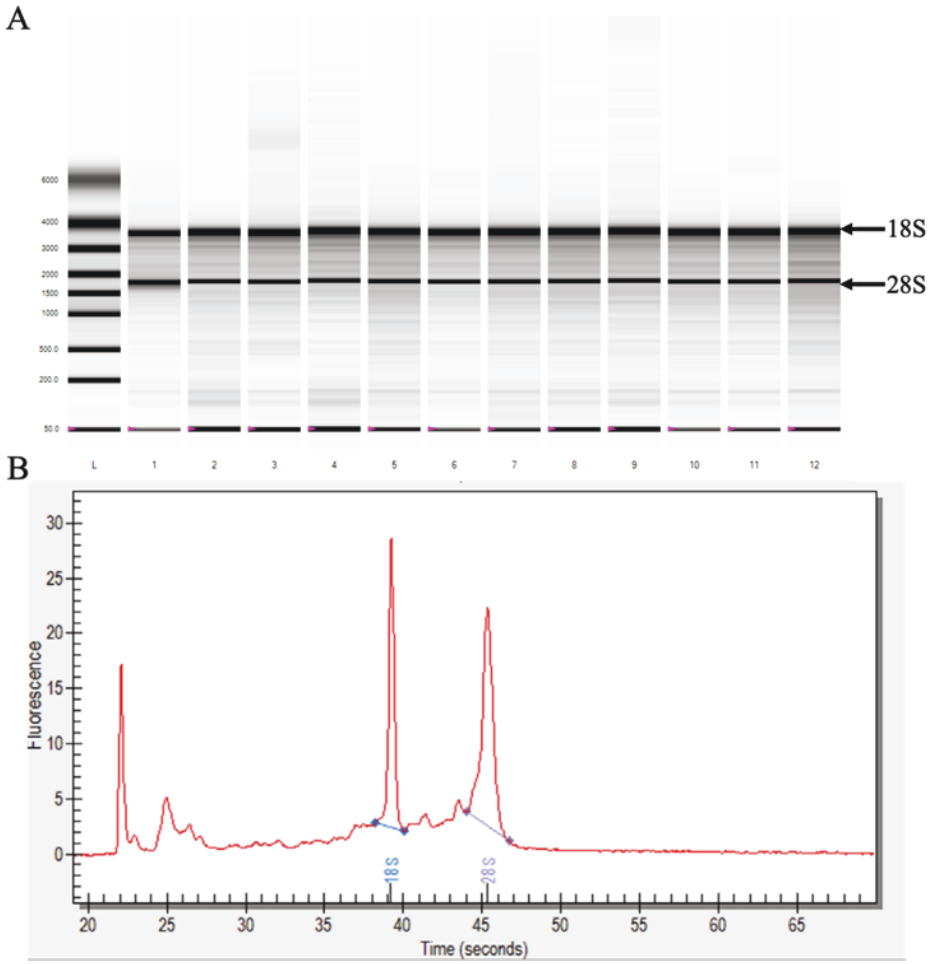

Figure 2.6. A representative virtual gel and electropherogram generated by the Experion RNA StdSens Analysis Kit. (A) The virtual gel showing two bands for 18S and 28S ribosomal RNA. (B) An electropherogram showing two peaks representing 18S and 28S ribosomal RNA.

2.13.3 Synthesis of cDNA using reverse transcription

After the integrity was assessed, the RNA was normalised to 220 ng/µL using the NanoDrop 2000 spectrophotometer (Thermofisher Scientific, MA, USA). Following this, the samples were reverse transcribed in duplicate using the Tetro cDNA Synthesis Kit (Bioline, UK). Briefly, a master mix was prepared containing 0.5 µL each of random hexamer, 10mM dNTP mix, RiboSafe RNase Inhibitor and Tetro Reverse Transcriptase, 2 µL of 5 x RT buffer and 4.7 µL of PCR water. Total RNA (1.3 µL) was added to give 1 µg of RNA per 10 µL reaction. Samples were incubated in the T100TM Thermocycler (Bio-Rad, CA, USA) for 10 mins at 25°C followed by 30 mins at 45°C. The reaction was terminated by incubating at 85°C for 5

mins. Duplicate samples were then pooled and diluted 1:3 with nuclease free water and stored at -20°C until testing was completed.

2.13.4 Real-Time PCR (qPCR)

Gene expression levels were quantified via real-time PCR (qPCR) using the SensiFast SBR No-ROS mix (Bioline, UK). Each reaction mix comprised of 5 µL of 2x SensiFAST SYBR No-ROS mix, 0.4 µL each of the forward and reverse primer (primer sequences shown in Table 2.3; 20 pmol/µL) and 1.2 µL of PCR water. The cDNA (3 µL) prepared as described (section 2.13.3) was then added to give approximately 100 ng of cDNA in a 10 µL reaction. The PCR plate was covered using a Microseal "B" PCR plate sealing film (Bio-Rad, CA, USA) followed by a brief centrifugation. Samples were then amplified in the CFX96 thermocycler (Bio-Rad, CA, USA) at 95°C for 2 mins for polymerase activation, 40 cycles of 5 secs at 95°C for denaturation, 10 secs at 60°C for annealing, and 10 secs at 72°C for extension. A melt curve was generated by incubating the cDNA at 65°C for 5 secs, then increasing the temperature to 95°C in 0.5°C increments.

2.13.5 Calculation of the fold changes in gene expression

Relative changes in mRNA levels were determined using the comparative analysis method ΔΔCq. The difference between the quantification cycle (155) value of the gene of interest (156) and the reference gene is given by ΔCq. The baseline ΔCq is set as the ΔCq for the W/T Saline administered mice. The ΔΔCq calculation was then determined by subtracting each sample's ΔCq and the baseline ΔCq. The Cq is exponentially related to copy number. Therefore, the absolute value for comparative expression level is given by the formula $2^{-\Delta\Delta}$Cq. For the current study the reference gene chosen was GAPDH (157, 158).

Table 2.3. PCR Primer Sequences for the in vivo experiment

Species	Gene ID	Description	F/R	Primer Sequences (5'-3')
Mouse	IL-6	Interleukin 6	F	GAACAACGATGATGCACTTGC
			R	TCCAGGTAGCTATGGTACTCC
	TNF	Tumour necrosis factor	F	CTATGTCTCAGCCTCTTCTC
			R	CATTTGGGAACTTCTCATCC
	GAPDH	Glyceraldehyde 6-phosphate dehydrogenase	F	GCTCACTGGCATGGCCTTCCG
			R	GTAGGCCATGAGGTCCACCAC

2.14 Protein extraction

Whole protein lysate was extracted from the cerebral cortex, hippocampus and SH-SY5Y cells, using RIPA lysis buffer (150 mM sodium chloride, 1 % triton X-100, 0.5 % sodium deoxycholate, 0.1 % sodium dodecyl sulphate, 50 mM Tris pH 8.0) supplemented 1/10 volume of protease inhibitor cocktail (Sigma Aldrich (MO, USA) containing 1.4 mm Zirconium oxide beads (Precellys 24, France) using a Minilys (Bertin Technologies, France). The samples were homogenised and incubated in the buffer on ice for 30 mins before being centrifuged at 12, 000 RCF to form a pellet. The supernatant containing the extracted protein was collected and stored at -80°C until required. The concentration of the extracted protein was quantified with a Pierce BCA Protein Assay Kit (Thermofisher Scientific, MA, USA, cat. 23225).

2.15 Aβ42 ELISA

To investigate whether air pollutant particles and CeO_2 nanoparticles are having an effect on insoluble Aβ42 aggregation, Aβ42 Human ELISA Kit (Thermofisher Scientific, MA, USA, cat. KHB3441) was completed with the extracted protein from SH-SY5Y cells. The protein (30 µg) was prepared in duplicate (50 µL) and added to the wells, along with standards and appropriate controls. The Aβ42 Detection antibody solution (50 µL) was added to each well and incubated at room temperature for 3 hours. Following this, the plate was aspirated and washed. The anti-rabbit IgG HRP (100 µL) was added to each well and incubated for 30 mins at room temperature. The plate was then aspirated and washed, and the stabilized Chromogen (100 µL) then incubated for a further 30 mins at room temp. Finally, the stop solution (100 µL)

was added, and the plate was read on the infinite M1000 PRO microplate reader (Tecan Sunrise, Grödig, Austria) at 450 nm. The results are expressed as Aβ42 (pg/mL).

2.16 Western blot analysis

For western blot analysis protein extracts (30 µg for the cerebral cortex and hippocampus and 20 µg for SH-SY5Y cells) were denatured by heating at 95°C for 5 mins, then mixed with 1:1 ratio of Laemmli loading buffer (BioRad, CA, USA). The samples were then loaded into wells on a 4-15 % Mini Protean TGX stain free protein gel (Bio-Rad, CA, USA). Electrophoresis was performed in the 10 x Tris/Glycine/SDS running buffer (BioRad, CA, USA) for 80 mins at 110v. The Precision Plus Protein Kaleidoscope™ ladder (BioRad, CA, USA) was included in each gel run. Resolved protein samples were transferred to a mini PVDF membrane (BioRad, CA, USA) using the Trans-Blot® Turbo™ Transfer System (Biorad, CA, USA), then blocked with skim milk (5 % (v/v) in 1 X TBST) for 2 hours at room temperature. Blots were then incubated with primary antibodies (Table 2.4) overnight at 4°C. After washing with TBST (3X), the membranes were incubated with appropriate secondary antibodies for 2 hours at room temperature, antibodies are listed in Table 2.4. Proteins were then visualised using ECL substrate (Bio-Rad, CA, USA) and a Bio-Rad Chemidoc Imaging System™. Protein bands were quantified by densitometry using the ImageJ 1.53a software (National Institute of Health, Maryland, USA).

Table 2.4. Antibodies used for Western Blot analysis

Protein	Dilution	Company	Catalogue
β-Actin	1:1000	Cell Signalling Technology, MA, USA	4970S
BDNF	1:1000	Abcam, UK	108319
GFAP	1:1000	Abcam, UK	33922
ICAM-1	1:1000	Abcam, UK	53013
iNOS	1:200	Cell Signalling Technology, MA, USA	12282S
Cox2	1:500	Cell Signalling Technology, MA, USA	13120S
Phospho-Tau (pS214)	1:500	Invitrogen, CA, USA	44742
ChK Total Tau	1:500	Abcam, UK	75714
Iba-1	1:1000	Abcam, UK	178847
NF-κB p65 (D14E12)	1:1000	Cell Signalling Technology, MA, USA	8242T
Phospho-NF-κB p65 (Ser536)	1:1000	Cell Signalling Technology, MA, USA	3033T
MAPK	1:1000	Cell Signalling Technology, MA, USA	8690S
Phospho-MAPK	1:1000	Cell Signalling Technology, MA, USA	4511S
JNK	1:1000	Cell Signalling Technology, MA, USA	9258S
Phospho-JNK	1:1000	Cell Signalling Technology, MA, USA	4668S
Tumour necrosis factor (TNF)	1:1000	Santa Cruz, CA, USA	sc-1350
Interleukin 6 (IL-6)	1:1000	Santa Cruz, CA, USA	sc-1265
Anti-rabbit Secondary (HRP conjugated)	1:5000	Cell Signalling Technology, MA, USA	7074P2
Anti-mouse Secondary (HRP conjugated)	1:5000	Cell Signalling Technology, MA, USA	7076P2
Anti-goat Secondary (HRP conjugated)	1:2000	Santa Cruz, CA, USA	sc-2350

2.17 Statistical Analysis

One-way ANOVA with Bonferroni's post-hoc test was used to determine statistical power in EPM, TST, NIRF in vivo brain imaging, β-secretase assay, neuronal cell counting, Aβ plaque counting, MTT assay, DCF assay, Griess assay, RT-qPCR, Aβ42 ELISA and western blot analysis. A an unpaired two-tailed t-test was used to determine the statistical significance of the NOR data. All statistical analysis was performed using the Graph-Pad Prism 9 software

(Graph-Pad, CA, USA) and the results are expressed as mean ± SEM. The treatment groups were considered significantly different if the p value was less than 0.05.

Chapter 3: Systematic and Bibliometric Analysis of Magnetite Nanoparticles and Their Applications in (Biomedical) Research

Submitted as:

Fleming, C., Golzan, M., Gunawan, C., McGrath, K., 2021. Systematic and Bibliometric Analysis of Magnetite Nanoparticles and Their Applications in (Biomedical) Research. Accepted to Global Challenges. Manuscript no. gch2.202200009.

Chapter Summary

The novel properties and potential for nanotechnological applications have generated increasing scientific interest in the use of nanoparticles. Of interest in this thesis, are magnetite particles which have been a popular nanomaterial. However, air pollutant magnetite particles found in human brains of people with AD, highlighting that a better understanding of magnetite's uses is pertinent. Herein, this chapter describes a systematic and bibliometrics analysis conducted on magnetite research from 1990-2020, highlighting the mechanism of formation, along with its extensive applications in various fields including environmental, industrial, and biomedical.

Systematic and Bibliometric Analysis of Magnetite Nanoparticles and Their Applications in (Biomedical) Research

Charlotte Fleming[1], Mojtaba Golzan[2], Cindy Gunawan[3#], Kristine McGrath[1#*]*

1. School of Life Sciences, Faculty of Science, University of Technology Sydney, Sydney, NSW 2008, Australia
2. Vision Science Group, Graduate School of Health, University of Technology Sydney, Sydney, NSW 2008, Australia
3. ithree Institute of Infection, Immunity and Innovation, University of Technology Sydney, Sydney, NSW 2008, Australia

Email:

Kristine.McGrath@uts.edu.au

Cindy.Gunawan@uts.edu.au

#These authors share senior authorship

Authors' contributions:

CF conducted the search, identified the studies, performed the systematic analysis and wrote the first draft of this manuscript. KM and CG conceptualized the study and supervised CF. KM and CG revised and edited the manuscript, and MG provided further edits to the manuscripts. All authors have read and approved the final version of the manuscript.

Charlotte Fleming	Production Note: Signature removed prior to publication.
Mojtaba Golzan	Production Note: Signature removed prior to publication.
Cindy Gunawan	Production Note: Signature removed prior to publication.
Kristine McGrath	Production Note: Signature removed prior to publication.

Systematic and Bibliometric Analysis of Magnetite Nanoparticles and Their Applications in (Biomedical) Research

Charlotte Fleming[1], Mojtaba Golzan[2], Cindy Gunawan[3#*], Kristine McGrath[1#*]

1. School of Life Sciences, Faculty of Science, University of Technology Sydney, Sydney, NSW 2008, Australia
2. Vision Science Group, Graduate School of Health, University of Technology Sydney, Sydney, NSW 2008, Australia
3. ithree Institute of Infection, Immunity and Innovation, University of Technology Sydney, Sydney, NSW 2008, Australia

Email:
Kristine.McGrath@uts.edu.au, Cindy.Gunawan@uts.edu.au

#These authors share senior authorship
Keywords: Magnetite, nanoparticles, composition, applications, bibliometric, review

3.1 Abstract:

Recent reports show air pollutant magnetite nanoparticles in the brains of people with Alzheimer's disease. Considering various field applications of magnetite nanoparticles because of developments in nanotechnology, the aim of this study was to identify major trends and data gaps in research on magnetite to allow for relevant environmental and health risk assessment. Herein, a bibliometric and systematic analysis of the published magnetite literature (n = 31, 567) between 1990 to 2020 was completed. Following appraisal, publications (n = 244) were grouped into four time periods with the main research theme identified for each as 1990-1997 "oxides", 1998-2005 "ferric oxide", 2006-2013 "pathology" and 2014-2020 "animal model". Magnetite formation and catalytic activity dominated the first two time periods, with the last two focusing on the exploitation of nanoparticle engineering. Japan and China had the highest number of citations for articles published. Longitudinal analysis indicated magnetite research for the past 30 years shifted from environmental and industrial applications, to biomedical and its potential toxic effects. Therefore, whilst this study presents the research profile of different

countries, the development in research on magnetite nanoparticles, it also reveals that further studies in the effects of magnetite nanoparticles on human health is much needed.

3.2 Introduction

Magnetite is an iron oxide (Fe_3O_4) rock mineral occurring naturally on Earth. Magnetite belongs to the spinel crystallizing group of minerals, with the formula $FeFe_2O_4$ (5). In the natural environment, magnetite is found in the form of igneous (basic rocks, basalts) and sedimentary rocks (banded iron formations, beach sands) formed via different ways, usually, the reaction between ferric iron mats and ferrous iron anaerobically (159). Magnetite can readily react with oxygen to produce hematite (Fe_2O_3) where it can be used to determine oxygen concentrations in rocks, due to the changes in the atmospheric oxygen content (160). Magnetite exhibits ferrimagnetism where dipole forces align in the same direction, permitting active magnetization to occur. This property of magnetite is influenced by size of the particles and is essential for the reconstruction of tectonics plates on the Earth's crust (160, 161). Overall, magnetite is a unique iron oxide compound that is it extremely versatile due to its magnetic, structural and redox characteristics (162).

Material and life scientists have shown particular interest in substances at nanoscale, referred to as nanomaterials or nanoparticles (163). Iron oxide magnetic nanoparticles or magnetite nanoparticles (MNPs) have become the focus for studies across various fields, including industrial, environmental, and biomedical applications of the nanoparticles. MNPs have been used extensively due to the fundamental properties of MNPs in the closely packed cubic lattice structure with the iron ions located at interstices between the oxygen ions, in either the tetrahedral or octahedral sites. The crystal structure of magnetite allows the movement from one ion to another (transitioning of valence states), exhibiting high conductivity, high catalytic performance, and regenerative abilities exhibiting ferromagnetic or superparamagnetic properties, which means the external magnetic field can magnetize the particles to a paramagnetic (weakly attracted to magnets) but with much larger magnetic susceptibility (161). MNPs can be chemically synthesised and is relatively cheap to manufacture on a large scale, thus it is abundantly available (164). The pliability of synthetic MNPs has allowed them to be used in various environmental, industrial and biomedical applications. For example, MNPs have been previously used to remove chromium, zinc, lead,

arsenic, palladium, copper and chloroform from polluted water and soil (165-169). In industries, MNPs (combined with carbon) have been shown to improve sodium and lithium battery life, improve rechargeable device efficiency, aid in the advancements of solar cells and biofuels due to thermal and catalytic properties (164, 170). In biomedical applications, superparamagnetic synthetic MNPs coated with organic materials has been shown to increase its stability and biocompatibility making it a safe and efficient biomedicine (163, 171). For example, in magnetic resonance imaging (MRI), MNPs have been used as a contrasting agent for tumour diagnosis, and hypothermia-based cancer therapies and for inflammatory diseases (172-177). The various applications of synthetic MNPs show their versatility, with manufacturer's exploiting the remarkable properties that they possess, which have been improved in many applications through the advancements in nanoparticle engineering and manufacturing (178, 179).

Whilst magnetite research over the last 30 years has yielded progress in our understanding of the properties of magnetite, and the ways in which we can exploit its properties for various uses, there are aspects of MNPs which are unknown, which include the way in which they are harmful to human health (180). For example, a study by Maher et al. has shown that air pollutant externally derived MNPs have been found in abundance in the brains of people suffering from Alzheimer's disease (AD) (181). The aim of this study therefore is to conduct a bibliometric analysis of the literature over the past three decades on MNPs related research and highlight future research needs.

3.3 Results

The term "magnetite" was searched in three different databases for scientific literature. A large difference in the number of publications was returned between each database, as seen in Table 3.1. However, the trend for all searches was similar, with the term "magnetite" producing the highest number of publications for all databases. Scopus database returned the highest number (31, 567 publications) of publications for all search terms compared to both Web of Science Core Collection (WoS) (8, 529 publications) and PubMed (938 publications). With the search term of "magnetite AND pathology" returning the smallest number of publications within the Scopus (2, 121 publications) and WoS (20 publications) database.

Table 3.1. Summary of the number of papers identified in searches of different databases in the years 1990-2020. Databases Web of Science (WoS), PubMed® and Scopus were accessed on the 14th of December 2020 and covered the article, title, abstract and keywords.

Search Terms	PubMed	WoS	Scopus
Magnetite	938	8529	31 567
(Magnetite) AND nanoparticle	741	1034	19 007
(Magnetite) AND pollution	22	58	4132
(Magnetite) AND pathology	222	20	2121

Topic Modelling

The dataset extracted on the PubMed database, from the search term "magnetite" was imported into the SWIFT-Review Software for topic modelling. The articles were triaged based on keywords, categorised into topic models and organised in ranking order. SWIFT-Review returned 100 topic models with an overview of the top 19 presented in Figure 3.1. Table 3.2 presents the top 19 topic models and includes a summary description of each topic formulated to provide a theme for each model identified (based on the topic model in the review by Reichel et al. 2020) (178). Most of the topics identified are associated with the magnetic properties and applications MNPs with the latter mostly focusing on advanced imaging techniques. This search was completed to identify the main research themes of MNPs studies conducted from 1990-2020, and to identify the main focus and applications of their use.

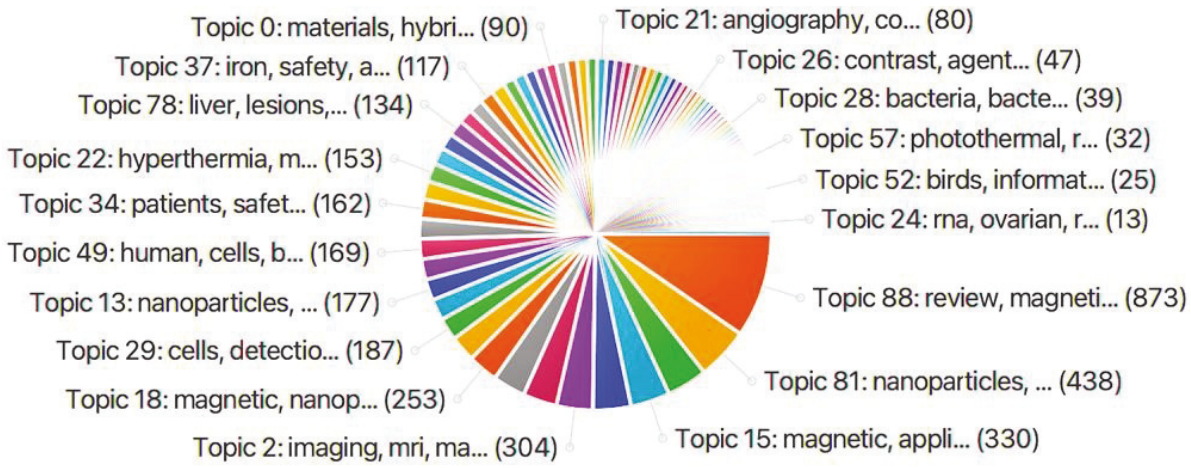

Figure 3.1. Topic models generated from PubMed dataset (938 publications) by SWIFT-Review software, using the search term "magnetite". This search was refined to clinical trials, meta-analysis, review, and systematic review articles. Accessed on 14th December 2020.

Table 3.2. Top 19 topic models generated from PubMed dataset (938 publications) by SWIFT- Review software, using the search term "magnetite". This search was refined to clinical trials, meta-analysis, review, and systematic review articles. The topics have been ordered by number of publications contributing to the topic model in descending order, with topic words and themes established. Accessed on 14th December 2020.

Topic Number	Topic Words	Number of Publications Contributing to Topic Model	Theme of Topic Model
88	Magnetic, applications, nanoparticles, review, recent, properties, biomedical, advances	873	Biomedical advances
81	Nanoparticles, clinical, applications diagnostics, therapeutics	438	Clinical applications
35	Magnetic, MNPs, biomedical, synthesis, properties, surface, imaging	340	Magnetic imaging properties
15	Iron, oxide, ultrasmall, MRI, superparamagnetic, contrast, imaging	330	Superparamagnetic property as contrast agent
27	Future, research, review, current, function, perspectives	319	Current research
2	Imaging, magnetic, resonance, function, probes, vivo, sensitivity	304	MRI use as contrast agent
23	Iron, oxide, nanoparticles, SPOINs, properties, applications, surface	285	Surface structure and properties
90	Size, magnetite, properties, synthesis, control distribution, specific, range	275	Formation and synthesis
18	Field, separation, particles, fields, external, application, surface, area, magnetic, nanoparticles	253	Conducting properties
3	Drug delivery, targeting, release, targeted, systems, anticancer, nanocarriers	217	Targeted drug delivery
29	Cells, detection, cancer targeting, early, specific, advanced, molecules, tumour, approach	187	Targeted cancer therapy
67	Studies, higher, data, larger, medical, form obtained, initial	178	Research analysis of magnetite
13	Clinical, agent, delivery, magnetic, therapy, gene, potential	177	Gene therapy agent
93	Agents, contrast, imaging, clinical media, tissue, extracellular	172	Clinical use to improve methodology
49	Human, cells, body, in vitro, external, material, found, toxicity, effect, tissues	169	Toxicity of MNPs to human cells
63	Nanoparticles, biological, inorganic, chemical, surface biomolecules, metal additives	169	Surface functionalized nanoparticles
34	Patients, safety, clinical, adverse, efficacy, event, injection, phase, safe, received	162	Clinical trials for biomedical applications
87	Dose, time, injection, effects, subjects, healthy, volunteers	154	Clinical trials for biomedical applications

22	Hypothermia, magnetic, treatment, cancer, therapy, heat	153	Hyperthermia based cancer therapy

Bibliographic analysis

To examine the growth of literature in research associated with magnetite, the Web of Science Core collection (WoS) database was used with the search term "magnetite" in the years 1990-2020, yielding 8, 529 publications. To create a visualisation of the co-occurrence of all keyword terms, the extracted dataset (title, abstract, and authors keywords) was imported into VOSviewer Software, Universiteit Leiden, Leiden, Netherlands, Version 1.6.15). The main characteristics obtained from an analysis of the co-occurrence of keywords included the frequency and proximity of similar words. The keywords were refined by a minimum of 20 occurrences, resulting in 134 keywords which were organised by VOSviewer into six main clusters, seen in Table 3.3. The main clusters have been organised to provide an overview of the main research that was carried out on "magnetite" from 1990-2020. Key discoveries within each cluster were identified with a lay description, seen in Table 3.3 and in a network visualisation map, segregated by colours in Figure 3.2. Cluster 1 (red) is focused on the biomedical applications of MNPs as a drug delivery system in cancer therapies and nanomedicine. Two of the clusters are closely linked to the magnetite formation and methodology used for research purposes (cluster 2 and 4; green and yellow respectively). Cluster 3 (blue) focuses on the antibacterial activity, morphology and composition of MNPs whilst cluster 5 (purple) highlights the chemical adsorbent properties of magnetite in terms of environmental remediation. Cluster 6 (aqua) reveals MNPs additives (e.g., nanocomposites, core-shell, doped and surface functionalized) for biomedical purposes. This analysis identified nanoparticle engineering enhancements and specific fields using nanotechnology (e.g., as biomedical therapies) which are further investigated.

Table 3.3. Summary of word clusters identified using VOSviewer and the WoS dataset obtained using a search for the term "Magnetite". The network analysis from 8, 529 publications from 1990-2020. The clusters are represented in a visualisation map (refer to Figure 3.2). Accessed on the 14th of December 2020.

Cluster	Lay/Description	Keywords
1 (red)	Cancer-based therapies	Cancer, contrast agents, design, drug-delivery, efficiency, ferrofluid, functionalization, hyperthermia, in-vitro, magnetite nanoparticles, MRI, release, shape, size, superparamagnetic, therapy, toxicity
2 (green)	Formation, structure and properties	Behaviour, biomineralization, carbon steel, concrete, corrosion, deposition, Fe2O3, hydrogen, kinetics, magnetotactic bacteria, magnetosome formation, microstructure, minerals, Mossbauer spectroscopy, oxidation, phase, surface
3 (blue)	Surface and morphological alterations	Antibacterial activity, chitosan, cytotoxicity, decomposition, gold, graphene, green synthesis, mechanical-properties, microspheres, nanocomposite, nanoparticle, performance, shell, silica
4 (yellow)	Synthesis, magnetic and physical characteristics. Visualisation methods	Conductivity, films, goethite, hematite, hydrothermal synthesis, maghemite, magnetic properties, magnetization, mechanism, Mossbauer, nanostructures, oxide, spectroscopy, system, temperature, transformation, transition, XPS spectra
5 (purple)	Environmental remediator properties and targets	Acid, adsorption, aqueous-solution, catalyst, copper, efficient, heavy-metal ions, humic acid, nanomaterials, nanotechnology, oxides, pH recovery, removal, stability, wastewater
6 (aqua)	Nanoparticle additives, and property characteristics	Carbon, nanotubes, dye, enhancement, graphene oxide, impact, interspecies electron-transfer, ions, methane production, reduction, separation, silver nanoparticles

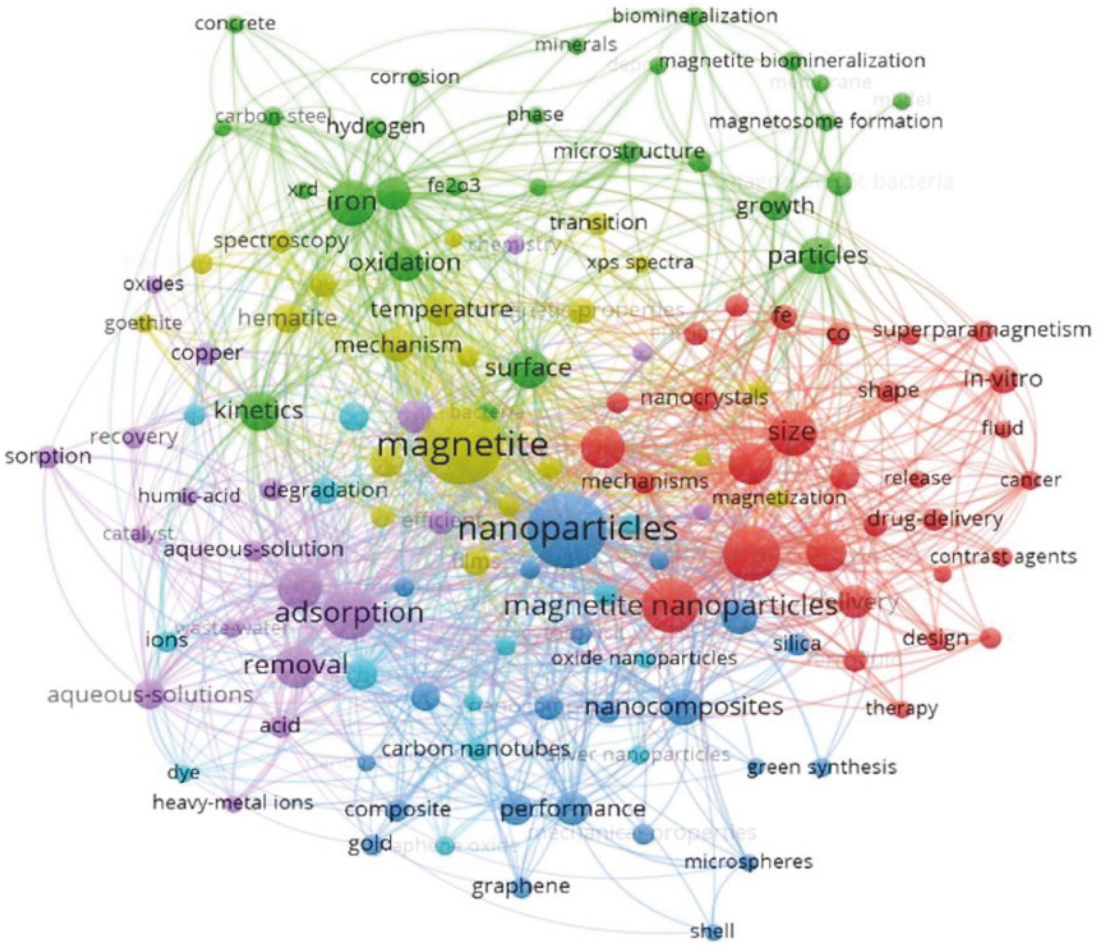

Figure 3.2. Network visualisation map showing six colour-coded clusters produced using VOSviewer and the Web of Science (WoS) dataset, with the search "Magnetite". The network map shows analysis of 8, 529 publications from 1990-2020. The colours represent the clusters of keywords displayed referred to in Table 3.3. Accessed on 14th December 2020.

SciMAT

Scientific research on magnetite has changed significantly over the last three decades, with studies initially investigating the thermal and oxidative properties of MNPs, then shifting focus onto the biomedical applications as a drug delivery and diagnostic agent, eventually looking into the effects of MNPs on the central nervous system, as seen in Figure 3.3. This shift is reflected in the longitudinal study performed using the SciMAT software with the Scopus database (31, 567 publications). Between 1990-1997 (1, 286 publications) the term "oxides" is associated with terms like "magnetics", "dextran" and "heat", indicating an additive of dextran coating of MNPs, with electron microscopy appearing as a common

technology for sedimentary formation analysis of MNPs (178). In the period of 1998-2005 (2, 439 publications) the term “ferric oxide” emerged as the main theme that is associated with words such as “remediation”, “unclassified drug” and “carbon”. In this period, Raman spectroscopy was a common technology used for soil analysis and chemical composition for remediation purposes. Of note in this period, studies were beginning to investigate the potential of MNPs as experimental drug delivery agents.

During 2006-2013 (8, 008 publications) the term “pathology” associated with “diagnostic use” emerged as the major theme. In line with this theme, high-frequency keywords including “tumour” and “diagnostic-agent” were present, with various animal models mentioned (“Wistar rats” and “nude mice”) along with tumour cell lines, being used for experimental studies. In 2014-2021 (19, 834 publications), analysis showed “animal model” as the main theme in association with terms like “inflammatory cell”, “liver function” and “amyloid-plaque” for studies of this period, suggesting that research focused on the role of MNPs in inflammatory and neurodegenerative diseases. The trajectory of MNPs research, initially focuses on the formation and characteristics of doped MNPs, as an anti-cancer agent, eventually leading to the *in vivo* and *in vitro* experiments highlighting the potential toxicity and role in neurodegenerative diseases.

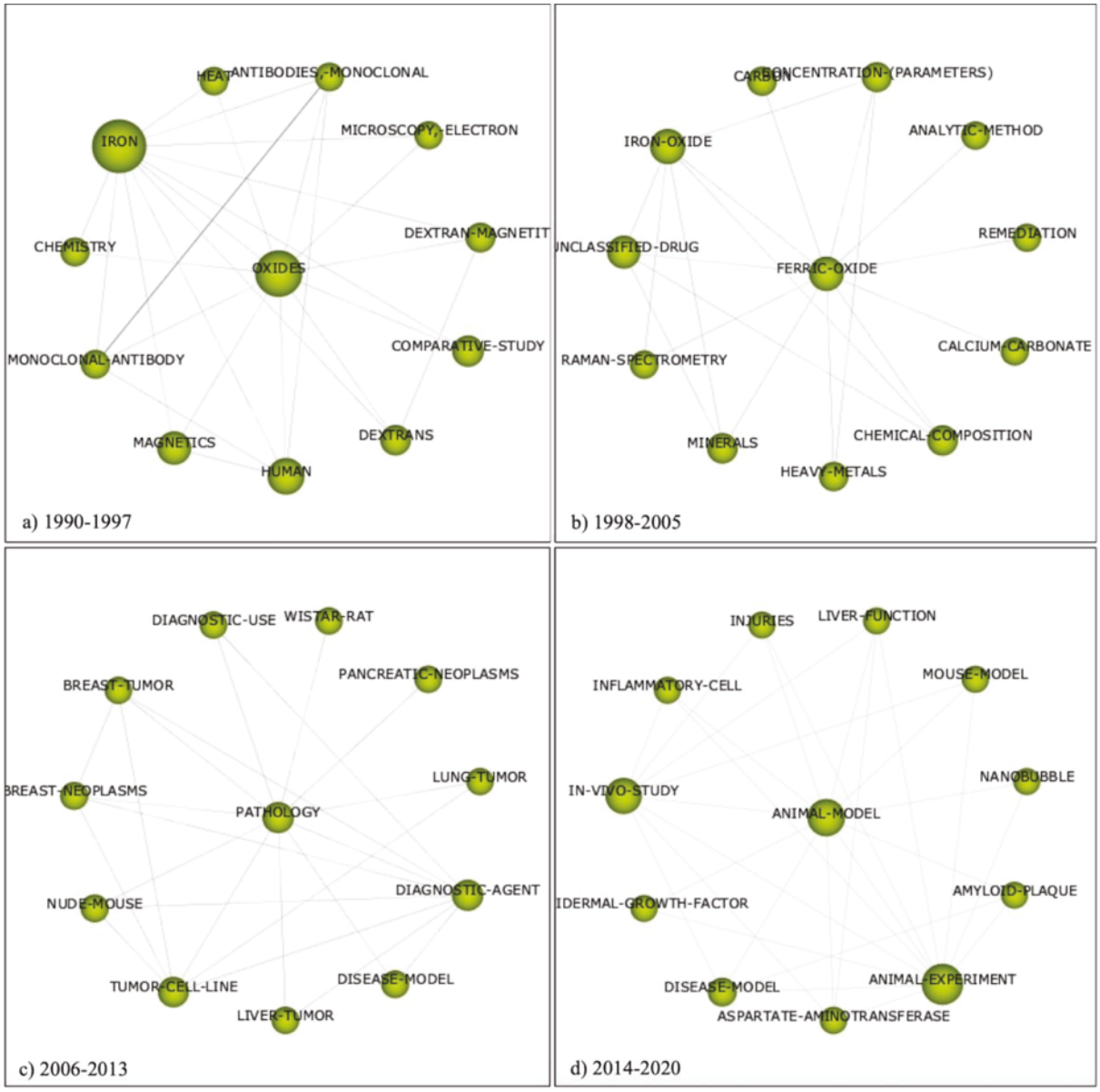

Figure 3.3. Main themes that emerged in magnetite-related publications extracted from the Scopus database (31, 567 publications), over four time periods using SciMAT ((a) 1990-1997 (1, 286 publications); ((b) 1998-2005 (2, 439 publications); ((c) 2006-2013 (8, 008 publications) and ((d) 2014-2021 (19, 834 publications). The figure shows the links between the keywords within the four major themes identified for each time-period. Accessed on the 14th of December 2020.

Systematic Review of Literature

The systematic literature analysis, on the Scopus database was completed to provide an analysis of literature from each theme established in the SciMAT search. This yielded a total of 244 scientific publications, refined by a citation ratio of greater than 6 (peer-acknowledged

quality threshold). The first time period (1990-1997) produced 9 publications ("oxides"), the second (1998-2005) produced 13 publications ("ferric oxide"), the third time period (2006-2013) produced 62 publications ("pathology"), and the last time period (2014-2020) produced the most with 160 publications ("animal model"), seen in Figure 3.4.

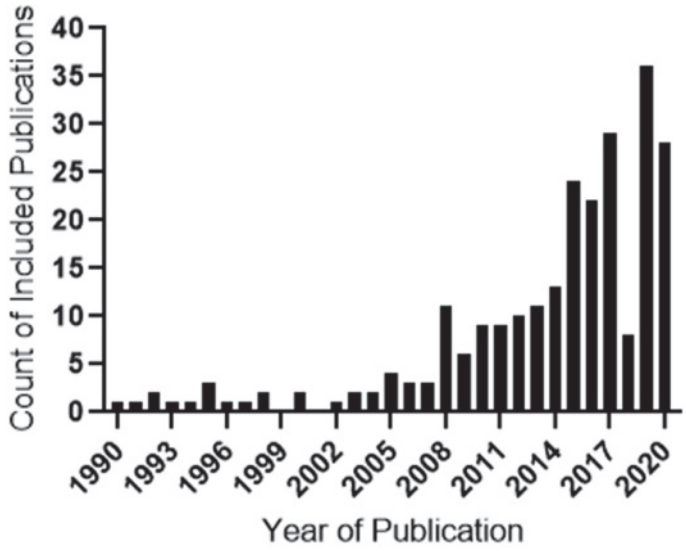

Figure 3.4. Frequency histogram of 244 publications derived from a systematic search of magnetite literature, conducted in the Scopus database for the search term "magnetite" AND oxides/ferric oxide/pathology/animal model, showing a peak publication between 2015-2020. The year 2019 demonstrated the highest number of publications. Accessed on the 14th of December 2020.

Time Period 1990 to 1997 (Magnetite and oxides)

This period yielded nine publications extracted from the literature search with four publications that focused on magnetite formation in sediment and its ability to leach chemical pollutants from soil and groundwater (182-185) One publication studied magnetite as an oxidising agent to better understand the reactivity of crystalline iron minerals in marine sediment formation (183). Two publications focused on magnetite isotope characteristics in sediment for geothermometers to measure temperature in deep sea deposits (184, 185). Three publications focused on the biomedical application of MNPs coated with polypeptide, polyoxymethylene-polypropylene copolymers, ferumoxides, ferumoxtran or ferumoxsil (dextran coated, dextran covered, or siloxane coated respectively) found to be superior for MRI contrasting and cell labelling compared to bare superparamagnetic MNPs (SPIONs) (186-188). Lastly, two publications highlighted the chemical properties and mechanisms of

magnetite transitioning between valence states (183, 189). The range of research on magnetite in this period covered many fields with the majority focused on naturally forming magnetite and the mechanistic properties that magnetite particle possess. This period also highlighted the use of coated MNPs as a biomedicine, which are all continued in the successive time periods.

Time Period 1998 to 2005 (Magnetite and ferric oxide)

A total of 13 publications were included in this time period, with some overlapping themes to the previous period; MNPs for environmental remediation and as a contrasting agent for MRI (190). Five publications highlighted formation, regenerative abilities, and abundance of magnetite in soil, with two studies investigating whether there is a link between the decrease in anerobic respiration, and another study focusing on magnetic properties in soil relating to future environmental change (191-195). Three publications highlighted environmental remediation studies using of MNPs with hydroxide coatings to extract arsenic and other heavy metals from soil, assessing the effects of particle size, surface texture and morphology (196-198). Three publications studied the valence electron transfer mechanism in MNPs coated with various organic compounds and its potential application to have increased regenerative abilities and improved catalytic capacity to increase battery charge (199-201). Two publications focused on MNPs and its potential as a biomedicine with one study adding bipolar surfactants to the high temperature synthesis reaction resulting in transition from hydrophobic to hydrophilic nanoparticles, increasing dispersibility for biomagnetic applications (e.g., MRI) (202). The second study used surface functionalized MNPs with hydrophilic organic molecules (e.g., tetramethylammonium hydroxide ($N(CH_3)_4OH$)) and reported enhanced MRI contrasting effects, increase cell viability in *in vitro* models (monkey kidney Cos-7 cells) and whole human blood samples. The surface modified/functionalized MNPs led to increased dispersion of the nanoparticles, enhancing contrasting abilities (190). While most of the publications in this period focused on the characterization and physicochemical biological effects of MNPs in soil and as an environmental remediator, the advancements in the design and engineering of the nanoparticles for biomedical purposes were also significant, the latter being the main theme of research in the next period.

Time Period 2006 to 2013 (Magnetite and pathology)

A total of 62 publications were included in this time period, with overlapping themes from the previous period where MNPs were investigated in removing contaminated waste in soil, as MRI contrasting agents and improvements battery life. The studies on the use of MNPs for environmental remediation increased substantially in this period (19 publications) targeting the removal of methylene blue, copper, chromium, arsenic, and chlorophenol as waste contaminants from water and soil (203-208). These MNPs were coated with various materials (e.g., methylene blue) or as nanocomposites (various compounds incorporated into a matrix of standard materials; ceria/MNPs, graphene oxide/MNPs and reduced graphene oxide/MNPs) and investigated the nanosheet structure for enhanced catalytic activity to degrade contaminants in soil (168, 204, 205, 207, 209, 210).

Three publications referred to MNPs and their role as a biosensor in a variety of biomedical, environmental, and industrial applications. One study utilised MNPs as a colorimetric biosensor, and proved to be extremely sensitive, detecting allergies, toxins in water and chronic diseases (211). The second, highlighted graphene oxide/MNPs nanocomposites, found to have improved dispersibility, compared to bare MNPs, thereby increasing electrocatalytic properties, indicating promise for energy (212). Lastly, a study used dopamine coated MNPs, being found to improve electrochemical efficiency and in turn, increasing lithium battery life (213).

Most of the publications in this period described the biomedical applications of MNPs (31 publications). Many studies (16 publications) focused on improving the design and manufacturing of MNPs, so they are more effective *in vivo (*209*)*. This was achieved by increasing the surface-to-volume ratio of MNPs and specifically superparamagnetic nanoparticles (SPIONs), which alter the magnetic property (e.g., as the size decrease, the magnetic anisotropy energy decreases; anisotropy is the energy that keeps the magnetic particles in a certain orientation) of MNPs (214, 215). Studies investigating the morphology of MNPs demonstrated the more compact nano-cubes have less oxygen vacancies and are more stable, compared to more oxygen vacancies, less stable and less compact nanorods and nanowires (209, 216, 217). There is limited evidence to suggest superior morphology, however the most widely used is nano-cubes and nanospheres, with one study suggested that nanowires were extremely effective hyperthermia-based cancer therapy (214, 215). The

composition of MNPs is the most commonly cited parameter, which is dependent on the synthesis method (e.g., gas phase, liquid phase, microemulsion, sol-gel, facile and solvothermal and thermal decomposition), nature of the dopant (e.g., magnetic or non-magnetic), which can affect the stability, dispersibility, coercivity (resistance of a material to changes in magnetization) and functionality of the nanoparticles (209, 218, 219). The composition is highly specific for the purpose of the nanoparticles (e.g., core-shell design also impacts the characteristics of MNPs, enhancing biocompatibility) providing another avenue for maximizing coercivity, and therefore biocompatibility (215, 220). Other biomedical applications of MNPs are more specialized, with one publication focusing on surface-functionalized MNPs with protamine sulphate, which gives a cationic surface charge on the magnetic particles, enhanced the transfection efficiency in an *in vitro* (mouse pLG2 liver cells) and *in vivo* (BALB/c mice, liver) model based on HVJ-E technology, finding that surface modifications can enhance gene transfer (via magnetic targeting) and potentially overcome gene therapy. Two publications investigated SPIONs, dextran coated (found to increase nanoparticle presence in blood circulation), mesoporous silica, (for controlled drug delivery, isolation of genomic and plasmid DNA), amorphous silica (isolation of biomolecules, drug delivery) and polyethylene glycol (221) as a nanowire (drug delivery agent, targeting drug resistant cancer cells) (217, 220, 222, 223). Coating the MNPs with polymer like materials (e.g., dextran and PEG), increases the targeting efficiency of SPIONs, showing these coating materials as a potential transport carrier across the blood brain barrier (BBB) (222). Three publications were found to focus on hyperthermia-based therapies and drug delivery applications, with one publication highlighting core-shell MNPs (used for chemotherapy, radiation and immunotherapy) and magnetic microcapsules (used for hyperthermia and drug delivery), finding that the latter was highly specific and also remained in circulation for a longer time (224). Similarly, another publication focuses on the potential for multi-functional modalities of hyperthermia and drug delivery having magnetite as the nanoparticle core with a polymer shell, as a nanocomposite, with targeting agents on the surface. This MNP design allowed for more controlled drug release, increased loading and greater stability of MNPs (225). Another publication found that iron oxide nano-cube chains, designed specifically for hyperthermia-based therapy, finding that these structures have superior thermal efficiency, as the cubic form can retain heat more readily than particles of similar size (226).

One publication reviewed the macrophage recognition to evade the immune response, however also identified the cytotoxic effects of MNPs *in vivo* (nude mice), finding that oxidative stress was increased, regardless of the composition and even mild exposures of MNPs. The observed toxicity was found to be size-dependent, and if small enough would escape phagocytosis, and lie within macrophages, promoting oxidative stress and ROS mediated activator protein 1(AP-1) and nuclear factor kappa B (NFκB) activation (227). This indicates the gaps in knowledge of MNPs as a biomedicine, which is further explored in the following period.

The research on MNPs in this period, provided insight into the physical changes of MNPs, and the physicochemical characteristics of the nanoparticles for specific environmental, biomedical, and industrial application. The various advances in doping, coating and adjusting the size, morphology and composition in this period was extensive, however the use of nanocomposites prevailed as the most common and effective nanostructure in this period. Combining these manipulations is seen in the later years of this period, which is followed through in the next.

Time Period 2014 to 2020 (Magnetite and animal model): Environmental, industrial, and biomedical applications

This period yielded the highest number of publications (160 publications) making up more than 50 % of all included publications in the final literature appraisal. The period also saw the highest number of publications (36 publications) from a single year (2019). The broad themes for this period are again on the environmental, industrial applications, with significant focus on the biomedical applications as well as toxicological studies of air pollutant MNPs. Many studies (9 publications) in this period described the synthesis process, characterisation, and engineering of MNPs in nanocomposites.

Publications focusing on the environmental applications of MNPs was the most extensive (76 publications). Research (24 publications) highlighted the ability of graphene oxide, cerium oxide, graphene carbon, silver, silica, carbon and polymer like/MNPs nanocomposites ability to efficiently adsorb heavy metals (e.g., chromium, lead, copper, caladium, mercury, arsenic, uranium and nickel), aromatic compounds (e.g., phenazopyridine, tetracycline,

sulfamethazine) and toxic dyes (e.g., methylene blue, organic dyes from polluted wastewater and sediment) (228-237). Microwave adsorption using nanocomposites was also extensively studied (7 publications) with graphene, carbon, yolk-shell and molybdenum disulfide/MNPs nanocomposites (238-240). All these nanocomposites have proven to be highly efficient due to the added activated oxygen sites exposed on the surface of these nanocomposites which readily form stable chelates with heavy metal ions and adsorb microwaves (229, 238, 241). Other publications (5 publications) focused on MNPs with a core shell of poly (m-phenylenediamine), manganese, and graphene oxide to adsorb/remove pollutants (chromium, cationic dyes, lead, copper, and arsenic) from wastewater (228, 233, 242, 243). These publications investigated different types of MNPs configuration including nanospheres, nanofibers, nanosheets, nanotubes, nanoflowers and nanoring's and textured surface for their distinct capacities to remove pollutant moieties (238, 239, 241, 244-247). The nanosphere structure has been most widely used for this purpose, however nanosheets, nanoflower-like and nanoring structures are highly efficient adsorbers as more surface area increases active sites. Similarly, the more porous a surface the more adsorptive (238, 239, 245, 247-249).

Many of the advances used for environmental applications of MNPs are also used for industrial applications focusing on renewable energy, with one publication using the catalytic nature of MNPs to increase methanogenic propionate degradation for renewable energy production (250). Nanocomposites are also widely used in this field with graphene oxide, sodium potassium and graphene aerogel combined with MNPs for enhanced electrochemical conductivity and supercapacitor performance (for efficient energy storage and usage) (251-253). Other studies used MNPs nanocomposites with lithium-sulphur (enhanced electrical conductivity, improved battery life in lithium-ion batteries) and polymethyl methacrylate functionalized MNPs (found to be flame retardant and be efficient electromagnetic wave adsorbents) as the structure enabled greater dispersion, and recyclable ability (251).

The biomedical applications of MNPs in this period are extensive, with subtopics reappearing in this period like contrasting agents, applications for therapy in cancer and drug delivery agents. MNPs as a contrasting agent in this period, focused on SPIONs, with one study using a small SPION agents (coated with carbohydrates), ferumoxide, which can be taken up by macrophages and the reticuloendothelial system to image lymph nodes and certain tumours for MRI imaging up to 11 months after injection (254). Other studies have tested core-shell

SPIONS coated with amino-functionalized octahedral carboxylate shells, further functionalised with PEG. This modification increased sensitivity, low toxicity, good biocompatibility and degradability both *in vitro* (KB cells - human epithelial carcinoma cells) and *in vivo* (BALB/C mice bearing KB tumours) making it a promising MRI contrasting agent (134, 178). Lastly, hyaluronic acid-modified MNPs/Gold (core/shell) nano-stars were investigated in *in vitro* (U87MG cells) and *in vivo* (BALB/c nude mice) models as an imaging and photothermal therapy of tumours, finding that the nanoparticles are water dispersible, colloidally stable, and biocompatible and therefore have great potential as a contrasting agent (255).

The use of MNPs as cancer treatments and drug delivery agents are extensively investigated in this period. Many studies (10 publications) highlighted the use of MNPs in various forms (magnetite fluid, hyaluronic acid-modified magnetite gold core/shell, coated with PEG, as ferumoxytol and SPIONs), which accumulate in and around the tumour effectively killing the cancer cells (178, 255-259). The photothermal nature (Fenton reaction) of MNPs initiate the production of ROS and the application of heat which work to kill cancer cells have been seen in *in vitro* (A549 cells and MMTV- PrMT-derived mammary carcinoma cells) and *in vivo* (female FVB/N mice) models as well as early mammary cancers and cancer metastases in the liver and lungs (173, 260-262). These studies found that the biocompatibility and physiological stability was improved, along with faster clearance enhanced permeability (257, 263, 264). Other publications used mesoporous silica (further functionalized with PEG) and gold, polymer-like shell loaded with doxorubicin that enhanced MNPs photothermal efficiency in killing cancer cells (162, 265, 266). Using MNPs as a diagnostic testing tool have been studied with immobilized surface antigen Hepatitis B on the surface of carbon coated MNPs to for better detection of Hepatitis B in serum and protein for diagnostic use (267).

Other biomedical applications of note in this period focus on the immune response, bone regeneration, and diagnostic testing methods. One publication uses MNPs surface functionalized with oleic acid to form a complex that is able to diagnose egg allergies (268). Another study uses dextran coated SPIONs core shell nano-worms incubated in human serum, to aid the in removal of proteins which may trigger an immune response to allergies, offering sight into safer nanomedicines for human subjects (269). MNPs have also been used

for bone regeneration studies, using porous poly-lactide/polyglycolic acid (PLLA/PGA)/MNPs nanocomposite to stimulate bone regeneration, tested on *in vitro* (MG63 cells) and *in vivo* (New Zealand white rabbits) models, finding that the bone tissue formation was significantly accelerated, along with increase cell proliferation and differentiation (270). Of particular interest is the synthesis of molecularly imprinted magnetite nanozymes, with one publication finding that is can improve specificity, activity, and mimic peroxidase-like activity as a drug delivery method, and another study using a nanozyme MNPs/carbon core shell nanocomposite, in the form a nanowires, for an assay to enhance signal amplification, and detection of platelet-derived growth factor, in human serum samples to in order to replace more costly (271, 272). Another study used PEG coated MNPs, for the detection of hydrochlorothiazide (anti-hypertensive agent) from human urine as a low cost, water compatible, environmentally friendly methods (273). It is apparent that advances in nanoparticle engineering and their exploitation of the physicochemical characteristics in conjunction with many other compounds for customised biological functions, has driven the significant progress of MNPs biomedical research in this period.

The advancements of nanoparticle engineering in this period are clear, with the extensive use of surface functionalized, coated, nanocomposite or a combination of these structural components. The biomedical applications of MNPs in this period are of particular interest, showing improvements in drug delivery, and cancer therapies, but also incorporating MNPs in a wide range of diagnostic testing methods, along with aiding and evading the immune response (e.g., allergies and antimicrobial resistance).

Time Period 2014 to 2020 (Magnetite and animal model): Toxicity

In relevance to the *in vivo* studies, toxicity publications (2 publications) also surfaced in this period, describing the potential impact of MNPs use on human health. As the extensive use of MNPs in various fields is established, the studies showing that nanoparticles including MNPs, may be toxic in many fields that use them. With publications finding the potential genotoxic (toxic to DNA) effects of MNPs with various coatings; polyaspartic acid (bone marrow cells), silica oxide (Hep3B cells), dextran (MCL5 human lymphoblastoid cell line) and bare MNPs (L-929 murine fibroblasts) (274-278). Of concern is bioaccumulation, biodistribution and toxicity of various nanoparticles showing damage to cell membranes by

increasing permeability, inducing cytotoxicity, and in the environment, inhibiting photosynthesis (169, 279). Scholarly research has also investigated the long-term repercussions of MNPs, those originating from anthropogenic sources, in neurodegenerative diseases. Ultrafine air pollutant MNPs have been previously implicated in cardiovascular diseases and neurodegenerative diseases (i.e., AD), as particles smaller than ~200 nm can enter the heart via the circulatory system, and the brain via the olfactory nerve through the blood brain-barrier (BBB) (280, 281). One publication detected presence of MNPs in the brains of AD patients, deducing that the nanoparticles were inhaled air pollutants with distinct spherical morphology and smooth surface texture unlike those of biological origins (from iron metabolisms) with octahedral morphology (178). Excess magnetite in the brain causes toxicity, increasing oxidative stress and ROS, found to be near amyloid-beta (Aβ) fibrils in the AD brain (181, 281-284). The toxicity studies highlighted the extensive use of MNPs in a variety of fields and their impact on human health, which is consistent with the recent evidence that air pollutant MNPs have been implicated in various diseases, including neurodegeneration (AD).

Author Network and Countries with Most Citations For "Magnetite" Research

Over the past 30 years, the direction of research into magnetite has been influenced by the catalytic and kinetic properties of magnetite, which has enabled the extensive application in the environmental, industrial, and biomedical fields, due to the advancements in technologies to direct the research through its manipulation for specific applications across various fields. To evaluate the authors involved in the advancements of magnetite research, an author network was established using VOSviewer software with the dataset obtained from the search "magnetite" in the years 1990 to 2020 from the WoS database (8, 529 publications). A bibliographic analysis for co-authorship (full counting method) refining authors with a minimum of 14 documents and 20 citations per author (used to as inclusion criteria for peer-acknowledged quality, h-index) resulted in 80 authors meeting this threshold (285). Figure S3.1, represents these authors in an overlay visualisation network providing the years in which these authors have published. The author's affiliations and number of citations were recorded and the percentage of citations per country was calculated and ordered by most to least citations (Figure 3.5). The top 13 countries were established, showing the highest number of citations from Japan (22 %), followed closely by China (21 %), suggesting that these countries have led the world in magnetite research over the past 30 years. Other

countries like Germany (13 %), USA (11 %), Iran (6 %), France (5 %), Romania (4 %), Brazil (3 %), Singapore, United Kingdom (2 %), Spain, Hungary, and Republic of Korea (1 %) have also contributed to magnetite research over the past 30 years.

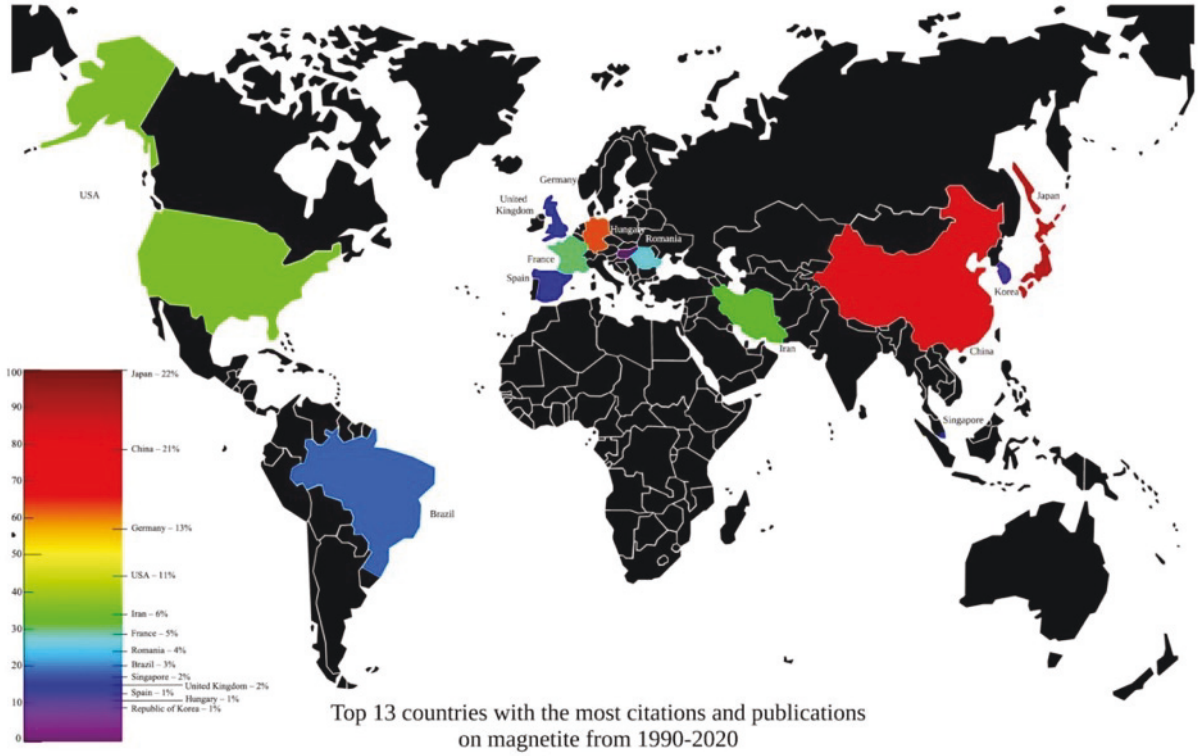

Figure 3.5. Top 13 countries with the highest percentage of citations (minimum 20) and publications (minimum 14) of authors, grouped by country affiliations, in descending order. Extrapolated from the dataset obtained from the Web of Science (WoS) database using the term "magnetite" in the years 1990 to 2020. Accessed on 14th December 2020.

3.3 Discussion

This systematic literature analysis revealed that scholarly studies on "magnetite" have been increasing worldwide with the highest percentage of publications originating from Japan and China. The results show research on "magnetite" have shifted over the last thirty years (Figure 3.6), from initially focusing on the formation of naturally occurring magnetite, into the synthetic development and manipulation of nanoparticles for various environmental, industrial and biomedical applications. Ultimately, to the advancements in biomedical applications which uncover the potential toxicity of MNPs and air pollutant MNPs being

implicated in various diseases including neurodegeneration and AD (181, 282, 286). Progress in MNP engineering has allowed applications in environmental remediation, batteries and solar cell, diagnostic and cancer therapy applications through tuning of the nanoparticles size, shape and surface components, as well as, equally important, the development of MNPs core-shell, nanocomposite and hybrid nanostructures.

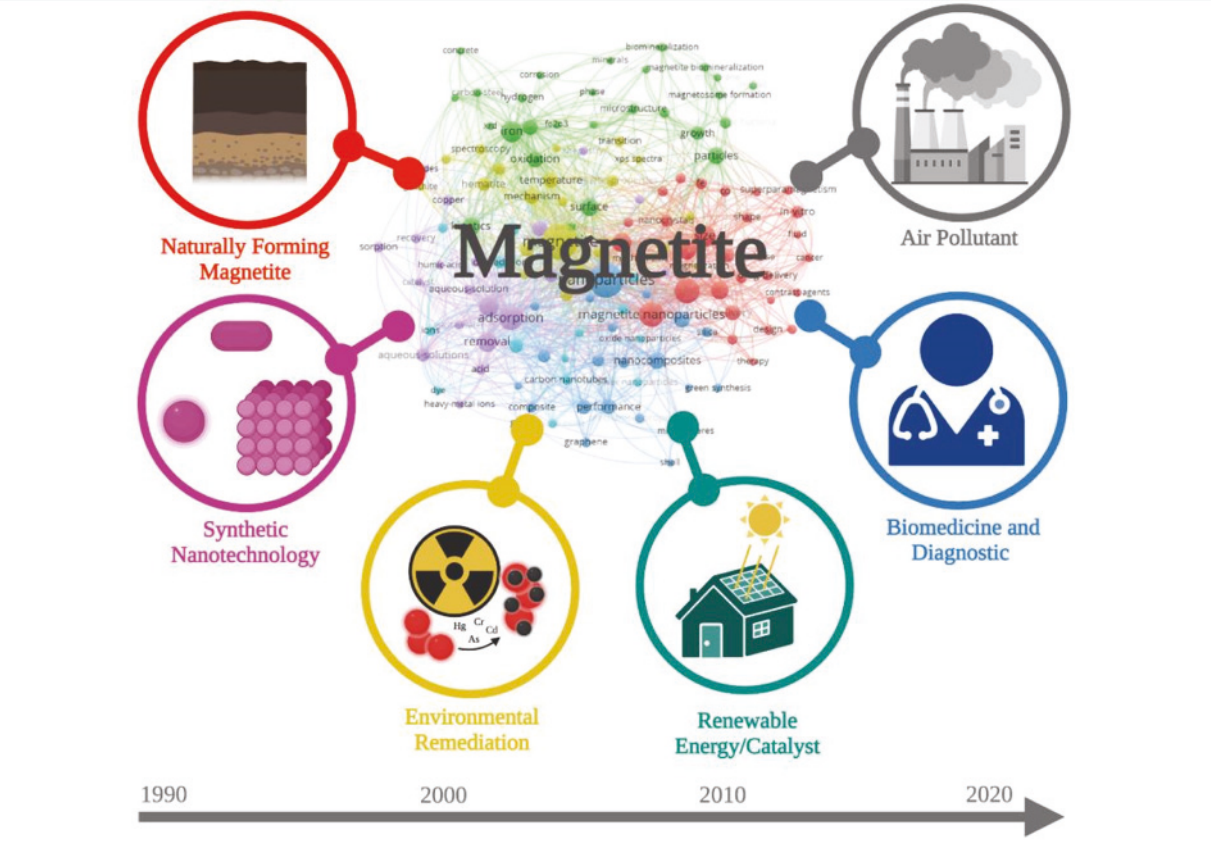

Figure 3.6. Timeline showing research on magnetite nanoparticle shifting from 1990 to 2020.

The VOSviewer software was used to analyse literature and identify clusters, highlighting magnetite research which focused on the kinetic and catalytic properties of MNPs, the adsorptive abilities and remediation targets as an environmental tool and the biomedical applications of MNPs (largely cancer-based therapies highlighting the surface and morphological alterations). The literature analysis using SciMAT software established themes for each time period; the first time period from 1990-1997 identified Magnetite AND oxides, with environmental remediation and biomedical applications of MNPs as the main themes. The environmental studies in this period mainly described magnetite distribution in soil, its crystalline reactivity structure and its ability to adsorb contaminants (e.g., arsenic)

(182-184). The biomedical applications of MNPs in this period are most interesting, with most publications referring to doped/coated MNPs. Doping is a widely used method for modifying the nanoparticles to enhance their electrical, optical and biological activities (287, 288). Doping provides more stability to the nanoparticle structure, as the dopant increases the hydrophilicity of the nanoparticle, therefore increasing dispersibility and in turn reducing cytotoxicity, thus improving biocompatibility (289). There are various synthesis methods, and parameters (e.g., temperature, dipping time and nature of surfactant) that affect the coating thickness, and therefore the overall size of the nanomaterial. For example, increasing concentration of silica (i.e., thicker coating) allows greater dispersion of nanoparticles and enhanced MRI contrasting performance with the use of an external magnetic field (222). Organic compounds, including surfactants and polymers represent a good choice for coating MNPs. In particular coating with dextran, a complex branched polysaccharide polymer chain unit of various lengths (from 1, 000, 000, 000 Da), has surfaced as advantageous with its biodegradable and water-soluble properties further enhancing MNP biocompatibility (290). Coating with dextran (i) prevented nanoparticle agglomeration and toxicity of magnetic particles and (ii) increase dispersibility and rapid clearing by macrophages from the blood, liver, spleen and lymph nodes, compared to bare MNPs (186, 291). Dextran is unique as it allows magnetite's magnetic structure to be extremely strong at the surface where strong magnetic disorder is usually occurs (290). Doping/coating of MNPs is observed to be extremely useful finding that there is reduced cytotoxicity, and consequently improving the potential application for diagnostic and therapeutic purposes, which is further investigated in later time periods (292).

The studies in the second period (1998-2005) focus primarily on the environmental and biomedical applications of MNPs, particularly focusing on the engineered surface chemistry. Both fields further explore the effects of coated MNPs, with adjustments to the surface (surface functionalization/modification) and morphology of the nanostructures. The environmental application of hydroxide coated MNPs indicated that the cubic spinel structure of MNPs (a cubic lattice structure, whereby Fe (III) ions occupy the tetrahedral and octahedral sites) renders the nanoparticles more hydrophilic and therefore, dispersing relatively easily in aqueous biological systems, enhancing the adsorptive properties. This is consistent with a hydrophilic polymer (polyethylene oxide) coated MNP study, in which the adsorption of heavy metals was improved due to the increased dispersion rate in solution (293). The

biomedical applications exploring surface modification/functionalization in this period is extensive, specifically referring to the surface chemistry (i.e., increasing, decreasing or neutralizing the surface charge) which strongly influences the properties of the system (e.g., polymers, small molecules, surfactants, dendrimers and biomolecules) (294-296). This occurs through the treatment of nanoparticles with specific agents, and is extremely valuable in enhancing cellular utilisation, cellular uptake, decreased toxicity, improved binding capacity, enabling selectivity and specificity, with longer retention time, or non-interactions (for evading the immune response) depending on its specific function (294, 295). Polymer surface functionalized NPs are extremely versatile, with the hydrophilic coating allowing increased circulation time. One study used dextran coated crosslinked (altering the charge to be more positive) surface modified MNPs, which reduced drug concentrations at non-target sites, due to increased dispersibility, overall resulting in fewer drug side effects (296). Another study used surface modification of MNPs with antibiotics, revealing that they could bind to bacterial cell walls, altering the cell wall integrity, due to its positive charge, demonstrating effective antimicrobial abilities. This was found to improve the antimicrobial inhibition against the pathogenic bacteria *Escherichia coli, Staphylococcus aureus* and *Pseudomonas aeruginosa* (295, 297). Like doping or coated additives, surface modification/functionalized, also increases biocompatibility by altering the surface charge, the nanoparticles can disperse more easily, and evade the immune response, due to the biocompatible additives on the surface, increasing reactive sites and for biomolecule attachments. This is further examined in later time periods, targeting the immune system, transportation of modulating agents and as potential vaccines (298).

In the 2006-2013 period, studies on MNPs focused on various morphological additives, particularly the use of nanocomposites due to the small size, increased dispersibility, enhanced adsorption and solar energy function for environmental and industrial applications (211). Nanocomposites are nanoparticles incorporated into a matrix, displaying improvements in thermal stability, increased surface defects, chemical resistance, and improved electrical conductivity (204). For example, graphene oxide/MNP and polymers/MNP nanocomposites were found to have increased adsorptive capabilities of heavy metals and aromatic compounds, due to the increased surface area (increased surface defects) of this matrix structure (236, 238, 299). The biomedical applications of MNPs, was the major research theme in this period, with MNP nanocomposites also being considerably

investigated. The use of nanocomposites has been found to be superior to doped/coated nanoparticles, as they behave more similarly to superparamagnetic nanomaterials, with a study displaying that polymer-like (PLGA)/MNP nanocomposites are more effective tumour targeting MRI contrasting agents compared to dextran coated MNPs of similar size (300). Another study using mesoporous dye doped silica MNP nanocomposites, loaded with doxorubicin (potent anti-cancer drug), found an improvement in MRI contrasting and tumour targeting abilities, whilst also being able to induce targeted cancer cell death (220). The combination of adding various nanoparticles into a nanocomposite structure, offers unique properties that are suggested to arise from the interactions of these materials in the matrix. This further proves the advancements in nanotechnology engineering with the improved thermal stability, dispersibility, increased surface exposure, thereby improved compatibility as a biomedicine, which is further explored in the successive time-period, targeting the immune system, transportation of modulating agents, but also as potential vaccines (298).

The most recent 2014-2020 period showed a shift in MNPs research with less proportion of publications dedicated on environmental remediation, and a clear surge in industrial and biomedical applications. MNP nanocomposite structures are again explored in this period, however there is a trend in studies focusing on the advancement in combining two or more additives (e.g., coating/doping, core-shell, surface modification/functionalized) into nanocomposite matrix, termed ‘hybrid’. The nanocomposite hybrid was investigated for industrial applications with one study, using lithium-sulphur coated MNP nanocomposites, surface functionalized with carbon, finding that the catalytic activity excelled due to the increased surface defects, enhancing recovery rate, thereby increasing battery life (301). In addition to focusing on the nanocomposite structure, the biomedical applications of MNPs in this time period, also focus on the MNP hybrid nanocomposites as more efficient contrasting agents for MRI and drug delivery agents for cancer therapies (e.g., hyaluronic acid-modified gold/MNPs nanocomposites) but extending further into the biomedical field by advancing the engineering of nano systems to overcome immunological barriers (255). The immune system responds to nanoparticles triggered through mechanisms that recognize surface molecules, peptides or foreign materials, modulating an immune response based on the size, morphology, surface characteristics and charge of the nanostructure. Therefore, evading the immune response relies on several properties of nanotechnological engineering, e.g., reducing nanostructure size, adjusting morphology to a more biocompatible shape (i.e., nanosphere

compared to nanocubes), and adding surface additives that increase the circulation time and overall biocompatibility (302). The manufacturing additives that can be applied to MNPs nanocomposites amplify the "stealth" ability, increasing circulation time, by which point they can provide active and specific targeting in the body (303). One study found that poly (caprolactone) coated MNPs loaded with doxorubicin hydrochloride, further surface functionalised with Arg-Gly-Asp enzymes, behaved like SPION nanocomposite microspheres, enhancing circulation time, whilst also exhibiting a quick magnetic response, advantageous for controlled drug release at tumour target site (304). This further confirms MNP nanocomposite hybrids as promising cancer and immune-modulatory therapies. The development of nanotechnology in the past three decades, has discovered the study of nanoparticle additives and most recently nanocomposite hybrids appear to fulfil the growing needs of multifunctional materials, being extremely versatile, with the most increased dispersion and retention rate, as well as the binding force and wear of the nanostructure (305).

Towards the final years of the 2014-2020 period, several research inquiries reported potential toxic effects of MNPs, being implicated with the environmental and biomedical applications. For example, the use of MNPs for environmental remediation used in wastewater and sediment treatment has led to extensive run off leading to an accumulation in aquatic environments. This accumulation leads to ROS/RNS production, causing damage to exposed organisms, stimulating delays of hatching, damage in cell wall and outer membranes, and depletion of oxygen exchange and hypoxia to an in vitro model (rainbow trout spermatozoon) (306). For biomedical applications, the cytotoxic effect of MNPs were tested using *in vivo* and *in vitro* models showing activation of activator protein 1 (AP-1) and nuclear factor kappa B (NFκB) pathways that subsequently results in increased oxidative stress and induced apoptosis regardless of dosage or composition (227, 307). MNPs coated with oleic acid and silica, were found to exhibit cytotoxicity in *in vitro* models (human neuroblastoma SH-SY5Y and glioblastoma A172 cells) through a decrease in cell viability (308). Similarly, MNPs coated with silica and polymer like materials for the purpose of cell labelling and hyperthermia treatments were also found to permeate cells, accumulating and causing cellular dysfunction (309). While these studies show the disadvantages of MNPs, the cytotoxic effects were shown to be dose dependent, with one study finding that MNPs cause toxicity to an *in vitro* model A549 cell line only at concentrations of greater than 50 µg/mL and that silica coated MNPs caused cellular dysfunction by impairing cellular adhesion properties at 0.1

μg/μL (307, 309). Therefore, establishing a safe and effective dose of MNPs as a biomedicine should be more closely investigated to prevent adverse side effects.

Toxicity studies also focused on the biological effects of air pollutant MNPs, more specifically on their potential links with the progression of neurodegenerative diseases like Parkinson's disease (PD) and AD (160, 310). Biogenic magnetite can be found in a wide range of organisms from bacteria to animals, including humans (311). Physiologically biogenic magnetite has been found to aid in the biological metabolism of iron (177, 312). Interestingly, Maher and colleagues showed that anthropogenic (synthetic) MNPs can be found in abundance in the brains of people suffering from AD, distinguished by differences in their morphology to biogenic MNPs (178). MNPs, like other air pollutant particulate matter (PM), is formed through frictional pressure at high temperatures. It is therefore no surprise that MNPs can be found in abundance in automotive diesel exhaust, grinding of trains on railway lines, welding factories, petroleum exhaust, and coal emission (313). Due to the formation process of these air pollutant MNP (< 200 nm), they can migrate into the central nervous system via the nasal canal and olfactory bulb (310). Inhaled air pollutant nanoparticles in the brain tissues are thought to trigger ROS/RNS production, leading to oxidative stress (314-316). This increase in oxidative stress, is believed to further contribute to chronic inflammation, and consequently increase Aβ fibril formation found near Aβ plaques in AD, however this is not confirmed. Therefore, consequent future studies should focus on understanding the effects of air pollutant MNPs in neurodegenerative diseases including AD.

3.4 Conclusion

In summary, the scholarly research on magnetite over the last three decades has generated knowledge of how the characteristics of MNPs affect the nanoparticle physical, catalytic and biological activities, and in turn, how the knowledge is being used to guide the engineering of the nanoparticles for specific environmental, industrial and biological applications (262). For the latter, being the most explored applications of MNPs, the tuning of the nanoparticle characteristics is also aimed to optimise biocompatibility, more specifically, for less aggregation, lower toxicity as well as enhancing cellular targeting and uptake, for use in disease diagnostic and therapy (317). Optimising the engineering of NPs for biomedical

applications has proven difficult, with the ability of the NPs to remain in circulation to achieve a desired goal, and on the other hand remaining too long in circulation causing toxicity, is a balance that has yet to be perfected. Future applications of MNPs in the biomedical field should focus on adjusting the size and morphology of the nanostructure, the "stealth" mechanism to evade the immune response which makes them an effective therapy or detection of human diseases. Considering the increasing evidence on the roles of air-pollutant MNPs and the onset and progression of neurodegenerative diseases, the next phase of research should also focus on elucidating the exact mechanisms of the nanoparticle-induced stress, including activation of inflammatory markers, while also focusing on epidemiology studies to determine any correlation between highly polluted sites and disease prevalence.

3.5. Methods

3.5.1 Topic Modelling

The database, Pubmed (https://pubmed.ncbi.nlm.nih.gov/), was used to search the term "Magnetite" (938 publications). The publications that were within the years, 1990-2020 and either a research or review articles were exported (PMID list file). They were then imported into the Sciome Workbench for Interactive Computer-Facilitated Text-mining (SWIFT) Review software (https://www.sciome.com/swift-review/) where the articles were segregated based on keywords, then organized into topic models of magnetite research and ranked in order from most to least prevalent topics. To enlarge the search range, other databases were used as a source of bibliographic data.

3.5.2 Bibliometric Analysis

The bibliographic data collected from a "Magnetite" search including, title, abstract, all citations, (accessed on 14 December 2020) for the period 1990-2020, was exported from the WoS database (txt. file). Duplicates identified were removed before all data were imported into the VOSviewer software (www.vosviewer.com). A bibliographic analysis was performed based on co-occurrence of authors keywords in the paper title (11, 949 keywords), using full counting, with a minimum of 20 occurrences in the dataset was specified (134 keywords).

3.5.3 Longitudinal Study

To undertake a review of the literature for the research on "Magnetite" over the past three decades, the bibliometric data present in Scopus (which included authors key words) for the topic "Magnetite" (Accessed on 14th December 2020) was obtained. This data (31, 567 publications) was imported into Science Mapping Analysis Software Tool (SciMAT) (https://sci2s.ugr.es/scimat/) for analyses; singular and plural version of the same words were grouped. The publications were arbitrarily assigned to four time periods (1990-1997, 1998-2005, 2006-2013, 2014-2021) so that changes over this chronological period could be analysed, using the workflow described (Figure 3.7). Normalisation was performed using the analysis function focusing on words and specifically authors keywords, with a frequency reduction minimum of 10, a co-occurrence matrix, the edge value reduction of 8, normalization of association strength, simple algorithm centres and core mapper, with quality measuring h-index and the longitudinal analysis with an evolution map (using Jaccard's Index) and an overlapping map (using Inclusion Index). Important motor-themes were identified by their location in the upper-right hand quadrant of the strategic diagram generated by SciMAT software.

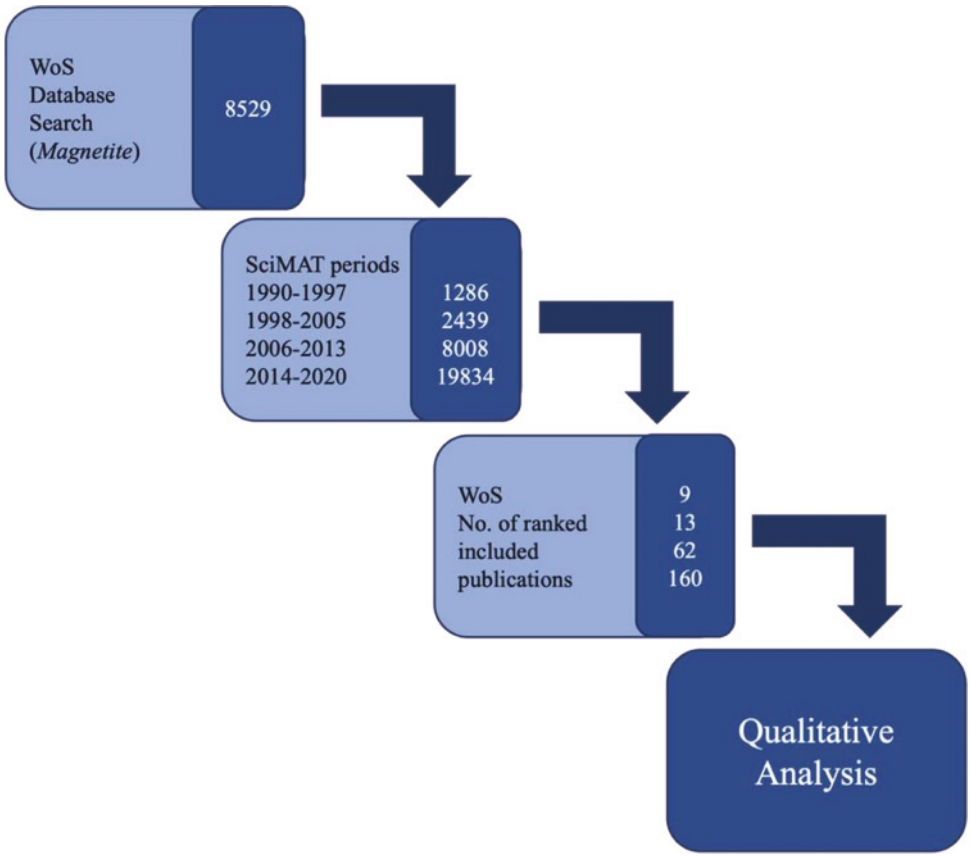

Figure 3.7. Graphical depiction of the systematic and bibliometric literature review process of the Web of Science (WoS) database (numbers represent the number of papers analysed at that step).

3.5.4 Systematic Review of Literature

A systematic review of the total available English language peer-reviewed literature on Magnetite in a Scopus database (date accessed 14 December 2020) was carried out on the four main themes (e.g., Magnetite AND oxides, 1990-1997) identified in SciMAT. Publications were restricted to the relevant time period related to the motor theme. The publications found were assessed according to the Field Citation Ratio (FCR) for all time periods. A total of 244 publications were included in this analysis. A value for the FCR of greater than 6 (as a proxy indicating peer-acknowledged quality) was used to justify inclusion of a publication in this study. Reviews, editorials and short communication were excluded from further analysis.

3.5.5 Author Network and Citation bursts

Co-authorship networks were constructed in VOSviewer software using the same dataset from the WoS database (new format, RIS file), from the search on "Magnetite" (accessed on 14th December 2020). The data was imported into the VOSviewer software, where a bibliographic database search was completed, for co-authorship using full counting method, finding a total of 46, 800 authors. The authors were further refined by a minimum of 14 documents and 20 citations per authors (used to as inclusion criteria for peer-acknowledged quality, h-index) resulting in 80 authors meeting this threshold. The authors affiliations, number of citations, along with the affiliated countries were recorded and the percentage of citations per country were calculated to determine the frequency of "magnetite' research around the world. The percentage of citations per country was calculated and ordered by most to least.

3.6 Supporting Information

Systematic and Bibliometric Analysis of Magnetite Nanoparticles and their Application in (Biomedical) Research

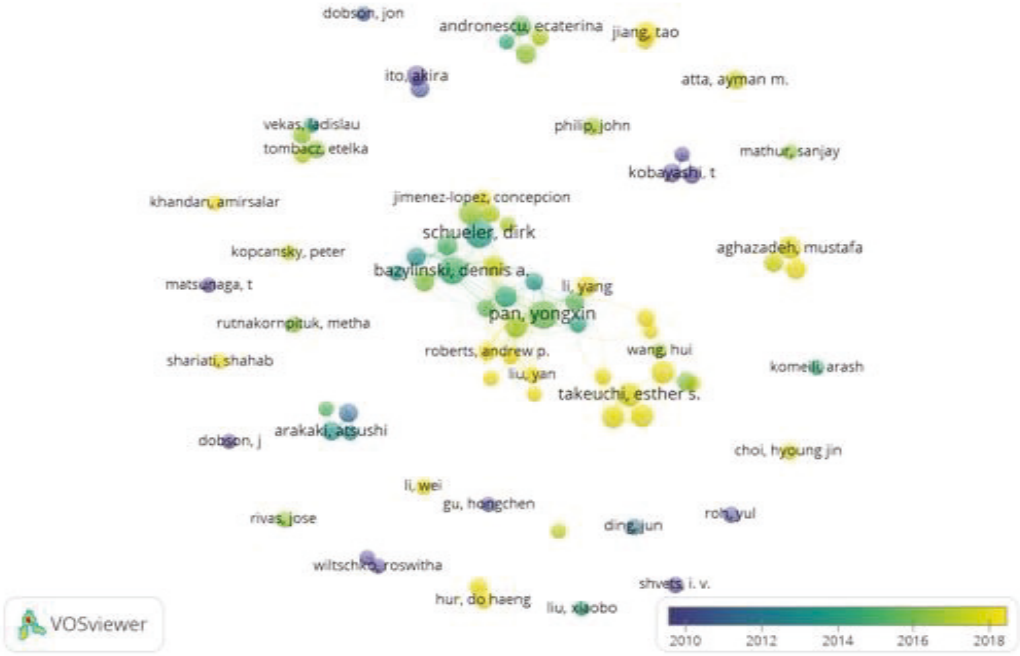

Figure S3.1. Overlay visualisation map of the author network obtained from the Web of Science (WoS) dataset using the VOSviewer software, with the search term “magnetite”. The network map shows the top 80 authors meeting the publication minimum of 14 and citation minimum of 20 from 1990-2020. The colours scale represents the year which these authors published (e.g., purple indicates 2010). Accessed on 14th December 2020.

Chapter 4: The Biological Roles of Air Pollutant Particulate Matters in the Early Onset Pathologies of Alzheimer's Disease

Intend to submit as:

Fleming, C., Golzan, M., Amal, R., Wong, R., Torpy, F., Irga, P., Gunawan, C., McGrath, K., 2022. The Biological Roles of Air Pollutant Particles in the Early Onset Pathologies of Alzheimer's Disease. *ACS Nano.*

Chapter Summary

The systematic and bibliometric review presented in Chapter 3 established that magnetite is a versatile particle that can be used for various applications; however, magnetite can exacerbate the pathologies associated with AD. For this reason and recent reports demonstrating the presence of magnetite particles in the brains of people with AD, has prompted the aim of this chapter. This chapter explores whether air pollutant particulate matter, iron, diesel and magnetite particles exacerbates the pathologies associated with AD, using a double transgenic APP/PS1 murine *in vivo* model and a human neuroblastoma SH-SY5Y *in vitro* model. This chapter has been written according to the guidelines of ACS nano of which the manuscript will be submitted to.

The Biological Roles of Air Pollutant Particulate Matters in the Early Onset Pathologies of Alzheimer's Disease

Charlotte Fleming[1], Mojtaba Golzan[2], Rose Amal[3], Roong Jien Wong[3], Fraser Torpy[4], Peter Irga[4], Cindy Gunawan[5#], Kristine McGrath[1#]**

1. School of Life Sciences, University of Technology Sydney, Sydney, Australia
2. Vision Science Group, Graduate School of Health, University of Technology Sydney, Sydney, Australia
3. School of Chemical Engineering, UNSW Sydney, Sydney, Australia
4. Centre for Green Technology, School of Civil and Environmental Engineering, University of Technology Sydney, NSW, Australia
5. ithree Institute, University of Technology Sydney, Sydney, Australia

Email:
Kristine.McGrath@uts.edu.au, Cindy.Gunawan@uts.edu.au
#These authors share senior authorship

Authors' contributions:

CF conducted the experiments, collected the data, analysed the data, produced the results and drafted the manuscript. KM contributed to the *in vivo* work. KM, CG and RA conceptualized the study. KM, CG and MJ contributed to result analysis and interpretation and supervised CF. CG revised and edited the manuscript. FT and PI provided the air pollutant iron and diesel particles for this study. RW conducted the particles characterization for this study. All authors contributed to the execution and approved the final version of the manuscript.

Charlotte Fleming	Production Note: Signature removed prior to publication.
Mojtaba Golzan	Production Note: Signature removed prior to publication.
Rose Amal	Production Note: Signature removed prior to publication.

Roong Jien Wong	Production Note: Signature removed prior to publication.
Fraser Torpy	Production Note: Signature removed prior to publication.
Peter Irga	Production Note: Signature removed prior to publication.
Cindy Gunawan	Production Note: Signature removed prior to publication.
Kristine McGrath	Production Note: Signature removed prior to publication.

The Biological Roles of Air Pollutant Particulate Matters in the Early Onset Pathologies of Alzheimer's Disease

Charlotte Fleming[1], Mojtaba Golzan[2], Rose Amal[3], Fraser Torpy[4], Peter Irga[4], Roong Jien Wong[5], Cindy Gunawan[6], Kristine McGrath[1]**

[1] School of Life Sciences, University of Technology Sydney, Sydney, Australia

[2] Vision Science Group, Graduate School of Health, University of Technology Sydney, Sydney, Australia

[3] iThree Institute, University of Technology Sydney, Sydney, Australia

*These authors contributed as senior authors

KEYWORDS magnetite, nanoparticles, oxidative stress, inflammation, neurodegeneration, Alzheimer's disease

Corresponding Author: Cindy.Gunawan@uts.edu.au, Kristine.McGrath@uts.edu.au

4.1 Abstract

The study describes the biological roles of air pollutant particles on the early onset of Alzheimer's disease (AD) pathologies. Different air particulate models – an iron (Fe^0) – iron oxide (Fe_3O_4) particles (d_{TEM} = 500–700 nm, referred to as 'iron'), particles generated from diesel combustion (d_{TEM} = 20 – 60 nm of hydrocarbon-based particles, 'diesel') and magnetite (Fe_3O_4, d_{TEM} = 100 - 400 nm, 'magnetite'), were studied on wild-type and AD-predisposed mice models. An increased anxiety and stress levels were seen in wild-type mice, while short-term memory impairment was observed in AD-predisposed mice. A detailed analysis revealed neuronal cell loss was present in both wild-type and AD-predisposed mice in the hippocampal and somatosensory cortex regions of the brain. Characteristically, there were no amyloid-beta plaque formations in the wild-type mice, however a significant increase was seen in the brains of the AD-predisposed mice. The air pollutant particles did however induce an increase in AD-

relevant inflammatory and oxidative stress responses in both wild-type and AD-predisposed mice, regardless of the presence of amyloid plaques in the AD-predisposed mice. The findings provide insight into how exposure to iron-based and carbon-based air pollutant particulate matter of various sizes can lead to AD-relevant pathological changes. The present work also highlights the need to study the pathological features in predisposed disease models.

4.2 Introduction

Alzheimer's disease (AD) is one of the most common forms of dementia affecting approximately 90 % of all dementia cases (318). The two characteristic pathologies of the disease are the formations of amyloid-beta (Aβ) plaques and neurofibrillary tangles (NFTs) (319, 320). Aβ plaques are aggregates of Aβ40 and Aβ42 peptide, derived from the large amyloid precursor protein (APP) *via* proteolytic cleavage (137, 138). NFTs are aggregates of hyper-phosphorylated tau protein, a microtubule binding protein (138). The plaque formation accumulates around neuron cells, while NFTs form intracellularly, with both pathologies known to cause neuronal cell death, leading to brain shrinkage, which is associated with AD-related behavioural changes, including increased anxiety and stress, memory impairment as well as mood changes (137).

In the present study, we investigated the biological effects of air pollutant particulate matter in early onset of AD pathologies. Unlike genetically linked familial AD, sporadic AD accounts for over 99 % of AD cases (138) and is thought to be associated with lifestyle and environmental factors (135). Among other anthropogenic factors, air pollutant particulate matter (PM) has been increasingly implicated in adverse biological activity, including DNA damage, neuronal cell death, and has been associated with neurodegenerative diseases (31, 136, 144, 321-323). Anthropogenic PM varies in composition and size, being primarily emitted into the atmosphere through combustion of fossil fuels, including coal, petroleum as well as natural gas (324). Pyrolisation (decomposition of materials at elevated temperatures) of unburnt fuel and engine wear can produce iron and iron oxide (magnetite; Fe_3O_4) pollutant particles, as well as the hydrocarbon-based diesel particulates (323). PM can range from less than 1 μm to 10 μm. Studies have shown that inhaled PM, in particular the sub-micron sized, can accumulate in the lower respiratory system, then further translocated across the alveolar-capillary barrier into the systemic circulation. Inhaled particles can also enter the brain via the

olfactory bulb, then travel across the blood brain barrier (BBB) and accumulate in the brain (325).

While studies have connected the presence of air pollutant PM to neurodegeneration, the exact pathological trigger and manifestation remains unclear (326). In 2016, Maher et al. found the presence of anthropogenically formed magnetite particles in the brain samples of AD patients (327). The spherical morphology of the submicron-sized particles (100 - 200 nm) are consistent with those formed at high temperature combustion reactions (327). Iron and iron oxides are naturally present in the brain and are essential for many metabolic processes, however excess iron can be toxic (319). Iron (II) (as Fe^{2+} ions) can react with hydrogen peroxide (H_2O_2) in biological environments to generate the highly reactive hydroxyl ($OH^{\bullet}$) radical via the Fenton reaction (319). Oxidative stress is a state of redox imbalance resulting from excess presence of reactive oxygen species (ROS) and reactive nitrogen species (RNS) that overwhelms the natural capacity of antioxidant defence mechanisms (328). Iron can mediate overproduction of ROS, leading to oxidative damage on proteins, lipids and nucleic acids (123, 329-331). Magnetite, is a ferrimagnetic iron oxide with alternating lattices of Fe^{2+} and Fe^{3+}, rendering the particles highly reactive with oxygen species, therefore readily able to generate reactive oxygen radicals (331). Increasing number of studies have indicated that the hallmark pathologies of AD, Aβ plaques and NFTs are driven by oxidative stress and neuroinflammation (332-334). The brain is a highly oxidative organ, extremely sensitive to foreign invasion, with macrophagic brain cells (e.g., microglial and astrocytes) becoming activated in response to foreign invasion, infection or an imbalance in homeostasis. These stimuli can activate immune responses, triggering various inflammatory and oxidative stress pathways (328, 334). This mechanism suggests that exposure to air pollutant particles induce that activation of microglia and astrocytic cells. These cells have been found in the vicinity of Aβ plaque deposits, suggesting that the plaque formation could also serve as a major stimulus for oxidative stress and inflammation in the AD brain (333). Understanding the biological processes that drive the pathologies associated with AD is extremely relevant to our study, as determining the role of air-pollutants in AD pathologies, will provide insight into the role of air pollutants in early onset of the disease. The present work carried out *in vivo* and *in vitro* investigations to study the AD-relevant biological activity of sub-micron sized air pollutant particulate models: (a) an iron (Fe^0) – iron oxide (Fe_3O_4) particles (referred herein to as 'IRON'), (b) a hydrocarbon-based diesel particulate emission ('DE') and (c) magnetite (Fe_3O_4; 'MAG'). *In vitro* studies

were performed using the human neuroblastoma SH-SY5Y cell line, an established neuronal cell model in neurodegenerative studies (335, 336). The results showed that the air pollutant particles could not only induce behavioural changes, but also induce an increase in oxidative stress and inflammation, whilst increasing the formation of Aβ plaques. These AD-relevant features interestingly manifest at different extents in the WT when compared to the AD-predisposed mice models.

4.3 Methods

Synthesis of model air pollutant particulate matters. The iron and iron oxide ('IRON') sample was produced by grinding hardened cast iron (rail track) with a fibreglass-reinforced grinding wheel (25 mm in diameter) at 37, 000 rpm. The particle samples (500 – 700 nm crystal size, irregular shape, Figure 4.1A) contained zero valent iron Fe^0 and iron oxide Fe_3O_4. The diesel emission particles ('DIESEL' or 'DE') were synthesized by burning retail grade diesel fuel in a spirit burner, with all effluent collected in an inverted conical flask, then washed with hexane and left to dry overnight, the particles were collected the next day. The samples (20 – 60 nm crystal size, Figure 4.1B) contained high boiling hydrocarbon-based particles, along with a range of sulphur and nitrogen compounds. The magnetite particles (Fe_3O_4, 'MAGNETITE' or 'MAG'; 100 – 400 nm crystal size, Figure 4.1C) were purchased from Sigma Aldrich (MO, USA, 97% purity, molecular weight 231.53).

Transmission Electron Microscopy (TEM). High resolution (HR)-TEM analysis was carried out for the assessment of primary particle size and morphology of iron and diesel and magnetite particles. Samples were dispersed in 95 % (w/v) ethanol and sonicated for 30 mins at room temperature. A drop of suspension was added to the copper grid and air dried before each measurement took place. TEM measurements were performed using a Phillips CM200 operating at 200kV with an SIS CCD camera.

Double Transgenic APP/PS1 *in vivo* model. The effects of the air pollutant particles were assessed in APP/PS1 double transgenic mice and C57BL/6 wild-type (WT) littermates for comparison (purchased from Professor Anna King, University of Tasmania, Tasmania Australia). The APP/PS1 model is a double transgenic mouse that expresses a chimeric mouse/human amyloid precursor protein (Mo/HuAPP695swe) and a mutant human presenilin 1 (PS1) on C57BL/6 (B6. Cg-Tg (APP6953DboTg (PSEN1dE9) S9Dbo) background (APP/PS1) (122). This model exhibits amyloid pathology that closely resembles the Aβ

deposits in the initial stages of AD and has been extensively used to study mechanisms of AD neuropathology (123). This model exhibits Aβ deposition as young as 6 weeks of age in the cortex and 3 - 4 months in the hippocampus (124, 125). Reactive glial cells appear around Aβ deposits at about 6 weeks of age, coinciding with a pro-inflammatory response (126). While global neuronal loss is not observed in the APP/PS1 model, modest neuronal loss in the dendate gyrus granule cells (127). Synaptic loss and cognitive impairment are also observed in this animal model at approximately 3 and 7 months of age (128). This animal model was chosen as the relevant AD pathological biomarkers are expressed at 5 - 7 months of age which coincided with the length of the animal study. The mice were house according to sex, with 2 - 5 mice per cage, and kept on a 12-hour light/dark cycle at room temperature 22/5 ± 2°C. Before commencing the *in vivo* experiments, the mice were allowed to acclimatize for 1 week. In week 1 of the animal experiment (13 weeks of age; W/T; n = 37, APP/PS1; n = 28), the mice were grouped to receive intranasal administration, every third day of (i) saline (ii) IRON (47) DE or (iv) MAG (66 μg/20 μL) for 4 months. The mice were monitored daily, and their weight was recorded weekly as seen in Figure S4.1. All animal experiments were conducted with the approval from the University of Technology Sydney Animal Care and Ethics Committee (ACEC ETH17-1418) and in accordance with the guidelines described by the Australian National Health and Medical Research council code of conduct for animals.

Preparation of particle suspension for *in vivo* model. The iron, diesel and magnetite particles used for this study were prepared at a concentration of 3.3 mg/mL, in sterile saline solution. Before administration particle solutions were sonicated, using the Q500 Sonicator (Q500 Sonica Sonicators, CT, USA) for 5 mins at 50 % amplitude to disperse particles. Once sonicated, all particles were ready for intranasal administration to the mice in their designated treatment groups.

Intranasal administration of particle suspension. Delivery of air pollutant particles was administered intranasally. To administer the particles, the mice were inducted in a chamber with 4 % isofluorane and 2 L/min oxygen until no movement was observed then 20 μl of air pollutant solution (3.3 mg/mL) was administered intranasally, and the mice were monitored for recovery. The air pollutant particle concentration was established based on the average ambient $PM_{2.5}$ intake of approximately 6-17.5 μg/day/person, based on urban environments in India, Portugal, Italy, Spain, Belgium, England and Poland etc. (129, 130).

Behavioural Assessments. At week 15 of the animal experiment (mice 28 weeks of age) the mice were subjected to behavioural tasks. All testing sessions were conducted between 10:00

- 16:00 hours and were video recorded. The assessment of short-term memory and anxiety and stress were assessed using the novel object recognition (NOR) test and the elevated plus maze (EPM) as previously described (337). Prior to the NOR the mice were acclimatized to the testing room for 1 hour prior to the assessment. There was no acclimatization for the EPM. Schematic representations of the NOR and EPM apparatus is seen in Figure 4.1. The APP/PS1 animal model is known to exhibit cognitive deficits and spatial learning and memory defects as young as 6 - 7 months of age (128) which is relevant to the behavioural testing time point in this study. Between each test the apparatus and object were cleaned with 80 % ethanol.

In vivo Quantification of Aβ Plaques. Following behavioural testing at week 15 (28 weeks of age) the development of Aβ species formation, detecting both the soluble (Aβ40) and insoluble (Aβ42) peptide aggregates, was assessed in the mice using a near-infrared fluorescence (NIRF) molecular imaging probe, CRANAD-2 (Abcam, Cambridge, UK) (141). The *in vivo* CRANAD probe detects for presence of the insoluble Aβ42 peptide aggregates. The CRANAD-2 probe was prepared in a mixture of 15 % DMSO, 15 % cremaphor and 70 % PBS at a concentration of 5 x 10^3 mg/mL. The mice heads were shaved and inducted in a chamber using 4 % isofluorane and 2 L/min oxygen. Baseline fluorescence of the brain was obtained using the IVIS fluorescent scanning machine (IVIS Lumina II; Caliper Life Sciences, MA, USA). The mice were then intravenously injected with the CRANAD-2 (5 mg/kg) before they were inducted again and fluorescence signals from the brain was recorded 5 mins after injection. A small circular region of interest (ROI), in the centre of the fluorescence region was established to be consistent, between mice measurements. The average radiance (p/s/cm^2/sr) in the region of interest was recorded.

Tissue harvest and blood collection. At experimental endpoint the mice were euthanized with isofluorane then placed on a nose cone until no reflex to pedal or ocular stimulation was observed. Cardiac puncture was performed via the left ventricle to collect approximately 1mL of blood using an 18-gauge syringe pre-coated with heparin (100 I.U/mL DBL Heparin Sodium Injection, Hospira, Vic, Australia). Following collection, the whole blood sample was immediately centrifuged (13, 500 RCF, 5 mins). The plasma layer was removed and stored at -80°C. To ensure the mouse was deceased before any further procedures, cervical dislocation was performed. For this study many different techniques were of interest, therefore the brains were halved; the right hemisphere was fixed in 4 % paraformaldehyde (PFA), while the left was dissected and the hippocampus and cerebral cortex were snap frozen in liquid nitrogen, then stored at -80°C until required.

Beta-secretase assay. β-secretase plasma levels have been found increase as AD patients both the peripheral blood and cerebrospinal fluid and therefore has been identified as a suitable early diagnostic biomarker (142, 143). To assess β-secretase levels in the plasma, the β-secretase fluorometric assay activity kit (BioVision, CA, USA, cat. K360) was completed following the manufacturer's protocol. Plasma samples were prepared in duplicate in a 96-well plate (50 µL per well) per well, along with appropriate controls. Reaction buffer (50 µL per well) was added to all wells and incubated at 37°C for 20 mins. β-Secretase substrate (2 µL per well) was added to all wells, then covered and incubated at 37°C for 20 mins. The plate was read on the infinite M1000 PRO microplate reader (Tecan Sunrise, Grödig, Austria) reader at 335 Ex/495 Em (excitation/emission). The results are expressed as percentage increase from control.

Tissue Fixation, Processing, Embedding and Cutting. The right hemisphere was fixed in 4 % PFA (Sigma-Aldrich, MO, USA) overnight, then rinsed with phosphate buffered saline (PBS) before being stored in 70 % ethanol for one week. Brain tissues were then placed in cassettes and processed using the ExcelsiorTM AS Tissue Processor (Thermo Fisher Scientific, MA, USA) for an overnight process involving two changes of formalin, increasing grades of ethanol and two changes of paraffin wax. After processing, brain tissues were embedded in paraffin wax and cut in sagittal sections using microtome (Epredia, MICH, USA). Brain sections were cut at a thickness of 10 µm, through the entire right hemisphere, resulting in approximately 25-30 slides (e.g., slide labelled #1 is closest to the midline) per tissue. Three brain tissue sections were mounted on every Platinum PRO adhesive glass slides (Trajan, VIC, AU), left to dry at 37°C overnight and stored at room temperature until required.

***Ex vivo* quantification of Aβ Plaques and neuronal cells.** For quantification of Aβ plaque formation and neuronal cell counting, sagittal brain tissue sections prepared on adhesive slides were stained with thioflavin S stain (1 % filtered aqueous solution), which detects the characteristic β-pleated sheets of Aβ plaque and cresyl violet (0.1 %) for differential neuronal cell staining respectively (338). Slides were placed in two changes of xylene followed by decreasing grades of ethanol (100 %, 95 %, 70 %) for 3 mins each. They were then hydrated in water for 6 mins. Slides were then immersed in thioflavin S stain (1% thioflavin S stain; Sigma-Aldrich, MO, USA) for 10 mins or cresyl violet (0.1% cresyl violet powder (wt/acetic acid); Sigma-Aldrich, MO, USA) for 3.5 mins. Slides were then rinsed with water for 5 mins, followed by dehydration in two changes of 100 % ethanol and two changes of xylene. Slides were cover-slipped using Dibutylphthalate polystyrene xylene (DPX) and left to dry overnight. All slides were imaged using the ZEISS AxioScan Digital Slide Scanner (Carl Zeiss

Microscopy, Germany) on the entire sagittal section at 20 x magnification, using fluorescence (thioflavin S stained tissue) or brightfield (cresyl violet stained tissue) imaging settings. W/T (C57BL/6) mice do not develop Aβ plaques, however APP/PS1 mice that are 6 - 12 months of age develop round dense Aβ plaque formations that are approximately 50 - 150 μm in diameter. The number of fluorescent Aβ plaque formations were automatically counted in a region of interest (ROI) in the neocortex above the hippocampus using Image J (IJ1.46r Revised Edition), by implementing a fluorescent and size (50-150 μm^2) threshold, highlighting the Aβ plaque formations in the brain tissue (147, 148). The hippocampus and somatosensory regions are responsible for memory and spatial recognition, and receiving and processing sensory information respectively (144, 145). The number of neuronal cell bodies were counted (with a range of 10-400 μm^2) using the QuPath Software Quantitative Pathology & Bioimage Analysis (QuPath) Software 0.2.3 (Edinburgh, UK) in regions of interest (ROI) in the hippocampus: cornu ammonis (Ca) 1, Ca3 and dentate gyrus (DG), and the somatosensory cortex (SS 2, 3, 4, 5, 6a) (146). Every brain tissue sample (n = 5-11 biological replicates) that was analysed had 9 technical replicates accounting for staining, imaging, and analysis bias.

Preparation of particle suspension for *in vitro* model. The iron, diesel and magnetite particles were prepared in filtered DMEM/F12 medium (Gibco, MA, USA) supplemented with 5 % foetal bovine serum (FBS) and 5 mM HEPES at a concentration of 100 μg/ml. Samples were sonicated, using the Q500 Sonicator (Q500 Sonica Sonicators, CT, USA) for 5 mins at 50 % amplitude, to disperse particles, due to the magnetic properties (339). After this, 100 μL and 1 mL of particle sample per well to a 96 - well and 6 - well plate respectively. This concentration was established based on preliminary testing from our lab, and also *in vitro* studies (e.g., human lung epithelial A549 and murine macrophage RAW 264.7) testing air pollutant induced toxicity for the same exposure time and concentration (150, 151).

Cell culture and particles suspension treatment. Human neuroblastoma (SH-SY5Y) cells were cultured in DMEM/F12 medium (Gibco, MA, USA) supplemented with 5 % foetal bovine serum (FBS) and 5 mM HEPES. The cells were cultured at 37°C in a humified atmosphere containing 5 % CO_2 until 80 – 90 % confluency. Unless otherwise stated, cells were seeded onto 6-well plates (80, 000 cells/well) for protein extraction or 96-well plates (30, 000 cells/well) for biochemical assays and allowed to settle overnight. The cells were then serum starved for 24 hours before exposure to 100 μL (96-well plate) or 1 mL (6-well plate) per well of iron, diesel, or magnetite particles (100 μg/mL) in DMEM/F12 containing 5 % FBS

for a further 24 hours, after which point, they were ready for protein and RNA extraction and biochemical assay analysis. Cells not exposed to nanoparticles acted as controls.

Total RNA and Protein Extraction. Total RNA was extracted from the snap frozen hippocampus, using the Isolate II RNA/DNA/protein kit following the manufacturer's instructions (Bioline, UK) (340). Whole protein lysate was extracted from the cerebral cortex and SH-SY5Y cells using the RIPA lysis buffer (1 % nonidea P-40, 0.1 % SDS, 0.5 % deoxycholate, 150 mM NaCl, 50 mM Tris pH 8) as previously described (341). The concentration of protein was quantified with the Pierce BCA Protein Assay Kit (Thermofisher Scientific, MA, USA, cat. 23225) and stored at -80°C.

Aβ42 quantification in SH-SY5Y cells. The extracted protein from SH-SY5Y cells was used to investigate Aβ42 concentration, using a Aβ42 Human ELISA Kit (Thermofisher Scientific, MA, USA, cat. KHB3441). This protocol was completed as per the manufacturer's instructions. The protein (30 µg) was prepared in duplicate and added to all wells with appropriate standards and controls. The Aβ42 detection antibody solution (50 µL per well) was added to each well and incubated at room temperature for 3 hours. Following this, the plate was aspirated and washed. The antirabbit IgG HRP (100 µL per well) was added to each well and incubated for 30 mins at room temperature. The plate was aspirated and washed, and the stabilized Chromogen (100 µL) was added and incubated for a further 30 mins at room temp. Finally, the stop solution (100 µL) was added, and the plate was read on the infinite M1000 PRO microplate reader (Tecan Sunrise, Grödig, Austria) at 450 nm. The results are expressed as Aβ42 (pg/mL).

Western Blot Analysis. Protein extracted from the cerebral cortex (30 µg) and SH-SY5Y cells (20 µg) were used for western blot analysis, as previously described (342). Proteins were visualized using ECL substrate (Bio-Rad, CA, USA) and a Bio-Rad Chemidoc Imaging System™. Protein bands were quantified by densitometry using the ImageJ 1.53a software (National Institute of Health, Maryland, USA) (342). All primary and secondary antibodies are listed in Table S4.1.

qPCR mRNA expression. Total RNA (1µg) was reverse transcribed to cDNA using Tetro cDNA synthesis kit (Bioline, MA, USA) following the manufacturer's instructions (340). Following this, cDNA samples were amplified by real-time PCR in master mixtures containing SensiFast SYBR No-ROX kit (Bioline, CA, USA) and primers (20 pmol of both forward and reverse primers). Amplification of samples was completed using the CFX96 thermocycler

(Bio-Rad, CA, USA) with the protocol; 95°C for 2 mins, followed by 40 cycles of 5 secs at 95°C, 10 secs at 60°C, and lastly 10 secs at 72°C. Relative mRNA levels were determined using the comparative analysis method ΔΔCq, using the difference between the gene of interest (156) and reference gene, glyceraldehyde 6-phosphate dehydrogenase (GAPDH) (157, 342). Primers are listed with sequences in Table S4.2.

Measurement of nitric oxide and intracellular reactive oxygen species levels. Following cell treatments, the media was collected and used to measure nitric oxide levels. The media collected was aliquoted (100 µL) in duplicates into wells on a 96-well plate before the addition of 100 µL of Griess reagent (40 mg/mL; Sigma Aldrich, MO, USA) was added into each well. The reaction mix was then incubated at room temperature for 15 mins followed by 30 mins in the dark at 37°C. An absorbance reading was obtained at 540 nm on the infinite M1000 PRO microplate reader (Tecan Sunrise, Grödig, Austria). The results are expressed as percentage increase from control. After the media was collected, intracellular ROS levels were measured in the remaining cells from each well using the DCF stain (Sigma Aldrich, MO, USA) as previously described (343). The results are expressed as percentage increase from control. Each biochemical assay that was performed with both cell lines, cells were seeded in a 96-well plate with 8 technical replicates per plate and per assay. Each assay was repeated 4 times (n = 4 biological replicates), at different passages to account for reproducibility issues (149) which is stated in the results.

Statistical analysis. One-way ANOVA with Bonferroni's post-hoc test was used to determine statistical power in EPM, NIRF in vivo brain imaging, neuronal cell counting, Aβ plaque counting, RT-qPCR, western blotting, Aβ42 ELISA, DCF assay and Griess assay analysis. A an unpaired two-tailed t-test was used to determine the statistical significance of the NOR data. A two-way ANOVA test was used when comparing the WT and APP/PS1 relative saline or air pollutant particle administered mice. All statistical analysis was performed using the Graph-Pad Prism 9 software (Graph-Pad, CA, USA) and the results are expressed as mean ± SEM. The treatment groups were considered significantly different if the p value was less than 0.05.

4.4 Results and Discussion

Exposure to air pollutant particles caused behavioural changes and neuronal cell loss in wild-type and AD-predisposed mice models

To evaluate the behavioural changes in the WT and the APP/PS1 mice following exposure to air pollutant 'iron' (Figure 4.1A), 'diesel' (Figure 4.1B) and 'magnetite' (Figure 4.1C) particles, we carried out the NOR and EPM behavioural tests. The EPM test assesses anxiety and stress levels (137, 138), while the NOR test assesses short-term memory impairment (135, 136). Anxiety and stress and short-term memory impairment are common symptoms of early onset AD (318-320). For the EPM test, the mouse was placed in a maze with open and closed arms and was allowed to move freely for 3 mins. The WT mice upon exposure to air pollutant particles spent more time in the closed arm ($p < 0.0018$ for iron, $p < 0.0309$ for diesel, $p < 0.0140$ for magnetite), relative to the WT saline-administered mice (Figure 4.1D). The increased time spent in the enclosed arm suggest that all pollutant particles induce anxiety and stress in the WT mice *(*138*)*. This is consistent with studies that have reported that excess iron is associated with anxiety-like behaviours, seen in an *in vitro* rat study (Sprague-Dawley rats) upon daily administrations of iron (321). To assess the anxiety effects on the AD-predisposed mice, we first compared the test results between the saline-administered APP/PS1 mice to WT mice (Figure S4.2A). The APP/PS1 saline mice spent more time in the closed arm ($p < 0.0225$) compared to the WT saline mice, indicating that this murine model exhibits an already anxious and stress response, even regardless of exposure to air pollutant particles. The observations are consistent with previous studies that show increased anxiety- and stress-like behaviours in APP/PS1 mice compared to WT mice (322). Exposure to the air pollutant particles did not seem to exacerbate the anxiety and stress responses of the APP/PS1 mice, with similar time spent in the closed arm, compared to that of the APP/PS1 saline mice (Figure 4.2E).

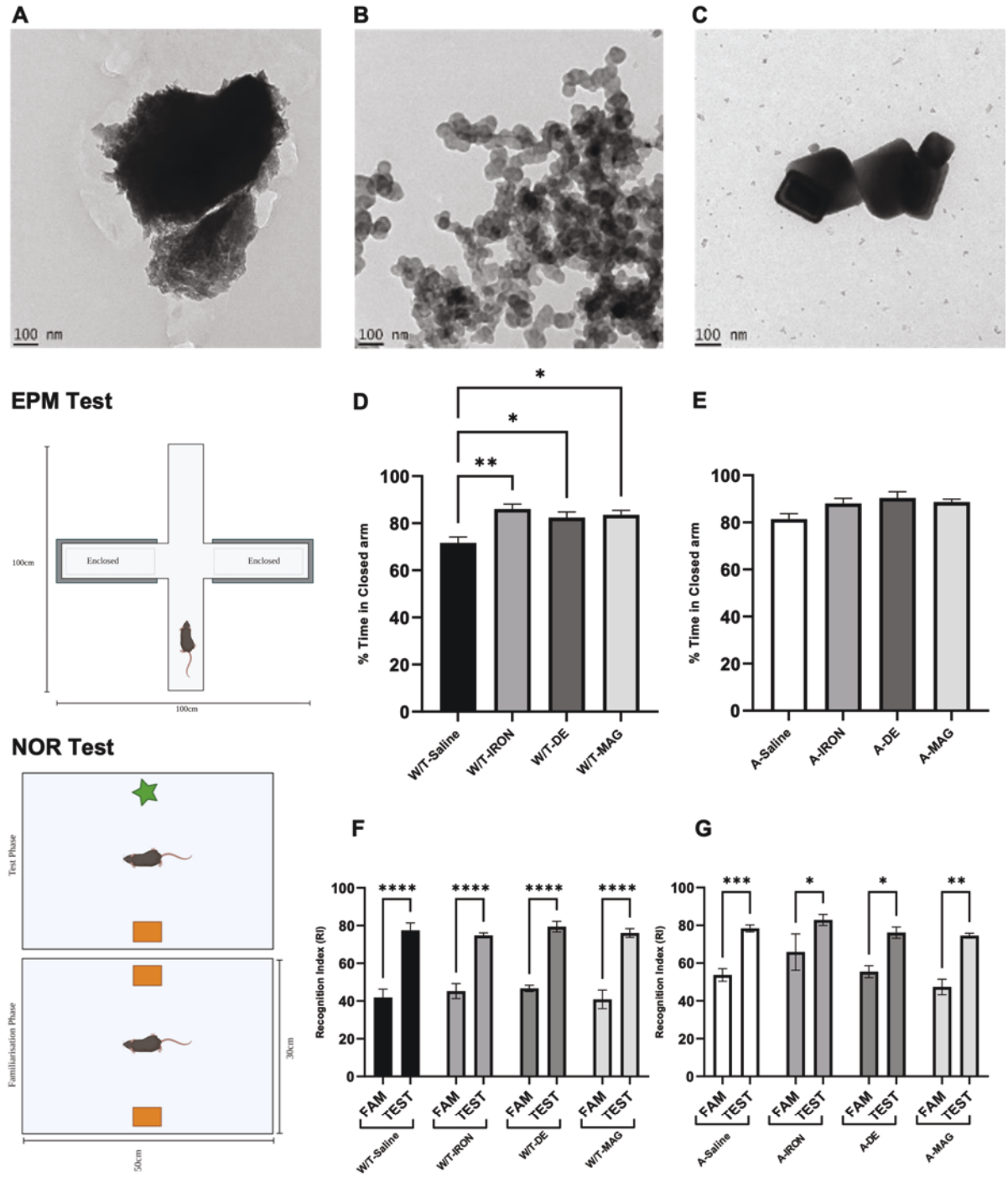

Figure 4.1. *In vivo* behavioural studies of the WT and APP/PS1 mice, following exposure to the air pollutant particles. Transmission electron microscopy (TEM) images of (**A**) IRON, (**B**) DE and (**C**) MAG. (**D**) The EPM test showing the time spent in the closed arm for W/T mice, **$p < 0.0018$ (WT-IRON), *$p < 0.0309$ (WT-DE), *$p < 0.0140$ (WT-MAG) with respect to WT-Saline, (**E**) Time spent in the closed arm for the APP/PS1 mice, note that there is no statistical significance for the particle-exposed groups relative to the A-Saline. (**F**) The NOR test showing the familiarization and test phase recognition indexes for the WT mice, ****p <

0.0001 for all particle groups and saline, (**G**) Recognition indexes for the APP/PS1 mice, ***p < 0.0005(A-Saline), *p < 0.0196 (A-IRON), *p < 0.0147 (A-DE), **p < 0.0015 (A-MAG). For the NOR test, the statistical significance represents discrepancies between the time spent in the test phase relative to the familiarization phase. All error bars indicate mean +/- SEM (n = 8). The schematic of the EPM and NOR tests are also shown.

The NOR test, in which a recognition index (RI) is used to refer to the time spent by the mice both the familiar and novel object (136). The test included a familiarisation phase, in which each mouse spends time with two identical objects, followed by a test phase, in which each mouse spends time with one 'familiar' and one 'novel' object. For the familiarisation phase, a RI is defined as the time spent exploring the familiar object relative to the total time spent exploring both the familiar and novel object. For the test phase, it is the time spent exploring the novel object relative to the total time spent exploring both the familiar and novel object. An indication of cognitive impairment is not present when the RI for both the familiarisation and test phase is statistically significant, as the 'novel' object is perceived as being 'novel' interpreted by more time spent with the object. The WT mice exhibited significantly different RI in the familiarisation phase compared to the test phase indexes in all WT mice groups, seen in Figure 4.1D. This suggests that no short-term memory loss has occurred after exposure to air pollutant particles in the WT mice. The APP/PS1 mice, on the other hand, exhibited discrepancies in the statistical significance of the familiarisation-test phase recognition indexes in all mice exposed to air pollutant particles ($p < 0.0196$ for iron, $p < 0.0147$ for diesel, $p < 0.0015$ for magnetite respectively), when compared to the saline system ($p < 0.0005$). Taken together, the results indicate short-term memory impairment upon the air pollutant particle exposures in the AD-predisposed mice, but not on WT mice. Of note, both WT and APP/PS1 saline administered mice, showed similar familiarisation and test phase RI, indicating that the predisposition of Aβ plaque development, which the APP/PS1 murine model possess, does not necessarily indicate the development of the associated human symptom of memory impairment.

Given the known association of anxiety, stress and memory impairment to neuronal cell loss in the hippocampal region of the brain, we next studied the effects of the air pollutant particles on cells in this region (324, 325). The hippocampus is important for memory storage and

retrieval, which is closely associated with stress and anxiety. Memory impairment can lead to increased stress and anxiety and *vice versa* with stress and anxiety known to disrupt working memory (322). The memory storage and retrieval process involves a chain of neuronal signalling, also known as the perforant pathway, that 'connects' the outer layer of the brain (cerebral cortex) – the parietal, temporal and prefrontal lobes, to hippocampus (344). More specifically, the pathway projects neuronal signalling from the lobes (including the somatosensory cortex (SSC) in the parietal lobe) via the entorhinal cortex (the primary input structure in hippocampus), which extends to the dentate gyrus (DG), cornu ammonis (Ca) 3 and Ca1 regions in the hippocampus (144, 145). As presented in Figure 4.2B and C, neuronal cell counting for the WT mice showed a decreased number of cells in the hippocampal DG region after exposure to air pollutant particles, with magnetite displaying a significant decrease in neuronal cells ($p < 0.0083$), when compared to saline-administered mice. Similar observations were also seen in the Ca3 ($p < 0.0010$ for magnetite, Figure 4.2D) and Ca1 ($p < 0.0001$ for magnetite, Figure 4.2E) regions, as well as with SSC cells ($p < 0.0394$ for diesel, $p < 0.0008$ for magnetite, Figure 4.2F). The neuronal cell loss results coincide with the increased anxiety and stress levels observed in the air pollutant particle-exposed WT mice in the EPM test. Neuronal cell dysfunction and death results in a loss of synaptic density and projections (transmission of electrical impulses between neuron cells) into various brain regions, including the DG and Ca3 regions in the hippocampus which has been known to correlate with increased stress in animal studies (31, 325).

In the EPM test, the APP/PS1 mice expressed predisposed anxiety and stress behaviour regardless of air pollutant particle exposure which is consistent when looking at the APP/PS1 saline administered mice, with less neuronal cell counts seen in the DG, Ca3 and Ca1 regions, compared to the WT saline administered mice (Figure S4.2B, C and D). This is consistent with studies finding that a decrease in Ca3 and Ca1 neuronal cell density has previously been reported in the APP/PS1 murine model (323, 345, 346). Following air pollutant particle exposure, neuronal cell counting in the APP/PS1 mice saw further neuronal cell loss with diesel particles inducing a significant decrease in the DG region ($p < 0.0369$, Figure 4.2B and G). Magnetite particles also induced a significant decrease in neuronal cell counts in the Ca3 ($p < 0.0428$, Figure 4.2H) and the Ca1 ($p < 0.0048$, Figure 4.2I) regions, with both diesel ($p < 0.0115$) and magnetite ($p < 0.0057$) responsible for a significant neuronal cell count in the SSC region (Figure 4.2J), compared to the APP/PS1 saline administered mice.

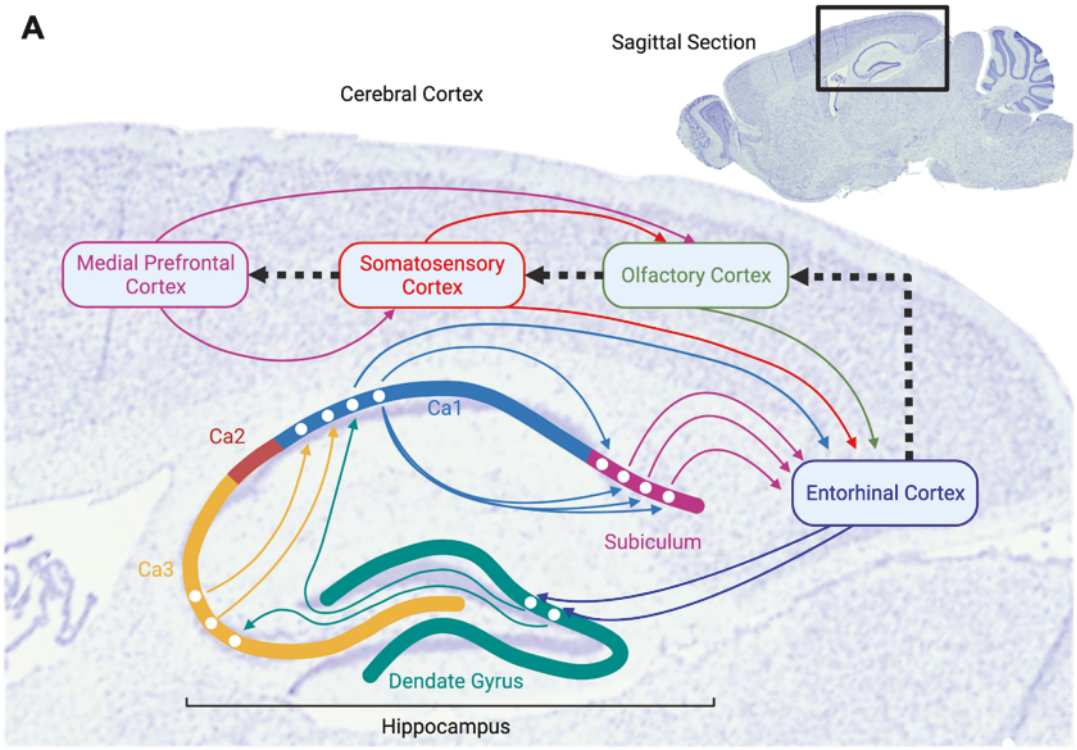
A
Sagittal Section
Cerebral Cortex
Medial Prefrontal Cortex
Somatosensory Cortex
Olfactory Cortex
Ca1
Ca2
Ca3
Entorhinal Cortex
Subiculum
Dendate Gyrus
Hippocampus

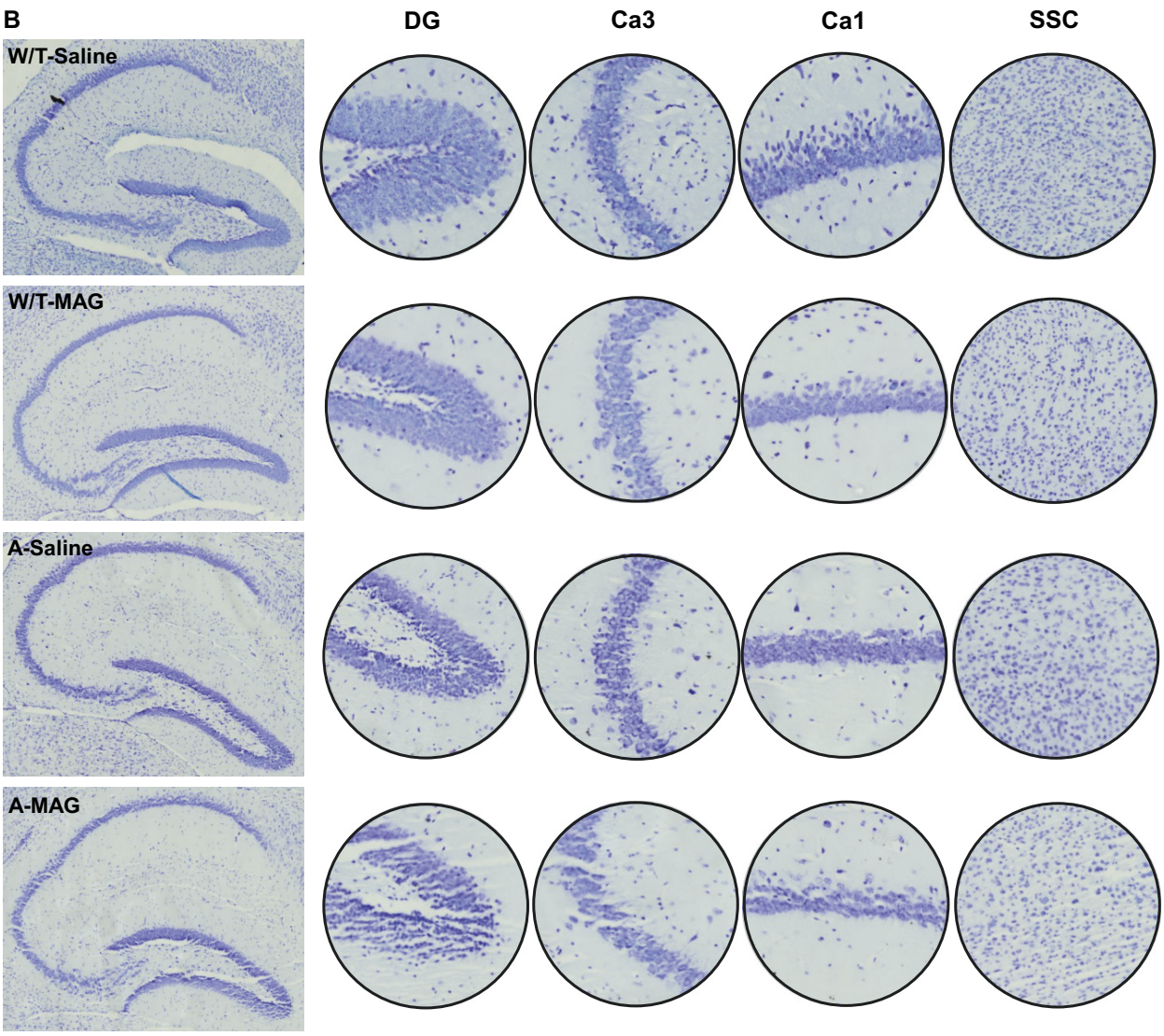
B
DG
Ca3
Ca1
SSC
W/T-Saline
W/T-MAG
A-Saline
A-MAG

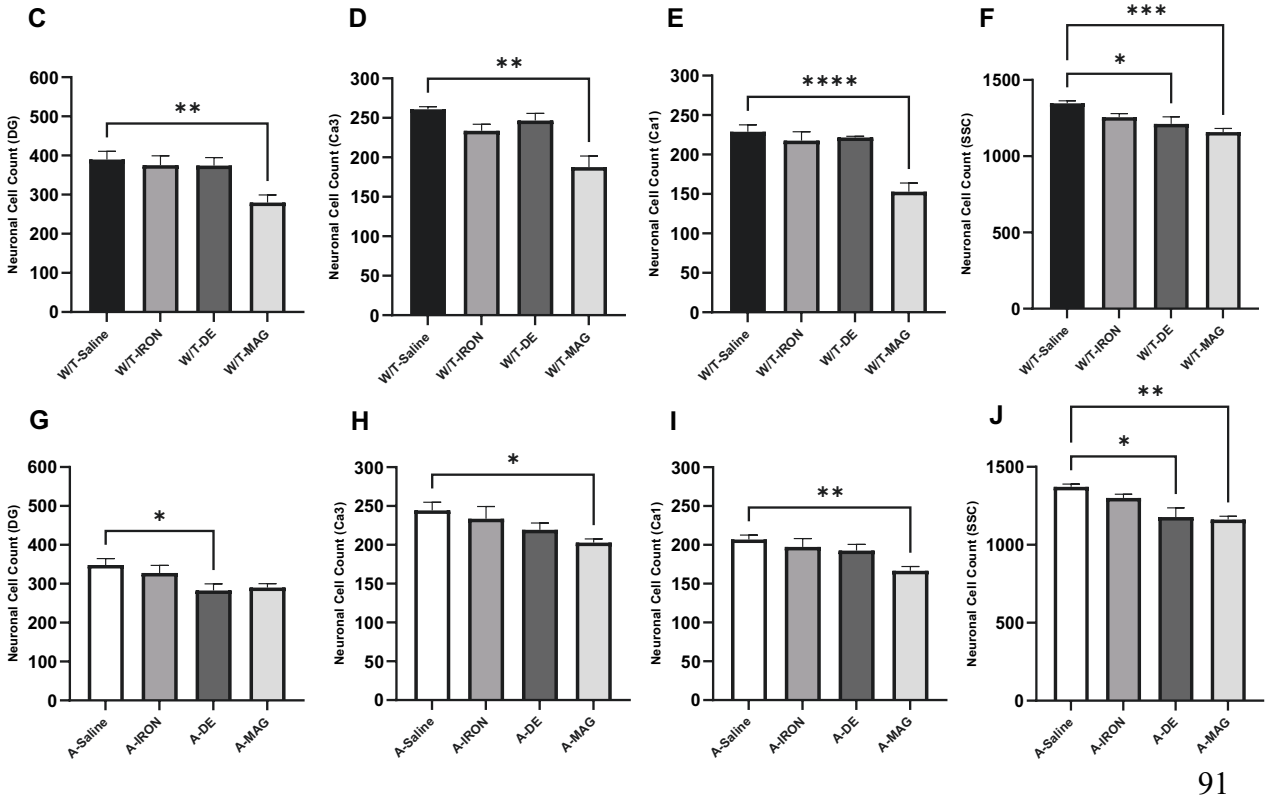
C
D
E
F
Neuronal Cell Count (DG)
Neuronal Cell Count (Ca3)
Neuronal Cell Count (Ca1)
Neuronal Cell Count (SSC)
W/T-Saline
W/T-IRON
W/T-DE
W/T-MAG
G
H
I
J
A-Saline
A-IRON
A-DE
A-MAG

Figure 4.2. *In vivo* analysis of neuronal cell loss following exposure to air pollutant particles in the hippocampus (DG, Ca3 and Ca1 regions) and somatosensory cortex (SSC 2, 3, 4, 5, 6a in the parietal lobe in cerebral cortex). (**A**) A schematic diagram showing the hippocampus and SSC regions in relation to the perforant pathway. (**B**) Brightfield microscopy images of the hippocampus – first column shows the overall hippocampus regions, with a zoomed in DG, Ca3, Ca1 regions in subsequent columns, and the SSC regions of the WT-Saline, WT-MAG, A-Saline and A-MAG mice. (**C, D, E, F**) Cell counting for particle-exposed WT mice; in the DG region **$p < 0.0083$ (WT-MAG) with respect to WT-Saline; in the Ca3 region **$p < 0.0010$ (WT-MAG) vs. WT-Saline; in the Ca1 region ****$p < 0.0001$ (WT-MAG) vs. WT-Saline; in the SSC region *$p < 0.0394$ (WT-DE), ***$p < 0.0008$ (WT-MAG) vs. WT-Saline. (**G, H, I, J**) Cell counting for the particle-exposed AD-predisposed mice; in the DG region, *$p < 0.0369$ (A-DE) vs. A-Saline; in the Ca3 region *$p < 0.0428$ (A-MAG) vs. A-Saline; in the Ca1 region *$p < 0.0048$ (A-MAG) vs. A-Saline; in the SSC region *$p < 0.0115$ (A-DE), **$p < 0.0057$ (A-MAG) vs. A-Saline. All error bars indicate mean +/- SEM (n = 6 - 8).

In summary, our air pollutant particle studies observed adverse behavioural changes in both WT and APP/PS1 mice, consistent with the detected neuronal cell loss observed. All air pollutant particles increased anxiety and stress levels in WT mice, with no further effect in the predisposed anxious and stressed APP/PS1 mice. Instead, the particles were found to cause memory impairment in the APP/PS1 mice. Neuronal cell loss was observed in the hippocampal regions (DG, Ca3 and Ca1) and the SSC regions for both WT and APP/PS1 mice suggesting that air pollutant particles induce a disruption in the perforant pathway associated with anxiety, stress and memory impairment. Studies have reported that disruptions of the perforant pathway in early onset AD patients, increase anxiety and stress levels whilst affecting short-term memory, including spatial recognition memory (323, 326, 327). In fact, studies have found that anxiety and stress-related symptoms are often linked to memory impairment in AD patients (347). Recalling the earlier mentioned link between behavioural changes and neuronal cell death to Aβ formation, we next looked for the development of the characteristic AD pathologies in the brain of the mice.

Exposure to air pollutant particles increased Aβ plaque formation and neurofibrillary tangles

We studied the potential formation of Aβ plaques using *in vivo* and *ex vivo* whole brain imaging on the WT and APP/PS1 mice. The *in vivo* NIRF CRANAD-2 probe detects for the presence of soluble (Aβ40) and insoluble (Aβ42) peptide aggregates (348), while the *ex vivo* fluorescence thioflavin S staining detects the characteristic β-pleated sheets of Aβ plaque (338). Unlike humans, C57BL/6 W/T mice do not develop Aβ plaques during the course of normal aging, however they are still able to develop Aβ peptide aggregates (349, 350), seen in the representative images of *in vivo* NIRF brain imaging (Figure 4.3A). These images display a brighter fluorescence was emitted in the WT and APP/PS1 mice that had been exposed to all air pollutant particles, compared to the saline administered mice. The NIRF probe (CRANAD-2) detects the presence of both soluble (Aβ40) and insoluble (Aβ42) peptides, and therefore does not accurately represent the formation of Aβ plaque deposits (large deposits of peptide principally Aβ42 peptide aggregates) (141). Therefore, the ex vivo fluorescence thioflavin S staining was completed to verify these results. Thioflavin S. stain detects the characteristic β-pleated sheets of Aβ plaques and as expected, no Aβ plaque formations were found in all W/T mice. There is a significant increase in Aβ plaque counting in the diesel ($p < 0.028$) and magnetite ($p < 0.0004$) particle exposed APP/PS1 mice, compared to the saline administered mice, seen in Figure 4.3B and 4.3C. The observations are indeed consistent with the elevated presence of β-secretase enzyme detected in the plasma of the particle-exposed WT mice, in particular with magnetite ($p < 0.0353$, Figure 4.3E). The enzyme β-secretase 1 (BACE1) catalyses the cleavage of APP (amyloid precursor protein) to form Aβ peptides (including Aβ42), which further aggregates to form the plaques (Figure 4.3I) (328, 330, 331, 351). The plasma levels of the β-secretase enzyme in the air pollutant particle-exposed APP/PS1 mice also seemed to increase, although with no statistical significance when compared to the saline administered mice (Figure 4.3F). Of note there is a correlation in the high plasma β-secretase enzyme levels ($p < 0.0283$, Figure S4.2E) presence in the APP/PS1 mice relative to the WT mice when comparing just the saline administered mice, which is anticipated (123, 329). Of note, the β-secretase levels in the plasma of WT particle exposed mice shows no difference from that of the APP/PS1 particle exposed mice, suggesting that particle exposure is inducing an increase in β-secretase plasma levels regardless of pathological vulnerability (Figure S4.2A, B, C). The observations indicate that exacerbation of Aβ plaque formation in the APP/PS1 mice is due to air pollutant particle exposure, with magnetite particles inducing the most consistent and detrimental effect.

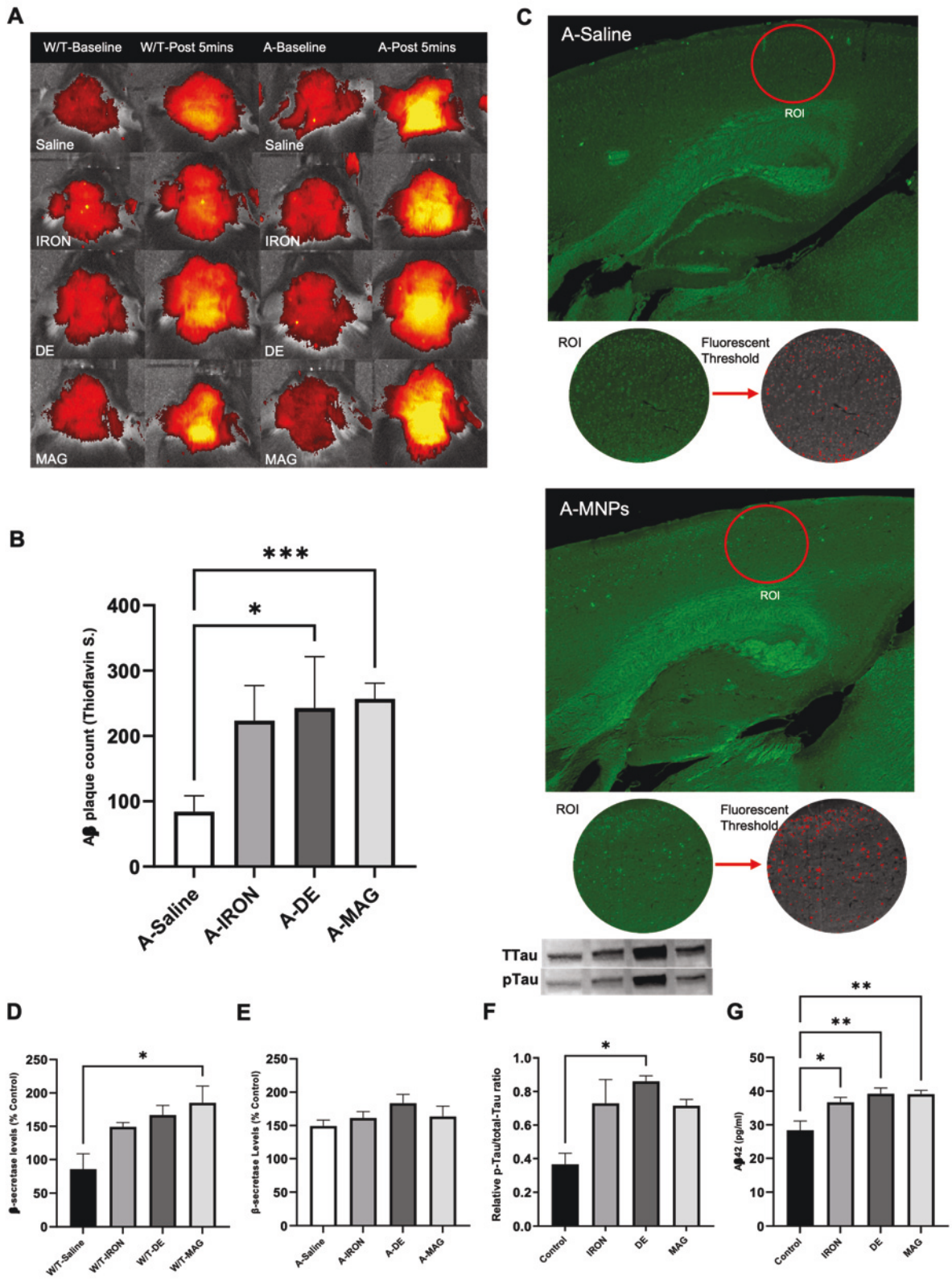
A
W/T-Baseline
W/T-Post 5mins
A-Baseline
A-Post 5mins
Saline
Saline
IRON
IRON
DE
DE
MAG
MAG
C
A-Saline
ROI
ROI
Fluorescent Threshold
A-MNPs
ROI
ROI
Fluorescent Threshold
TTau
pTau
B
***
*
400
300
200
100
0
Aβ plaque count (Thioflavin S.)
A-Saline
A-IRON
A-DE
A-MAG
D
*
250
200
150
100
50
0
β-secretase levels (% Control)
W/T-Saline
W/T-IRON
W/T-DE
W/T-MAG
E
250
200
150
100
50
0
β-secretase Levels (% Control)
A-Saline
A-IRON
A-DE
A-MAG
F
*
1.0
0.8
0.6
0.4
0.2
0.0
Relative p-Tau/total-Tau ratio
Control
IRON
DE
MAG
G
**
**
*
50
40
30
20
10
0
Aβ42 (pg/ml)
Control
IRON
DE
MAG

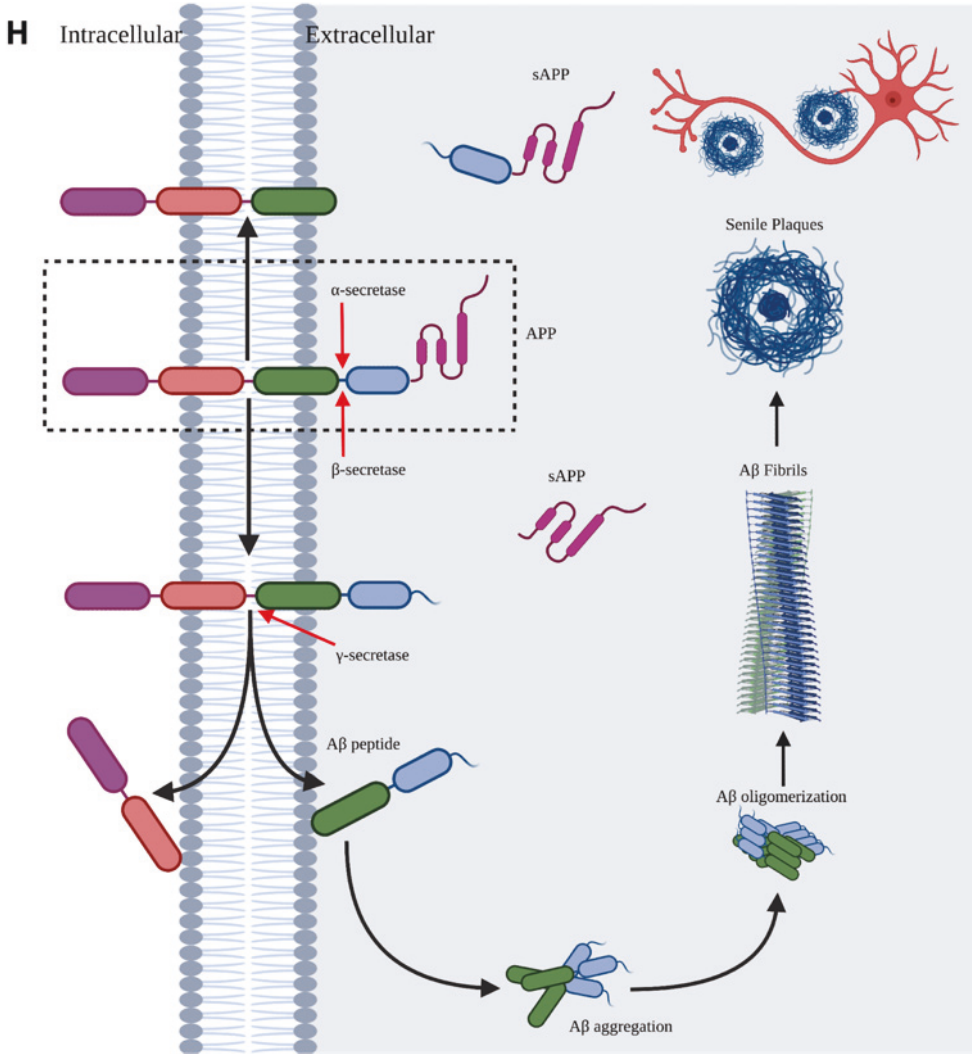

Figure 4.3. *In vivo* and *in vitro* studies of hallmark AD characteristics. (A) Aβ42 aggregates detected in the brain of the particle-exposed WT and AD-predisposed mice, showing fluorescent radiance before (baseline) and after (post 5 mins) intravenous injection of the NIRF probe (CRANAD-2). Aβ plaque counting (based on thioflavin S staining) for (B) AD-predisposed mice *p < 0.028 (A-DE), ***p < 0.0004 (A-MAG) vs. A-Saline, (n = 8). (C) Thioflavin S fluorescence imaging of Aβ plaque in A-Saline and A-MAG mice groups (with zoomed-in hippocampal images). (D) Percentage increase of plasma β-secretase (BACE-1) levels, for (E) WT mice *p < 0.0409 (WT-MAG) vs. WT-Saline (n = 8), (F) APP/PS1 mice (n = 8), note that there is no statistical significance for the particle-exposed groups relative to the A-Saline. (G) *In vitro* detection of phosphorylated (Ser214) Tau/total Tau protein in SHSY5Y cells *p < 0.0468 (DE) vs. Control (n = 5-6). (H) Aβ42 peptide levels in SHSY5Y cells *p < 0.0244 (IRON), **p < 0.0022 (DE), **p < 0.0017 (MAG) vs. Control (n = 8). (I) Schematic

showing Aβ plaque formation after cleavage with β-secretase. All error bars indicate mean +/- SEM.

Taken together, it is evident that exposure to the air pollutant particles increased the formation of Aβ species in the WT mice, and even more in APP/PS1 mice leading to the exacerbated formation of Aβ plaques. The formation of Aβ plaques are associated with NFT formation in AD development. For example, it has been shown that Aβ plaques can destabilise microtubule-associated tau protein (found predominantly in axons, promoting tubulin polymerization for axonal function) by rendering it prone to extensive phosphorylation (333, 334, 352). The hyperphosphorylated tau protein, in turn, aggregates into bundled filaments and subsequently forms the NFTs inside the neuronal cells (333, 334, 352). NFTs are known to be toxic to neuronal cells, and is often associated with neuronal degeneration and death, resulting in the release of intracellular NFTs into the extracellular environments, which then cause toxicity to surrounding neurons. Hyperphosphorylated tau contains a unique double-site phosphor-epitope AT100 which consists of both anti-phosphoThr (Thr212) and anti-phosphoSer214 (Ser214) (61, 62). Phosphorylation of tau at Ser214 inside the neuron decreases the binding of tau to microtubules, affecting the stability of the cytoskeleton and promotes tau fibrillation (353). Therefore, investigating the protein expression of phosphorylated Ser214 protein-to-total tau ratio inside neuronal cells was completed with the SH-SY5Y cells to gain insight into the potential development of NFTs and associated neuronal damage, after exposure to air pollutant particles. Figure 4.3G shows SH-SY5Y cells after exposure to air pollutant particles particularly diesel ($p < 0.0468$), resulted in an increase in phosphorylation of Ser214-to-total tau protein ratios, compared to control samples. While the presence of phosphorylated Ser214 tau does not necessarily mean that NFTs are present or that they will form, phosphorylated Ser214 tau is important as it alone can potentially disrupt microtubule binding, leading to destabilised microtubules resulting in the eventual formation of NFTs, and subsequently neuronal death, hallmark features of AD (332). We also detected elevated presence of Aβ42 peptide in the particle-exposed cell samples ($p < 0.0244$ for iron, $p < 0.0022$ for diesel, $p < 0.0017$ for magnetite, Figure 4.3H) relative to the control. In the next study, we investigated the effects of the pollutant particles on AD-relevant biomarkers and inflammatory molecules. These findings agree with the earlier described changes in mice behaviour as well as neuronal cell loss, indicative of early onset AD, and indeed, our *in vitro* studies also detecting increased presence of phosphorylated tau protein after exposure to air pollutant particles.

Air pollutant particles increased levels of immune system biomarkers and inflammatory molecules

To obtain insights on the roles of air pollutant particles on AD pathologies, we studied how the particles are affecting a number of AD-relevant inflammatory biomarkers and mediators. Herein, we focused on the presence of biomarkers that are produced by major immune cells in the CNS, microglia and astrocytic cells. Microglia and astrocytes are macrophagic cell, responding to foreign entities, whereby microglia have enhanced phagocytic capacity to remove debris, while astrocytes increase their size to physically guard the BBB and protect the brain (354). In the case of AD progression, microglial and astrocytes have been known to upregulate specific biomarkers and inflammatory cytokines (38, 355), which have been assessed in brain samples of the WT and APP/PS1 mice. Our study also assessed biomarkers that are associated with central MAPKs (mitogen-activated protein kinases) pathway, a major signalling network that initiates a physiological response, including the activation of various inflammatory molecules when exposed to external stimuli (356, 357).

Firstly, we had a look on the levels of the biomarkers and inflammatory molecules in WT mice. Exposure to the air pollutant particles were found to induce an increase in immune system cells in the WT mice, with increased BDNF protein expression detected in the cerebral cortex brain regions through western blot analysis ($p < 0.0001$ for iron, diesel and magnetite normalised to β-actin) compared to WT saline administered mice (Figure 4.4A). Exposure to air pollutants also saw higher protein expression of ICAM-1 ($p < 0.010$ for magnetite normalised to β-actin, Figure 4.4C) in the cerebral cortex samples. BDNF is a growth factor released by microglia cells to repair neuron cells (358), while ICAM-1 is a transmembrane glycoprotein presented on the surface of both microglia and astrocytes to facilitate interactions of immune system cells (359). Studies have found that increased presence of Aβ species, observed in this study in the whole brain fluorescence imaging, can indeed upregulate BDNF synthesis (358), as well as increase the surface presentation of ICAM-1(360). AD studies have reported increased BDNF levels in damaged brain regions, as well as increased ICAM-1 levels (serum), when compared to healthy individuals (361-365). In the APP/PS1 mice, exposure to air pollutant particles increased BDNF protein expression ($p < 0.021$ for iron normalised to β-actin, Figure 4.4B) and ICAM-1 protein expression ($p < 0.010$ for iron normalised to β-actin, Figure 4.4D) compared

to the APP/PS1 saline mice. Particle exposures on the APP/PS1 mice also saw higher protein expression of cerebral cortex Iba-1 ($p < 0.0385$ for iron normalised to β-actin, Figure 4.4F) compared to the APP/PS1 saline mice. Iba-1 is expressed in microglia with studies indicating its role in the actin (cytoskeletal protein) cross-linking involved in membrane ruffling of microglia (366). The latter is a process essential for microglia activation and in turn, the phagocytic activity of microglia (367). Studies have correlated upregulation of Iba-1 synthesis with activation of microglia (367), and indeed, an increased cerebral cortex Iba-1 levels have been detected in AD cases (366). We also compared in air pollutant particles APP/PS1 mice, relative to the air pollutant particle exposed WT mice.

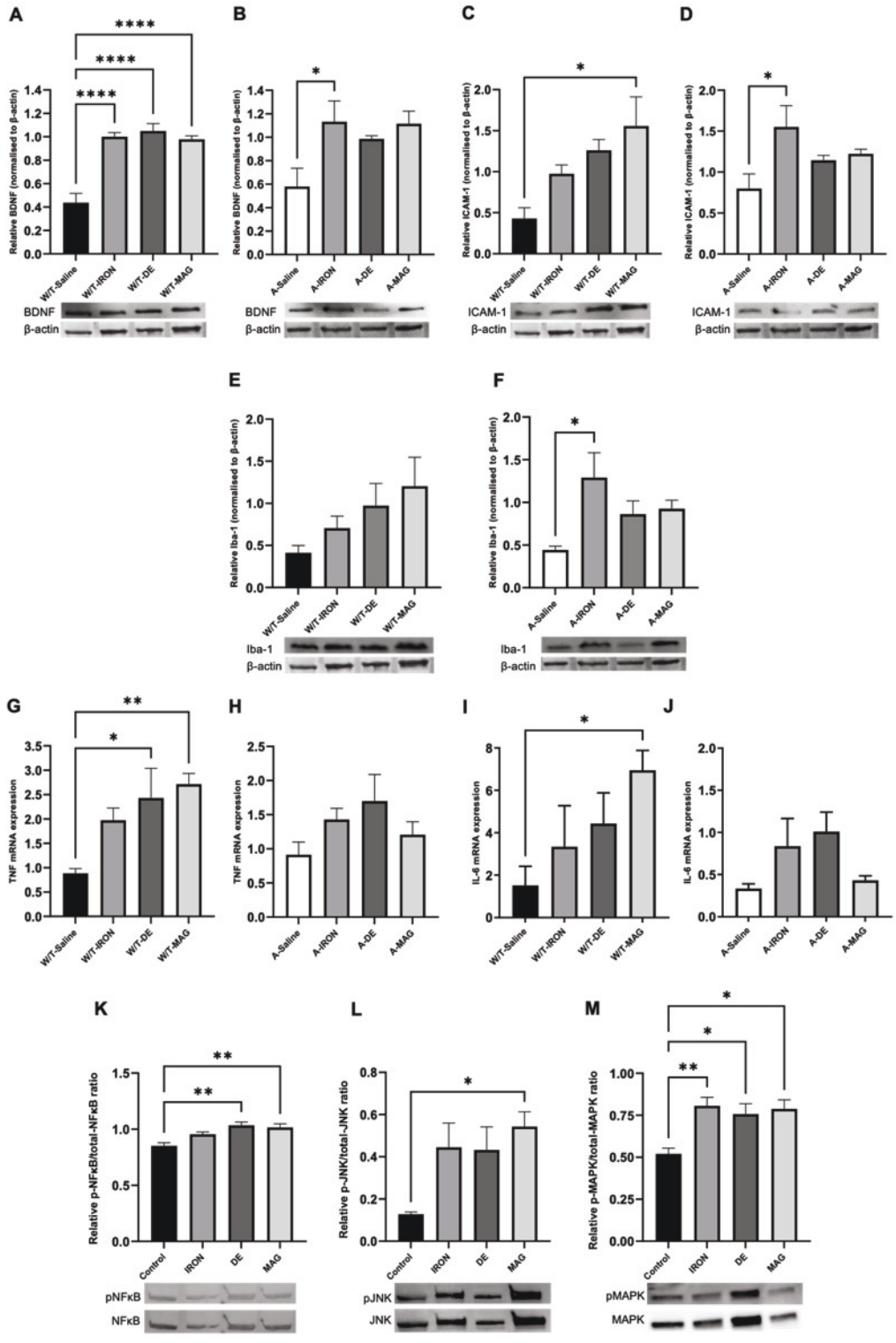

Figure 4.4. *In vivo* and *in vitro* studies of AD-relevant inflammatory biomarkers and mediators. (**A, B**) Relative BDNF protein expression levels in the cerebral cortex of WT mice (n = 5-8) ****p < 0.0001 (for all particle groups) vs. WT-Saline; and the APP/PS1 mice (n = 5-8) *p < 0.021 (A-IRON) vs. A-Saline. (**C, D**) Relative ICAM-1 protein expression levels in the cerebral cortex of WT mice (n = 5-8) *p < 0.01 (WT-MAG) vs. WT-Saline; and the

APP/PS1 mice (n = 5-8) *p < 0.010 (A-IRON) vs. A-Saline. (**E, F**) Relative Iba-1 protein expression levels in the cerebral cortex, WT mice (n = 5-8), note that there is no statistical significance for the particle-exposed groups relative to WT-Saline; and the APP/PS1 mice (n = 5-8) *p < 0.0385 (A-IRON) vs. A-Saline normalised to β-actin. (**G, H**) TNF mRNA expression in the hippocampus, WT mice (n = 8) *p < 0.0291 (WT-DE), **p < 0.0054 (WT-MAG) vs. WT-Saline; and the APP/PS1 mice (n = 8), no statistical significance for the particle-exposed groups relative to the A-Saline. (**I, J**) IL-6 mRNA expression in the hippocampus, WT mice (n = 8), *p < 0.0137 (WT-MAG) vs. WT-Saline; for the AD-predisposed mice (n = 8), no statistical significance for the particle-exposed groups relative to the A-Saline. (**K**) Relative pNFκB/NFκB in SH-SY5Y cells (n = 5-6), **p < 0.007 (DE and MAG) vs. Control. (**L**) Relative pJNK/JNK in SH-SY5Y (n = 5-6), *p < 0.030 (MAG) vs. Control. (**M**) Relative pMAPK/MAPK in SH-SY5Y (n = 5-6), **p < 0.007 (IRON), *P<0.030 (DE and MAG) vs. Control. All error bars indicate mean +/- SEM.

The results so far indicate that exposure to air pollutant particles increases the activity of the CNS immune system, evident from the higher levels of microglia and astrocytic biomarkers in the mice cerebral cortex, in both WT and APP/PS1 mice. Next, we looked for the potential upregulation of inflammatory molecules. During the early stages of the CNS immune response, both microglia and astrocytes have been known to upregulate cytokine synthesis (355) and herein, we detected higher TNF and IL-6 gene expressions in the air pollutant particle exposed WT mice, in particular with diesel ($p < 0.0291$ for TNF) and magnetite ($p < 0.0054$ for TNF and $p < 0.0137$ for IL-6, Figure 4.4G and 4.4I), in their hippocampal regions, relative to the WT saline-administered mice. The observations agree with earlier studies detecting increased expression of TNF and IL-6 genes in the hippocampal regions of AD patients *(*355*)*. The Inflammation is a biological immune response, and these inflammatory cytokines have been known to induce a number of physiological responses in AD pathologies, including oxidative stress, as later described (368). Although not statistically significant, a trend towards an increase in TNF and IL-6 mRNA gene expression levels were also seen in the APP/PS1 mice relative to the saline group (Figure 4.4H and 4.4J). The increased levels of inflammatory markers in the WT mice compared to that of the APP/PS1 mice is interesting and is somewhat consistent with a study testing for low-grade chronic inflammation, which showed that there was an increase in microglial activation observed in the cortex of the APP/PS1 mice, and in the hippocampus of the WT mice 2 hours after peripheral LPS injection as the inflammatory

stimuli (369). This suggests that the hippocampus in the WT mice can exhibit an increased inflammatory response compared to the APP/PS1 equivalent particle exposed groups, perhaps due to the neuronal loss and other AD pathologies associated with 7-8-month-old APP/PS1 transgenic mice.

Next, we investigated the biomarkers associate with the major physiological MAPK signalling pathways involved in the immune system. Activation of the MAPK pathway has been known to subsequently activate the three-tier NFκB, JNK and p38 MAPK modules in the development of AD (357). We found that exposures to the air pollutant particles increased the levels of biomarkers for these modules. Our *in vitro* studies with the SH-SY5Y cell line detected higher levels of phosphorylated nuclear-factor kappa B p65 (p-NFκB subunit 65)-to-total NFκB ($p < 0.007$ for diesel and magnetite), phosphorylated c-Jun N-terminal Kinase (p-JNK) ($p < 0.030$ for magnetite)-to-total JNK and phosphorylated (p38) MAPK ($p < 0.007$ for iron, $p < 0.030$ for diesel and magnetite)-to-total MAPK protein expression in cells exposed to air pollutant particles compared to control samples (Figure 4.4K, L and M respectively). The protein complex NFκB is a family of transcription factors that controls expressions of genes various biological processes, including cytokine production (370). The levels of these biomarkers, more specifically, the p65 NFκB, p-JNK and p38 MAPK, have been found to increase in AD studies (344, 371). NFκB has in fact been indicated to upregulate the synthesis of β-secretase 1 enzyme (BACE1), this is also seen with the particle-exposed mice (in particular the WT mice), and in turn the formation of Aβ peptides (344, 372). Further, recalling the observed short-term memory impairment in the AD-predisposed mice (from the NOR behavioural test), research inquiries have indeed linked cognitive decline in mice to activation of the JNK pathway (371). Studies have also linked the activation of the p38 MAPK pathway to an increase in tau phosphorylation (371), which is consistent with our *in vitro* results.

Taken together, exposure to the air pollutant particles increased a number of AD-relevant brain microglia and astrocytic immune responses, increasing the protein expression of the neurotrophic growth factor, BDNF and the surface glycoprotein, ICAM-1. The latter plays a significant role in immune cell interactions, along with proteins that are involved in the immune cell activation of Iba-1. These responses were seen in both the WT and AD-predisposed mice. Our studies further observed an increase in the mRNA gene expression of the inflammatory

cytokines, TNF and IL-6. These inflammatory cytokines are known to be produced by phosphorylated transcription factors like p38-MAPK, p65-NFκB and JNK, which is consistent with the *in vitro* data, showing an increase in expression of these cytokines in SH-SY5Y cells exposed to air pollutants. Next, in our final studies, we investigated the oxidative stress phenomena, with studies linking immune responses to oxidative stress in AD pathologies. Immune system stimuli, including cytokines, as well as the transcription factor NFκB, have been indicated to mediate the generation of damaging ROS, therefore we next investigated the effects of exposure to air pollutant particles on the oxidative stress phenomena.

Air pollutant particles induce oxidative stress

We studied the levels of the oxidative stress-related microglia and astrocytic enzymes, iNOS and Cox2, in brain samples of the WT and APP/PS1 mice. Exposure of WT mice to the air pollutant particles saw an increase cerebral cortex iNOS protein expression, particularly with diesel ($p < 0.0406$ normalised to β-actin) and magnetite ($p < 0.0014$ normalised to β-actin), when compared to the WT saline-administered mice (Figure 4.5A). We also observed an increase in cerebral cortex iNOS protein expression in the APP/PS1 mice exposed to the air pollutant particles compared to the saline mice, however there was no significance (Figure 4.5B). This indicates that the air pollutant particles do not exacerbate the effects on APP/PS1 mice due to similar iNOS protein expression levels observed in the APP/PS1 saline administered mice, which is evident when comparing the iNOS protein expression in the WT and APP/PS1 saline administered mice ($p < 0.0451$ normalised to β-actin, Figure S4.2F). iNOS, an inducible nitric oxide synthase which catalyses the synthesis of nitric oxide (NO) from the amino acid *L*-arginine. NO is a cellular signalling molecule important for neural development (373). Increased presence of iNOS and in turn, excess of NO, has been seen in AD studies (374). Indeed, we detected higher cellular NO levels in the SH-SH5Y cells exposed to air pollutant particles ($p < 0.018$ for iron, $p < 0.0001$ for diesel, $p < 0.0023$ for magnetite, Figure 4.5E), compared to the controls. We also detected higher cellular presence of other ROS (general ROS presence) in the SH-SY5Y cells exposed to air pollutant particles ($p < 0.0239$ for iron, $p < 0.0001$ for diesel, $p < 0.0147$ for magnetite, Figure 4.5F). Earlier AD studies have reported increased cellular ROS levels closely linked to increased Cox2 protein expression. Cox2, a cyclooxygenase enzyme, mediates ROS generation with studies indicating its stimulation is due to excess presence of cellular NO (375-377). Indeed, we detected increased protein expression of Cox2 in the cerebral cortex of WT mice exposed to air pollutant particles

($p < 0.040$ for iron, $p < 0.0236$ for diesel, $p < 0.0155$ for magnetite normalised to β-actin, Figure 4.5C). As with iNOS, there is no significant increase in Cox2 protein expression levels in the APP/PS1 mice after exposure to air pollutant particles, compared to the APP/PS1 saline mice (Figure 4.5D). Neurons are sensitive to oxidative stress which have been known to correlate with neuronal cell loss, consistent with the neuronal cell loss seen in the hippocampal and SSC regions of both the WT and APP/PS1 mice seen in this study (316).

To determine the mechanism of ROS generation, we incorporated an NFκB inhibitor into *in vitro* air pollutant particle exposure systems. As shown in Figure 4.5G and 4.5H, less cellular ROS levels ($p < 0.0001$ for all particles), including NO levels ($p < 0.0012$ for iron, $p < 0.0001$ for diesel, $p < 0.0167$ for magnetite), were detected when in the presence of the NFκB inhibitor for all air pollutant particle exposed SH-SY5Y cells. The observations suggest that ROS generation is inhibited from transcription of iNOS and Cox2 in the presence of the NFκB inhibitor (378, 379) indicating that NFκB plays a significant role in ROS generation, whilst also confirming the close relationship that neuroinflammation and oxidative stress hold.

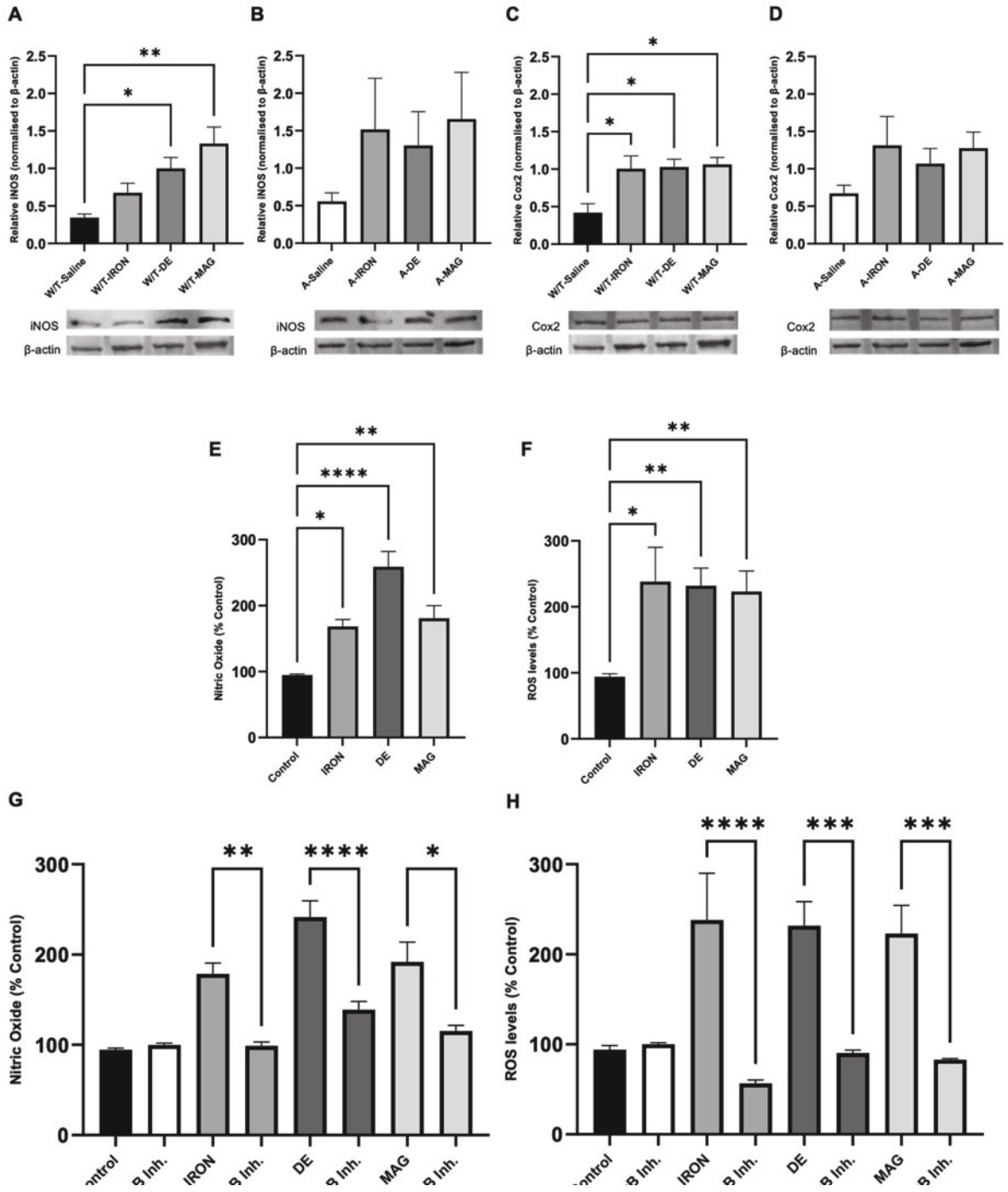

Figure 4.5. *In vivo* and *in vitro* studies of oxidative stress responses. (**A, B**) Relative iNOS protein expression levels in the cerebral cortex of the particle-exposed wild-type mice (n = 5-8) *p < 0.0406 (WT-DE), **p < 0.0014 (WT-MAG) vs. WT-Saline; for the particle-exposed AD-predisposed mice (n = 5-8), note that there is no statistical significance for the particle-exposed groups relative to the A-Saline, normalised to β-actin. (**C, D**) Relative Cox2 protein expression levels in the cerebral cortex, WT mice (n = 5-8), *p < 0.040 (WT-IRON), *p <

0.0236 (WT-DE), *p < 0.0155 (WT-MAG) vs. W/T-Saline; for the AD-predisposed mice (n = 5-8), no statistical significance for the particle-exposed groups relative to the A-Saline, normalised to β-actin. (**E**) NO levels (relative to the cell-only control) in SH-SY5Y cells (n = 4) *p < 0.0180 (IRON), ****p < 0.0001 (DE), ** p < 0.0023 (MAG) vs. Control. (**F**) ROS levels (relative to the cell-only control) in SH-SY5Y (n = 4) * p < 0.0239 (IRON), ** p < 0.0001 (DE), ** p < 0.0147 (MAG) vs. Control. (**G**) NO levels in SH-SY5Y in the presence of NFκB inhibitor (n = 4) ** p < 0.0012 (IRON), **** p < 0.0001 (DE), * p < 0.0167 (MAG) vs. NO levels without the inhibitor. (**H**) ROS levels in SH-SY5Y in the presence of NFκB inhibitor (n = 4) **** p < 0.0001 (IRON, DE, MAG). All error bars indicate mean +/- SEM.

A working model and differential effects of air pollutant particles on AD pathologies

The present *in vivo* and *in vitro* studies aimed to determine the potential roles of exposure to air pollutant particle on the early onset of AD. Firstly, consistent with the detected neuronal cell loss in the hippocampus and SCC regions, we found that all the tested particles; iron, diesel and magnetite caused anxiety and stress in the WT mice, while prompting short-term memory impairment in the APP/PS1 transgenic mice. The exposure to the air pollutant particles is thought to disturb the outer brain lobes (including SSC)-to-hippocampus neuron signalling via the perforant pathway, which plays a significant role in working memory. The impairment of this pathway has also been linked to anxiety and stress (319). Next, we found that exposure to air pollutant particles increased the formation of the Aβ species in both the WT and APP/PS1 mice, when considering the *in vivo* NIRF probe brain imaging and the β-secretase plasma levels. There was also an increase in Aβ plaque development in the APP/PS1 mice, which correlates with the short-term memory impairment in this mice model. An increase in Aβ42 protein aggregation was also seen in the SH-SY5Y cell after exposure to the air pollutant particles. We also observed an increase in phosphorylated tau protein levels, in the SH-SY5Y cells exposed to the air pollutant particles. While this does not reflect the AD hallmark feature of NFTs, phosphorylated tau is a precursor to the paired helical tau tangles that make up the NFT formation in the neuronal cell. Seen herein with both the WT and AD-predisposed mice, we hypothesized that exposure to air pollutant particles induces an increase in Aβ species formation (as also implied in earlier study (358)) an increase in microglia and astrocyte activation leading to increased production of inflammatory biomarkers, like BDNF, ICAM-1 and Iba-1 in the cerebral cortex, which repair damaged neuronal cells, mediate immune cell

interactions and further activates microglial cells respectively. It is also apparent that exposure to air pollutant particles can initiate AD-relevant inflammation as well as oxidative stress seen in both the WT and APP/PS1 mice. The air pollutant particles induced an increase in the hippocampal mRNA expression of TNF and IL-6 inflammatory cytokines. Our *in vitro* data (with SHSY5Y cells) linked the inflammation, at least in part, to the activation of the MAPK signalling pathway, that is, on the activity of the three-tier NFκB, JNK and p38 MAPK signalling modules. Indeed, we also deduced the role of NFκB in the generation of ROS and oxidative stress. Exposure to the air pollutant particles exposures were found to increase the levels of cellular NO (as well as reactive oxygen species (ROS) in general). The transcription factor NFκB is thought to control the expression of the NO-synthesizing enzyme iNOS, as well as Cox2, an enzyme that mediates ROS generation. Elevated presence of these enzymes were detected in the cerebral cortex regions in the mice exposed to the air pollutant particles.

Taken together, the exposure to air pollutant particles can induce AD-relevant behavioural changes and neuronal cell loss, with the detection of the hallmark Aβ species. The exposures were also shown to increase AD-relevant immune responses including those involved in inflammation, as well as oxidative stress. These air pollutant particle-induced biological effects were seen in both the WT and APP/PS1 mice. This study also revealed that among the tested air pollutant particle models, magnetite seemed to inflict the most changes (increased anxiety and stress, neuronal cell loss, Aβ species formation, as well as increasing the inflammatory and oxidative stress responses), followed by diesel particles on the WT mice. The air pollutant iron particles in this study are the largest (500 - 700 nm crystal diameter), and they appear to have the least consistent damaging effects in the WT mice and in the *in vitro* studies compared to both diesel and magnetite air pollutant particles. The smaller the size of air pollutant particles is directly associated with extent of migration and penetration (50). The air pollutant diesel particles in this study are the smallest in size (20 - 60 nm crystal diameter) and show consistent toxicity in both the WT mice and in the *in vitro* studies, however the air pollutant magnetite particles appear to induce the most damage in the WT mice and *in vitro* studies overall. The magnetite particles are 100 – 400 nm crystal diameter in size, suggesting that the size of the air pollutant particles is associated with the extent of damage, however the composition of magnetite (transitioning from $Fe_{2+}O_{4-}$ (reduced) to $Fe_{3+}O_{4-}$ (oxidised) state) is the most significant factor in a highly oxygen rich environment like the brain (76, 78). The trends were, however, rather inconclusive with the APP/PS1 mice, with no clear tendencies on which particles induced the

most damaging effects. Finally, comparing the WT and APP/PS1 groups, we can deduce that in general there is no particle-induced exacerbation of the effects in the APP/PS1 mice, more specifically on the immune system and oxidative stress responses, despite detection of the high Aβ plaque presence.

4.5 Conclusion

In summary, the present work reported the ability of air pollutant particles to induce pathological features implicated in early onset AD. In both WT and APP/PS1 mice models, exposure to the iron-based and carbon-based particles of varying sizes led to behavioural changes and different extents of neuronal cell loss, inflammatory as well as oxidative stress responses, with magnetite particles appearing as the most consistent in inducing the development of AD-related changes. Exposure to the particles, however, does not seem to exacerbate the inflammatory and oxidative stress response in the APP/PS1 mice, with pre-existing AD pathological vulnerabilities, despite the more abundant presence of the AD hallmark Aβ plaques in the latter. Future studies are needed to investigate the exact trigger of the air pollutant particle-induced AD pathologies, which will also give insight into the effects currently observed in the AD-predisposed cases.

4.6 Supporting Information

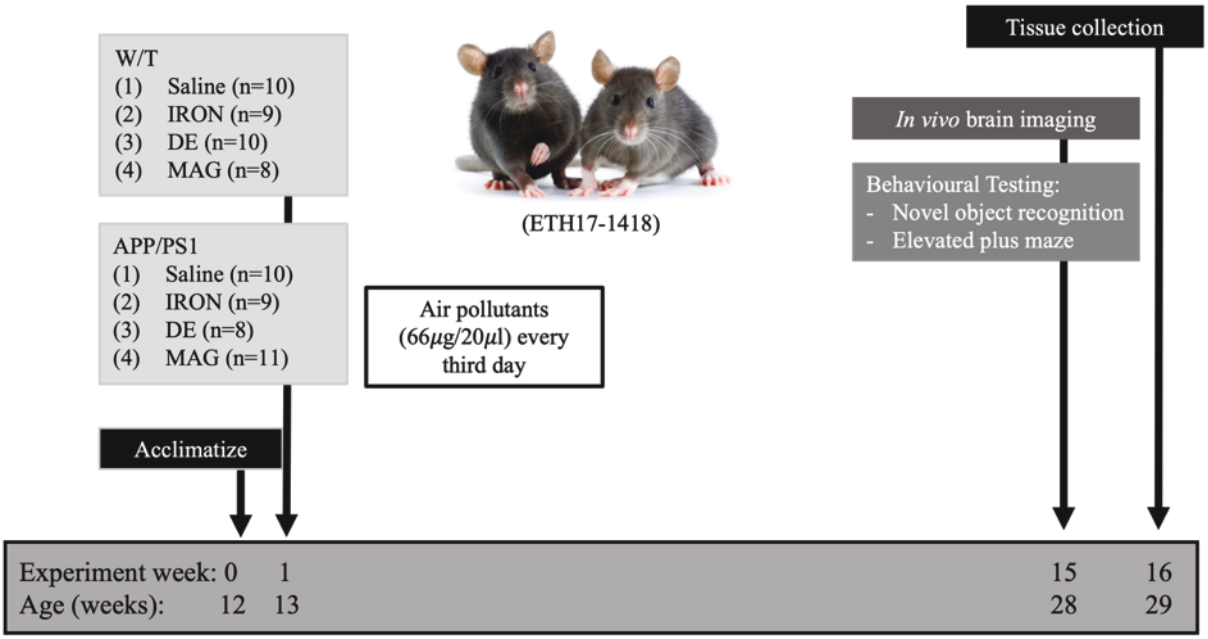

Figure S4.1. A timeline summary of the *in vivo* study. After 1 week of acclimatizing the mice were divided into eight groups to receive either saline, IRON, DE or MAG (66 µg/20 µL) every third day. In week 15 the mice underwent behavioural testing and *in vivo* brain imaging, and in week 16 the tissue was collected.

Table S4.1. Primary and secondary antibodies used in western blot analysis

Protein	Dilution	Company	Catalogue
β-Actin	1:1000	Cell Signalling Technology, MA, USA	4970
BDNF	1:1000	Abcam, UK	108319
GFAP	1:1000	Abcam, UK	33922
ICAM-1	1:1000	Abcam, UK	53013
Iba-1	1:1000	Abcam, UK	178847
iNOS	1:200	Cell Signalling Technology, MA, USA	12282S
Cox2	1:500	Cell Signalling Technology, MA, USA	13120S
Phospho-Tau (pS214)	1:500	Invitrogen, CA, USA	44742
ChK Total Tau	1:500	Abcam, UK	75714
NF-κB p65	1:1000	Cell Signalling Technology, MA, USA	8242T
Phospho-NF-κB p65 (Ser536)	1:1000	Cell Signalling Technology, MA, USA	3033T
MAPK p38	1:1000	Cell Signalling Technology, MA, USA	8690S
Phospho-MAPK p38	1:1000	Cell Signalling Technology, MA, USA	4511S
JNK	1:1000	Cell Signalling Technology, MA, USA	9258S
Phospho-JNK	1:1000	Cell Signalling Technology, MA, USA	4668S
Anti-rabbit Secondary (HRP conjugated)	1:5000	Cell Signalling Technology, MA, USA	7074P2
Anti-mouse Secondary (HRP conjugated)	1:5000	Cell Signalling Technology, MA, USA	7076P2

Table S4.2. PCR Primer Sequences for qPCR analysis

Specie	Gene ID	Description	F/R	Primer Sequences (5'-3')
Mouse	IL-6	Interleukin 6	F	GAACAACGATGATGCACTTGC
			R	TCCAGGTAGCTATGGTACTCC
	TNF	Tumour necrosis factor	F	CTATGTCTCAGCCTCTTCTC
			R	CATTTGGGAACTTCTCATCC
	GAPDH	Glyceraldehyde 6phosphate dehydrogenase	F	GCTCACTGGCATGGCCTTCCG
			R	GTAGGCCATGAGGTCCACCAC

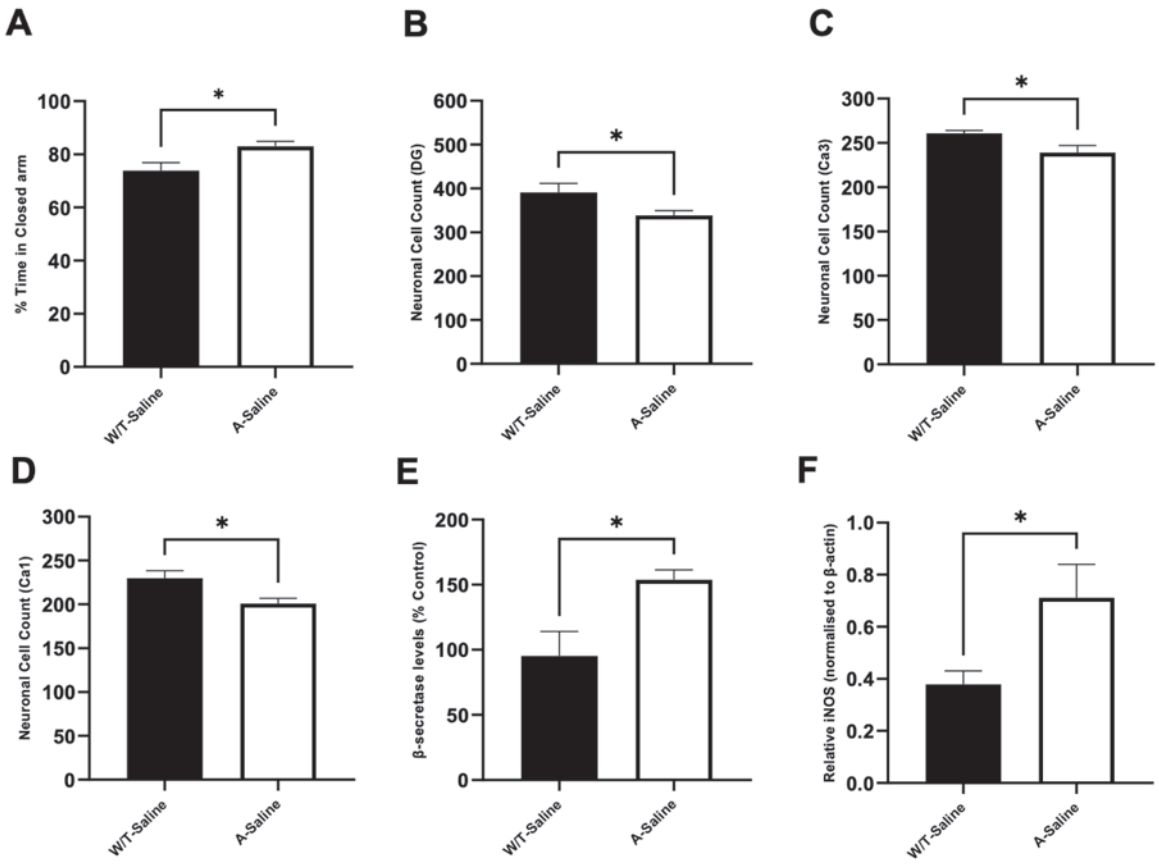

Figure S4.2. *In vivo* studies comparing the AD pathologies in WT saline and APP/PS1 saline mice. (**A**) Behavioural analysis of time spent in the closed arm in the EPM for WT and APP/PS1 saline mice, *$p < 0.0225$. (**B**) Neuronal cell counting in the DG region for WT and APP/PS1 saline mice, *$p < 0.0419$. (**C**) Neuronal cell counting in the Ca3 region for WT and APP/PS1 Saline groups, *$p < 0.0439$. (**D**) Neuronal cell counting in the Ca1 region for WT and APP/PS1 Saline groups, *$p < 0.0321$. (**E**) Percentage increase of β-secretase levels in plasma, for WT and APP/PS1 Saline groups, ($n = 8$), *$p < 0.0283$. (**F**) Relative iNOS protein expression levels in the cerebral cortex, for WT and APP/PS1 saline groups, normalised to β-actin ($n = 5$-8), *$p < 0.0451$. All error bars indicate mean +/- SEM.

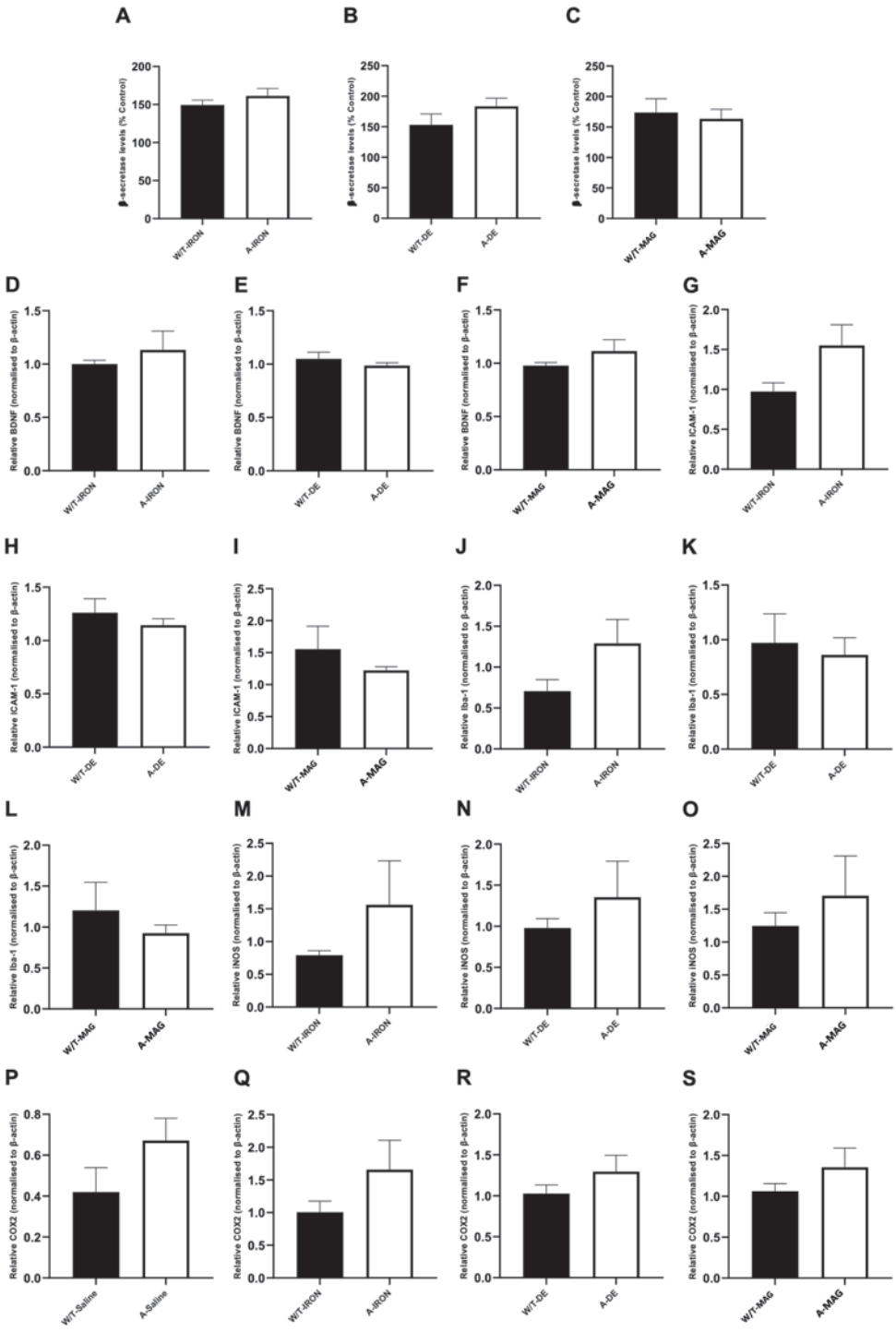

Figure S4.3. *In vivo* studies comparing the AD pathologies in the WT air pollutant particles and APP/PS1 air pollutant particles exposed mice. Percentage increase of β-secretase levels in plasma, for **(A)** WT and APP/PS1 iron groups (n = 8), **(B)** WT and APP/PS1 diesel groups (n = 8), **(C)** WT and APP/PS1 magnetite groups (n = 8). Relative BDNF protein expression levels in the cerebral cortex, **(D)** WT and APP/PS1 iron groups, **(E)** WT and APP/PS1 diesel groups, **(F)** WT and APP/PS1 magnetite groups, normalised to β-actin (n = 5-8). Relative ICAM-1 protein expression levels in the cerebral cortex, **(G)** WT and APP/PS1 iron groups,

(H) WT and APP/PS1 diesel groups, **(I)** WT and APP/PS1 magnetite groups normalised to β-actin (n = 5-8). Relative Iba-1 protein expression levels in the cerebral cortex, **(J)** WT and APP/PS1 iron groups, **(K)** WT and APP/PS1 diesel groups, **(L)** WT and APP/PS1 magnetite groups normalised to β-actin (n = 5-8). Relative iNOS protein expression levels in the cerebral cortex, **(M)** WT and APP/PS1 iron groups, **(N)** WT and APP/PS1 diesel groups, **(O)** WT and APP/PS1 magnetite groups normalised to β-actin (n = 5-8). Relative Cox2 protein expression levels in the cerebral cortex, **(P)** WT and APP/PS1 saline groups, **(Q)** WT and APP/PS1 iron groups, **(R)** WT and APP/PS1 diesel groups, **(S)** WT and APP/PS1 magnetite groups normalised to β-actin (n = 5-8)**.** All error bars indicate mean +/- SEM.

Chapter 5: Insights from a bibliometrics-based analysis of publishing and research trends on cerium oxide during 1990-2020

Intend to submit as:

Fleming, C., Wong, J., Golzan, M., Gunawan, C., McGrath, K., 2021. Insights from a bibliometrics-based analysis of publishing and research trends on cerium oxide during 1990 – 2020. *Dovepress.*

Chapter Summary

The field of nanomaterials as industrial, environmental, and of greater interest for biomedical applications has expanded due to the advancements in nanoparticle engineering, and in turn the range of pathological conditions for which nanomaterials may be used for. Relevant to this thesis, CeO_2 has been a prevalent nanomaterial, surfacing as a potential neurodegenerative and AD therapy, therefore a greater understanding of its properties and characteristics is necessary. Hence, this chapter describes the systematic literature review on the CeO_2 research trends from 1990-2020, discovering its remarkable properties and its extensive use in a variety of applications including environmental/industrial and biomedical.

Insights from a bibliometrics-based analysis of publishing and research trends on cerium oxide during 1990-2020

Charlotte Fleming[1], Jessie Wong[1], Mojtaba Golzan[2], Cindy Gunawan[3#], Kristine McGrath[1#*]*

1. School of Life Sciences, Faculty of Science, University of Technology Sydney, Sydney, NSW 2008, Australia
2. Vision Science Group, Graduate School of Health, University of Technology Sydney, Sydney, NSW 2008, Australia
3. ithree Institute of Infection, Immunity and Innovation, University of Technology Sydney, Sydney, NSW 2008, Australia

Email:
Kristine.McGrath@uts.edu.au, Cindy.Gunawan@uts.edu.au
#These authors share senior authorship

Authors' contributions:

CF conducted the search, identified the studies, performed the systematic analysis and wrote the first draft of this manuscript. JW contributed to the initial interpretation and first draft of this manuscript. KM and CG conceptualized the study and supervised CF. KM and CG revised and edited the manuscript, and MG provided further edits to the manuscripts. All authors contributed to interpretation and revision of the manuscript. All authors have read and approved the final version of the manuscript.

Charlotte Fleming	Production Note: Signature removed prior to publication.
Mojtaba Golzan	Production Note: Signature removed prior to publication.
Jessie Wong	Production Note: Signature removed prior to publication.

Cindy Gunawan	Production Note: Signature removed prior to publication.
Kristine McGrath	Production Note: Signature removed prior to publication.

Insights from a bibliometrics-based analysis of publishing and research trends on cerium oxide during 1990-2020

Charlotte Fleming[1], Jessie Wong[1], Mojtaba Golzan[3], Cindy Gunawan[2*], Kristine McGrath[1*]

[1] School of Life Sciences, University of Technology Sydney, Sydney, NSW, Australia

[2] iThree Institute, University of Technology Sydney, Sydney, NSW, Australia

[3] Graduate School of Health, University of Technology Sydney, Sydney, NSW, Australia

*These authors contributed equally as senior author

Correspondence:

Dr Kristine McGrath/Dr Cindy Gunawan

University of Technology Sydney

PO Box 123, Broadway

Ultimo, NSW, 2007, Australia

Ph: 612 9514 9773

Email: kristine.mcgrath@uts.edu.au or cindy.gunawan@uts.edu.au

5.1 Abstract:

Background: Research into nanomedicine is influencing the trajectory of therapies for various diseases, using nanoparticles (1-100 nm in diameter). Cerium oxide nanoparticles have received attention due to their environmental, industrial and more recently, biomedical applications. This report aimed to assess research trends on cerium oxide from 1990-2020 and identify gaps in knowledge in its emerging application(s).

Methods: Bibliometric methods were used to identify themes in database searches extracted from PubMed, Scopus and Web of Science Core Collection using SWIFT-Review, VOSviewer and SciMAT software programs. A systematic review was then completed on the published cerium oxide literature extracted from the Scopus database (n = 17, 115), identifying themes relevant to its industrial, environmental and biomedical applications.

Results: A total of 172 publications were included in the systematic analysis and categorized into four time periods with research themes; "doping additives" (n = 5, 1990-1997), "catalysts" (n = 32, 1998-2005), "reactive oxygen species" (n = 66, 2006-2013) and "pathology" (n = 69, 2014-2020). The catalytic features of cerium oxide nanoparticles were prevalent themes in the first two periods, followed by a pivot into the biological effects in more recent periods, with an increased focus on nanoparticle engineering development. China and the USA showed the highest number of citations for articles published in the past 30 years.

Conclusion: Longitudinal analysis shows cerium oxide has been extensively used for various applications due to its catalytic properties. Advancements in nanoparticle engineering like doping, and more recently surface modification or functionalization have further enhanced its antioxidant abilities. In more recent years, CeONP additives were able to broaden its potential for therapy in a range of pathologies, including neurodegenerative diseases like AD. Consequently, this study presents the versatility of cerium oxide, however, addresses the necessity to investigate the potential beneficial but also adverse effects that its extensive application may have on human health.

Keywords: nanoceria, nanoparticles, composition, applications, biomedicine, review

5.2 Introduction

Cerium oxide (CeO_2), also referred to as nanoceria, is a well-known rare earth element of moderate abundance, found in the lanthanide group in the periodic table (380). Over the years, CeO_2 has received much attention because of as a biomedicine, due to its extraordinary catalytic ability (381-385). The numerous applications of CeO_2 are due to its unique structural properties, altering its electron configuration such that it can exist in both the trivalent (Ce^{+3}) reduced state and the stable tetravalent (Ce^{+4}) oxidized state (380). This property enhances oxygen storage and release (i.e., antioxidant), resulting in its ability to regenerate, based on the redox cycling in its immediate environment (108, 386, 387). Cerium (Ce), when added to oxygen (O_2) in nanoparticle formulation (CeONPs) adopts a cubic crystalline structure, akin to a fluorite type structure, enabling the rapid diffusion of oxygen as a function of the number of oxygen vacancies (108, 380).

CeONPs have been extensively used in the biomedical field, particularly harnessing its antioxidant mimetic properties, reflecting the behaviour of enzymes like superoxide dismutase (SOD), catalase, and peroxidase, targeting and scavenging reactive oxygen species (ROS) and reactive nitrite species (RNS) (388). Widespread application of these nanoparticles includes as an antioxidant, anti-inflammatory, antibacterial, anti-cancer activity and as drug delivery agents, due to the redox imbalances that play an underlying role in a myriad of pathological conditions (107, 389, 390). While this shows the advantages of CeONPs as biomedicines, studies have also found that CeONPs can induce toxicity, however it is dependent on dosage, and nanostructure size, shape, morphology, and composition. The aim of this study is to conduct a bibliometric analysis of the literature on CeO_2 over thirty years from 1990 - 2020 highlighting key research elements, focusing on the various applications of CeONPs but also the nanoparticles structural integrity for different research purposes, which will aid in current and future studies.

5.3 Material and methods

Topic Modelling

The PubMed (https://pubmed.ncbi.nlm.nih.gov/) database was used to search the term "*cerium oxide OR ceria OR nanoceria OR nano ceria"* from 1990 – 2020 (accessed on 17th September

2020). The publications extracted (129 publications; included research and review articles) were exported as a PMID list file and imported into the SWIFT (Sciome Workbench for Interactive Computer-Facilitated Text-mining) - Review software **(**https://www.sciome.com/swift-review/**)**, where the articles were segregated based on keywords, then organized into topic models of cerium oxide research and ranked in order from most to least prevalent topics. To enlarge the search range, other databases were used as a source of bibliographic data. All databases were accessed in September and October 2020.

Bibliometric Analysis

Bibliographic data (title, abstract, all citations) for the period of 1990 - 2020 were exported (txt file) from the Web of Science Core Collection (WoS) database (accessed on the 17th of September 2020) using the search "*cerium oxide OR ceria OR nanoceria OR nano ceria".* The dataset was then imported into the VOSviewer software **(**www.vosviewer.com**).** Any duplicates in the search were removed and a bibliometric analysis (yielding 7, 862 publications), was performed based on co-occurrence of authors keywords in the paper title (9, 253 keywords) using full counting, which was then further refined to a minimum of 20 occurrences, yielding 144 keywords.

Longitudinal Study

A bibliographic search was performed to undertake a review of the literature over the past three decades, using the Scopus database (accessed on the 9th of October 2020) with the search term "*cerium oxide OR ceria OR nanoceria OR nano ceria"* from 1990 - 2020. The dataset was exported (authors keywords) and imported into Science Mapping Analysis Software Tool (SciMAT) (https://sci2s.ugr.es/scimat/) software for analysis. Within the data set, identical and similar words were grouped to identify the literature trends and themes. Publications were reviewed in four time periods (1990 - 1997, 1998 - 2005, 2006 - 2013 and 2014 - 2020) for ease of investigation in a chronological manner, using the workflow presented in Figure 5.1. Normalization of all the publications was completed using the analysis function, focusing on keywords and specifically authors keywords, with a frequency reduction minimum of 10, a co-occurrence matrix, the edge value reduction of 8, normalization of association strength, simple algorithm centres and core mapping was used. The quality index (h-index) was used, and for the longitudinal analysis, the inclusion index was used on the overlapping map and the

Jaccard's index was used for the evolution map. The important motor-themes (main themes) in each period were identified by their location in the upper right-hand quadrant of the strategic diagram generated by SciMAT software.

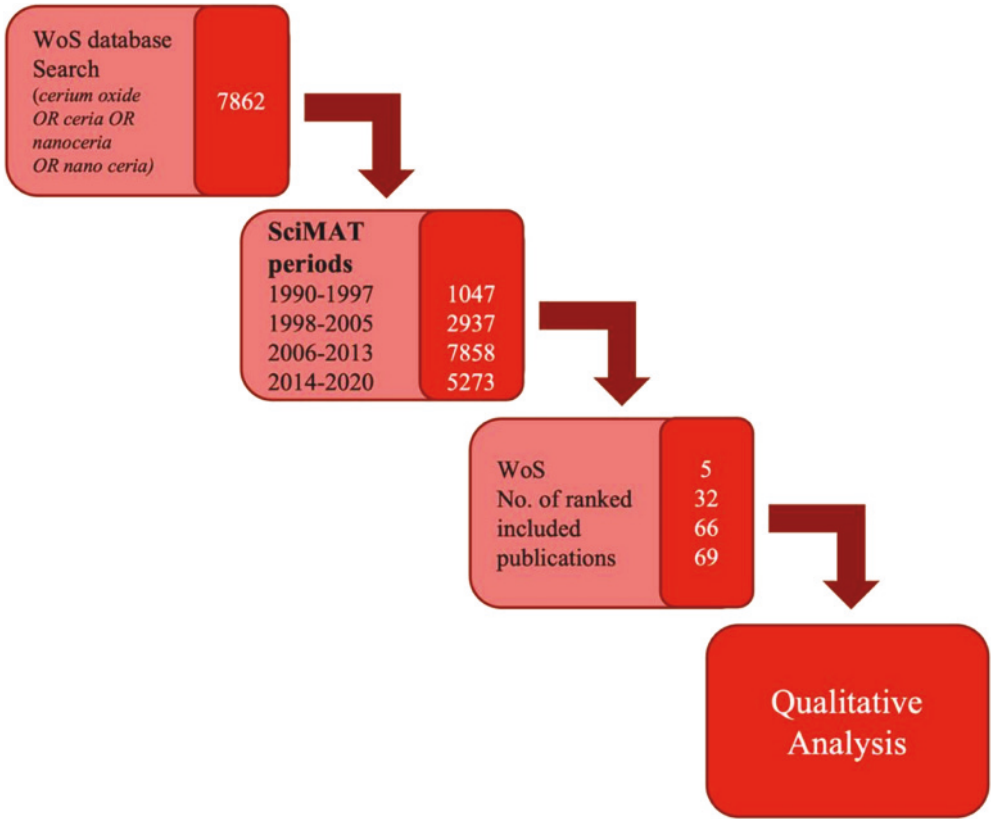

Figure 5.1. Graphical depiction of the systemic literature review process of the WoS database (numbers represent the number of publications analysed at that step).

Systematic Review of literature

Using the four main motor themes generated from the SciMAT software, a systematic review of the peer-reviewed literature was carried out using the Scopus database (accessed on the 9th of October 2020). In this search, the four main motor themes identified in SciMAT were included in the time frame of 1990 - 2020 (e.g., "*cerium oxide OR ceria OR nanoceria OR nano ceria AND doping additives AND catalyst AND reactive oxygen species AND pathology, 1990 - 2020")*. The publications were restricted to the relevant time period related to the motor theme. The publications were assessed according to the Field Citation Ratio (FCR) for all time periods. A total of 172 publications were included in this analysis. A FCR value of greater than

6 was included, indicating peer-acknowledged quality for each publication in this review. Reviews, editorials and short communication were excluded from further analysis.

Author Network

To establish a co-authorship network, the dataset obtained from the WoS database (new format, RIS file), from the search *cerium oxide OR ceria OR nanoceria OR nano ceria* in the years 1990 – 2020 (accessed on the 9th of October 2020) was imported into VOSviewer software. A bibliographic database search, using full counting method, was then completed for co-authorship which resulted in 25, 580 authors identified. The authors were further refined by a minimum of 10 documents and 10 citations per author (used as the inclusion criteria for pear-acknowledge quality, h-index) yielding 68 authors. The authors affiliations, number of citations, along with the affiliated countries were recorded and the percentage of citations per country were calculated to determine the frequency of "magnetite' research around the world. The percentage of citations per country was calculated and ordered by most to least.

5.4 Results

The results from the three databases using the search terms "*cerium oxide OR ceria OR nanoceria OR nano ceria"* yielded the highest number of publications regardless of the database used. A large difference in the number of publications returned between the databases was noted, with WoS returning ~ 238 % and ~ 180 % more papers compared to PubMed and Scopus, respectively (Table 5.1). The search term "*cerium oxide OR ceria OR nanoceria OR nano ceria AND pathology"* returned the smallest number of publications with ~ 57 % less for WoS, ~ 87 % less for PubMed and ~99 % less Scopus.

Table 5.1. Summary of the number of papers identified in searchers of different databases (PubMed, WoS and Scopus) using the search terms "*cerium oxide OR ceria OR nanoceria OR nano ceria"* from the years 1990 - 2020.

Search Terms	**PubMed**	**WoS**	**SCOPUS**
Cerium oxide	122	27674	22467
Cerium oxide AND nanoparticles	59	16252	738

Cerium oxide AND pathology	17	13350	193
Cerium oxide AND toxicity	29	14533	624

Notes: Accessed on the 17th of December 2020, and covered the article, title, abstract, and keywords.

Topic modelling

Using the PubMed database, the search "*cerium oxide OR ceria OR nanoceria OR nano ceria"* was completed, yielding 129 publications which was imported into SWIFT-Review software. The SWIFT-Review software analysed the articles and segregated them based on keywords, where they were then categorized into topic models and organized in ranking order. The SWIFT-Review software found 100 topic models with an overview of the top 19 topic shown in Figure 5.2. Table 5.2 presents the top 19 models, including a brief summary and description formulated to clearly explain the categorized topics (based on the topic model in the review by Reichel et al. 2020) (391). The topics identified mainly focus on the biomedical applications of CeONPs, focusing on targeted treatments highlighting the oxidative properties and surface modifications. This search was completed to identify the main research themes of CeONPs studies conducted from 1990-2020, and to identify the focus and applications of their use.

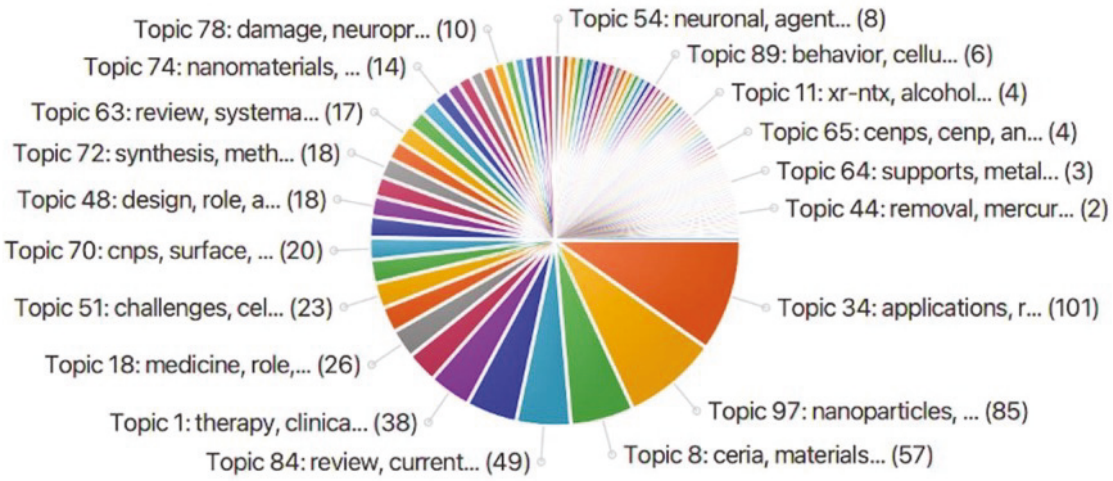

Figure 5.2. The top 19 topic models formulated from the dataset collected from PubMed (129 publications) with the SWIFT-Review software, using the search term "*cerium oxide OR*

ceria OR nanoceria OR nano ceria". This search was refined to review, clinical trials, meta-analysis, and research articles. Accessed on the 17th of September 2020.

Table 5.2. Top 19 topic models generated from PubMed dataset (129 publications) by SWIFT-Review software using the search terms "*cerium oxide OR ceria OR nanoceria OR nano ceria"*. This search was refined to review, clinical trials, meta-analysis, and research articles. The topics have been ordered by number of publications contributing to the topic model in descending order, with topic words and themes established.

Topic No.	Topic word	No. of Publications in Topic Model	Brief Description of Topic
34	Applications, properties, synthesis, review, biomedical, advances	101	Properties for biomedical applications
97	Nanoparticles, oxide, cerium, review, activity, properties, oxidative, research	85	Oxidative Properties
8	Ceria, materials, surface, application, energy, properties, systems, structure, material	57	Surface materials and structure
84	Current literature, include, increase, therapies, existing conditions	49	Therapies
5	Antioxidant, potential, species, effects vivo reactive, stress, biological, ROS, oxygen	46	Antioxidant properties
1	Therapy, clinical outcomes, patients, improved, scientific approaches	38	Clinical approaches
93	Catalysts, catalytic, reactions, oxidation, reaction, ceria-based, catalyst, high activity, organic	28	Catalytic properties
18	Medicine, role, toxicity, regenerative, promising, industry, recent	26	Medicinal therapies
21	HIV, trial, study, incarcerated, months, release, randomized, results, observed treatment	23	Randomized trials
51	Challenges, cells, order, progress, systems, target, addition, improve, medical barriers	23	Targeted treatments
28	Model, studies, hydrogen, techniques, design, kinetics, water-gas, knowledge, modelling, advanced	21	Kinetic studies
70	CNPs, surface, oxygen, vacancies, lattice, results, experimental, presence, evidence	20	Surface structure
86	Nanoceria, cells, CONPs, particles, anti-cancer, data, point, improve, agent normal	19	Anti-cancer agent
48	Design, role, aims, emissions, reviews, interest, carbon, focusing, develop, materials	18	Carbon emission materials
69	Health, effects, exposure, fuel, engineered, risk, toxicological, studies, air	18	Air pollution
72	Synthesis, methods, synthetic, number, template, products, implications, function, metals, enhanced	18	Synthesis methods
38	Treatment, development, growth, pathway, inhibitors, target, tumour, kinase, receptor, phase	17	Tumour kinase pathway
63	Review, systematic, studies, outcomes, articles, results, reported, included published, gaps	17	Systematic reviews
85	Control, research, populations, article, needed, major, practice, describes, provided, discussion, gaps	16	Research gaps

Notes: Accessed on the 17th of September 2020. Refined to review, clinical trials, meta-analysis, and research articles.

Bibliometric Analysis

To examine the broad development of literature in the research associated with CeONPs, the search "*cerium oxide OR ceria OR nanoceria OR nano ceria"* in the years 1990-2020 was implemented in the WoS database, yielding 7, 862 publications. To create a visualization of the co-occurrence of all keyword terms, the extracted dataset (title, abstract and author keywords) was imported into the VOSviewer Software (www.vosviewer.com, Universiteit Leiden, Leiden, Netherlands, Version 1.6.15). The main characteristics obtained from an analysis of the co-occurrence of keywords included the frequency and proximity of similar words. The keywords were further refined to a minimum of 20 occurrences, yielding 144 keywords, then designated by VOSviewer into 9 main cluster groups (Table 5.3). Each cluster represents major themes of CeO_2 studies between 1990 - 2020. Important findings within each cluster are established with a lay description (Table 5.3) and a corresponding visualization map with the clusters coded by colour presented in Figure 5.3. Cluster 1 (red) refers to the biocompatibility and antioxidant properties of CeONPs in biomedicine. Some of the clusters are closely associated; clusters 2 and 4 (green and yellow respectively) highlight the different doping additives, as well as changes in the nanostructure to increase efficiency in various applications. Clusters 3 (blue), 5 (purple) and 6 (aqua) all refer to CeONP application in environmental remediation and industrial implementation as biofuels. Cluster 7 (orange) refers to CeONPs as additives to biofuels and as a potential therapy for wound healing. Lastly, clusters 8 (brown) and 9 (pink), mention the oxygen defects (vacancies) on the surface and antioxidant activity of CeONPs. This analysis identified nanoparticle engineering enhancements and also specific fields of nanoparticle use (i.e., environmental remediation) which are further investigated.

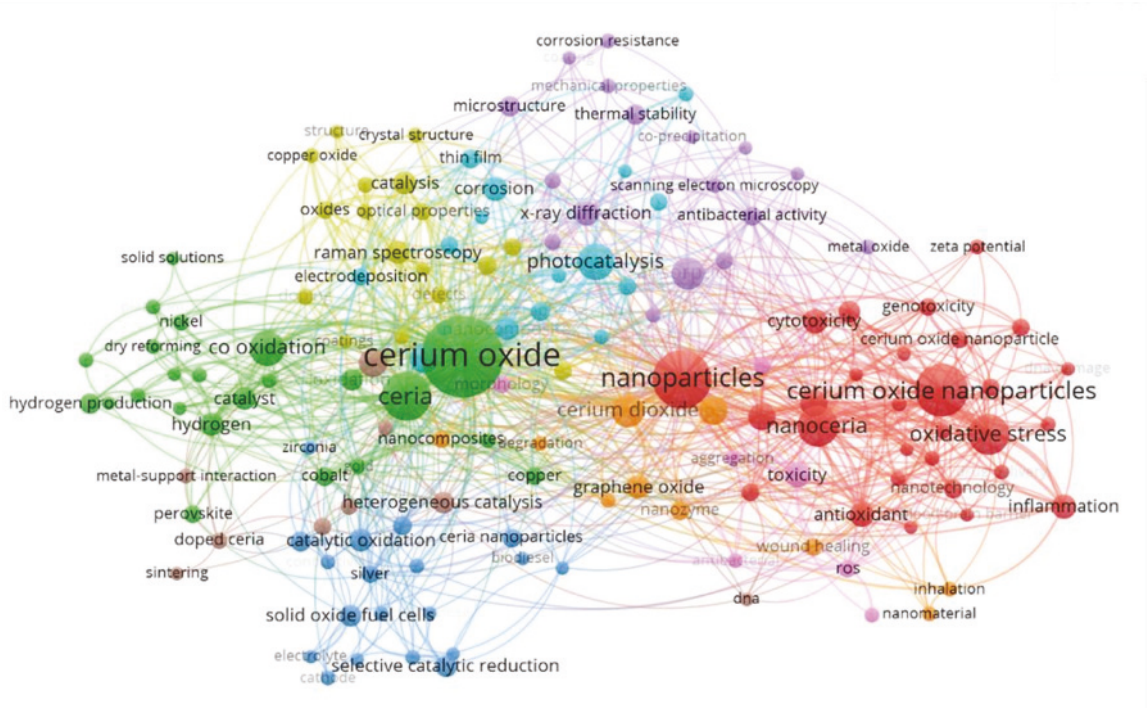

Figure 5.3. Network visualization map showing nine color-coded clusters produced using the VOSviewer and the WoS Database with the search "*cerium oxide OR ceria OR nanoceria OR nano ceria"*. The network analysis from 7, 862 publications and 144 author key words, from 1990 - 2020. The colours represent the clusters of keywords presented in Table 5.3. Access on the 17th of September 2020.

Table 5.3. Summary of the word clusters identified using VOSviewer and WoS dataset using the search term "*cerium oxide OR ceria OR nanoceria OR nano ceria"*. The network analysis from 7, 862 publications from 1990 - 2020. The clusters are also represented in a visualisation map (Figure 5.3).

Cluster	Lay/Description	Keywords
1	Biocompatibility as a biomedical application	Antioxidant, apoptosis, biocompatibility, blood-brain-barrier, catalase, cerium oxide nanoparticles, cytotoxicity, drug delivery, genotoxicity, inflammation, nanoceria, nanomedicine, nanotechnology, oxidative stress, translocation
2	Surface coating additives	Catalyst, cerium oxide, cobalt oxide, copper, hydrogen production, hydrogen peroxide, hydrogen production, interface, methane, nickel, oxygen reduction reaction
3	Catalytic properties remediation	Biodiesel, catalytic oxidation, cathode, ceria nanoparticles, conductivity, electrolyte, manganese oxide, metal oxides, methanol, palladium, reaction mechanism, stability
4	Manufacturing alterations	Catalysis, ceramics, coatings, copper oxide, crystal structure, defects, doping, nanostructures, optical properties, oxides, photocatalytic activity, ramen spectroscopy, solid solution, structure
5	Advancements in thermal stability	Adsorption, antibacterial activity, co-precipitation, coating, corrosion, resistance, electron microscopy, hydrothermal synthesis, kinetics, mechanical properties, metal oxide, microstructure, thermal stability, x-ray diffraction
6	Advancements in manufacturing (nanocomposites) improved efficiency	Corrosion, electrochemical sensors, electrodeposition, ionic conductivity, lanthanum oxide, mechanism, nanocomposite, oxygen vacancies, photocatalysis, rare earth metals, reduced graphene oxide, thin film, titanium dioxide, zinc oxide
7	Degradation, air pollutant and biomedical applicant	Catalytic ozonation, cerium dioxide, degradation, graphene oxide, inhalation, nanomaterial, nanozyme, wound healing
8	Catalytic interaction of doped cerium oxide	Doped ceria, heterogenous catalysis, metal-support interaction, oxygen vacancy, sintering, synergistic effect
9	Antioxidant activity	Aggregation, anti-bacterial, antioxidant activity, morphology, ROS, silver nanoparticles, toxicity

Note: Accessed on the 17th of September 2020.

SciMAT

Scientific research on CeO_2 has shifted over the last 30 years, with studies focusing on the manufacturing alterations of CeONPs to enhance a specific purpose, followed by the exploitation of its remarkable catalytic and antioxidant abilities, into the most recent years revealing its application on the biomedical field as a drug agent and therapy (Figure 5.4). This is shift is reflected in the longitudinal bibliometric study performed using the SciMAT software, from the Scopus dataset (17, 115 publications). The results show a clear trajectory of CeO_2 research interests, initially focusing on the manufacturing alterations Between 1990 - 1997 (n = 1, 047) the term "doping additives" emerged as a main theme suggesting the manufacturing alterations and additives to CeONPs (e.g. doping/coating, loading, nanocomposites and hybrid nanostructures) and morphological alterations with associated terms like "copper-oxides", "crystal defects" and "crystal lattice", indicating that this period aimed to enhance the properties of CeO_2 (Figure 5.4A). The term "catalyst" appeared as a main theme in 1998 - 2005 (n = 2, 937) associated with the terms "thermostability", "oxygen transport" and "exhaust gas" suggesting its catalytic role as a potential air pollutant adsorber or a biofuel (Figure 5.4B). In the period of 2006 - 2013 (n = 7, 858 publications), "reactive oxygen species" is a main theme, with terms like "cell survival", "cell death", "free radicals", "catalase" and "glutathione", indicating the research focused on antioxidant properties on cellular models (Figure 5.4C). The final period between 2014 - 2020 (n = 5, 273 publications), found "pathology" as a main theme, with "apoptosis", "cell proliferation" and "drug effect" appearing as associated terms, suggesting that research in this period, focused on CeONPs and its effects on gene expression and cell proliferation as a biomedicine (Figure 5.4D).

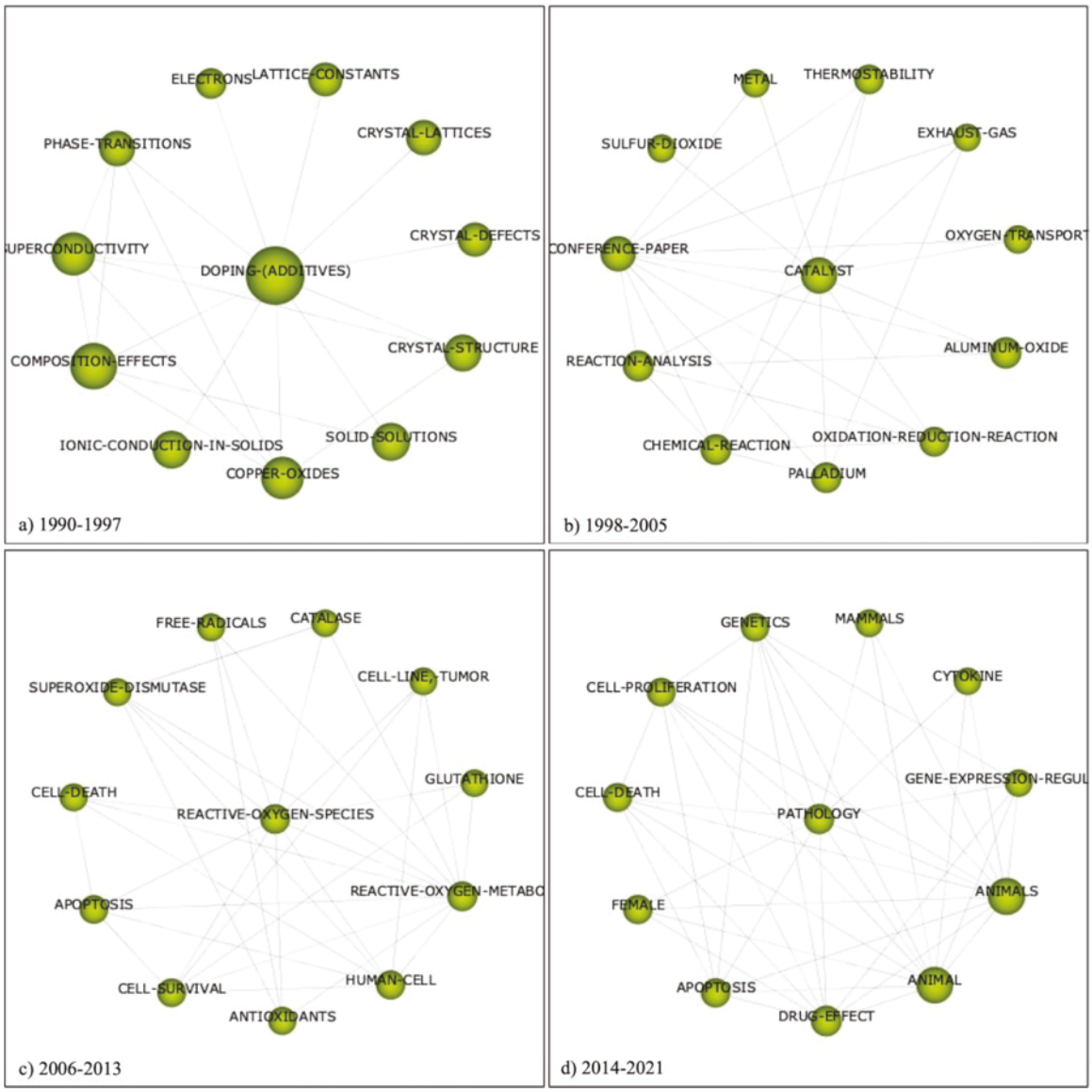

Figure 5.4. Main themes in the cerium oxide related publications from the Scopus database, over four time periods identified using SciMAT software (a) 1990 - 1997 (n = 1, 047); (b) 1998 - 2005 (n = 2, 937); (c) 2006 - 2013 (n = 7, 858); (d) 2014 – 2020 (n = 5, 273). The figure demonstrates the development of cerium oxide investigation and the links in terms of the major themes, identified for each period. Accessed on the 9th of October 2020.

Systematic Review of Literature

A refined search on the Scopus database was then completed to provide a systematic analysis of the literature from each theme identified from the SciMAT software. A total of 172 publications were included in this study, refined by a citation ratio of greater than 6 (peer-acknowledged quality threshold). Figure 5.5 shows the total publications that met the citation criteria; 5 publications were from 1990 to 1997 ("doping additives"), 32 publications from 1998 to 2005 ("catalyst"), 66 publications from 2006 to 2013 ("reactive oxygen species"), and 69 publications from 2014 to 2020 ("pathology").

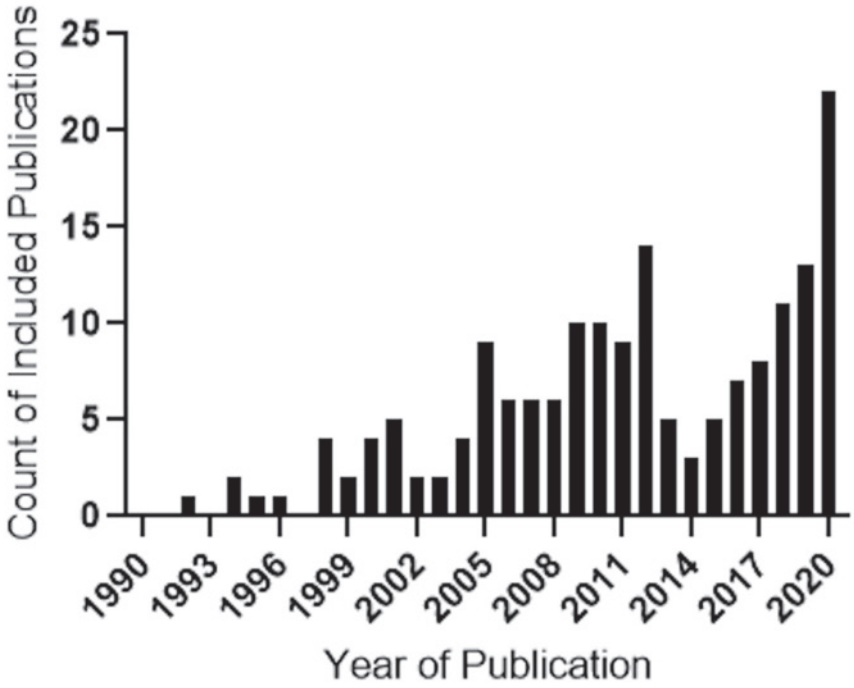

Figure 5.5. Frequency histogram of 172 publications, derived from a systematic search of cerium oxide literature, conducted in the Scopus database for search terms: "cerium oxide OR ceria OR nanoceria OR nano ceria" AND doping-additives/catalysts/reactive oxygen species/pathology, showing the surge of publication activity across all four themes between 2019 - 2020. The year of 2020 demonstrating the highest number of publications. Accessed on 17th of September 2020.

Time period 1990 to 1997 – "Cerium oxide AND Doping-(additives)"

SciMAT extracted five publications from this period meeting the citation ratio of above 6, focusing on the combined environmental and industrial applications of CeONPs. To enhance

CeONPs ionic conductivity for electrolyte fuel cell efficiency, one study doped the CeONPs with zirconia, samaria and gadolinia which resulted in increased oxygen vacancies (or oxygen defects) on its surface, thereby making it more reactive (392). Samaria and gadolinia-doped CeONPs exhibit high electrical conductivity due to the close ionic radii of Sm^{3+} Gd^{3+} to that of Ce^{4+} (392). The reduction of ceria electrolyte at the fuel side could be suppressed by doping with a thin film of stabilized zirconia on the ceria surface (392).

While the theme of this time periods is "doping-additives" of CeONPs, the remaining studies included in this analysis focus mainly on the morphological enhancements of CeONPs due to the FCR threshold implemented. Two publications focused on using bare CeONPs to eliminate contaminants in automobile gas exhaust (393). Bare CeONPs have less oxygen vacancies thereby increasing nanoparticle stability, suitable for interactions between small molecules e.g., hydrogen, carbon dioxide, oxygen and nitric oxide (393, 394). Another publication in this time period focused on the structural properties (i.e., oxygen defects) of CeONPs with numerous studies finding that morphology and surface characteristics greatly influence the behaviour of the nanoparticles, e.g., lattice structure with increased surface area exposed, thereby having more oxygen vacancies, resulting in a less compact nanostructure but increased reactivity (395). The last publication in this time focused on CeONPs as an effective industrial catalyst by increasing the efficient of the WGS reaction, which was achieved at low temperature, thereby conserving energy (394). The research on CeONPs in this period, highlight its potential as an environmental/industrial fuel cell and energy converting catalytic alternative to fossil fuel sources, which is a topic further investigated in successive time periods.

Time period 1998 to 2005 – "Cerium oxide AND Catalyst"

In this time-period, 32 publications met the citation ratio criteria, overlapping themes from the previous period, including the environmental/industrial applications with advancements (e.g., additives to CeONPs) in renewable energy and as a potential biomedicine in its pure form.

The environmental/industrial applications of CeONPs in this period, make up most of the publications (n = 23), and extend on the previous period with different additives and structural changes were further investigated for example the nanocomposite structure (incorporation of

nanosized particles into a matrix of standard material, resulting in improved strength, electrical and thermal properties) (396). Many publications focused on CeONPs as renewable energy sources to replace combustion fuel sources (e.g., natural gas, diesel fuel, biodiesel blends, petroleum and coal), with one study using poly-alkene doped CeONPs in a crystalline form with a porous surface, increasing surface and oxygen vacancies enhancing the thermo-catalytic stability in solar cells to replace organic dyes (384, 397). Gadolinia-doped CeONPs, as a solid fuel electrolyte, was found to have high stability at reduced oxygen pressures improving fuel cell performance while maintaining textural and mechanical integrity, increasing the electrolyte composition therefore making it a promising recyclable renewable source for turbine power (398-400). Other studies highlighted the use of copper and nickel loaded CeONPs, doped with lanthanum in a hybrid nanocrystalline structure (i.e., hybrid - combination of doping, loading, surface functionalized or nanocomposite additives) (401). These hybrid structures were highly dispersed due to the doping and loaded component interactions, enhancing their catalytic activity, through the increased oxygen vacancies of the added components, thereby increasing WGS reaction efficiency (401). CeONPs have also been used as effective pollutant adsorbers, decontaminating wastewater and sediment, with one study using magnesium oxide/ aluminium oxide/titania oxide-CeONPs nanocomposites, for the removal of heavy metals and organic compounds finding that the redox potential to adsorb the contaminants was increased, suggesting the additives and nanostructure enhanced these activities (402-406). CeONPs nanocomposites have also been investigated as highly efficient catalysts (e.g., copper, zirconia, nickel, aluminium/CeONPs nanocomposites) for methane oxidation (methane is a potent greenhouse gas in the atmosphere and needs to be broken down by combustion, producing heat and therefore making it a useful fuel source) (402, 403, 407, 408). These nanocomposite structures are ideal for methane oxidation due to catalytic nature of CeO_2, achievable at lower temperatures, hence conserving more energy. Platinum and gold/CeONPs nanocomposites in a crystal lattice fluorite structure showed increased reactivity and reducibility for a more efficient catalyst in the WGS reaction as the temperature can be lowered allowing for enhanced energy to be conserved (409-413). The morphology of CeONPs (n = 7) has been studied in this period to enhance the properties for a specific purpose, with nano-polyhedral, nano-rods, and nanotubes shown to have increased oxidative properties compared to those of the nanosphere (414). The crystal plane structure of CeO_2 nano-rods, was found to have higher oxidation activity, compared to crystal lattice structure, as more oxygen vacancies are exposed making the structure more reactive and superior fuel cells and environmental remediators (415, 416). A reoccurring theme for environmental/industrial

catalysts in this period, highlight the manipulation in manufacturing nanotechnology to increase oxygen vacancies on the surface of the nanostructures which improves the catalytic activity. This is further explored in the following time period.

The biomedical applications in this period (n = 2) highlighted CeONPs as potential cancer therapies. One study investigated the cellular uptake of polymer micelle coated CeONPs in human lung fibroblasts *in vitro* models (ATCC and MRC-9 cell lines), displaying that these nanostructures had increased adsorption, agglomeration, dispersion, and retention time compared to bare CeONPs, therefore proving to be a superior cancer therapy (417). The second demonstrated that bare CeONPs in a crystal lattice structure showed differential effects with 99% protection against radiation-induced cell death in human breast carcinoma epithelial *in vitro* model (MCF-7 cell line) whilst no protection was conferred for the normal human breast epithelial *in vitro* model (CRL8798 cell line) (418). These studies provide a good foundation into the successive periods of CeONPs as a biomedicine, with its potential as a cancer drug delivery agent and in chemotherapy radiation.

Time period 2006 to 2013 – "Cerium oxide AND Reactive Oxygen Species"

A total of 66 publications met the citation criteria in this period, with overlapping themes from the previous period; CeONPs as an effective environmental/industrial renewable resource for fuel cells and its biomedical application as a cancer therapy. The environmental/industrial uses of CeONPs in this period (n = 47) highlight the manufacturing manipulations focused on increasing the amount of oxygen vacancies through nanoparticle engineering in adjusting the additives and morphology of the nanostructures. Two studies focused on the effectiveness of CeONPs as an electrolyte fuel cell, with studies using samaria- and carbon-based polymer doped CeONP hybrids, increasing oxygen vacancies, inducing higher energy conversion rates that subsequently improved efficiency, coinciding with low emissions (419, 420). Other studies have again highlighted CeONPs as solid electrolyte fuel cells, however in the lattice fluorite structure. This structure improved ionic conductivity and overall efficiency when doped with lower charged cations like zirconia oxide, aluminium oxide and palladium oxide due to the increased oxygen vacancies on the surface and the interactions between these components (421, 422). Of particular significance in this period, was the platinum oxide, titania oxide, copper oxide, and particularly gold oxides/CeONPs nanocomposites, extensively investigated

for further improved efficiency in the WGS reaction (423-431). Adding heterogenous "- oxide" nanoparticles to the CeONP nanocomposite further enhanced the facilitation and formation of oxygen vacancies on the surface, which increased the catalytic activity of these nanostructures (423-431). Various studies used CeONPs nanocomposites (e.g., platinum and zirconia/CeONPs) for remediating automotive exhaust gas, finding that the nanowire structure (having increased oxygen vacancies) further improving catalytic and recyclable efficiency (432-436). These studies display the innovative advancements in nanostructure engineering enhancing the efficiency of the catalytic property, which is enhanced through the increased amount of oxygen vacancies thereby increasing reactivity with surrounding molecules. This increased reactivity allows CeONPs to effectively scavenge and reduce free radicals like superoxide (O_2^-), hydroxide (OH^-), hydroxyl (OH) and hydrogen peroxide (H_2O_2), nitric oxide (NO) and peroxynitrite ($ONOO^-$) which are volatile ROS and are produced from various biological processes like automotive exhaust gas and other pollutant bio-products, thereby appropriate for environmental remediation (37). This ROS scavenging is also prevalent in the biomedical application of CeONPs.

The biomedical research on CeONPs (n = 15) in this period further investigated the potential of CeONPs and exploited the advancements in nanoparticle engineering additives like doping, surface modification and nanocomposites. CeONPs have been found to be protective against ischemic stroke in a cardiac progenitor *in vitro* model showing no toxicity, in fact increasing cell viability and decreasing apoptosis compared to copper and zinc nanoparticles (437-439). CeONPs have also been used as probes in bioanalysis and diagnostic tests, in the form of a bioactive sensing paper for glucose and H_2O_2 testing to replace the use of organic dyes, measuring multiple cycles (440). Studies have shown that CeONPs have antioxidant catalytic properties, having the capacity to mimic superoxide dismutase (SOD), specifically converting superoxide to oxygen and hydrogen peroxide with high specificity and efficiency, highlighting its ability to scavenge ROS and RNS and therefore an effective antioxidant (222, 441, 442). Doping consists of the insertion of a specific ion into a crystal lattice structure, not originally present in the starting material whereby coating consists of a thin film, applied to the surface, encapsulating a nanomaterial (443). Doping of CeONPs with polymers (e.g., polyacrylic acid, animated poly (acrylic acid), dextran-coated) were found to enhance CeO_2 ability to mimic oxidase-like activity, enhancing targeting abilities and increasing cellular uptake in *in vitro* models (lung carcinoma - A549, cardiac myocytes - H9c2, embryonic kidney - HEK293 and

breast carcinoma - MCF-7 cell lines) (444, 445). In addition to enhancing its oxidase-like ability, dextran-doped CeONPs was exhibited neuroprotective effects in the human dermal fibroblast *in vitro* (HDF cell line) model via its ROS scavenging ability (112). One study investigated polymer-like (polyethylene glycol; PEG) doped CeONPs to enhance circulation of the nanoparticles in the blood stream, showed a reduction to non-specific binding and increase uptake into organs, in an ovarian hamster *in vitro* model (CHO-K1 cell line) (446). Whilst doping served to enhance its antioxidant catalytic property it has also been found to increase retention time, with one study reported in a human bronchial epithelial *in vitro* model (16HBE cell line) that surface modified/functionalized CeONPs with ligands stabilized the antioxidant abilities of CeO_2 (447). Another study investigated yttrium oxide/CeONP nanocomposites on a nerve cell *in vitro* model (HT22 cell line) finding that they exhibit neuroprotective properties, reducing oxidative stress and cell toxicity (448). These studies show the broad range of biomedical uses and disease pathologies which CeONPs could be used for, highlighting the nanotechnology advancements which improve the biocompatibility of the nanostructures (e.g., increased circulation time and cellular uptake). These studies have directly influenced the biomedical applications of CeONPs in the following period (2014 - 2020).

Four publications in this period reported the potential toxicity and hazards that CeONPs and other nanoparticles poses to human health and the environment. Exposing pure CeONPs to a human lung epithelial *in vitro* model (A549 cell line) induced cell death with increased catalase, glutathione (GSH) and reductase enzymes reported (449). These enzymes are effective ROS scavengers and plays key roles in the inflammatory and oxidative stress pathways (449). Another study found that CeONPs induced oxidative damage and led to decreased lifespan in an *in vivo* model (*Caenorhabdotis Elegans* cell line) (450). Similarly, exposure of CeONPs decreased cell viability and increased ROS production in a human skin melanoma *in vitro* model (A375 cell line) (451). In acidic conditions the antioxidant ability of CeO_2 nanoparticles is lost, behaving instead much like a strong oxidant, which may influence the oxidation of intracellular and extracellular components to induce apoptosis (111). This ability to become cytotoxic has been found to induce oxidative stress, could be attributed to cancer cells being more acidic than normal cells (112, 113). The bifunctional characteristic of CeONPs allows it to exhibit both ROS scavenging and cytotoxic effects is possible due to its ability to change structural composition in valency depending on the environment (106, 114).

These toxicology studies provide insight into the various therapeutic applications of CeONPs, which is further examined in the final period of CeO_2 research.

Time period 2014 to 2020 – "Cerium oxide AND Pathology"

This period yielded the highest number of publications (n = 69), with the highest number of publications (n = 22) from a single year (2020). Following on from the previous period, the broad themes are the same, with most publications highlighting the environmental/industrial applications of CeONPs, with several studies focusing on its biomedical uses.

Environmental/industrial applications of CeO_2 make up most of the publications in this period (n = 63) like the previous period, CeONPs were investigated as renewable resources, efficient fuel cells, and remediating the environment through implementing hybrid CeONPs complexes. Of particular interest is the advancement of the single atom catalyst, with one study using platinum single atoms on the surface of CeONPs (surface modified/functionalized support) demonstrating higher reactivity, better selectivity and less agglomeration when heated, resulting in a superior compound compared to the platinum/CeONPs nanocomposite complex (452). The fluorite lattice structure of CeONPs were exploited in this period with studies using various additives (e.g., titania/CeONPs, lanthanum/CeONPs nanocomposites and nickel, zirconia oxide/CeONP nanocomposites surface functionalized with palladium) for methane combustion and removal of organic dye (e.g., Rhodamine-B dye) with enhanced catalytic performance compared to bare CeONPs (453-455). Another study found that CeONPs supported platinum-selenium clusters (as surface modified/functionalized additives) extending the catalytic reaction which unearthed full regeneration, increased dispersibility and stability of the complex for CO oxidation (456). The use of the core-shell nickel encapsulated between silica oxide/CeONP nanocomposites was useful in reforming biogas, leading to increased nickel dispersion and reductivity, compared to nickel-silica or nickel-ceria alone, therefore resulting in the development of a potential sustainable hydrogen fuel source (457). All these studies extend on the previous periods of CeONPs research further highlighting the versatility of CeO_2 manipulation, leading to additional advancements in catalytic control and improved performance from an environmentally conscious and industrial perspective.

The remaining publications highlight the biomedical applications of CeONPs in this period are consistent with the environmental/industrial applications in terms of exploiting the advanced nanoparticle engineering of doping, loading, nanocomposite, surface functionalization and hybrid complexes to enhance their function. Following on from the previous period, montmorillonite loaded CeONP nanocomposites and porphyrin surface modified/functionalized CeONPs have been explored as diagnostic tools to detect hydrogen peroxide (H_2O_2) and glucose (458, 459). These nanostructures were found to exhibit peroxidase (enzyme that reacts with H_2O_2 to catalyse oxidation of a number of inorganic compounds in samples) like catalytic activity demonstrating a colorimetric sensitive and specific method, indicating its potential for biochemical assays, clinical diagnosis and environmental monitoring (458, 459). Advancing the idea of CeONP as a therapy in cancer in this time period, one study demonstrated the use of manganese doped-CeONP nanocomposites inducing higher cytotoxicity effects in an adenocarcinoma *in vitro* model (MCF7 cell line) compared to bare CeONPs (460). The enhanced cytotoxic effect is likely due to the higher oxygen vacancies generated from adding manganese, producing increased ROS generation which target and kill the cancerous cells, therefore demonstrating its potential as a promising cancer targeting therapy (460). The bifunctional properties of CeONPs allow it to change its role from antioxidant to pro-oxidant, depending on its surrounding environment, with an acidic environment inducing a pro-oxidant cytotoxic property allowing it to target cancer cells (110). CeONPs as a drug delivery agent was also investigated for its use in acute kidney injury (AKI). In this instance, exposure of surface modified/functionalized CeONPs with triphenylphosphine, doped with an ROS-responsive organic polymer (PEG - polylactic acid-glycolic acid copolymer), and further loaded with atorvastatin, resulted in protection against tubular cell apoptosis and tubular necrosis in an LPS-induced AKI *in vivo* model. This study showed the successful modification of CeONPs to target the kidney and selectively release the drug in response to ROS (461). Another study highlighted CeONPs as an effective drug delivery agent, using CeONPs encapsulated within zeolithic imidazole framework-8. This nanostructure could penetrate the blood brain barrier (BBB), accumulate in the brain tissue and reduce oxidative damage and apoptosis of neurons, in an ischemic stroke middle cerebral artery occlusion (MCAO) *in vivo* mouse model, indicating its potential as a therapy for ischemic stroke (462). CeO_2 as neuroprotective agent has further been investigated, with one study adding triphenyl phosphonium (TPP)-conjugated CeONPs as potent ROS/RNS scavengers due to its recyclable ability, reducing oxidative stress in an *in vivo* Alzheimer's disease (AD) mouse model (5XFAD transgenic mice) (463).

The advancements in nanoparticle engineering in this period is clear, with extensive use of doping, nanocomposite, surface functionalized or hybrid (doped and nanocomposite) nanostructures, designed for their specific purpose, considering the morphology, surface texture and additives. The biomedical applications of CeONPs in this period, for their ROS scavenging abilities, as anti-inflammatory therapy, as a diagnostic testing method and of particular interest, the neuroprotective properties for neurological diseases and neurodegeneration.

Author Network and Countries with Most Citations for Cerium Oxide research

The **s**ystematic literature search found a wide range of ground-breaking research into CeONPs over the last 30 years identifying advancements in nanoparticle engineering which has increased the understanding of CeO_2 properties whilst uncovering a larger body of scientific work for renewable resources, solid fuel cells, along with its potential as cancer, inflammatory and neuroprotective therapies. To evaluate the authors contributing to CeO_2 research, an author network was created from the dataset obtained from the WoS database (7, 862 publications) using the term "*cerium oxide OR ceria OR nanoceria OR nano ceria"* in the years 1990 - 2020 (accessed on the 17$^{th\ of}$ September 2020). The data from this search was imported into the VOSviewer software, where a bibliographic database search was completed for co-authorship using full counting method resulting in a total of 25, 580 authors. The authors were further refined by a minimum of 10 documents and 10 citations per author (using as an inclusion criterion for peer-acknowledged quality, h-index) which resulted in 68 authors **(**285**)**. Figure S5.1, represents these authors in an overlay visualization network providing the years in which these authors have published. The author's affiliations and number of citations were recorded and the percentage of citations per country was calculated and ordered by most to least citations (Figure 5.6). The top 11 countries were identified, showing the highest number of citations from China, encompassing a total of 37 %, indicating that China has led the world in CeO_2 over the last 30 years. Other countries like USA (26 %), Iran and India (8 %), Canada (5 %), Sweden and Spain (4 %), Italy (3 %), Czech Republic (3 %), Netherlands (1 %) and Russia (0.4 %) have also contributed to CeO_2 research over the past 30 years.

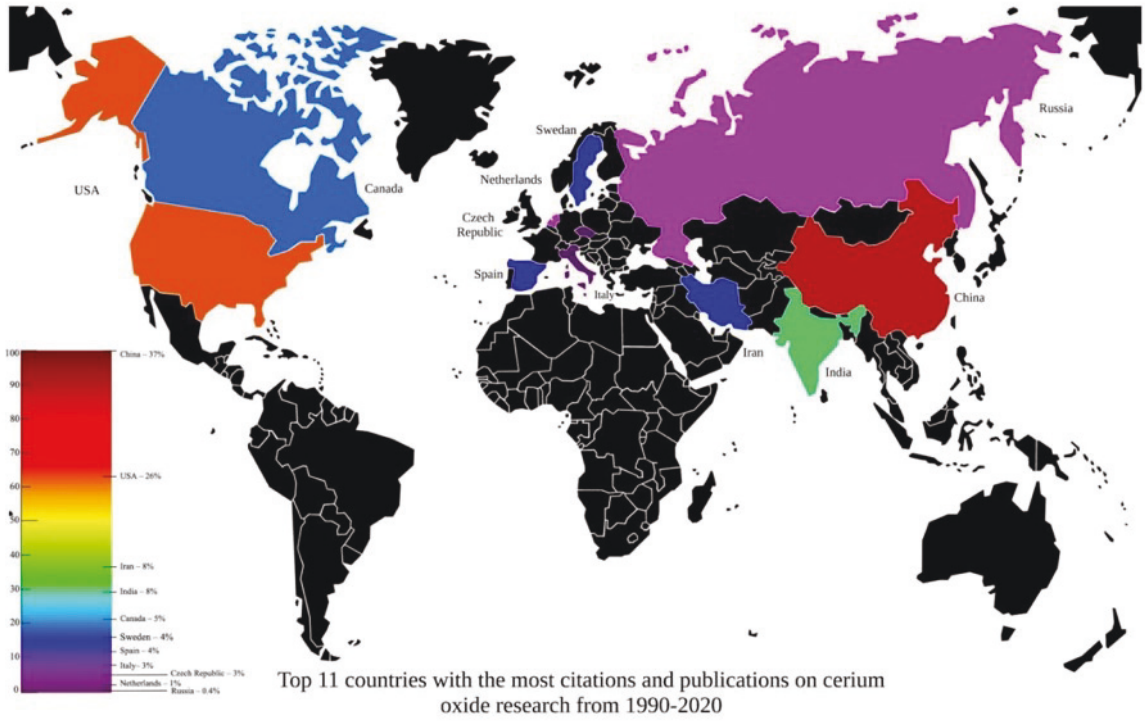

Figure 5.6. Top 11 countries, with the highest citations (minimum 10) and documents (minimum 10) per authors, grouped by country affiliations. Extrapolated from the dataset obtained from the WoS database, using the term "*cerium oxide OR ceria OR nanoceria OR nano ceria"* in the years 1990 - 2020. Accessed on the 9th of October 2020.

5.5 Discussion

This systematic literature analysis found that the research on "*cerium oxide*" has developed over the past three decades from initially focusing on understanding the unique physicochemical properties of cerium oxide, into the extensive environmental and industrial applications, and finally focusing on CeONPs as a biomedicine. The biomedical applications of CeONPs in the more recent time periods have uncovered the advancements in nanoparticle engineering (e.g., dopants, coating, surface functionalization, core-shell structures, nanocomposites, and hybrid structures). CeONPs additives were able to increase the already remarkable biological effects of CeONPs as cancer therapeutics, for therapy in inflammatory disease and as diagnostic tools. Moreover, its unique ability to induce cytotoxic effects to cancerous cells whilst inducing protective effects against cytotoxicity in non-cancerous cells indicates its potential for development as therapy for range of pathologies (Figure 5.7).

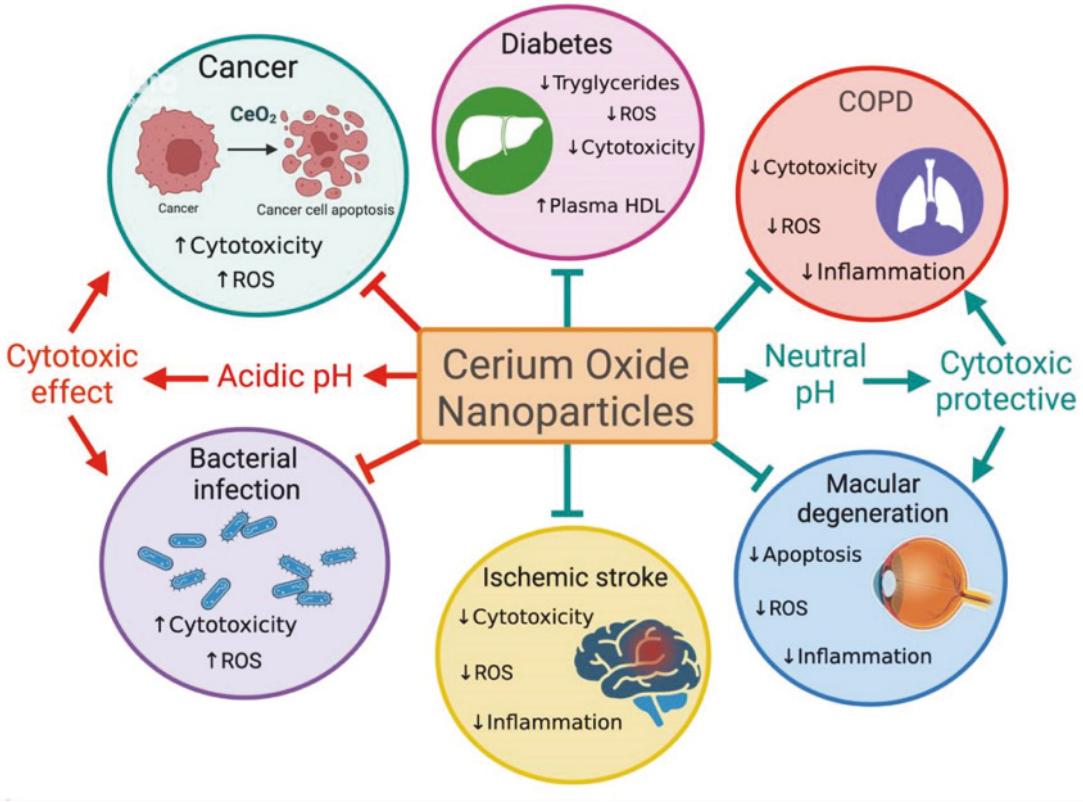

Figure 5.7. Graphical depiction of the various biomedical applications of cerium oxide nanoparticles as therapies for a wide range of pathologies including cancer, diabetes, cardiovascular pulmonary disease, macular degeneration, ischemic stroke and bacterial infection due to the bifunctional nature of CeO_2. In acidic conditions the antioxidant ability of CeO_2 nanoparticles is lost, behaving instead much like a strong oxidant, which may influence the oxidation of intracellular and extracellular components to induce apoptosis. This ability to become cytotoxic has been found to induce oxidative stress, could be attributed to cancer cells being more acidic than normal cells. Created with BioRender.com

The scientific literature on CeO_2, over the past 30 years, presented in the topic modelling found the catalytic applications of CeONPs was prominent particularly in the WGS reaction. However, most of the topics that were identified referred to the potential biomedical applications, highlighting its oxidative, antioxidant, catalytic and anti-cancer properties. Further analysis of the topic models using the VOSviewer software, identified nine clusters, highlighting the various fields and developments of CeONP applications largely focusing on the surface and morphological alterations of the nanostructures across various environmental/industrial and biomedical fields.

The SciMAT software was used for a systematic literature analysis, established themes for each time-period. The first period (1990 - 1997) focused on the environmental/industrial applications of doped and undoped CeONPs, for the enhancement of solid fuel electrolyte cells found to increase the efficiency of the WGS reaction to replace non-renewable resources (e.g., coal, natural gas, oil and nuclear energy) (464). Replacing non-renewable resources is a major problem for humanity, however, is necessary to create an environmentally sustainable lifestyle. The WGS reaction is significant for this, reforming hydrocarbons to produce hydrogen as an energy source (464). Fuels produced from hydrogen can be used as direct replacements for oil and gas as low carbon emitting alternatives, which is more environmentally sustainable (465). CeONPs have been found to be a more effective catalysts for the WGS reaction compared to noble gases (e.g., platinum and manganese) and transition metals (e.g., copper) due to its oxygen storage capacity, facilitated by the ability of transitioning from the trivalent (Ce^{3+}) to the tetravalent (Ce^{4+}) state (466). This property is enhanced by doping CeONPs with various metal (e.g., platinum, manganese, nickel, cobalt, zirconia and gold) and non-metal (e.g., silica and selenium) catalysts, achieving a powerful catalytic system with increased surface area exposing more oxygen vacancies, resulting in long-term stability and reproducibility, as well as higher CO conversion activity at lower temperatures (464, 467-469). In light of these enhanced properties, doping, another manufactured additive is highly utilized in this period and has been shown to be crucial in influencing and controlling the surface reactivity of CeONPs. The doping of CeONPs in this period, focused on increasing the oxygen vacancies (active sites) overall improving catalytic performance and compatibility. This suggests that increasing oxygen vacancies for improved performance is an alteration that is still investigated currently with various studies using additives like titania, lanthanum, zirconia, palladium, yttrium and zinc CeONP structures which have increased oxygen vacancies as environmental remediators (e.g., degrade crystal violet dye, Rhodamine-B dye and methane combustion) (453-455, 470).

The environmental/industrial and biomedical application using CeONPs in the second period (1998 to 2005) continued to focus on the manufacturing alterations of CeONPs to further enhance its performance. The environmental/industrial applications of CeONPs highlight the influence that chemical composition has on its catalytic activity regarding the WGS reaction and environmental remediation. As the catalytic performance relies heavily on oxygen vacancies, the crystal plane and nanorod morphologies of CeONP were found to exhibit the

highest catalytic performance compared to crystal lattice, nanocube and nanosphere structures (414-416). The increased oxygen vacancies had significant impact on the electrostatic surface charge of the nanostructures which affect the agglomeration rate and overall stability of the complex (466). Nanocomposites incorporate nanosized particles into a matrix, which has increased oxygen vacancies compared to single nanoparticle structures, but also has enhanced reducibility due to the interactions that occur between the nanoparticles in the matrix further improving catalytic performance (396). CeONPs nanocomposites combined with copper, nickel, zirconia, aluminium, platinum and gold nanoparticles have been extensively used for the WGS reaction in this period (471). CeONPs nanocomposites are still investigated currently in renewable energies, with a study highlighting the use of silica oxide/CeONPs nanocomposites in reforming biogas, and a potential sustainable hydrogen fuel source (457).

Consistent with the environmental/industrial applications of CeONPs in this period (1998 to 2005), manipulations of CeONPs size, morphology, and additives were investigated for its biomedical application, particularly as a cancer targeting therapy. CeONPs have been found to have anti-tumour properties, becoming cytotoxic towards cancer cells pro-oxidant producing ROS to target them (i.e., pro-oxidant), whilst having little to no effect to the surrounding healthy cells (110). This is due to the enzymatic abilities in effectively switching valence states from the Ce^{3+} (reduced form) to the Ce^{4+} (oxidised form) donating an electron (106, 109). Nanoparticle studies have found that sharp edged, large nanostructures are less biocompatible as they may inflict mechanical damage on cell membranes and organelles while triggering an immune response (466). A study using ultrafine bare CeONPs, whilst being an effective ROS scavenging agent, also exhibited cell differentiation protective qualities, targeted and inducing cytotoxicity in a breast carcinoma *in vitro* model (MCF-7 cell line) (418). Another study showed that tumour cells create an acidic environment, which induces oxidant like behaviour in CeONPs. This study used murine fibrosarcoma tumour cells (WEH164 cell line) which were injected in the flank of a murine *in vivo* model (BALB/c). The CeONPs (< 50 nm) were extremely efficient in targeting and aggregating at tumour site, finding that enhanced permeability and retention plays a crucial role in delivering the CeONPs to tumour cells (472). These studies provide further evidence for CeONPs as potent ROS scavengers, and potential as effective cancer therapies. Of note, doping CeONPs for biomedical applications surfaced in this period, showing clear advantages, in preventing agglomeration and toxicity compared to undoped equivalents (466). This is consistent with a study that used dextran-coated CeONPs

in an osteosarcoma *in vitro* model (MG-63 cell line), finding that these nanostructures induced increased toxicity compared to bare-CeONPs. This effect was shown to be dose dependent with increasing toxicity as dextran coating concentration increased (473). Another study using polymer-doped CeONPs in a human lung fibroblasts *in vitro* model (ATCC and mRC-9 cell lines) demonstrated rapid adsorption, increased retention time and increase dispersion, compared to the bare CeONP equivalent (417). Doping CeONPs has been found to improve its antioxidant abilities, more effectively scavenging ROS/RNS, enhancing solubility, stability and dispersion of the nanoparticles, which is further investigated in successive time periods (474). These studies suggest that CeONPs are effective anti-cancer therapies due to their unique ability to differentiate between healthy and cancerous cells with polymer coated CeONPs showing enhanced efficacy in this ability to target the cancerous cells.

The third period (2006 to 2013), saw further developments in the environmental/industrial applications of CeONPs as a heterogenous catalyst (multiple catalysts in a nanocomposite structure). The use of metal oxide/CeONPs nanocomposites as heterogenous catalysts were used having increased oxygen storage for the WGS reaction (475). This is seen in a study using metal (platinum, titania, gold) oxide/CeONPs nanocomposites to generate a more efficient catalyst, as the hybrid materials incorporated into the crystal lattice structure provide active support and new oxygen vacancies at the metal oxide/CeONPs interface (475, 476). The biomedical applications in this period, provided support for CeONPs as an anti-cancer agent, however, transitioned into targeting inflammatory driven diseases and wound healing, highlighting its antioxidant abilities. CeONPs are effective cancer targeting therapies due to the pro-oxidant properties which they exhibit (112, 113). These mechanisms of CeONPs are highly reliant on the pH of the surrounding environment being more acidic (pH 6) which is attributed to cancer cells being more acidic than normal cells (477-479). In a more alkaline pH (e.g., pH 7, 9) the antioxidant abilities of CeONPs are exhibited, inducing strong ROS scavenging properties (111). This bifunctional property is due to alternating valence states and hence the ability to regenerate oxygen vacancies, which are active sites for redox reactions (ROS/RNS scavenging) to take place (388, 466). This property of CeONPs is important because oxidative stress is considered central to the progression of chronic inflammation and inflammatory diseases (480). A study used micro-RNA 146a (miR146a)/CeONPs nanocomposites to treat a colitis *in vivo* murine model (C57BL/6), finding that this nanostructure induced an anti-inflammatory and antioxidant response, decreasing

inflammatory cytokines; tumour necrosis factor (TNF) and interleukin 6 (IL-6) coinciding with reduced oxidative stress (481). Similarly, *in vitro* models, adipocyte (3T3-L1 cell line) and myoblast (C2C12 cell line) of diabetes mellitus were exposed to selenium/CeONPs nanocomposites, showing a decrease in extracellular ROS production (482). These studies show that CeONPs nanocomposites are potent ROS scavengers in reducing oxidative stress and inflammation. Oxidative stress has been found to increase bone loss and limit bone repair through the formation and maintenance of low-grade chronic inflammation. Spherical CeONPs, exhibited immune protective effects, by enhancing cell proliferation, osteogenic differentiation and mineralization using on a murine macrophage *in vitro* model (RAW264.7 cell line) and human bone derived mesenchymal stem cell model (hBMSCs cell line). This study showed the multifunctional effects of CeONPs for healthy tissue and bone regeneration under acute or chronic conditions (483). These studies further demonstrate the remarkable properties of CeONPs as a potent anti-inflammatory and antioxidant agent, demonstrating their potential use in a wide variety of inflammatory associated diseases. CeONPs nanocomposites emerging in this period highlight the advancements in nanoparticle manufacturing, pioneering current nanotechnology research studies.

The most recent period (2014-2020) showed a significant development in environmental/industrial applications of CeONPs in the single atom catalysts for the WGS reaction. Single atom catalysts have been developed to increase catalytic performance, due to the increased dispersion rate and the active sites encapsulated on the support structure, achieving higher turnover rates compared to larger nanoparticles (464). One study used a platinum single atom supported on CeONP catalysts (1.7 nm in diameter), reported a high number of surface oxygen vacancies and increased dispersibility, due to the synergistic effects of platinum and CeO_2 (484). Noble metals atomically dispersed on solid oxide supports have currently become the superior form of heterogenous catalysis, with palladium doped CeONPs single atom catalysts having increased interactions between the metal-support crucial to maintain stability (485).

The CeONPs biomedical applications in this period are the most interesting, identifying a clear trajectory of research into CeONPs as therapies for neurological diseases and in particular neurodegenerative diseases. CeONPs have emerged as potential neurodegenerative therapies

due to the ease at which these nanoparticles can be manipulated to adjust the size and additives, for passage through the BBB. One study investigated the effects of CeONPs in an anaplastic astrocytoma *in vitro* model (grade II glioma), displaying selective cytotoxicity targeting astrocytoma cells (486). PEG coated CeONPs can easily cross the BBB, therefore various studies exploring treatment for ischemic stroke and multiple sclerosis (MS) have emerged (487). Studies tested these nanoparticles in *in vivo* murine models of ischemic stroke and MS effectively scavenging ROS/RNS and reducing overall oxidative stress injury (486, 487). Another study used citrate EDTA stabilized CeONPs in an *in vitro* murine model (SOD1G93A cell line) of amyotrophic lateral sclerosis (ALS), finding that the ROS/RNS scavenging ability assisted in prolonging lifespan after muscle weakness was observed (487). These studies demonstrate that CeONPs are able to induce both protective and cytotoxic effects efficient against oxidative stress/inflammatory driven diseases as well as cancer (488). This dual effect of CeONPs to be both protective and selectively cytotoxic is remarkable and is found to rely on the surrounding pH (110). In acidic conditions the cytotoxic ability of CeONPs is activated and the antioxidant ability is lost, behaving instead much like a strong oxidant, which may influence the oxidation of intracellular and extracellular components to induce apoptosis in the presence of cancerous cells (111). This ability to become cytotoxic has been found to induce oxidative stress, could be attributed to cancer cells being more acidic than normal cells (112, 113). The bifunctional characteristic of CeONPs allows it to exhibit both ROS scavenging and cytotoxic effects is possible due to its ability to change structural composition in valency and its interaction with the surrounding environment (106, 114, 489). The This makes it an extremely versatile and remarkable compound for various biomedical applications including an efficient drug targeting therapy and also oxidative stress driven diseases like neurodegenerative diseases (106).

CeONPs as a therapy for neurodegeneration and particularly AD has emerged in recent years due to the driving pathological features where oxidative stress and inflammation is now recognized as playing a key role in disease progression (490, 491). Various studies have tested CeONPs in human neuroblastoma *in vitro* model (SH-SY5Y cell line) treated with amyloid-beta (Aβ) protein (protein that aggregates and forms Aβ senile plaques, a hallmark pathology of AD) (487, 492). Similarly, the use of CeONPs but coated with an anti-amyloidogenic agent, inhibited amyloidogenic activity with no toxicity present in an *in vitro* human glial model (U87MG cell line) (493). These studies highlight CeONPs antioxidant, anti-inflammatory and

neuroprotective properties, as well as the ability to permeate the BBB, for its development as a promising therapy for neurological and/or neurodegenerative diseases like AD.

The advancements in nanotechnology over the years have led to the extensive applications of CeONPs in the environmental/industrial and biomedical fields. Whilst the use of CeONPs have mostly been beneficial, adverse effects have been reported. For example, increased dosage and sized of CeONPs was associated with varied toxicity levels and apoptosis in human neuroblastoma cells (IMR32 cell line) (494). Similarly, oxidative stress and cytotoxicity was increased following exposure to CeONPs in human lung adenocarcinoma cells (A549 cell line) (116). In contrast, CeONPs showed neuro- and cardio-protective effects through suppression of decrease ROS and oxidative stress (446, 495). These studies indicate that whilst CeONPs has great potential for biomedical applications, future research is still necessary to optimize CeONPs as a therapy, particularly focusing on dosage, administration, particle composition, size and shape which have known effects on their interactions with molecular mechanisms of various cells and tissues in biological systems (Figure 5.8).

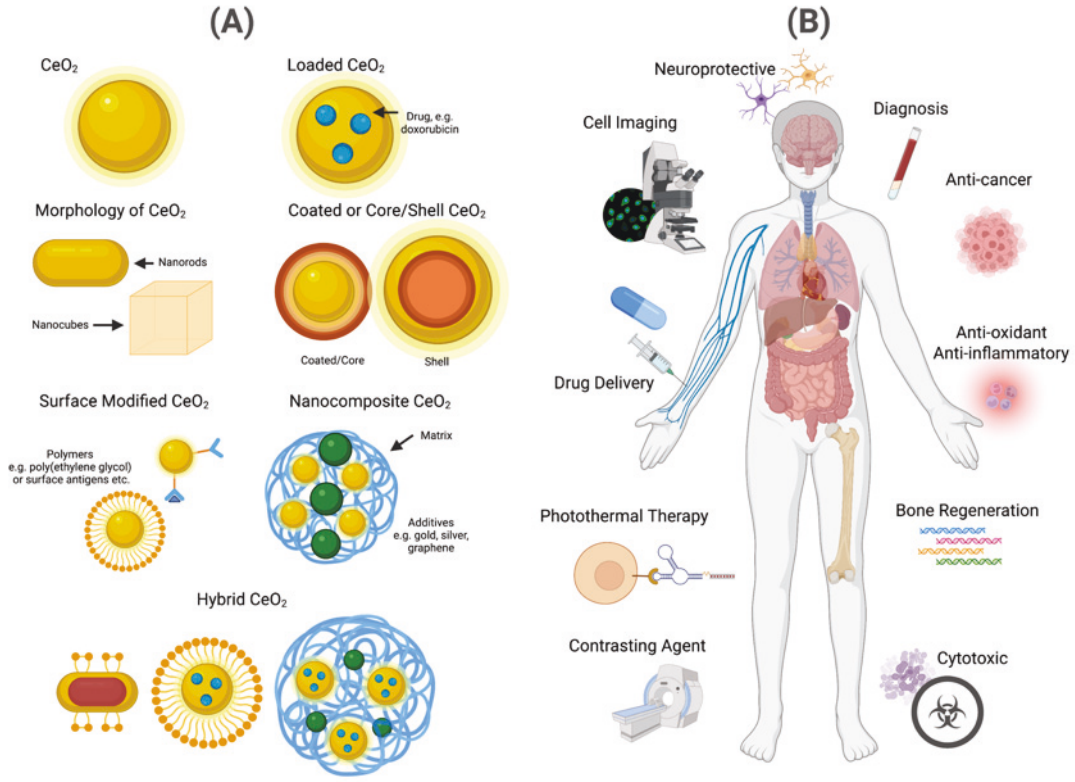

Figure 5.8. Graphical representation of the various nanoparticle engineering manipulations of cerium oxide that have been implemented in various biomedical applications (e.g., drug

delivery agent, diagnosis, anti-cancer agent and contrasting agent etc.). Created with BioRender.com.

5.6 Conclusion

The research over the last three decades on CeO_2 nanoparticles have made progress in environmental and industrial applications as an effective catalyst, for environmental remediation and replacing fossil fuels with renewable resources. The biomedical applications have also increased our understanding of the properties and characteristics of CeO_2, leading to the manipulation and enhancements of CeO_2 nanostructures. The unique redox property of CeO_2 makes it a potent antioxidant when compared with other ROS modulators, including promising applications in cancer, inflammatory diseases, neurological diseases, and neurodegeneration. The key to CeONPs as a neurological therapy, is its facilitation to cross the BBB, which is easily obtainable due to the advancements in nanotechnological engineering. Further research in both *in vitro* and *in vivo* studies need to be undertaken, to fully understand the exact anti-inflammatory mechanism that CeO_2 possesses and the synergistic therapeutic effect of oxidative stress reduction. This will aid in developing therapies for various diseases, showing remarkable potential as a biomedicine for inflammatory diseases, but also for neurodegenerative diseases like AD.

Chapter 6: Effects of cerium oxide nanoparticles in a mouse model of Alzheimer's disease exposed to magnetite pollution particles

Intend to submit as:

Fleming, C., Golzan, M., Amal, R., Esmailour, A., Gunawan, C., McGrath, K., 2022. Effects of cerium oxide nanoparticles in a mouse model of Alzheimer's disease exposed to magnetite pollution particles. *ACS Nano.*

Chapter Summary:

The management of AD is challenging, with current therapies focused on managing the symptoms of the disease, rather than targeting the underlying driving pathological mechanisms. Oxidative stress is a central pathogenic process in AD development, with the antioxidant CeO_2 emerging as a promising therapy. Considering the potential risk that air pollutant magnetite particles have on the development of AD pathologies, this study was conducted to investigate whether CeO_2 nanoparticles could delay or reverse the AD pathologies induced by air pollutant magnetite particles. This study was conducted using a double transgenic APP/PS1 murine *in vivo* model and human neuroblastoma SH-SY5Y and murine microglial BV-2 *in vitro* models. This chapter has been written according to the guidelines of ACS nano of which the manuscript will be submitted to.

Effects of cerium oxide nanoparticles in a mouse model of Alzheimer's disease exposed to magnetite pollution particles

Charlotte Fleming[1], *Mojtaba Golzan*[2], *Rose Amal*[3], *Ali Asghar Esmailpour*[3], *Cindy Gunawan*[4#]*, *Kristine McGrath*[1#]*

1. School of Life Sciences, University of Technology Sydney, Sydney, Australia
2. Vision Science Group, Graduate School of Health, University of Technology Sydney, Sydney, Australia
3. School of Chemical Engineering, UNSW Sydney, Sydney, Australia
4. ithree Institute, University of Technology Sydney, Sydney, Australia

Email:
Kristine.McGrath@uts.edu.au, Cindy.Gunawan@uts.edu.au
#These authors share senior authorship

Authors' contributions:

CF conducted the experiments, collected the data, analysed the data, produced the results and drafted the manuscript. KM contributed to the *in vivo* work. KM, CG and RA conceptualized the study. KM, CG and MJ contributed to result analysis and interpretation and supervised CF. CG revised and edited the manuscript. FT and PI provided the air pollutant iron and diesel particles for this study. RW conducted the particle synthesis and characterization for this study. All authors contributed to the execution and approved the final version of the manuscript.

Charlotte Fleming	Production Note: Signature removed prior to publication.
Mojtaba Golzan	Production Note: Signature removed prior to publication.
Rose Amal	Production Note: Signature removed prior to publication.
Ali Esmailpour	Production Note: Signature removed prior to publication.

Cindy Gunawan	Production Note: Signature removed prior to publication.
Kristine McGrath	Production Note: Signature removed prior to publication.

Effects of cerium oxide nanoparticles in a mouse model of Alzheimer's disease exposed to magnetite pollution particles

Author names Charlotte Fleming[1], Mojtaba Golzan[2], Rose Amal[3], Roong Jien Wong[3], Cindy Gunawan[4]*, Kristine McGrath[1]*

Author address [1]School of Life Sciences, University of Technology Sydney, Sydney, Australia; [2] Vision Science Group, Graduate School of Health, University of Technology Sydney, Sydney, Australia; [3]School of Chemical Engineering, UNSW Sydney, Sydney, Australia; [4] ithree Institute, University of Technology Sydney, Sydney, Australia

Keywords cerium oxide, magnetite particles, air pollutant, nanoparticles, antioxidant, inflammation, Alzheimer's disease

6.1 Abstract

Inhalation of air pollutant nanoparticles are likely candidates for triggering oxidative stress that can impact human health. In recent years, air pollutant magnetite particles found to be present in human brains and has come to light as potentially increasing the risk of Alzheimer's disease. The current therapies for Alzheimer's disease focus on managing the symptoms, rather than targeting the underlying driving forces such as oxidative stress. Herein, we synthesized amorphous blue silica doped cerium oxide nanoparticles with increasing reducing properties, to compare its effects bare to cerium oxide nanoparticles in in vitro (neuronal and microglial cells) and in vivo in an Alzheimer's disease mouse model that were exposed to air pollutant magnetite particles. In vitro, we found that magnetite particles induced oxidative stress and inflammation in the key cells that plays a role in Alzheimer's disease. Both cerium oxide nanoparticles (doped vs. undoped) decreased oxidative stress and suppressed inflammation, in part, via the MAPK and NFκB pathway. In vivo, exposure of magnetite particles induced an increase in (i) pro-inflammatory cytokines, (ii) amyloid plaque, (iii) neuronal loss in the hippocampus region and (iv) short term memory loss that was delayed or perhaps reversed following treatment with cerium oxide nanoparticles. This study demonstrates the detrimental effects of air pollutant magnetite particles whilst showing the potential of cerium oxide nanoparticles in air pollutant induced Alzheimer's disease.

6.2 Introduction

Alzheimer's disease (AD) is the most common form of dementia, accounting for approximately 90 % of all cases (496). It is the fifth leading cause of death in adults over 65 years of age, estimating a total of healthcare costs to be approximately $305 billion, worldwide in 2020 alone (496). Whilst genetics can play a role in the development of AD, 95 % of all AD cases (called Sporadic AD) develop without genetic predisposition (5). The triggers leading to the development of sporadic AD remains largely unknown, however several factors have been recognized to significantly contribute its progression. These include lifestyle factors such as inactivity and environmental factors such as air pollution and underlying health issues such as cardiovascular disease, diabetes, and obesity (497). Air pollution is the fourth greatest overall risk factor for human health, and in recent years has been implicated in neurodegeneration and AD development (498).

It has been reported that nanosized ambient air pollutant particulate matter (< 200 nm in diameter; PM) generated from industrial sources (e.g., fossil fuels, agricultural waste and vehicle emissions etc.) contains a diverse mixture of volatile compounds (e.g., graphite, organic chemicals, carbon monoxide, nitrates, sulphates, iron and iron oxides (magnetite) that can migrate through the blood brain barrier (BBB) and accumulate in the brain (72, 499-501). Moreover, air pollutant magnetite particles were found in abundance in brain samples obtained at autopsy from older people (< 65 years at death) with AD but also from younger people (< 40 years at death) who resided in Mexico City where the average concentration of outdoor ambient air pollution is > 25 µg/m^3, more than double the limit set by the World Health Organization of 10 µg/m^3 (49, 88). Numerous in vivo studies (e.g., male fisher rats, male C57BL/6 mice and CD36-deficient (CD36$^{-/-}$) have explored various vehicle emission air pollutant PM samples, as aerosols to investigate the translocation of air pollutant PM, suggesting that it can migrate into the brain (97, 502, 503). Air pollutant PM have been found to enter the brain through the olfactory bulb via the nasal canal and BBB or be ingested into the lungs translocating into the circulatory system where they are able to enter the brain by passing through the BBB (97, 502). The cellular response in the brain varies based on the chemical composition, size and shape of the air pollutant particles however an overall immune response that is typically activated reflects that of an infection, pathogen or foreign body (502, 503). The immune response attempts to remove foreign material in the brain, resulting in the activation of microglia and astrocytic cells resulting in an increase in neuroinflammation and

oxidative stress after exposure to re-aerosolized PM. The microglia and astrocytic cells are involved in the activation of transcription factors like nuclear factor kappa B (NFκB) and its downstream targets including pro-inflammatory cytokines/mediators such as interleukin-1β (IL-1β), IL-6, tumour necrosis factor (TNF), intercellular adhesion molecular 1 (ICAM-1), inducible nitric oxide synthase (iNOS) and cyclooxygenase 2 (Cox2) (502). Adding to the progression of neuroinflammation is oxidative stress which results from an imbalance in antioxidative defence and the excessive radical production of reactive oxygen species (ROS) and reactive nitrogen species (RNS) (314, 504). This is consistent with an *in vitro* (mixture of astrocyte and microglia primary rat cells) study conducted using the same particulate matter, finding a toxic response coinciding with an increase in inflammatory mediators and an increase in nitric oxide (NO) production - a free radical that contributes to the formation of RNS (502).

While the pathogenesis of AD is still not fully understood, the two hallmark pathologies: extracellular amyloid plaques (Aβ plaques) and neurofibrillary tangles (NFTs) consisting of hyperphosphorylated tau, are thought to be driven by inflammation and oxidative stress (10, 17, 505). A study using an in vivo (male fisher rats) model, showed exposure to aerosolized diesel exhaust emissions over 6 months reported a dose dependent increased in inflammatory cytokines (IL-6, TNF and IL-1β) and Aβ42 protein aggregation (the main component of Aβ plaque deposits) levels in the midbrain (313). While this study refers to carbon-based air pollutants, significant neurotoxicity induced by air pollutant PM has occurred with transition metals in the mixture, as these structures can increase oxidative potential, thereby increasing oxidative stress (502). Maher et al. (2016) (181) found magnetite (a volatile iron oxide nanoparticle that is abundant in our ambient air) in the brains of people with AD. The magnetite nanoparticles were consistent in morphology to combustion derived nanoparticles, formed at high temperatures (e.g., vehicle emissions, electrical powerplants) like the burning of fossil fuels, (e.g., coal, petrol, natural gas, oil shales, and diesel exhaust) for energy (47, 48). Such findings provide evidence that air pollutant particulate matter can mount neuroinflammatory and oxidative responses that can lead to the onset or progression of AD pathologies.

Current therapies for AD focus on managing the symptoms, e.g., cholinesterase inhibitors, donepezil, tacrine, and N-methyl-D-aspartate (NMDA)-receptor modulator memantine (90). While they have been very effective at managing symptoms, the underlying pathologies of the

disease still progress. Disease modifying strategies have been the recent focus for delaying the progression of AD, including targeting the underlying significant factors; oxidative stress and neuroinflammation (103). The brain is the most active organ in the body, highly susceptible to oxidative stress due to the high oxygen content and utilization, therefore antioxidants such as cerium oxide (CeO_2) has surfaced as a potential therapy for neurodegeneration and AD (105). CeO_2 has remarkable enzymatic mimicking abilities of superoxide dismutase (SOD) and catalase, transitioning between the more reduced (Ce^{3+}) and oxidized (Ce^{4+}) state, allowing it to be a highly efficient ROS and RNS scavenger, therefore a promising therapy for neurodegeneration and AD (109, 506). Extensive research on CeO_2 nanoparticles reported its potential to treat a number of diseases of which includes inflammatory and neurological diseases (116). Moreover, CeO_2 nanoparticles have been shown to have the ability to differentiate between cancer vs healthy cells, inducing cytotoxicity and decreasing cell viability via increased ROS production whilst displaying minimal toxicity and providing protection against ROS in normal tissues (507, 508). In acidic conditions the antioxidant ability of CeO_2 nanoparticles is lost, behaving instead much like a strong oxidant, which may influence the oxidation of intracellular and extracellular components to induce apoptosis (111). This ability to become cytotoxic has been found to induce oxidative stress, could be attributed to cancer cells being more acidic than normal cells (112, 113). The bifunctional characteristic of CeO_2 nanoparticles is possible due to its ability to change structural composition in valency depending on the environment (e.g., pH) (106, 114). This makes it an extremely versatile and a remarkable compound for various biomedical applications including neurodegeneration and AD, as oxidative stress plays a significant role in the progression of neurodegenerative diseases (106).

Limitations to using bare CeO_2 nanoparticles however include agglomeration increasing their size to ~ 40 nm in diameter, which reduces cellular uptake, resulting in cytoplasmic accumulation resulting in an increase in ROS production, thereby reducing overall efficiency. Doping of $CeO_{2\ \text{nanoparticles}}$ with polymer, starch, silica oxide has been found to reduce agglomeration, and increase the oxygen vacancies on the nanomaterials surface (enhancing its catalytic and redox properties), inducing higher ROS scavenging abilities in turn, improving its antioxidant and anti-inflammatory capabilities (117, 119). Silica oxide coated CeO_2 ($SiCeO_2$) nanoparticles have been studied previously demonstrated to decrease CeO_2 induced lung inflammatory responses, in the male Sprague-Dawley rats (118). Silica oxide coating also

has found to improve biocompatibility, through increased dispersibility, increased retention rates due to the increased amounts of oxygen vacancies on the surface of the nanoparticle structure, seen in Figure 6.1 (118, 119). Encouraged by these findings, the aim of the current study is two-fold. The first is to investigate the effects of magnetite particles in neuroinflammation and oxidative stress and the second is to investigate the potential of amorphous silica doped CeO_2 that have been further engineered to create more oxygen vacancies and therefore enhanced ROS scavenging ability as a potential therapeutic agent for AD. The characterization of nanoparticles is essential for toxicity studies as the size, shape, surface reactivity, solubility and degree of aggregation is substantial in the differential response in biological systems (115, 116).

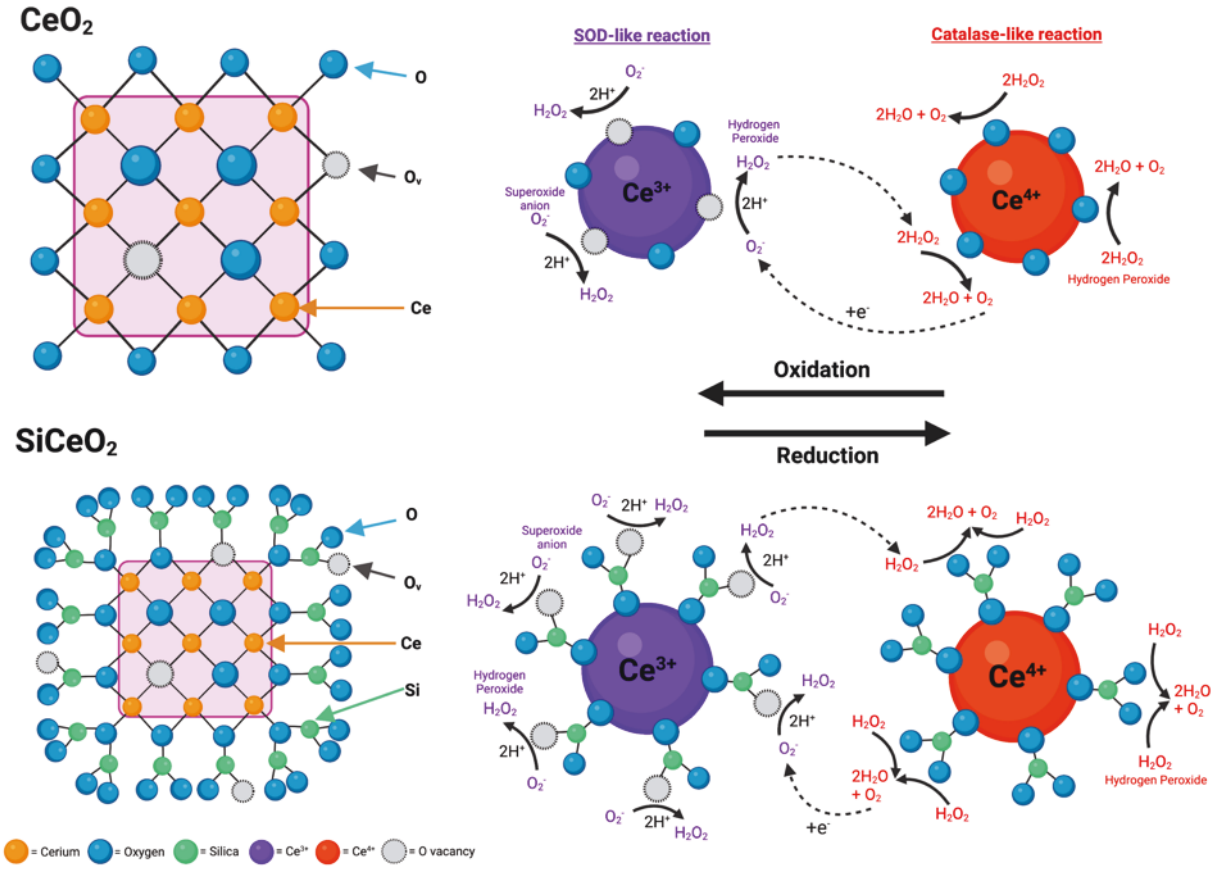

Figure 6.1. Schematic representation of the oxygen vacancies (O_v) in CeO_2 and $SiCeO_2$ nanoparticles, and the SOD-like and catalase-like enzymatic mechanisms that they exhibit. Created with BioRender.com.

6.3 Methods

Characterization of nanoparticles. The CeO_2 and blue $SiCeO_2$ nanoparticles were synthesized using flame spray pyrolysis (FSP), described previously (120, 121). For the CeO_2 nanoparticles, cerium (Ce) 2-ethylhexanoate (Alfa Aesar, 49 % in 2-ethylhexanoic acid) was dissolved in xylene with a final Ce concentration of 0.5 M, fed to the centre of the flame by a syringe pump at 1-10 mL/min, then dispersed with 5 L/min oxygen to control to rate of combustion and manipulate nanoparticle size. A constant pressure drop of 1.5 bar was maintained by adjusting the orifice gap. The spray flame was surrounded and ignited by a premixed methane/oxygen (1.5/3.2 L/min, respectively) flame from an annular gap (0.15 mm spacing, at a radius of 6 mm from the centre of nozzle). A sintered metal plate ring (8 mm wide, at inner radius of 9 mm from the centre of nozzle) provided an additional 5 L/min O_2 as a sheath for the supporting flame. Additionally, a modified set up was used where the flame was enclosed in a quartz tube to maintain the sheath gas at 20 L/min O_2 and preserve heat. This temperature gradient causes the metal vapour to supersaturate to form nuclei as the flame temperature reduces downstream. The nuclei coalesce, sinters and agglomerates before leaving the flame as nanoparticles, and is then collected on glass fibre filter. The average nanoparticle diameter of the crystalline structure is approximately 7 nm. Two separate precursors (Si:Ce) in a 20:80 ratio, were combined by adding hexamethyldisilane, (HMDSO, Sigma Aldrich) and cerium 2-ethylhexanoate (Alfa Aesar, 49 % in 2-ethylhexanoic acid) dissolved in xylene, with a final Si:Ce concentration of 0.5 M, which was fed to the centre of the flame by a syringe pump at a rate of 3 mL/min. “Blue” $SiCeO_2$ was prepared by hydrogenation of these nanoparticles, by heating 1200 mg of the sample in a carbonite tube furnace. A constant flow of 50 mL/min of 10 % H_2 in N_2 was implemented and the furnace was heated at a rate of 5°C/min to 500°C and then held for 180 min. The average diameter of the crystal structure is approximately 7.5 nm. The magnetite particles (MAG) were synthesized by Sigma Aldrich (MO, USA) to pure 97 % sample (molecular weight 231.53) and the crystal structure is approximately 100 - 400 nm in diameter.

Transmission electron microscopy (TEM). High resolution (HR)-TEM analysis was carried out for the assessment of primary particle size and morphology of CeO_2, blue $SiCeO_2$ nanoparticles, and magnetite particles (MAG). Samples were dispersed in 95 % (w/v) ethanol and sonicated for 30 mins at room temperature. A drop of suspension was added to the copper grid and air dried before each measurement took place. TEM measurements were performed using a Phillips CM200 operating at 200 kV with an SIS CCD camera.

Preparation of nanoparticles suspensions for treatment in vivo. The magnetite particles (MAG) were prepared, at a concentration of 3.3 mg/mL in in sterile saline solution. The CeO_2 and blue $SiCeO_2$ nanoparticles were prepared 1.65 mg/mL in a sterile saline solution. Before administration, (nano)particle solutions were sonicated, using the Q500 Sonicator (Q500 Sonica Sonicators, CT, USA) for 5 mins at 50 % amplitude.

Alzheimer's disease animal model. The effects of the magnetite particles and CeO_2 and blue $SiCeO_2$ nanoparticles were assessed in APP/PS1 transgenic mice and C57BL/6 wild-type (W/T) littermates for comparison (purchased from Professor Anna King, University of Tasmania, Tasmania Australia). The AD mouse model (APP/PS1) used for this study was a double transgenic mouse that expresses a chimeric mouse/human amyloid precursor protein (Mo/HuAPP695swe) and a mutant human presenilin 1 (PS1) on C57BL/6 (B6. Cg-Tg (APP6953DboTg (PSEN1dE9) S9Dbo) background (APP/PS1) (122). This model exhibits amyloid pathology that closely resembles the Aβ deposits in the initial stages of AD and has been extensively used to study mechanisms of AD neuropathology (123). This model exhibits Aβ deposition as young 6 weeks of age in the cortex and 3 - 4 months in the hippocampus (124, 125). Reactive glial cells appear around Aβ deposits at about 6 weeks of age, coinciding with a pro-inflammatory response (126). While global neuronal loss is not observed in the APP/PS1 model, modest neuronal loss in the dendate gyrus granule cells (127). Synaptic loss and cognitive impairment are also observed in this animal model at approximately 3 - 7 months of age (128). The APP/PS1 model can develop age-related depressive-like and anxiety-like behavioural changes at approximately 7 - 9 months old and are very prominent at 12 months of age (139). This animal model was chosen as the relevant AD pathological biomarkers are expressed at 5 - 7 months of age which coincided with the length of the animal study. The mice were house according to sex, with 2 - 5 mice per cage, and kept on a 12-hour light/dark cycle at room temperature 22/5 ± 2°C. Before commencing the *in vivo* experiments, the mice were allowed to acclimatize for 1 week. In week 1 of the animal experiment (W/T; n=37, APP/PS1; n=28) at 11 weeks of age, the mice were grouped to receive intranasal administration of (i) saline (ii) MAG (66 µg/20 µL of saline) every third day for 4-months. At weeks 16 of the animal experiment (27 weeks of age) the mice were further subdivided to receive (i) saline, (ii) MAG, (47) MAG+CeO_2 (iv) MAG+blue $SiCeO_2$ nanoparticles for 4 months. All mice were monitored daily, and their weight recorded on a weekly basis in Figure S6.1. All animal experiments were conducted with the approval from the University of Technology Sydney Animal Care and Ethics Committee (ETH19-4326) and in accordance with the guidelines

described by the Australian National Health and Medical Research council code of conduct for animals.

Preparation of particle suspension for *in vivo* model. The magnetite particles used for this study were prepared at a concentration of 3.3 mg/mL, and the CeO_2 and blue $SiCeO_2$ nanoparticles were prepared at a concentration of 1.65 mg/mL in sterile saline solution. Before administration particle solutions were sonicated, using the Q500 Sonicator (Q500 Sonica Sonicators, CT, USA) for 5 mins at 50 % amplitude to disperse particles. Once sonicated, all particles were ready for intranasal administration to the mice in their designated treatment groups.

Intranasal administration of particle suspension. Delivery of magnetite particles and CeO_2 and blue $SiCeO_2$ nanoparticles was administered intranasally. To administer the particles, the mice were inducted in a chamber with 4 % isofluorane and 2 L/min oxygen until no movement was observed then 20 μL of air pollutant solution (3.3 mg/mL) was administered intranasally, and the mice were monitored for recovery. For the groups receiving both magnetite and CeO_2 or blue $SiCeO_2$ nanoparticles, the administration was conducted on different days, so each treatment could be ingested more uniformly. The air pollutant particles concentration was established based on the average ambient $PM_{2.5}$ intake of approximately 6-17.5 μg/day/person, based on urban environments in India, Portugal, Italy, Spain, Belgium, England and Poland etc.) (129, 130).

Behavioural assessments. At week 31 of the animal experiment (42 weeks of age) the mice were subjected to behavioural assessments. All testing sessions were conducted between 10:00 - 16:00 hours and were video recorded. The assessment of short-term memory and anxiety and stress were assessed using the novel object recognition (NOR) test and the elevated plus maze (EPM) as previously described (337). The tail suspension test (TST) is widely used method for measuring depressive-like symptoms, seen in Figure S6.2 (140). Prior to the NOR and TST the mice were acclimatized to the testing room for 1 hour prior to the assessment. There was no acclimatization for the EPM. For the TST each animal was placed upside down hanging from the centre of the box by their tail for 3 mins for observation of their mobility during this time. Decreased mobility time (seconds) indicates depressive-like symptoms which is an indicator early AD that closely correlate with anxiety and stress and the development of cognitive impairment (44, 45).

In vivo quantification of Aβ plaques. At week 31 of the animal experiment (42 weeks of age) the development of Aβ species formation, detecting both the soluble (Aβ40) and insoluble (Aβ42) peptide aggregates, was assessed using a near-infrared fluorescence (NIRF) molecular imaging probe, CRANAD-2 (Abcam, Cambridge, UK) (141). The *ex-vivo* fluorescence CRANAD staining probes for presence of the insoluble Aβ42 peptide aggregates. The CRANAD-2 probe was prepared in a mixture of 15 % DMSO, 1 5% cremaphor and 70 % PBS at a concentration of 5 x 10^3 mg/mL. The mice heads were shaved and inducted in a chamber using 4 % isofluorane and 2 L/min oxygen. Baseline fluorescence of the brain was obtained using the IVIS fluorescent scanning machine (IVIS Lumina II; Caliper Life Sciences, MA, USA). The mice were then intravenously injected with the CRANAD-2 (5 mg/kg) before they were inducted again and fluorescence signals from the brain was recorded 5 mins after injection. A small circular region of interest (ROI) in the centre of the fluorescence region was established, and the average radiance (p/s/cm^2/sr) in the region of interest was recorded, seen in Figure S6.3.

Tissue Collection. At experimental endpoint (43 weeks of age) the mice were euthanized with isofluorane then placed on a nose cone until no reflex to pedal or ocular stimulation was observed. Cardiac puncture was performed via the left ventricle to collect approximately 1mL of blood using an 18-gauge syringe pre-coated with heparin (100 I.U/mL DBL Heparin Sodium Injection, Hospira, Vic, Australia). Following collection, the whole blood sample was immediately centrifuged (13, 500 RCF, 5 mins). The plasma layer was removed and stored at -80°C. To ensure the mouse was deceased before any further procedures, cervical dislocation was performed. For this study many different techniques were of interest, therefore the brains were halved; the right hemisphere was fixed in 4 % paraformaldehyde (PFA), while the left was dissected and the hippocampus and cerebral cortex were snap frozen in liquid nitrogen, then stored at -80°C until required.

Tissue Fixation, Processing, Embedding and Cutting. The right hemisphere was fixed in 4 % PFA (Sigma-Aldrich, MO, USA) overnight, then rinsed with phosphate buffered saline (PBS) before being stored in 70 % ethanol for one week. Brain tissues were then placed in cassettes and processed using the ExcelsiorTM AS Tissue Processor (Thermo Fisher Scientific, MA, USA) for an overnight process involving two changes of formalin, increasing grades of ethanol and two changes of paraffin wax. After processing, brain tissues were embedded in paraffin wax and cut in sagittal sections using microtome (Epredia, MICH, USA). Brain sections were cut at a thickness of 10 µm, through the entire right hemisphere, resulting in

approximately 25-30 slides per tissue. Three brain tissue sections were mounted on every Platinum PRO adhesive glass slides (Trajan, VIC, AU), left to dry at 37°C overnight and stored at room temperature until required.

Ex vivo Quantification of Aβ Plaques and neuronal cells. For quantification of Aβ plaque formation and neuronal cell counting, sagittal brain tissue sections prepared on adhesive slides were stained with thioflavin S stain (1 % filtered aqueous solution), which detects the characteristic β-pleated sheets of Aβ plaque [31] and cresyl violet (0.1 %) for differential neuronal cell staining respectively. Slides were placed in two changes of xylene followed by decreasing grades of ethanol (100 %, 95 %, 70 %) for 3 mins each. They were then hydrated in water for 6 mins. Slides were then immersed in thioflavin S stain (1% thioflavin S stain; Sigma-Aldrich, MO, USA) for 10 mins or cresyl violet (0.1% cresyl violet powder (wt/acetic acid); Sigma-Aldrich, MO, USA) for 3.5 mins. Slides were then rinsed with water for 5 mins, followed by dehydration in two changes of 100 % ethanol and two changes of xylene. Slides were cover-slipped using Dibutylphthalate polystyrene xylene (DPX) and left to dry overnight. All slides were imaged using the ZEISS AxioScan Digital Slide Scanner (Carl Zeiss Microscopy, Germany) on the entire sagittal section at 20 x magnification, using fluorescence (thioflavin S. stained tissue) or brightfield (cresyl violet stained tissue) imaging settings. W/T (C57BL/6) mice do not develop Aβ plaques, however APP/PS1 mice that are 6-12 months of age develop round dense Aβ plaque formations that are approximately 50-150 μm in diameter (147, 148). The number of fluorescent Aβ plaque formations were automatically counted in a region of interest (ROI) in the neocortex above the hippocampus, using Image J (IJ1.46r Revised Edition), by implementing a fluorescent and size (50-150 μm^2) threshold, highlighting the Aβ plaque formations in the brain tissue (147, 148). The hippocampus and somatosensory regions are responsible for memory and spatial recognition, and receiving and processing sensory information respectively (144, 145). The number of neuronal cell bodies were counted (with a range of 10-400 μm^2) using the QuPath Software Quantitative Pathology & Bioimage Analysis (QuPath) Software 0.2.3 (Edinburgh, UK) in regions of interest (ROI) in the hippocampus: cornu ammonis (Ca) 1, Ca3 and dentate gyrus (DG), and the somatosensory cortex (SS 2, 3, 4, 5, 6a) (146). Every brain tissue sample (n = 5-11 biological replicates) that was analysed had 9 technical replicates accounting for staining, imaging and analysis bias.

Cell Culture models. Human neuroblastoma (SH-SY5Y) cells and murine microglial (BV-2) cells were cultured in DMEM/F12 medium (Gibco, MA, USA) supplemented with 5 % foetal

bovine serum (FBS) and 5 mM HEPES. The cells were cultured at 37°C in a humified atmosphere containing 5 % CO_2 until 80-90 % confluency. Unless otherwise stated, cells were seeded onto 6-well plates (80, 000 cells/well) for protein extraction or 96-well plates (30,000 cells/well) for biochemical assays and allowed to settle overnight. The cells were serum starved (0 % FBS) for 24 hours before exposure to magnetite and CeO_2 nanoparticles.

Preparation of particle suspension for *in vitro* model. The magnetite particles were prepared at a concentration of 100 μg/mL and both CeO_2 nanoparticles were prepared at a concentration of 50 μg/ml in filtered DMEM/F12 medium (Gibco, MA, USA) supplemented with 5 % foetal bovine serum (FBS) and 5 mM HEPES at a concentration of 100 μg/mL. Samples were sonicated, using the Q500 Sonicator (Q500 Sonica Sonicators, CT, USA) for 5 mins at 50 % amplitude, to disperse particles, due to the magnetic properties (339). After this, 100 μL and 1 mL of particle sample per well to a 96 - well and 6 - well plate respectively. This concentration was established based literature of *in vitro* studies (e.g., human lung epithelial A549 and murine macrophage RAW 264.7) testing air pollutant induced toxicity for the similar exposure times and particles concentration (150, 151). The concentration of both CeO_2 and blue $SiCeO_2$ nanoparticles was established based on preliminary in vitro studies investigating the effects of CeO_2 nanoparticles in various concentrations on both SH-SY5Y and B-V2 cells (Figure S6A-D), where the concentration of 50 μg/mL for 24 hours was chosen (152, 153). The cell viability, ROS and NO production was further tested on both cell types with LPS being used as the inflammatory stimuli (Figure S6E-J). For each biochemical assay that was performed with both cell lines, cells were seeded in a 96-well plate with 8 technical replicates per plate and per assay. Each assay was repeated 4 times (n = 4 biological replicates), at different passages to account for reproducibility issues (149) which is stated in the results.

Protein Extraction. Whole protein lysate was extracted from the hippocampus and SH-SY5Y cells performed using RIPA lysis buffer (1 % nonidet P-40, 0.1 % SDS, 0.5 % deoxycholate, 150 mM NaCl, 50 mM Tris pH 8) as previously described (341). The concentration of protein was quantified with the Pierce BCA Protein Assay Kit (Thermofisher Scientific, MA, USA; cat. 23225) and stored at -80°C.

Aβ42 Quantification in SH-SY5Y cells. The extracted protein from SH-SY5Y cells was used to investigate Aβ42 concentration, using a Aβ42 Human ELISA Kit (Thermofisher Scientific, MA, USA; cat. KHB3441). This protocol was completed as per the manufacturer's instructions. The protein (30 μg) was prepared in duplicate and added to all wells with

appropriate standards and controls. The Aβ42 detection antibody solution (50 µL) was added to each well and incubated at room temperature for 3 hours. Following this, the plate was aspirated and washed. The anti-rabbit IgG HRP (100 µL) was added to each well and incubated for 30 mins at room temperature. The plate was aspirated and washed, and the stabilized Chromogen (100 µL) was added and incubated for a further 30 mins at room temp. Finally, the stop solution (100 µL) was added and the plate was read on the infinite M1000 PRO microplate reader (Tecan Sunrise, Grödig, Austria) at 450 nm. The results are expressed as Aβ42 (pg/ml).

Western Blot Analysis. Protein extracted from the hippocampus (30 µg) and SH-SY5Y cells (20µg) were used for western blot analysis, as previously described (342). Proteins were visualized using ECL substrate (Bio-Rad, CA, USA) and a Bio-Rad Chemidoc Imaging System™. Protein bands were quantified by densitometry using the ImageJ 1.53a software (National Institute of Health, Maryland, USA). Protein bands were quantified by densitometry using the Fiji software. as previously described (342). All primary and secondary antibodies in Table S6.1.

Measurement of cell viability. The MTT assay is cell viability was assessed using *M*ethylthiazolydiphenyl-tetrazolium bromide (MTT) dye (Sigma Aldrich, MO, USA), a widely used method for cell viability and cytotoxicity (154). The MTT dye was prepared at a concentration of 5 mg/mL in PBS. Following treatment of cells, MTT dye (10 µL) was added to each well and incubated in dark sterile conditions at 37°C for 3 - 4 hours - until purple coloured formazan crystals were observed visually. The MTT dye is utilised by cell mitochondria, converting the dye to formazan, forming insoluble purple granules. Once the purple-coloured formazan crystals were observed visually, the media and dye were removed followed by adding 100 µL of DMSO (Sigma Aldrich, MO, USA) each well to solubilize formazan and turn the solution purple. The absorbance at 570 nm was obtained on the infinite M1000 PRO microplate reader (Tecan Sunrise, Grödig, Austria). The results are expressed as percentage increase from control.

Measurement of nitric oxide and intracellular reactive oxygen species levels. Following cell treatments, the media was collected and used to measure nitric oxide (NO) levels. The media collected was aliquoted (100 µL per well) in duplicates into wells on a 96 well plate before the addition of 100 µL of Griess reagent (40 mg/mL; Sigma Aldrich, MO, USA) into each well. The reaction mix was then incubated at room temperature for 15 mins followed by 30 mins in the dark at 37°C. An absorbance reading was obtained at 540 nm on the infinite M1000 PRO microplate reader (Tecan Sunrise, Grödig, Austria). The results are expressed as

percentage increase from control. After the media were collected, intracellular ROS levels were measured in the remaining cells from each well using the DCF stain (Sigma Aldrich, MO, USA) as previously described (343). The results are expressed as percentage increase from control.

Statistical analysis. One-way ANOVA with Bonferroni's post-hoc test was used to determine statistical power in EPM, TST, NIRF in vivo brain imaging, neuronal cell counting, Aβ plaque counting, MTT assay, DCF assay, Griess assay, Aβ42 ELISA and western blot analysis. A an unpaired two-tailed t-test was used to determine the statistical significance of the NOR data. All statistical analysis was performed using the Graph-Pad Prism 9 software (Graph-Pad, CA, USA) and the results are expressed as mean ± SEM. The treatment groups were considered significantly different if the p value was less than 0.05.

6.4 Results and Discussion

Characterization and synthesis of nanoparticles

CeO_2 nanoparticles have emerged as effective nanomedicines, used extensively due to the physicochemical properties of transitioning between Ce^{3+} (fully reduced) or Ce^{4+} (fully oxidized) valence states, exhibiting enzymatic and regenerative capabilities (108). The CeO_2 and blue $SiCeO_2$ nanoparticles used in this study were synthesized using flame spray pyrolysis. Representative high resolution transmission electron microscopy (HR-TEM) reveals the rhombohedral morphology of the CeO_2 nanoparticles with an average crystalline diameter of 7 nm (Figure 6.2B) in single crystal particles with high crystallinity. The angular shape and small size of these nanoparticles exposes more oxygen vacancies on the surface, contributing to an increase in the uptake of nanoparticles from surrounding cells that subsequently enables effective ROS scavenging activity (489). These properties have been shown to play a role in the effectiveness of CeO_2 nanoparticles as an anti-cancer, anti-inflammatory and anti-bacterial agents (509). CeO_2 nanoparticles however have been shown to have a natural tendency to agglomerate in their bare state which has been shown to lead to increased inflammation and toxicity especially, in the lungs and liver (506). Advancements in nanoparticle engineering for biomedical applications have found that doping CeO_2 nanoparticles can increase the hydrophilicity of the nanostructure, increasing dispersibility and overall improving biocompatibility (108, 506, 510).

Silica coated CeO_2 nanoparticles have been previously found to be protective against inflammatory responses in the lung, decreasing fibrosis (118, 119). Doping CeO_2 nanoparticles with silica has been shown to improve nanoparticle stability, dispersibility and cellular uptake (119). The representative TEM image reveals that the blue $SiCeO_2$ nanoparticles were mostly uniform in morphology, spherical in shape and with an average crystalline diameter of 7.5 nm (Figure 6.2A). In addition, the amorphous silica coating is clearly visible showing the crystalline CeO_2 core. The nano-thin amorphous silica layer is synthesized through the flame spray pyrolysis method and has been designed specifically to reduce CeO_2 -mediated toxicity (118). Amorphous silica coating has been found to reduce pulmonary inflammatory responses in rats, compared to crystalline silica coated equivalents, which are found to be more redox reactive however less stable (118). The "blue" component of the silica coated CeO_2 nanoparticles was prepared by hydrogenation, heating 1200 mg of the sample in a carbonate tube furnace. This step further reduced the nanostructure (increasing the Ce^{3+}/Ce^{4+} ratio) thereby increasing the oxygen vacancies, resulting in a highly stable and catalytic redox nanostructure which is expected to increase its antioxidant and anti-inflammatory capabilities, compared to bare CeO_2 nanoparticles (108, 506).

The magnetite particles used in this study were a representative for magnetite particles found in air pollutant samples. Air pollutant magnetite particles can be formed through combustion reactions where the frictional heat generated from brake pads, diesel exhaust emissions, power plants or incineration from industrial facilities causes a release of melted, condensed, and partially oxidative materials (88, 511). In agreement with Maher *et al* (2016), the magnetite particles used in this study have smooth distinct cuboidal morphology (Figure 6.2C) consistent with those formed from frictional pressure at high temperatures. The small size of these particles (< 200 nm in diameter) allows easy absorption through the skin and mouth into the cardiovascular and respiratory system, where they can enter the brain through circulation. Alternatively, they can directly enter the brain through the BBB via the nasal canal and olfactory bulb (53, 512-514).

Cerium oxide nanoparticles decrease oxidative stress and improve cell viability after exposure to magnetite particles in in vitro models

Oxidative stress plays a significant role in exacerbating AD pathologies, arising as a result of an imbalance between ROS and RNS production and their removal (316). ROS and RNS are produced by microglia and astrocytic cells in the brain to regulate synaptic and non-synaptic communication between neurons and glial cells (314, 316). Two cell lines were used for this study, the first; human neuroblastoma SH-SY5Y cells, a well-established model for neuronal cells and the second; murine microglial BV-2 macrophage cells, both used for the neurodegenerative research (515, 516). To evaluate the effects of CeO_2 nanoparticles on oxidative stress, a DCF assay was used to measure total ROS, including superoxide, hydroxyl, hydrogen peroxide, nitrogen oxide and nitrogen dioxide species. Both SH-SY5Y and BV-2 cells exposed to magnetite particles showed an increase in ROS levels to 177.3 ± 18.1% ($P < 0.0001$) and a 139.8 ± 15.6% ($P < 0.05$) respectively, compared to the controls (Figure 6.2D and G). Treatment with CeO_2 and blue $SiCeO_2$ nanoparticles were able to significantly reduce ROS levels in the SH-SY5Y cells to 99.9 ± 6.7% ($P < 0.0001$) and 97.4 ± 9% ($P < 0.0001$) compared to control. This trend was also seen in the BV-2 cell with CeO_2 and blue $SiCeO_2$ nanoparticles reducing ROS levels to 88.7 ± 4.8% ($P < 0.0001$) and 90.5 ± 6.9% ($P < 0.0001$) compared to magnetite exposed particles, consistent to those observed for both control cell types. We next examined the effect of the nanoparticles on NO levels which acts as a precursor to nitrogen-oxide, -dioxide and RNS (517). Magnetite particles was shown to increase NO levels to 153.3 ± 6.07% in SH-SY5Y and 321.1 ± 26.2% in BV-2 cells ($P < 0.0001$ for both SH-SY5Y and BV-2) compared to control (Figure 6.2E and H). This effect was abrogated in the BV-2 cell line, returning the NO levels to 206.4 ± 14.1% ($P < 0.0001$) and 154.6 ± 11.6% ($P < 0.0001$) after treatment with CeO_2 and blue $SiCeO_2$ nanoparticles respectively and in the SH-SY5Y cells, returning NO levels to 102.5 ± 7.8% ($P < 0.0001$) after treatment with blue $SiCeO_2$ nanoparticles (Figure 6.2E and H). CeO_2 nanoparticles are effective ROS and RNS scavengers due to the presence of mixed valence states (Ce^{3+} and Ce^{4+}), allowing easy regenerative abilities, due to the changing number of oxygen vacancies on their surface (518). This structural ability allows it to mimic superoxide dismutase (SOD) and catalase enzymatic activity (108). It needs to be noted however that no significant decrease was observed in SH-SY5Y cells treated with CeO_2 nanoparticles (Figure 6.2E). Therefore, whilst both CeO_2 and blue $SiCeO_2$ nanoparticles can effectively scavenge the ROS produced from magnetite particle exposure, it can be postulated that CeO_2 nanoparticles are less effective in reducing NO

production, and therefore have less RNS scavenging ability compared to the blue $SiCeO_2$ nanoparticles. This could be due to the fact that the blue $SiCeO_2$ nanoparticles are in a more reduced state (Ce^{3+}/Ce^{4+} ratio is higher) which allows for more oxygen vacancies, increased enzymatic and regenerative ability (519).

To assess whether both nanoparticle treatments had any effects on SH-SY5Y and BV-2 cells without exposure to magnetite particles, we further tested CeO_2 and blue $SiCeO_2$ nanoparticles on the effects of ROS and NO levels with lipopolysaccharide (LPS) as a positive control (Figure S6.4E, F, H and I). LPS is an endotoxin derived from outer membrane gram-negative bacteria and is a powerful mediator of systemic inflammation (520). Both SH-SY5Y and BV-2 cells exposed to LPS showed to have an increase in ROS levels to 119.1 ± 2.6% ($P < 0.0001$) and 116.1 ± 3.64% ($P < 0.001$) respectively, compared to the controls (Figure S6.4E and H). Treatment with CeO_2 and blue $SiCeO_2$ nanoparticles, showed significantly less ROS levels compared to LPS, which is consistent with the controls in both SH-SY5Y and BV-2 cells. Similarly, LPS was found to induce and increase in NO levels to 135.4 ± 3.1% ($P < 0.0001$) and 162.8 ± 3.4% ($P < 0.0001$) in the SH-SY5Y and BV-2 cells compared to the controls (Figure S6.4F and I). Again, treatment with CeO_2 and blue $SiCeO_2$ nanoparticles were found to be consistent with their corresponding controls for both SH-SY5Y and BV-2 cells. These results suggest that both CeO_2 and blue $SiCeO_2$ nanoparticles have no ROS or NO inducing effects at this concentration.

An increase in oxidative stress occurs in conjunction with decreased cell viability in the development of AD as an accumulation of ROS and RNS, contributes to protein misfolding, increased microglial activation and mitochondrial dysfunction, resulting in cellular apoptosis (316, 521, 522). Therefore, we next investigated the effects of the nanoparticles on cell viability in SH-SY5Y and BV-2 cell lines. After exposure to magnetite nanoparticles cell viability was shown to decrease to 75.1 ± 2.5% ($P < 0.001$) in SH-SY5Y cells and 57.1 ± 5.12% ($P < 0.05$) in BV-2 cells compared to control (Figure 6.2F and I). In contrast, cell viability was increased (BV-2 cells) or returned to those observed for control cells (SH-SY5Y) following treatment with either CeO_2 or blue $SiCeO_2$ nanoparticles, suggesting that they exhibit neuroprotective effects. Our results are consistent with studies using the MTT assay on SH-SY5Y cells treated with copper ions or alpha-synuclein (α-syn; a neuronal protein associated with the

development of Parkinson's disease) inducing cell death, and that after CeO_2 nanoparticle administration an increase in cell viability was observed (221, 523). The cell viability of the BV-2 cells is noteworthy (Figure 6.2I), with both CeO_2 and blue $SiCeO_2$ nanoparticle treatments shown to increase cell viability to 220.5 ± 16.0% ($P < 0.001$) and 227.3 ± 13.7% ($P < 0.05$) compared to the control, further supporting CeO_2 nanoparticle's neuroprotective role but also its differential effect on neuronal cells (SH-SY5Y) compared to microglial cells (BV-2). To assess whether CeO_2 or blue $SiCeO_2$ nanoparticles alone had any effect on cell viability another MTT assay was performed on both cell lines (Figure S6.4G and I). Exposure to LPS induced a decrease in cell viability to 76.4 ± 1.6% ($P < 0.05$) in the SH-SY5Y and 80.9 ± 2.2% ($P < 0.001$) in the BV-2 cells compared to the controls. Treatment with blue $SiCeO_2$ nanoparticles alone were found to have significantly increased cell viability to 110.4 ± 8.9% ($P < 0.001$) in the SH-SY5Y cells, compared to LPS treated cells, and in the BV-2 cells both CeO_2 and blue $SiCeO_2$ nanoparticles showed significantly higher cell viability increased to 118 ± 4.2% ($P < 0.0001$) and 112.8 ± 6.5% ($P < 0.0001$) respectively, compared to LPS alone treated cells. When compared to neuronal cells, microglial cells are known to proliferate particularly during infection or injury and therefore, we suggest that CeO_2 nanoparticles are inducing a cell proliferation effect on the BV-2 microglial cells. While CeO_2 nanoparticles have been found to prohibit cell proliferation in a variety of cancer cell studies (e.g., primary osteoblasts and colorectal cancer cells; HCT 116) where the surrounding environment is more acidic (e.g., pH 6), they have also been found to have anti-apoptotic effects on macrophages and can exhibit cell proliferation effects at a pH of 9 (477-479). This anti-apoptotic and cell proliferation effect that CeO_2 nanoparticles exhibit, coincides with its strong antioxidant abilities (479). This is reflected in this study, as cell viability, ROS and NO levels were seen to be consistent with the controls after exposure to CeO_2 and blue $SiCeO_2$ nanoparticles. This suggests that both CeO_2 and blue $SiCeO_2$ nanoparticles are having a protective effect on both SH-SY5Y and BV-2 cells in reducing oxidative stress and increasing cell survival, perhaps through an anti-apoptotic effect or cell proliferation effect which needs to be further investigated.

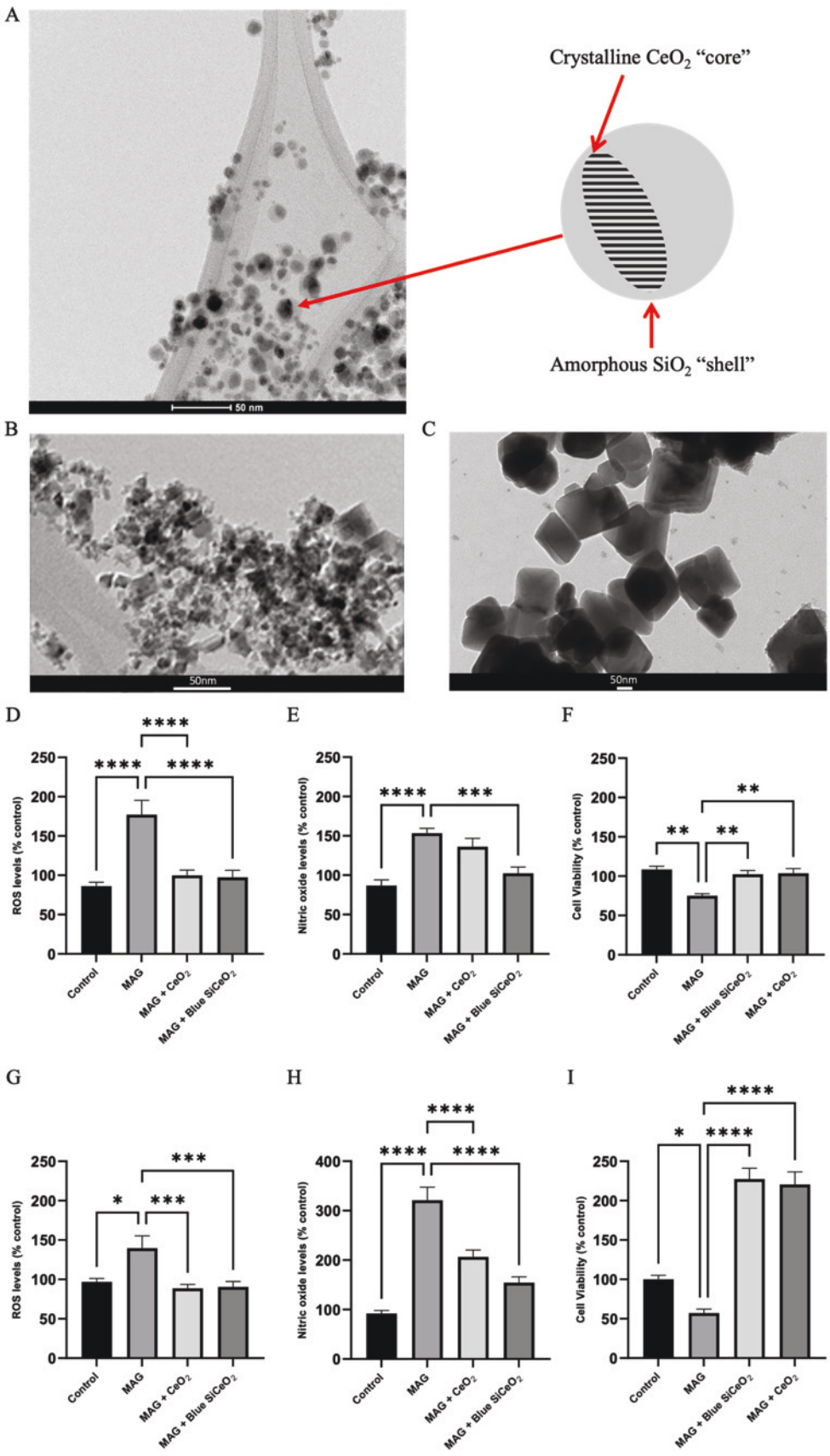

Figure 6.2. *In vitro* analysis of oxidative stress markers, after exposure to magnetite particles and CeO_2 nanoparticles. (A) TEM image of amorphous blue $SiCeO_2$ nanoparticles (50

nm). (B) TEM image of CeO_2 nanoparticles (50 nm). (C) TEM image of magnetite particles (50 nm). (D) Percentage of ROS production compared to control, SH-SY5Y cells (n = 4). (E) Percentage of NO production compared to control, SH-SH5Y cells (n = 4). (F) Percentage of cell viability compared to control, SHSY5Y cells (n = 4). (G) Percentage of ROS production compared to control, BV-2 cells (n = 4). (H) Percentage of NO production compared to control, BV-2 cells (n = 4). (I) Percentage of cell viability compared to control, BV-2 cells (n = 4). * $P < 0.05$, ** $P < 0.001$, *** $P < 0.0001$, **** $P < 0.0001$. All error bars indicate mean ± SEM.

Cerium oxide nanoparticles decrease inflammatory markers, associated with AD development, after exposure to magnetite particles in in vitro and in vivo models

Neuroinflammation is closely associated with an increase in oxidative stress in the progression of various chronic inflammatory diseases, including neurodegenerative diseases like AD (524). The inflammatory defensive response is a coordinated activation (by microglial and astrocytes cells) of signalling pathways, transcription factors and cytokines, that regulate inflammatory mediators which then further recruit inflammatory cells (525). In light of our results observed for oxidative stress and cell viability we therefore investigated the effects of the CeO_2 nanoparticles on two major transcription factors that play key roles in the control of inflammatory pathways - mitogen-activated protein kinase (MAPK) and NFκB. MAPK is a family of transcription factors, consisting of four subgroups, one of interest is the p38-MAPK (526). The p38-MAPK transcription factor is activated by phosphorylation and is essential in the production of pro-inflammatory cytokines (TNF, IL-6 and IL-1β), chemokines, induction of enzymes, adhesion molecules, proliferation, apoptosis and differentiation (526). The p38-MAPK transcription factor has been found to be an up-regulatory mediator of NFκB (527). NFκB is another important family of transcription factors, similarly to p38-MAPK, directly activating pro-inflammatory cytokines, chemokines, adhesion molecules, but also indirectly, cell proliferation, apoptosis, and differentiation (528, 529). The most abundant form of NFκB is the heterodimer with two subunits (p50 and p65) (529). Following exposure to magnetite particles, the ratio of phosphorylated to total p38-MAPK and p65- NFκB transcription factors was found to have significantly increased protein expression to 0.87 ± 0.04 ($P < 0.0001$) and 0.88 ± 0.043 ($P < 0.001$), compared to the control samples 0.49 ± 0.03 and 0.52 ± 0.08 respectively (Figure 6.3A and B). After treatment with blue $SiCeO_2$ nanoparticles, there was a significant reduction observed in the phosphorylated p38-MAPK and p65-NFκB protein

expression to 0.62 ± 0.04 ($P < 0.05$) and 0.61 ± 0.6 ($P < 0.0001$) relative to the total p38-MAPK and p65-NFκB protein expression levels respectively, suggesting that blue $SiCeO_2$ nanoparticles are able to decrease the phosphorylation of p38-MAPK and p65-NFκB, thereby decreasing their activity. These results are consistent with studies showing that CeO_2 nanoparticles, can inhibit MAPK and NFκB phosphorylation, which in turn prevented LPS induced cytokine release, thereby mediating severe sepsis (530, 531). Of note, no significant changes were observed following treatment with CeO_2 nanoparticles, which indicates that these nanoparticles do not have the same effect, or perhaps having a delayed effect on these transcription factors. CeO_2 nanoparticles are not coated, therefore tend to agglomerate more easily, decreasing the cellular uptake compared to the blue $SiCeO_2$ nanoparticles. These findings suggest that blue $SiCeO_2$ nanoparticles show better efficacy than CeO_2 in decreasing the phosphorylation and therefore activation of two major transcription factors that play key roles in neuroinflammation.

The activation of both MAPK and NFκB transcription factors results in the production of proinflammatory cytokines, TNF and IL-6, which further progress and exacerbate neuroinflammation (526). The SH-SY5Y cells show magnetite particles increased TNF protein expression to 0.93 ± 0.14 ($P < 0.001$; normalised to β-actin), compared to the control 0.26 ± 0.04 (Figure 6.3C). There was a significant reduction in TNF protein expression after treatment with both CeO_2 (0.36 ± 0.07; $P < 0.001$ normalised to β-actin) and blue $SiCeO_2$ (0.41 ± 0.05; $P < 0.05$ normalised to β-actin) nanoparticles in the SH-SY5Y cells. Encouraged by our results of the CeO_2 nanoparticles, we then conducted analysis using an in vivo model of AD. These results demonstrated a similar trend in the hippocampus, with magnetite particle exposed W/T and APP/PS1 mice having a significant increase in TNF protein expression to 0.46 ± 0.02 ($P < 0.001$; normalised to β-actin) and 0.76 ± 0.1 ($P < 0.001$; normalised to β-actin) correspondingly, compared to saline treated mice (Figure 6.3D and E). APP/PS1 mice exposed to magnetite particles and CeO_2 or blue $SiCeO_2$ nanoparticles was found to have significantly decreased TNF protein expression to 0.28 ± 0.08 ($P < 0.001$; normalised to β-actin) and 0.28 ± 0.08 ($P < 0.001$; normalised to β-actin) respectively. While there is a decrease in TNF protein expression observed in the W/T mice exposed to magnetite particles and CeO_2 or blue $SiCeO_2$ nanoparticles there was no significance.

Exposure of magnetite particles also resulted in an increase in IL-6 protein expression levels to 0.48 ± 0.02 ($P < 0.05$; normalised to β-actin) in W/T and 0.61 ± 0.07 ($P < 0.05$; normalised to β-actin) in APP/PS1 mice, compared to saline. Following the exposure to magnetite particles, treatment with CeO_2 and blue $SiCeO_2$ nanoparticles returned the IL-6 protein expression back to those observed for APP/PS1 saline mice (Figure 6.3G). While there is a decrease in IL-6 levels seen after treatment with CeO_2 and blue $SiCeO_2$ nanoparticles in W/T mice exposed to magnetite particles, there is no significance (Figure 6.3F). W/T mice are littermates of the APP/PS1 mice and are not prone to developing the pathologies associated with AD, they are expected to have similar immune responses (e.g., inflammatory response) as the APP/PS1 strain is on a C57BL/6 background, which is consistent when comparing the graph trends in this study, however the W/T model is showing a decreased overall inflammatory response compared to the APP/PS1 model. The APP/PS1 murine model, expresses a chimeric APP and mutant PS1, which both play a role in Aβ plaque deposition, occurring as young as 6 weeks of age (123-125). Aβ plaque deposition is known to induce microglial and astrocyte activation, resulting in an increased inflammatory response (126). As this is the first study to show magnetite particles can lead to neuroinflammation in a mouse model of AD and that CeO_2 and blue $SiCeO_2$ nanoparticles have the potential to suppress the inflammatory response, future studies need to investigate the potential of the CeO_2 nanoparticles using different strains of mice to confirm the results shown in this study and to further confirm its potential as a therapy for sporadic AD. Nevertheless, our results for TNF and IL-6 protein expression observed in SH-SY5Y cells, W/T and APP/PS1 mice are in agreement with the study by Turco et al. (2013), which showed that CeO_2 nanoparticles reduced TNF and IL-6 protein expression and ROS production in human umbilical vein endothelial cells (HUVECs) (532). Similarly, another study found that CeO_2 nanoparticles reduce inflammatory cytokines (TNF, IL-6 and IL-1β) and NFκB activation in LPS induced macrophages (RAW264.7 cell line) (533). Our findings therefore are in line with previous literature demonstrating that CeO_2 and blue $SiCeO_2$ nanoparticles can reverse the inflammatory effects induced after exposure to magnetite particles.

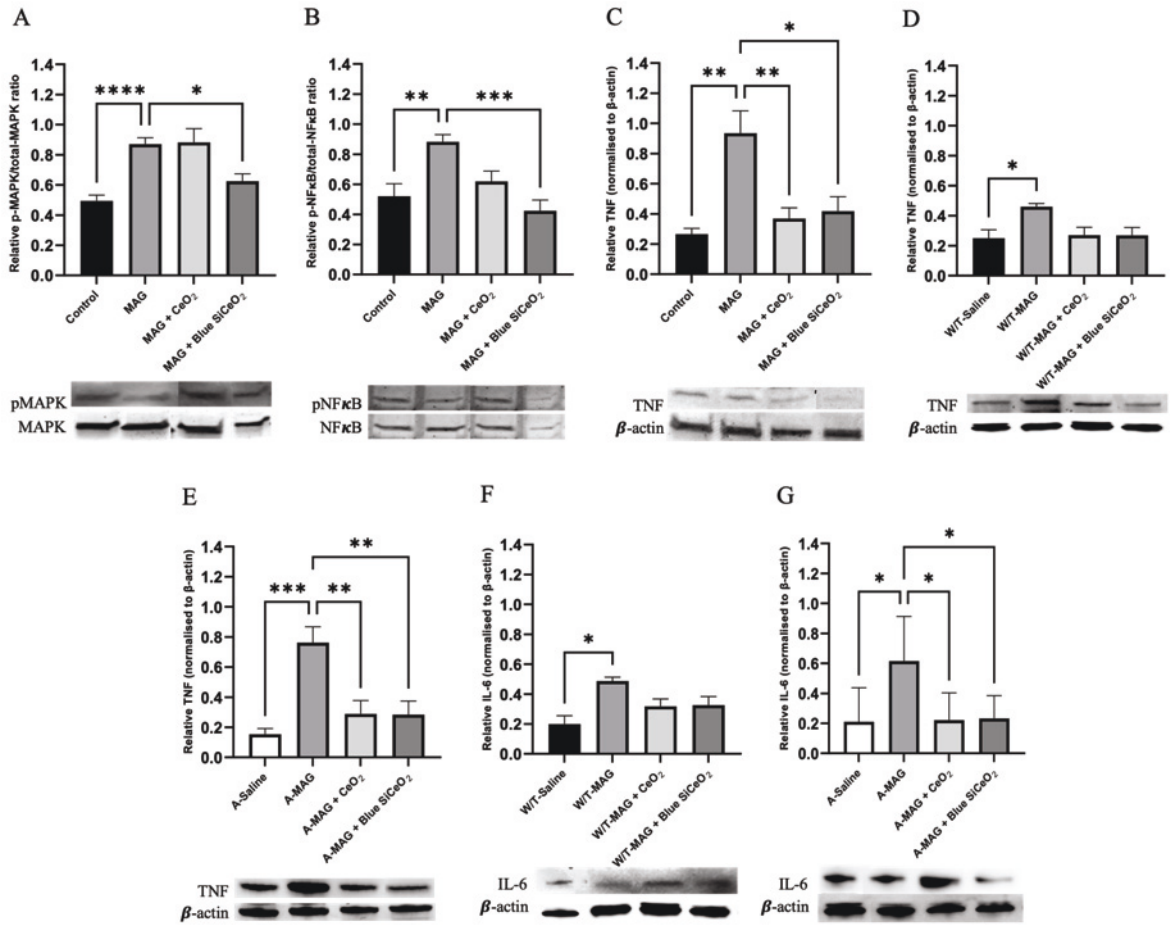

Figure 6.3. *In vitro* and *ex vivo* analysis of inflammatory transcription factors cytokines, in SH-SY5Y cells and the hippocampus respectively, after exposure to magnetite particles and CeO_2 nanoparticles. (A) Relative pMAPK/MAPK protein expression levels, SH-SY5Y cells (n = 5-6). (B) Relative pNFκB)/NFκB protein expression levels, SH-SY5Y cells (n = 5-6). (C) Relative TNF protein expression levels normalised to β-actin, SH-SY5Y cells (n = 5-6). (D) Relative TNF protein expression levels normalised to β-actin, W/T mice (n = 5-6). (E) Relative TNF protein expression levels normalised to β-actin, APP/PS1 mice (n = 5-6). (F) Relative IL-6 protein expression levels normalised to β-actin, W/T mice (n = 5-6). (G) Relative IL-6 protein expression levels normalised to β-actin, APP/PS1 mice (n = 5-6). * $P < 0.05$, ** $P < 0.001$, *** $P < 0.0001$, **** $P < 0.0001$. All error bars indicate mean ± SEM.

During the initial stages of inflammation immune cells invade the central nervous system (CNS) through the BBB via the endothelium of small vessels and tight junctions of astrocytes (534). This immune response is mediated by inflammatory markers, including intercellular adhesion molecule 1 (ICAM-1), which plays a key role in the inflammatory response (535,

536). ICAM-1 expression is induced by TNF and mediated by p38-MAPK (537). After exposure to magnetite particles in the SH-SY5Y cells, we observed an increase in ICAM-1 protein expression to 0.77 ± 0.06 ($P < 0.0001$, normalised to β-actin) compared to control (0.18 ± 0.04; normalised to β-actin) seen in Figure 6.4A. This was also seen in the APP/PS1 mice exposed to magnetite particles (0.87 ± 0.1, $P < 0.001$ normalised to β-actin) compared to saline (0.26 ± 0.08 normalised to β-actin), no effect was observed in the W/T littermates (Figure 6.4B and C). After treatment with CeO_2 and blue $SiCeO_2$ nanoparticles there was a decrease in ICAM-1 protein expression seen in the SH-SY5Y cells to 0.32 ± 0.08 ($P < 0.0001$, normalised to β-actin) and 0.23 ± 0.032 ($P < 0.0001$, normalised to β-actin) respectively, compared to cells exposed to magnetite particles. Similarly, APP/PS1 mice treated with blue $SiCeO_2$ nanoparticles also showed a decrease in ICAM-1 protein expression to 0.27 ± 0.07 ($P < 0.001$, normalised to β-actin) compared to APP/PS1 mice exposed to magnetite particles alone. ICAM-1 has been found near Aβ plaque formations in AD brains and is known to be upregulated when there is partial damage to the BBB, which corresponds to the influx and activation of immune cells (e.g., microglial and astrocytes) that is observed in AD development (534, 538). This suggests that the anti-inflammatory effects of CeO_2 and blue $SiCeO_2$ nanoparticles may be able to decrease phosphorylation of transcription factors which in turn decrease the production of pro-inflammatory cytokines resulting in a downstream inhibition of mediators like ICAM-1.

ICAM-1 expression in the CNS is often associated with the expression of glial fibrillary acidic protein (GFAP)-immunoreactive astrocytes marker (534). GFAP is the principle intermediate filament protein in astrocytes, thought to maintain astrocytic function, with an increased expression closely correlating with early pathological manifestations of AD (534, 539, 540). Exposure to magnetite particles in both W/T and APP/PS1 mice was found to induce a significant increase in GFAP protein expression to 0.70 ± 0.06 ($P < 0.05$, normalised to β-actin) and 1.02 ± 0.10 ($P < 0.05$, normalised to β-actin) respectively, compared to saline administered mice (Figure 6.4D and E). After treatment with blue $SiCeO_2$ nanoparticles in APP/PS1 mice, there was a decrease in GFAP protein expression to 0.45 ± 0.09 ($P < 0.05$, normalised to β-actin) compared to magnetite exposed mice. While CeO_2 nanoparticles did induce a decrease in GFAP protein expression compared to APP/PS1 magnetite exposed mice, it was not significant. While there was a decreased trend in GFAP protein expression in W/T mice treated with CeO_2 and blue $SiCeO_2$ nanoparticles, there was no significance (Figure

6.4D). These results demonstrate that magnetite particles induced an increase in GFAP protein expression, and that after exposure to blue $SiCeO_2$ nanoparticles, GFAP protein expression were decreased. These findings are consistent with a study in an AD murine model (5XFAD), which found that GFAP astrocytic activity was decreased following treatment with CeO_2 nanoparticles (463). These results are also consistent with the ICAM-1 protein expression levels suggesting that CeO_2 nanoparticles are indeed having less of an anti-inflammatory effect compared to blue $SiCeO_2$ nanoparticles, due to the morphological and physiological properties. Alternatively, due to the known increase in agglomeration tendency of bare CeO_2 nanoparticles compared to blue $SiCeO_2$ nanoparticles, could also explain the ICAM-1 protein expression levels in the *in vivo* model (119). Further investigation into the effects of CeO_2 nanoparticles in both microglial and astrocytic cells therefore this needs to be addressed to clarify the underlying anti-inflammatory mechanisms of these nanoparticles.

Brain derived neurotrophic factor (BDNF) is another important neuroinflammatory biomarker, that stimulates and controls growth of new neurons from neural stem cells (neurogenesis), playing a key role in energy homeostasis (541-543). Moreover, accumulating evidence indicates that reduced BDNF expression in human brains is closely associated with the pathogenesis of AD (544). Reduced BDNF levels have been linked directly to degeneration of specific neurons, eventually leading to dementia (105). This was observed in our study with the APP/PS1 mice exposed to magnetite particles showing a significant decrease in BDNF protein expression to 0.25 ± 0.06 ($P < 0.05$, normalised to β-actin) compared to saline (0.79 ± 0.16, normalised to β-actin) (Figure 6.4H). There is a trend towards a decrease in intracellular BDNF protein expression after magnetite particle exposure observed in SH-SY5Y (0.41 ± 0.3, normalised to β-actin) and W/T mice (0.32 ± 0.08, normalised to β-actin), compared to their corresponding controls, however there is no significance (Figure 6.4F and G). After treatment with both CeO_2 and blue $SiCeO_2$ nanoparticles in the SH-SY5Y cells, there is a significant increase in BDNF protein levels to 1.21 ± 0.1 ($P < 0.001$, normalised to β-actin) and 0.98 ± 0.16 ($P < 0.05$, normalised to β-actin) compared to the magnetite exposed cells (Figure 6.4F). While there is an upward trend in BDNF levels after both CeO_2 and blue $SiCeO_2$ nanoparticles in both W/T and APP/PS1 mice, there is no significance. These results suggest that air pollutants containing magnetite particles can lead to reduced BDNF levels, therefore inhibiting cell survival and proliferation, and that exposure to CeO_2 and blue $SiCeO_2$ nanoparticles can potentially promote cell survival, seen through an increase in BDNF levels. In agreement with

an AD study, using SH-SY5Y cells treated with an Aβ cell line which induced cytotoxicity, were treated with CeO_2 nanoparticles which resulted in an alteration to the BDNF signal transduction pathways, which protects neuronal cells against apoptosis induced by AD onset (521, 545). In agreement with an AD study, using SH-SY5Y cells treated with an Aβ cell line, which induced cytotoxicity, were treated with CeO_2 nanoparticles (546). With this in mind, perhaps CeO_2 and blue $SiCeO_2$ nanoparticles are having a direct effect in promoting BDNF initiation to counteract neuronal cell death and promote cell survival, indicating a potential a neurotrophic role which is in agreement with another study by D-Angelo, B. et al (2009) (492).

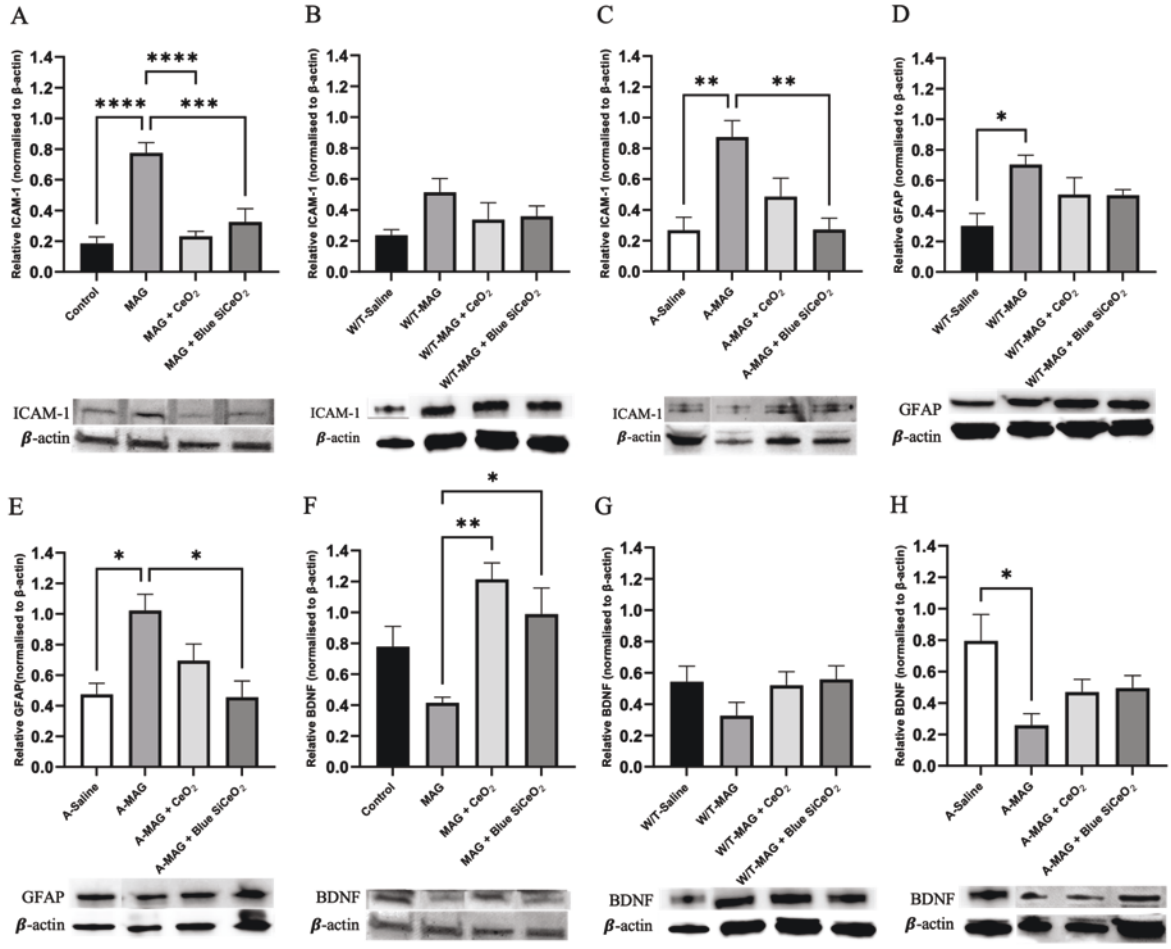

Figure 6.4. *In vitro* and *ex vivo* inflammatory transcription factors and mediators, in SH-SY5Y cells and the hippocampal region respectively, after exposure to magnetite particles and CeO_2 nanoparticles. (A) Relative ICAM-1 protein expression levels, SH-SY5Y cells (n = 5-6). (B) Relative ICAM-1 protein expression levels, W/T mice (n = 5-6). (C) Relative ICAM-1 protein expression levels, APP/PS1 mice (n = 5-6). (D) Relative GFAP protein expression levels, W/T mice (n = 5-6). (E) Relative GFAP protein expression levels, APP/PS1 mice (n =

5-6). (F) Relative BDNF protein expression levels, SH-SY5Y cells (n = 5-6). (G) Relative BDNF protein expression levels, W/T mice (n = 5-6). (H) Relative BDNF protein expression levels, APP/PS1 mice (n = 5-6). All normalised to β-actin. * $P < 0.05$, ** $P < 0.001$, *** $P < 0.0001$, **** $P < 0.0001$. All error bars indicate mean ± SEM.

While these results show a consistent trend between the in vitro and in vivo models, there are treatment group discrepancies. This could be due to the difference between an acute and chronic inflammatory response. An acute inflammatory response is consistent with the in vitro model due to the short magnetite particle exposure time (24-hours) associated with the spike or drop in inflammatory mediators that is observed (547). This contrasts to the in vivo model which more closely represents low-grade chronic inflammation that is sustained over a long period of time (8-months), a key feature in AD pathogenesis. Low-grade chronic inflammation, while it does contribute to disease pathology, can also occur independently as a result of age-related physiological changes like cellular senescence and accumulation of cellular debris, which is difficult to translate into an in vitro model (548). Overall, these results not only demonstrate the potent anti-inflammatory properties of CeO_2 nanoparticles but also highlights its neuroprotective capability. Moreover, the BDNF results display the robust cell survival and proliferative role that CeO_2 nanoparticles exhibit, indicating that they may play a role in neurotrophic signalling pathways (e.g., PI3K, Akt, ERK and CaMK) which need to be further explored as the decrease seen among the other inflammatory mediators suggests that there is a change in macrophage polarization, in decreasing pro-inflammatory mediator production (Figure 6.5). Therefore, future studies should on better the mechanism of CeO_2 nanoparticles and their effects on microglial and astrocytes.

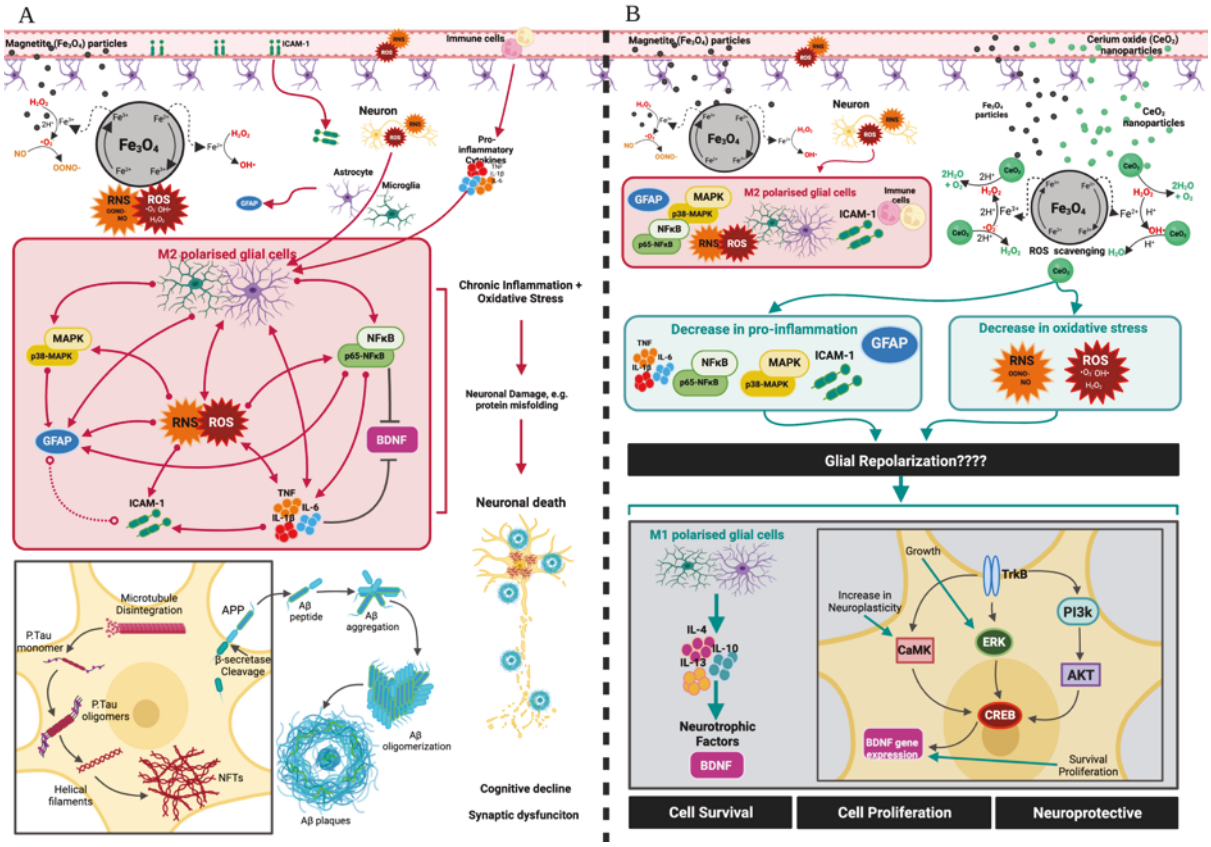

Figure 6.5. (A) This schematic representation shows magnetite particles inducing and exacerbating oxidative stress and chronic inflammation contributing to the development of AD. Magnetite particles increase ROS and RNS production, leading to an increase in M2 polarised astrocytic and microglial cells, which promote the production of pro-inflammatory cytokines and mediators leading to chronic inflammation and oxidative stress. This causes neuronal dysfunction leading to the formation of Aβ plaques and NFTs, eventually neuronal death and cognitive decline. (B) The schematic representation shows CeO_2 nanoparticles inhibiting oxidative stress and pro-inflammation, induced by the presence of magnetite particles. CeO_2 nanoparticles are effective antioxidants, scavenging ROS and RNS thereby decreasing pro-inflammation. A proposed mechanism of CeO_2 nanoparticles is the initiation of glial repolarisation from M2 to M1, promoting anti-inflammation through the upregulation of various pathways and associated transcription factors (i.e., TrkB, CaMK, ERK, P13K, AKT and CREB) which promote the regulation of neurotrophic factors (i.e., BDNF) which promote cell survival and proliferation. Created with BioRender.com.

Cerium oxide nanoparticles delay the development of Aβ species formation after exposure to magnetite particles in an AD mouse model

Aβ plaques are one of two major neuropathological features in AD brains (16). Neuroinflammation is another hallmark feature of AD development and is considered another theory in the pathogenesis of the disease (29). In this theory, the accumulation of Aβ plaques trigger the activation of microglial and astrocytic cells that in turn produces numerous inflammatory cytokines and mediators subsequently leading to chronic inflammation within the brain (549). Therefore, we next investigated the effects of the nanoparticles on the development of Aβ species in the double transgenic APP/PS1 mouse model, using the W/T littermates as a comparison. Aβ plaques are large accumulations of Aβ peptides, primarily the Aβ42, the principal deposit of Aβ plaques (16). To assess the effects of the nanoparticles on the accumulation of Aβ plaques, we performed in vivo brain imaging using a NIRF probe that targets Aβ aggregates in the brain (Figure S6.4) and thioflavin S. staining of the left hemisphere at experimental endpoint. Representative images from in vivo brain imaging shows brighter fluorescence was emitted in the W/T and APP/PS1 mice that had been exposed to magnetite particle (Figure 6.6A). Analysis of the images show an increase in the average radiance to 2.09 ± 0.31 ($P < 0.05$) in W/T mice and 2.3 ± 0.28 ($P < 0.05$) in APP/PS1 mice exposed to magnetite particles, compared to saline (1.2 ± 0.14 and 1.03 ± 0.06 respectively, Figure 6.6B and C). The NIRF probe (CRANAD-2) detects for the presence of soluble (Aβ40) and insoluble (Aβ42) peptides, and do not necessarily detect the presence of Aβ plaques (large deposits of peptide principally Aβ42 peptide aggregates) (141). Unlike humans, C57BL/6 W/T mice do not develop Aβ plaques during the course of normal aging, however they are still able to develop Aβ peptide aggregates (349, 350), seen in Figure 6.6A. These results indicate that exposure to magnetite particles induces an increase in both soluble (Aβ40) and insoluble (Aβ42) peptides, and that there is less soluble and insoluble Aβ peptides after treatment with both CeO_2 and blue $SiCeO_2$ nanoparticles (Figure 6.6B and C). Thioflavin S. stain detects the characteristic β-pleated sheets of Aβ plaques, therefore stained brain tissue samples were then analysed. As expected, there were no Aβ plaque formations in all W/T mice (Figure S6.5), however there was an increase in Aβ plaque amounts in the APP/PS1 magnetite exposed mice to 241.3 ± 27.4 plaque counts ($P < 0.001$), compared to the saline administered mice (78.7 ± 20.8, Figure 6.6D and F). After exposure to blue $SiCeO_2$ nanoparticles there is a decrease in Aβ plaque amounts to 112.3 ± 36.3 plaque counts, compared to the APP/PS1 magnetite exposed mice, however no

significance is seen (Figure 6.6D and F). While there are decreased Aβ plaque amounts after CeO_2 nanoparticle treatments in APP/PS1 mice there is no significance. The SH-SY5Y cells were also investigated for Aβ42 aggregates, displaying a significant increase in Aβ42 protein levels (39.10 ± 1.12 $P < 0.0001$), in magnetite particle exposed cells compared to the control, and while a trend towards a decrease in Aβ42 aggregation can be observed after CeO_2 or blue $SiCeO_2$ nanoparticles exposure there is no significance (Figure 6.6E). These results indicate magnetite particles can induce the formation of Aβ species and pose a risk to the development of AD, consistent with the study by Maher et al (2016) (181), that theorized the possible link between air pollutant magnetite PM and the development of AD. Aβ42 aggregation can also occur as result of increased inflammation and oxidative stress, therefore we suggest that the downstream antioxidant and anti-inflammatory effects of CeO_2 or blue $SiCeO_2$ nanoparticles had not yet taken place, and therefore CeO_2 nanoparticle exposure time needs to be further investigated in in vitro studies to determine this.

While this mechanism is not well understood, it is possible that CeO_2 nanoparticles can initiate the breakdown of Aβ40 and Aβ42 aggregates, through its potent antioxidant, anti-inflammatory and neuroprotective properties, thereby preventing or delaying the development of Aβ plaques, however its effects on well-established Aβ plaques is unknown. Research into the APP/PS1 model has found that Aβ plaque deposition is almost exclusively driven by Aβ42 protein aggregation, due to the genetic mutations in the APP and PS1 proteins (16). Evidence has been found that CeO_2 nanoparticles can reduce the formation of amyloid species and β-sheets (precursors to Aβ plaques), confirming that their presence limited the formation of well-defined fibrillar structures (221). While the CeO_2 and blue $SiCeO_2$ nanoparticles are primarily consistent in reducing Aβ species in the in vitro and in vivo models, there is a clear decrease in Aβ plaque amounts in the APP/PS1 mice after treatment with blue $SiCeO_2$ nanoparticles compared to CeO_2 nanoparticles. The blue silica coating induces a more reduced state (higher Ce^{3+}/Ce^{4+} ratio), exhibiting higher SOD mimetic activity. SOD mimetic activity is known to shift the production to increase formation of the soluble (Aβ40) peptide over the insoluble (Aβ42) protein aggregates, ultimately decreasing the propensity for aggregation and neurotoxicity (521). Overall, these results are consistent with the previous in vitro and in vivo data presented, displaying that treatment with blue $SiCeO_2$ nanoparticles induce a more prominent antioxidant and anti-inflammatory effect, compared to CeO_2 nanoparticles, thus signifying it as a superior choice for a neurodegenerative therapy.

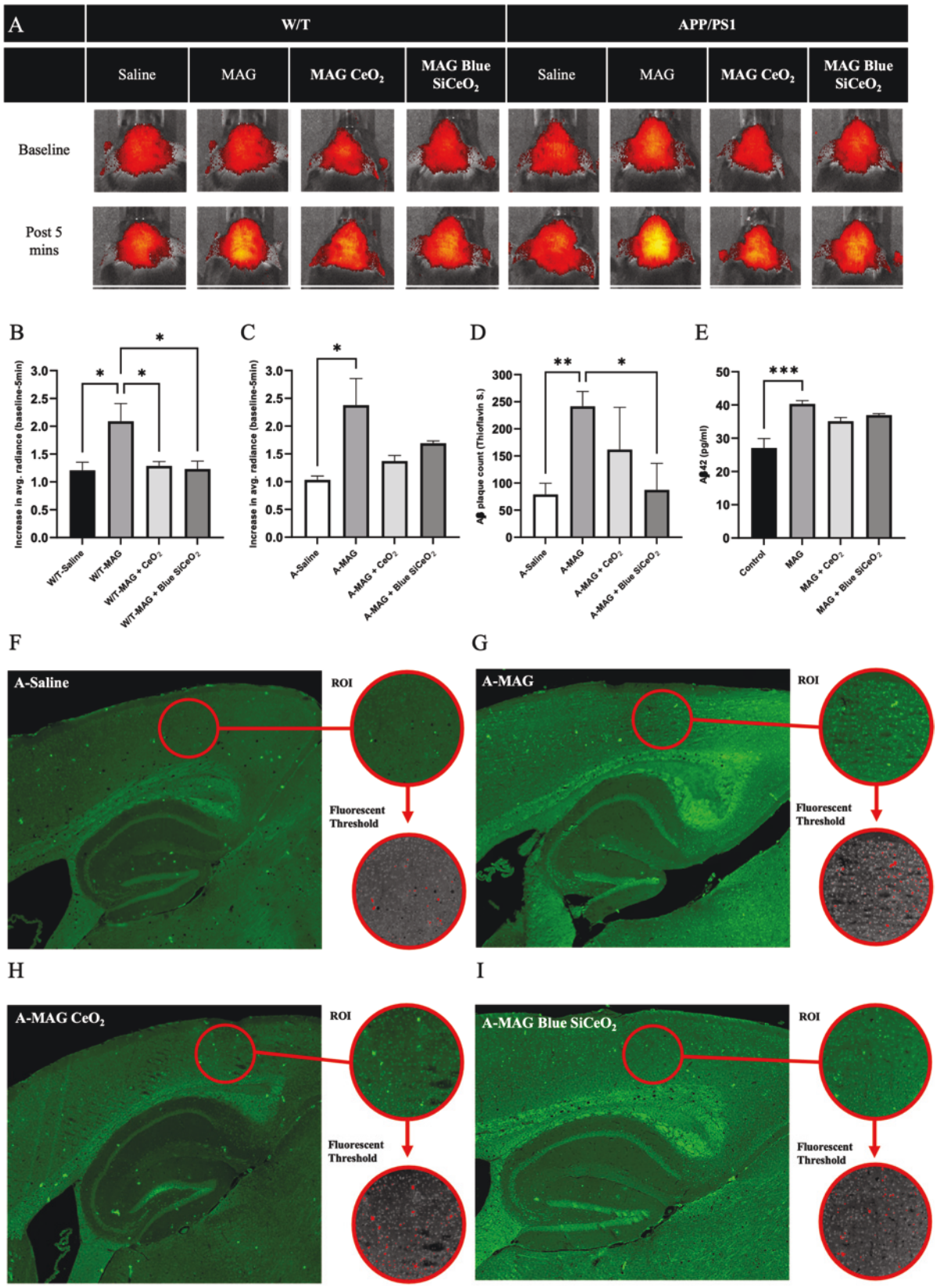

Figure 6.6. *In vivo*, *ex vivo* and *in vitro* analysis of Aβ species, after exposure to magnetite particles and CeO_2 nanoparticles. (A) NIRF *in vivo* brain imaging (baseline and post 5 mins),

W/T mice and APP/PS1 mice. (B) Increase in average radiance of Aβ plaque formation in W/T mice (baseline - post 5 minutes), (n = 5-11). (C) Increase in average radiance of Aβ plaque formation in APP/PS1 mice (baseline - post 5 minutes), (n = 5-11). (D) Aβ plaque count, from Thioflavin S. stained brain tissue in APP/PS1 mice, (n = 5-11). (E) Aβ42 protein levels, SH-SY5Y cells (n = 8). (F) Thioflavin S. stained brain tissue from A-Saline, (G) A-MAG, (H) A-MAG + CeO_2 and (I) A-MAG + Blue $SiCeO_2$ mice, the arrows indicate the Aβ plaques. * $P < 0.05$, ** $P < 0.001$, *** $P < 0.0001$, **** $P < 0.0001$. All error bars indicate mean ± SEM.

Blue Silica Cerium oxide nanoparticles delays neuronal cell loss in W/T mice after exposure to magnetite particles

During the development of AD, there is an increase in Aβ aggregates and Aβ plaques deposits, forming in and around neuronal cells leading to the disruption of several important regulatory pathways, causing dysfunction and eventually cell death, a clinical feature of AD patients, with the hippocampal region being the most vulnerable (31-35). The hippocampus is essential for episodic memory function, relying on pathway interactions from various stimuli (e.g., visual, auditory, olfactory and sensory), consisting of four main regions; the cornu ammonis (Ca), dendate gyrus (DG), subiculum, entorhinal cortex (EC; five layered region) (31, 550). The perforant pathway connects the parietal, temporal and prefrontal cortices to the hippocampus, where the axons in the entorhinal cortex (EC), extends into the DG, then further project into either the (i) Ca3 region or the (ii) Ca1 regions of the hippocampus (31, 144). The pyramidal cells in the Ca1 region send their axons to the subiculum and then to entorhinal cortex (31). An increase in Aβ species formation and plaques have been associated with neuronal cell loss in AD development, therefore, the hippocampus region of the brain was stained with cresyl violet to allow for neuronal cell counting. Representative images of the hippocampus region showing stained neurons are shown for the DG, Ca3 and Ca1 regions for W/T saline, magnetite particle and blue $SiCeO_2$ nanoparticle exposed mice as well as APP/PS1 saline and magnetite particle exposed mice (Figure 6.7A-E). Neuronal cell counting shows that regardless of the mouse model (W/T or APP/PS1), exposure to magnetite particles results in a significant reduction in neuronal cells in all regions of the hippocampus (Figure 6.7F-K). These results are consistent with the previous Aβ species data, and agrees with a study, which found that Aβ plaques may act synergistically with magnetite to enhance cellular toxicity and induce cell death in cortical neurons from rat embryos (E18-19 Sprague-Dawley) (551). Therefore, we suggest that the increased oxidative stress and inflammation induced by magnetite, induces an increase in Aβ

species formation, which in turn induces neuronal toxicity and cell death. After treatment with blue $SiCeO_2$ nanoparticles, there is a significant increase in neuronal cell counts to 393.5 ± 11.9 ($P < 0.05$) in the DG region, 233.6 ± 8.4 ($P < 0.05$) in the Ca3 region and 194.4 ± 8.16 ($P < 0.001$) in the Ca1 region compared to magnetite exposed mice in the hippocampus of the W/T mice (Figure 6.7F, H and J). Treatment with CeO_2 nanoparticles in W/T mice showed only a slight increase in neuronal cell amounts compared to magnetite exposed mice, however this was not significant. Of note, treatment with both CeO_2 and blue $SiCeO_2$ nanoparticles in the APP/PS1 mice showed no increase in neuronal cell amounts compared to magnetite exposed mice (Figure 6.7G, I and K). At experimental endpoint all mice were 10.5 months old, with extensive AD neuropathology's present (123). While CeO_2 nanoparticles are known to promote cell survival, the mutations exhibited by the APP/PS1 mice may delay the neuroprotective effects of these treatments. Overall, these results indicate that magnetite particles induce neuronal cell death in both W/T and APP/PS1 mice, and that after treatment with blue $SiCeO_2$ nanoparticles in W/T mice, neuronal cell death is delayed, prevented or reversed (i.e., inducing cell proliferation effects) promoting cell survival. This is consistent with the BDNF in vitro and in vivo results (Figure 6.7H-J), suggesting that the blue $SiCeO_2$ nanoparticles induce antioxidant and anti-inflammatory effects, exhibiting neuroprotective properties which promote cell survival, further supporting their possible role in inducing cell proliferation. These results further indicate that blue $SiCeO_2$ nanoparticles are inducing a more consistent and wholistic therapeutic effect, signifying the benefits of silica oxide coating and the more reduced form of CeO_2 nanoparticles.

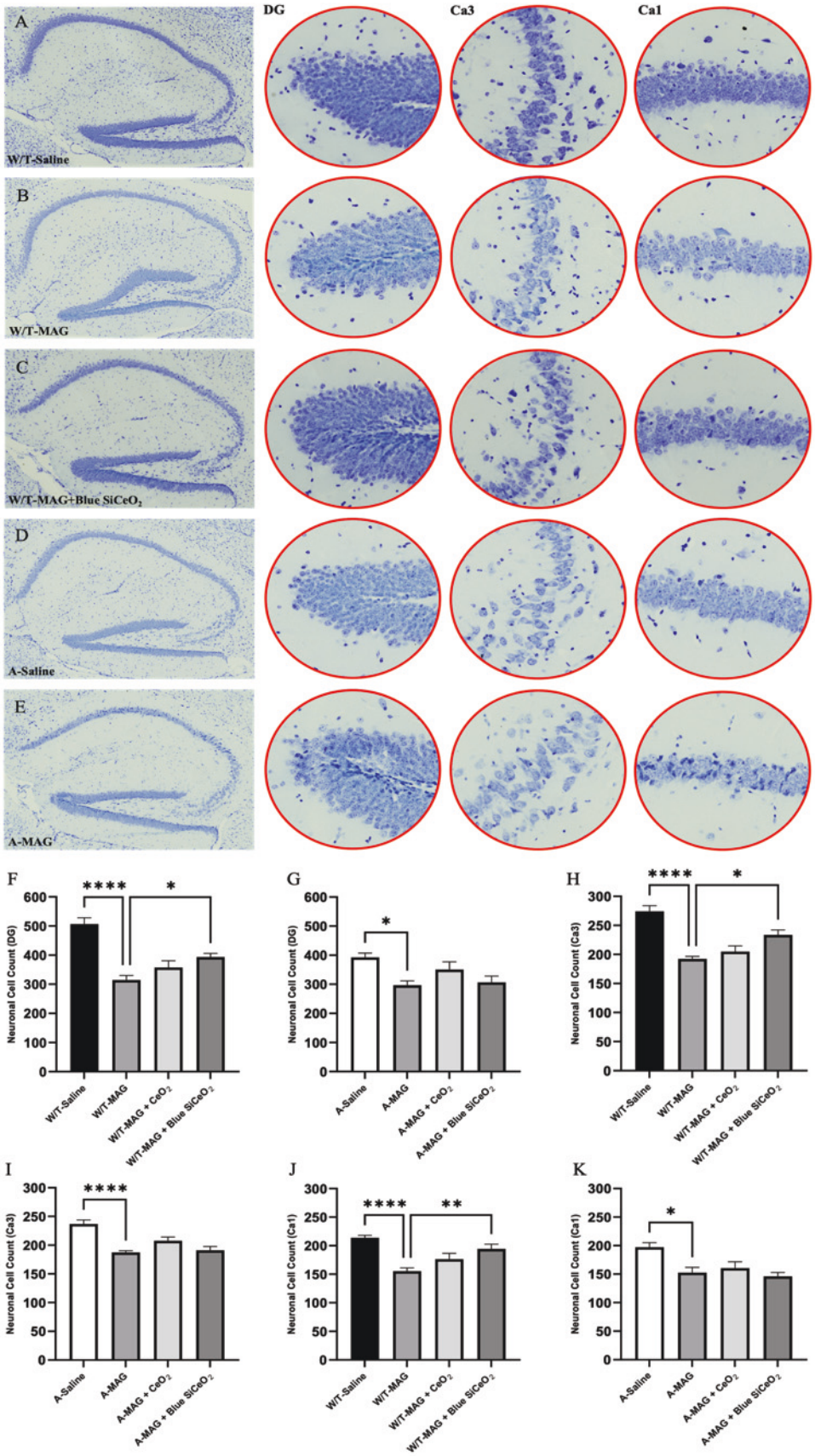

Figure 6.7. *In vivo* analysis of neuronal cell viability and death in the hippocampus regions; DG, Ca3 and Ca1 and in SH-SY5Y cells after exposure to magnetite particles and CeO_2

particles. (A) Brightfield image of hippocampus regions (DG, Ca3 and Ca1) in W/T - Saline, (B) W/T - MAG, (C) W/T – MAG + Blue $SiCeO_2$, (D) A - Saline and (E) A - MAG. (F) Neuronal cell counting in the DG region, W/T mice (n = 5-11). (G) Neuronal cell counting in the DG region, APP/PS1 mice (n = 5-11), * $P < 0.0327$ (control vs. MAG). (H) Neuronal cell counting in the Ca3 region, W/T mice (n = 5-11). (I) Neuronal cell counting in the Ca3 region, APP/PS1 mice (n = 5-11). (J) Neuronal cell counting in the Ca1 region, W/T mice (n = 5-11). (K) Neuronal cell counting in the Ca1 region, APP/PS1 mice (n = 5-11). * $P < 0.05$, ** $P < 0.001$, *** $P < 0.0001$, **** $P < 0.0001$. All error bars indicate mean ± SEM.

Cerium oxide nanoparticles delay/alleviate cognitive impairment, a behavioural change associated with AD pathologies in an in vivo model

The progression of AD is closely associated with neuronal cell death via several complex interactions including the development of Aβ plaques (318). Neuronal cell death causes brain shrinkage, a common AD pathophysiological trait, by which point the symptoms of AD (e.g., memory loss, poor judgement, increased anxiety and stress, apathy and withdrawal or depression and an inability to perform everyday tasks) are expressed (318, 325). Behavioural testing was completed in the final two weeks of the animal experiment, to determine the effects of the nanoparticles on AD development.

The NOR test assesses short-term memory and cognitive impairment, established by implementing the recognition index (RI) to assess if the mice could distinguish the novel object from the familiar one (135, 136). Analysis of the RI revealed that regardless of the mouse model (W/T and APP/PS1), exposure to magnetite particles resulted in increased cognitive impairment seen from the lack of significance in time spent with the familiar object compared to the novel with respect to the W/T saline mice ($P < 0.0001$) and the APP/PS1 saline ($P < 0.001$) (Figure 6.8A and B). Cognitive impairment is a typical symptom of AD diagnosis, which is associated with increased neuronal cell loss (552). The hippocampal region experiences severe neuronal cell loss in the development of AD and is responsible for many forms of learning and memory (553). Cognitive function relies on the synaptic function and plasticity of the granule cells in the DG region of the hippocampus to project signals into the pyramidal cells in both the Ca3 and Ca1 regions. This process is highly sensitive to change in homeostasis with the development of Aβ plaques associated with synaptic dysfunction and loss

(554, 555). Therefore, these results indicate that magnetite particles are inducing cognitive impairment, coinciding with neuronal cell loss (Figure 6.7F-K). Treatment with both CeO_2 and blue $SiCeO_2$ nanoparticles appears to decrease the degree of cognitive impairment, seen in the significant difference in time spent with the familiar object compared to the novel object in the W/T mice ($P < 0.0001$ and $P < 0.001$) and APP/PS1 mice ($P < 0.001$ and $P < 0.05$) respectively. The increased neuronal cell count observed in the W/T blue $SiCeO_2$ nanoparticle exposed mice (Figure 6.7F, H and I) is consistent with these results, however, this is not the case for the W/T CeO_2 nanoparticle and APP/PS1 CeO_2 and blue $SiCeO_2$ nanoparticle exposed mice. While the novel objection recognition test is extensively used for AD research, it assesses the working memory, as opposed to spatial navigation, learning and memory, which is severely impeded by the development of AD and is a significant function of the hippocampal region (552, 556). Therefore, with attention to recent literature, a spatial learning memory test, like the Morris water maze, relying on the mice to navigate the perimeter of an open swimming arena to locate the submerged platform is considered a more accurate behavioural study in AD development, closely associated with the degree of neuronal damage in the hippocampal region (557). Evidence has shown that this test is able to measure hippocampally dependent spatial navigation and reference memory, found to be sensitive across a range of experimental treatment effects (552).

Anxiety and stress are symptoms that are associated with AD diagnosis and are closely associated with increased cognitive impairment in the development of AD (318-320, 347). In this study, we used the EPM to assess for anxiety and stress, which is identified by the increased time spent in the closed arms compared to the open arms of the maze (137, 138). The EPM test for the W/T mice showed that the magnetite exposed mice spent significantly less time in the closed arm, compared to saline to 126.3 ± 6.6 seconds ($P < 0.001$) seen in Figure 6.8C. The trend is similar for the magnetite particle exposed APP/PS1 mice however no significance was shown (Figure 6.8D). No significant effects were observed for W/T or APP/PS1 mice treated with CeO_2 and blue $SiCeO_2$ nanoparticles. This is also seen in the tail suspension test, analysing the depressive-like symptoms, as preclinical AD is often characterized by social withdrawal in both human and mice (140, 558, 559). Depressive-like symptoms are characterized by lack of mobility (i.e., time spent mobile), which is found after treatment with magnetite particles in the W/T mice to 49.1 ± 3.9 seconds ($P < 0.05$) compared to W/T saline (80.8 ± 9.6 seconds; Figure 6.8E). A decrease in mobile time is also seen in the APP/PS1 mice exposed to magnetite

particles, to 55 ± 3.3 seconds compared to APP/PS1 saline 84.4 ± 18.1 seconds, however there is no significance (Figure 6.8F). While there is an upward trend of increased mobility seen in W/T and APP/PS1 CeO_2 and blue $SiCeO_2$ nanoparticle exposed mice, there is no significance (Figure 6.8E and F). These observations suggest that both W/T and APP/PS1 mice exhibit anxiety, stress and depressive like behaviours following exposure to magnetite particles, with CeO_2 and blue $SiCeO_2$ nanoparticle exposure having no alleviating effect on these symptoms. Stress and anxiety are critically involved in the development and progression of AD, with studies suggesting that they can exacerbate the symptoms like depression that coincide with AD development (560). When exposed to a stressful situation the pituitary gland produces ACTH, subsequently releasing cortisol by the adrenal cortex, which play central roles in exacerbating AD by stress (560, 561). Cortisol exhibits anti-inflammatory properties however, a study for Cushing's disease (a condition that occurs from exposure to chronic high cortisol levels) has found a correlation in hypercortisolism coincided with chronic oxidative stress and inflammation (562). While this example is based on adipose tissue, elevated cortisol levels have been found in the AD patients. While the exact mechanism of magnetite particles is still unknown, these results suggest that the presence of the particles increase anxiety, stress and depressive like behaviours which are side effects to the increased oxidative stress and inflammation that magnetite particles induce. Moreover, regardless of CeO_2 and blue $SiCeO_2$ nanoparticle exposure, these behavioural changed induce by magnetite particles were unable to delayed or reversed by the animal experimental endpoint, and therefore this demonstrates that magnetite induces behavioural changes associated with AD development.

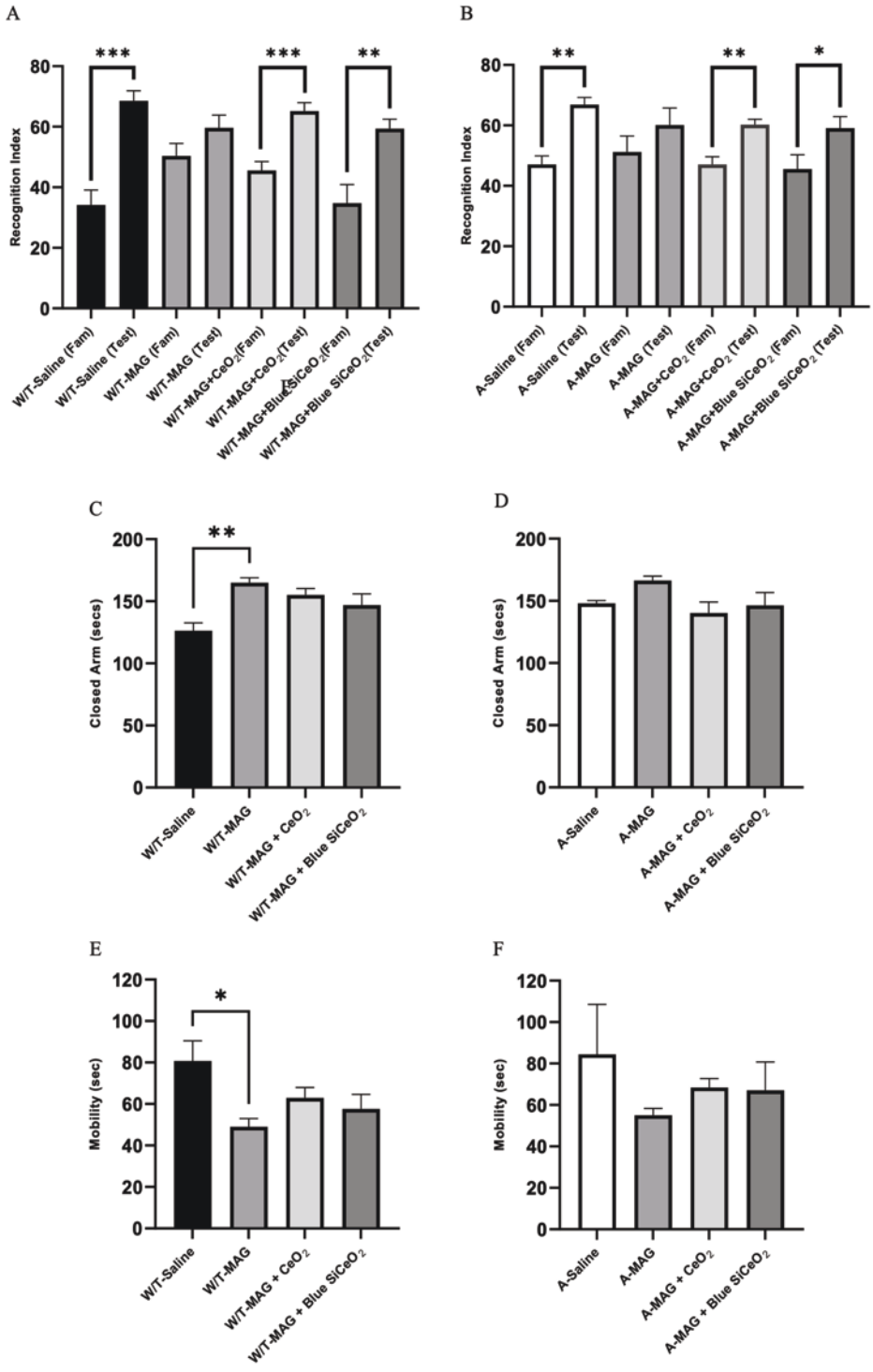

Figure 6.8. *Ex vivo* analysis of the behavioural changes associated with the development of AD in W/T and APP/PS1 mice, after exposure to magnetite particles and CeO_2 nanoparticles. (A) NOR analysis with the recognition index, W/T mice (n = 5-11). (B) NOR analysis with the recognition index, APP/PS1 mice (n = 5-11). (C) Time spent in the closed arm in the EPM, W/T mice (n = 5-11). (D) Time spent in the closed arm in the EPM, APP/PS1 mice (n = 5-11). (E) Mobility time (secs) from TST, W/T mice (n = 5-11). (F) Mobility time

(secs) from TST, APP/PS1 mice (n = 5-11). ** P < 0.001, *** P < 0.0001, **** P < 0.0001. All error bars indicate mean ± SEM.

Mouse models for AD have been instrumental in further understanding the pathophysiology and behavioural characteristics of the disease, however there are some limitations to mouse models and therefore to this study. This study used a combination of male and female mice, however during the analytical process the mice were not further segregated by gender, and therefore the potential gender effects were not analysed which is a limitation to the study. The concentration of both CeO_2 and blue $SiCeO_2$ nanoparticles was established based on preliminary in vitro testing. Both SH-SY5Y and B-V2 cells were tested with CeO_2 nanoparticle concentrations ranging from 3.13 – 50 μg/mL, for 24 hours resulting in little to no effect on cell viability (Figure S6.4A-D). The concentration of 50 μg/mL was chosen, and further preliminary studies were conducted, again assessing the cell viability, ROS and NO production on both SH-SY5Y and B-V2 cells, compared to an inflammatory stimulus (e.g., LPS) ranging between 1-120 μg/mL for 24 hours (Figure S6.4E-I) (152, 153).

It is important to note that CeO_2 and blue $SiCeO_2$ nanoparticle treatments alone were not included in the in vivo experiment as control groups, and therefore should be further explored as this will also influence the dosage and route of administration in future studies. In this study, administration of CeO_2 and blue $SiCeO_2$ nanoparticles every third day may not be easily translated into a clinical setting, and therefore investigation into the route of administration and dosage needs to be explored. One study found that a single bolus dose of CeO_2 nanoparticles could alleviate depressive-like symptoms, which was accompanied by a decrease in oxidative stress, inflammation, improvement of hippocampal cell viability, cell proliferation and neurite growth, emphasizing the neuroprotective effects of CeO_2 nanoparticles neuroprotective in the stress-induced model of depression (e.g., rat model of unpredictable induce chronic mild stress) (563). A study using an *in vivo* model (Sprague Dawley rats) were exposed to 7.65, 5 and 2.65 g/cm^3 depending on weight of animal, of CeO_2 nanoparticles and amorphous $SiCeO_2$ nanoparticles, and a combination of these nanoparticles, finding that amorphous $SiCeO_2$ nanoparticles completely reduced acute lung inflammation and injury in 28 days post exposure, not seen in other treatment variations (118). Therefore, a personalized treatment option considering weight could be implemented, however this needs to be further investigated.

6.5 Conclusion

Based on the data obtained, magnetite particles have been found to induce the pathologies associated with AD, and that after CeO_2 and particularly blue $SiCeO_2$ nanoparticle treatments, these pathologies are reduced. This study shows the remarkable antioxidant, anti-inflammatory and neuroprotective properties of CeO_2 nanoparticles. Most interestingly, CeO_2 nanoparticles possible mediation of signalling pathways that potentially promote cell proliferation, signifies a possible alteration in microglial and astrocytic polarization and activation. However, this needs to further be elucidated. Overall, this study displays that air pollutant magnetite particles induce the pathologies associated with AD, and that CeO_2 nanoparticles and most consistently, blue $SiCeO_2$ nanoparticles can delay and, in some cases, reverse these pathologies and therefore prove to be a promising therapy for AD.

6.6 Supplementary Information

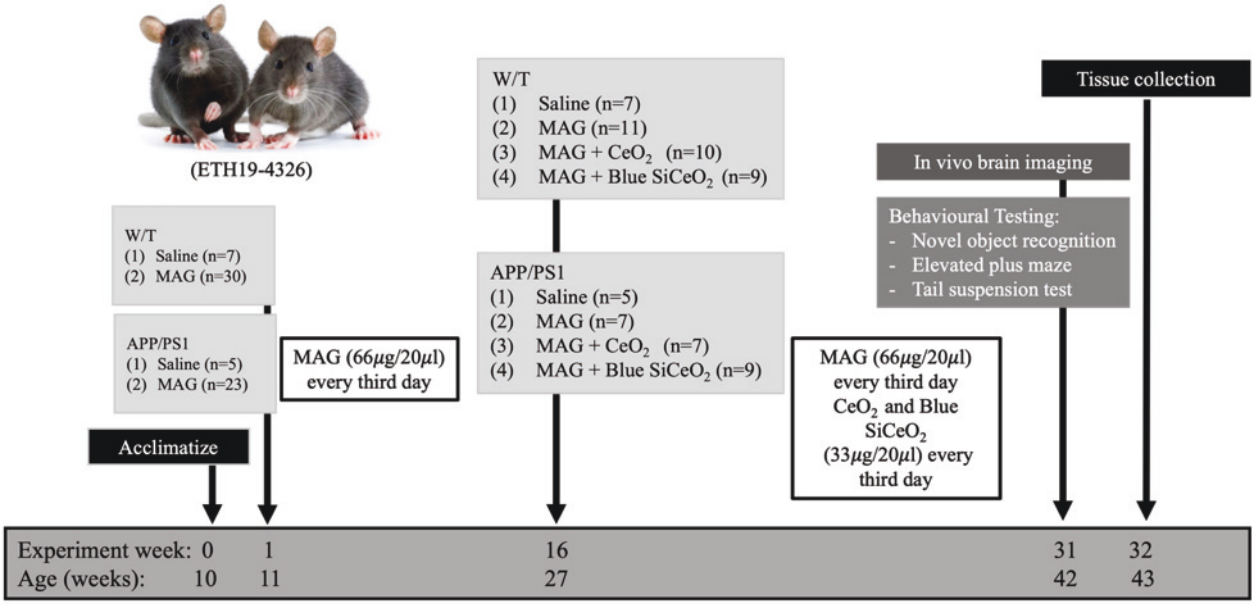

Figure S6.1. A timeline summary of the *in vivo* study. Sixty-five female and male wild-type (W/T; C57BL/6) mice were genotyped and divided into four groups; W/T-Saline, W/T-MAG, APP/PS1-Saline and APP/PS1-MAG. Animals were intranasally administered with magnetite particles (66μg/20μl) every third day for 4 months. In week 16 of the animal experiment, the mice were further sub-divided into eight groups; W/T-Saline, W/T-MAG, W/T-MAG+CeO_2, W/T-MAG+Blue $SiCeO_2$, APP/PS1-Saline, APP/PS1-MAG, W/T-MAG+CeO_2 and W/T-MAG+Blue $SiCeO_2$. Animals continued to be intranasally administered with magnetite particles (66μg/20μl) or every third day, with some groups also having intranasal administration of CeO_2 or blue $SiCeO_2$ nanoparticles (33μg/20μl) every other third day for 4 months. In week 31 of the animal experiment the mice underwent behavioural testing and *in vivo* brain imaging.

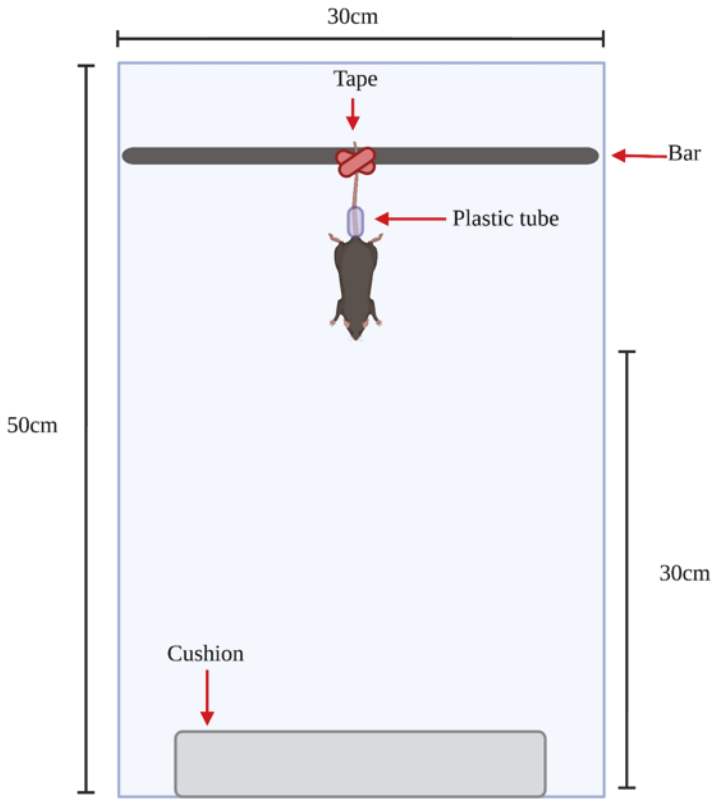

Figure S6.2. Schematic representation of the TST experiment. The mice were placed upside with their tails taped to the bar, and the mobility time was recorded. Created with BioRender.com.

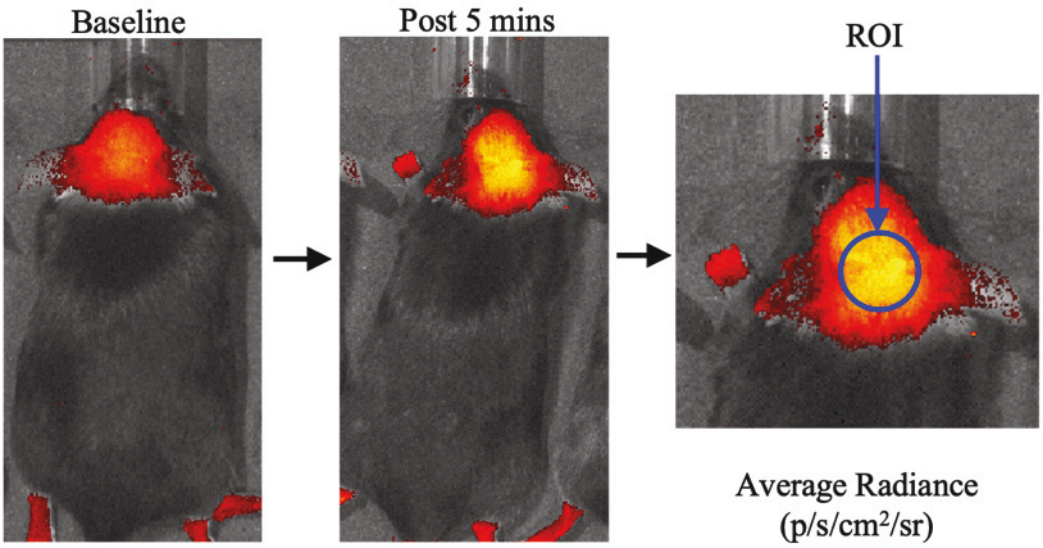

Figure S6.3. Schematic representation of *In vivo* NIRF brain imaging. A NIRF molecular imaging probe was used to target Aβ42 protein aggregation. A baseline fluorescence image was obtained prior to intravenous injection of the NIRF probe, followed by another fluorescence image obtained 5 minutes post injection. The average radiance (p/s/cm^2/sr) was recorded from the region of interest (ROI).

Table S6.1. Antibodies used in Western Blot analysis

Protein	Dilution	Company	Catalogue
β-Actin	1:1000	Cell Signalling Technology, MA, USA	4970S
BDNF	1:1000	Abcam, UK	108319
GFAP	1:1000	Abcam, UK	33922
ICAM-1	1:1000	Abcam, UK	53013
NF-κB p65	1:1000	Cell Signalling Technology, MA, USA	8242T
Phospho-NF-κB p65 (Ser536)	1:1000	Cell Signalling Technology, MA, USA	3033T
MAPK	1:1000	Cell Signalling Technology, MA, USA	8690S
Phospho-MAPK	1:1000	Cell Signalling Technology, MA, USA	4511S
Tumour necrosis factor (TNF)	1:1000	Santa Cruz, CA, USA	sc-1350
Interleukin 6 (IL-6)	1:1000	Santa Cruz, CA, USA	sc-1265
Anti-rabbit Secondary (HRP conjugated)	1:5000	Cell Signalling Technology, MA, USA	7074P2
Anti-mouse Secondary (HRP conjugated)	1:5000	Cell Signalling Technology, MA, USA	7076P2
Anti-goat Secondary (HRP conjugated)	1:2000	Santa Cruz, CA, USA	sc-2350

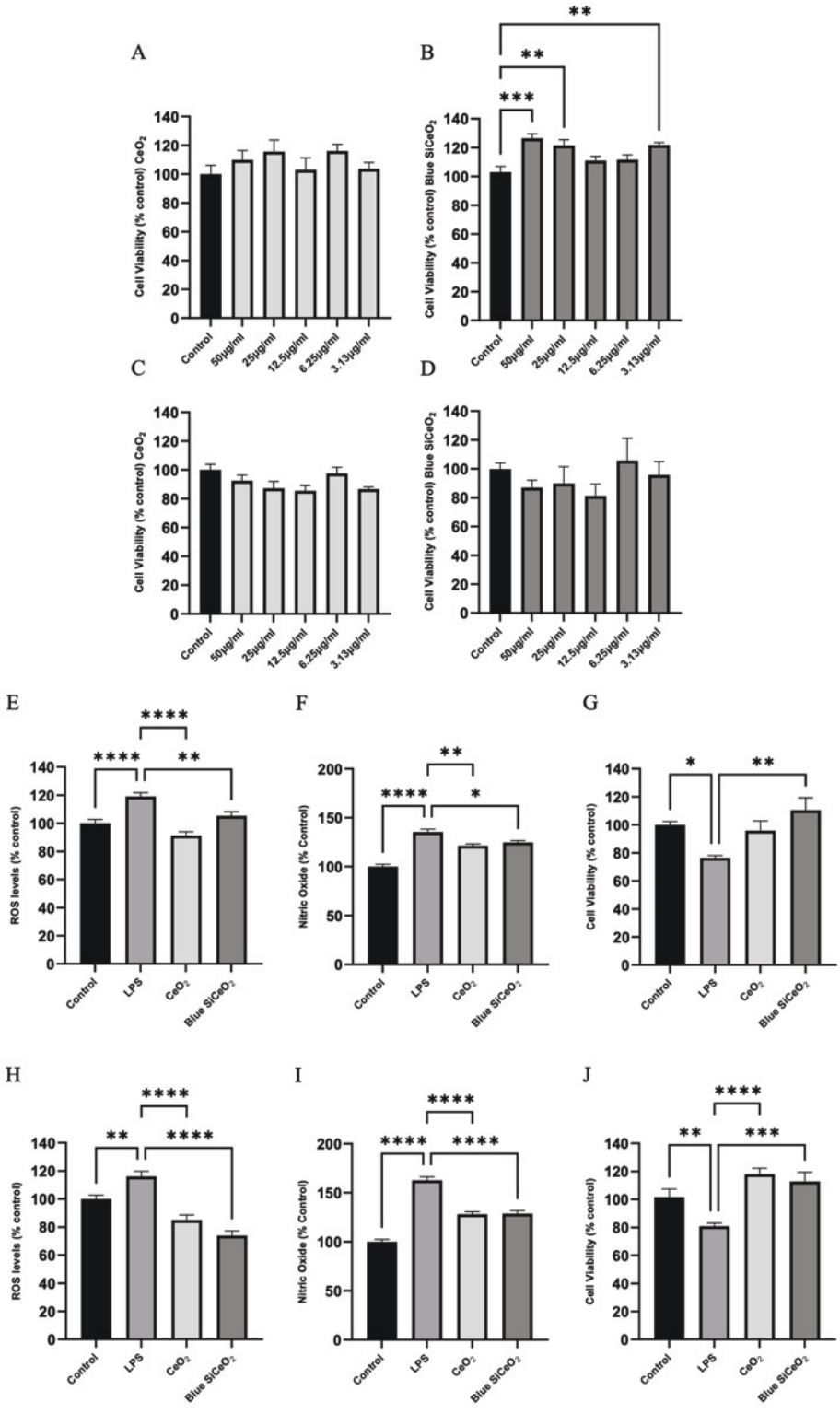

Figure S6.4. *In vitro* analysis of oxidative stress and cell viability responses after exposure to CeO_2 and blue $SiCeO_2$ nanoparticles. (A) Percentage of cell viability from control testing various concentrations of CeO_2 nanoparticles, SH-SY5Y cells, (n = 4). (B) Percentage of cell viability from control testing various concentrations of Blue $SiCeO_2$ nanoparticles, SH-SY5Y cells, (n = 4). (C) Percentage of cell viability from control testing various concentrations of

CeO_2 nanoparticles, B-V2 cells, (n = 4). (D) Percentage of cell viability from control testing various concentration of Blue $SiCeO_2$ nanoparticles, B-V2 cells, (n = 4). (E) Percentage of ROS production from control, SH-SY5Y cells, (n = 4). (F) Percentage of NO production from control, SH-SH5Y cells, (n = 4). (G) Percentage of cell viability from control, SHSY5Y cells, (n = 4). (H) Percentage of ROS production from control, BV2 cells, (n = 4). (I) Percentage of NO production from control, BV2 cells (n = 4). (J) Percentage of cell viability from control, BV2 cells, (n = 4). *P < 0.05, **P < 0.001, ***P < 0.0001, ***P < 0.0001. All error bars indicate mean +/- SEM.

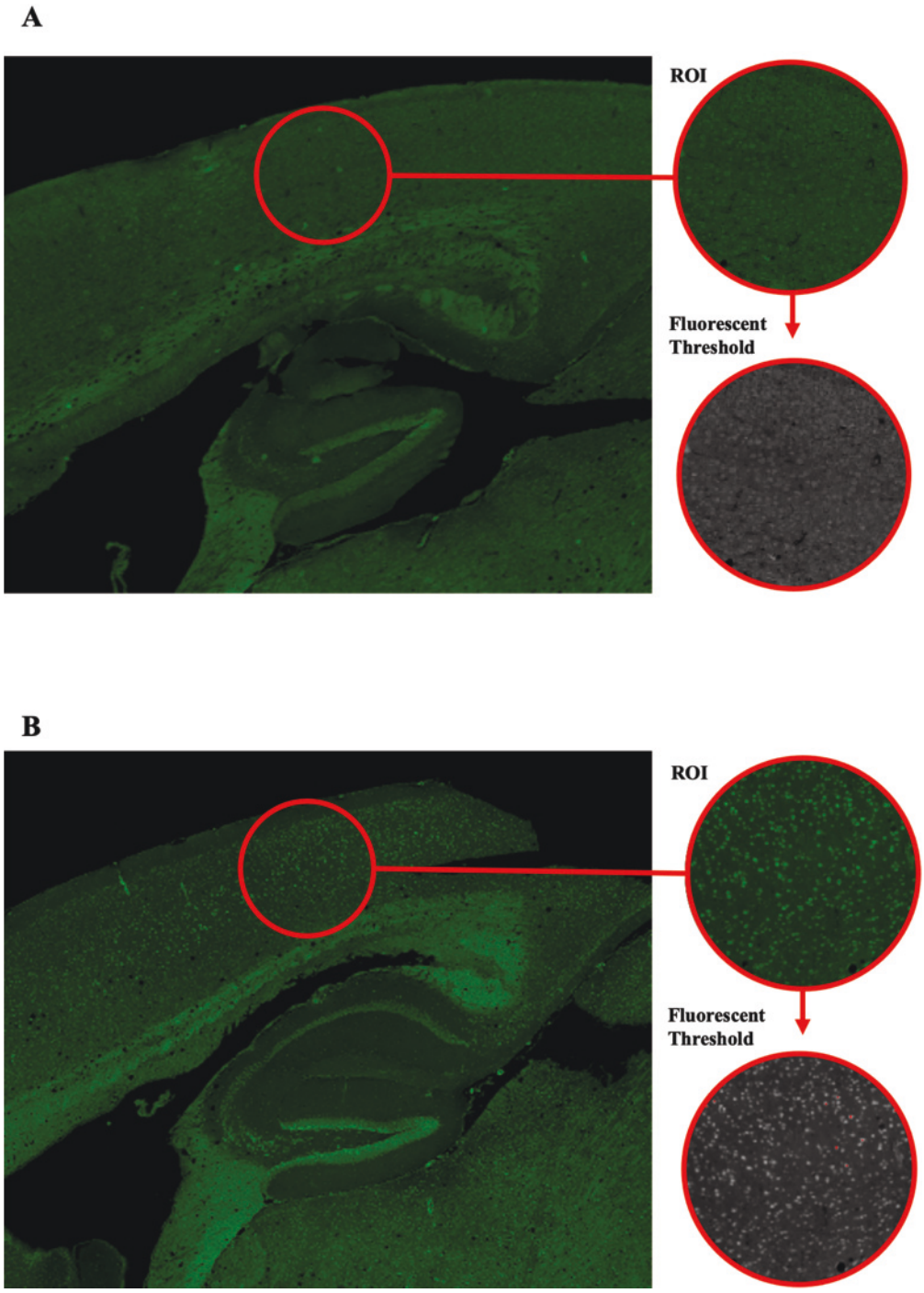

Figure S6.5. *Ex vivo* analysis of Aβ plaques, after exposure to magnetite particles and CeO_2 nanoparticles. (A) Thioflavin S. stained brain tissue from W/T saline mice and (B) W/T magnetite exposed mice.

Chapter 7: Conclusions and Future Perspectives

Chapter Summary

This chapter will provide a general discussion of the key findings of the present PhD project. This chapter also presents the limitations of the studies presented in this thesis as well as an outline of future directions for research in the field of magnetite particles risk to human health and the development of CeO_2 nanoparticles as therapies for neurodegeneration and AD.

7.1 Conclusions

It is well known that there is increased risk of adverse health effects associated with exposure to air pollutant particulate matter. With numerous epidemiological studies showing that increased air pollutant PM present in ambient air correlates with increased morbidity and mortality rates related to many diseases (47, 564). In fact, there are countless studies, over the last 15 years that highlight the adverse effects of air pollution associated with increased risk of lung, head, neck, and nasopharyngeal cancer, all of the upper aerodigestive tract, however, far less have focused on its role in the development of neurodegenerative diseases like AD and PD (565). Diesel exhaust emissions and air pollutant iron particles have been previously implicated in various adverse health effects as well as being implicated in neurodegenerative like AD and PD (284, 313).

Magnetite is an iron oxide mineral, that is abundant in ambient air. Like iron, magnetite forms naturally in the brain, however excessive amounts can have adverse effects on brain health (84). Magnetite is a volatile particle, with alternating lattice structure, from the $Fe_{2+}O_{4-}$ (reduced) to $Fe_{3+}O_{4-}$ (oxidised), thereby having increased redox potential (84-86). Air pollutant magnetite particles are produced in copious amounts, similarly to diesel, from combustion sources (84). A study by Maher et al (2016), found magnetite consistent to externally derived air pollutant MNPs in excessive quantities in the brain tissue of people with AD (85, 88). There have been few studies to confirm this, and therefore the systematic review of magnetite studies was completed (Chapter 3) revealing the mechanism of naturally forming magnetite as well as its various environmental, industrial and biomedical applications of magnetite from 1990 - 2020 (259, 566, 567). More significantly, this study uncovered the cytotoxic effects of magnetite particles through its extensive use as a biomedicine and more recently its potential implication as an air pollutant in the form of PM correlating with neurodegenerative diseases (280, 284, 568). This study displays the wide variety of applications of magnetite particles from 1990-2020 bringing to light the gaps in knowledge about the long-term and potential side effects of magnetite particles as a biomedicine, and the future studies that need to be undertaken to establish its role in neurodegenerative diseases like AD.

Chapter 4 established that that air pollutant particles, particularly magnetite, had significant detrimental effects on anxiety and stress, while cognitive impairment was increased after

exposure to all air pollutants, with magnetite particles inducing the most neuronal cell loss. Further histological analysis showed that neuronal cell loss correlated with an increase in Aβ species formation in both the *in vivo* and *in vitro* models. These observations led to an exploration into relevant neuroinflammatory and oxidative stress markers in the pathogenesis of AD. Gene expression analysis found that air pollutant particles induced an increase in inflammatory cytokines. Further testing with western blot and biochemical analysis showed varying inflammatory and oxidative stress changes associated with AD pathogenesis in both the *in vivo* and *in vitro* models. The air pollutant particles induced NO and ROS production *via* the activation of the NFκB pathway in the *in vitro* models, therefore indicating the universal inflammatory and oxidative stress response that the air pollutant particles are inducing, suggesting their significant role in the development of AD pathogenesis. As the C57BL/6 WT mice do not develop Aβ plaques, therefore this suggests that the air pollutant particles induce an increase in neuroinflammation, oxidative stress and Aβ species formation regardless of AD pathological vulnerabilities that the APP/PS1 mice possess (147, 148). While this is the case, the APP/PS1 mice have developed more pathologies associated with AD compared to the WT mice, suggesting that the presence of Aβ plaques will speed up AD-pathological features, rendering the brain more vulnerable to neurodegeneration. This also indicates that the presence of neuroinflammation and oxidative stress in this study does correlate with an increase in Aβ species formation, and hence indicates a strong association between these driving pathological processes which is consistent with current literature supporting both the neuroinflammation and oxidative stress theories as to the trigger of AD development (332-334). Overall, magnetite particles stimulated the most consistent damaging effects in inducing the pathologies associated with AD in both the W/T and APP/PS1 mice, and therefore could play a role in the onset or progression of sporadic AD.

The management of AD is extremely challenging, with a number of therapies currently on the market as symptomatic therapeutics for AD; cholinesterase inhibitors, donepezil, rivastigmine, galantamine, and tacrine, and N-methyl-D-aspartate (NMDA)-receptor modulator memantine (90). These therapies are unable to prevent or reverse the disease progression, however, they have been extremely effective in replacing damaged or dysfunctional mediators (90). Recent research into therapies for AD have focused on targeting the underlying drivers of the disease like oxidative stress and inflammation.

Inflammation is also a process that has been closely related to the onset of various neurodegenerative diseases, including AD, where the inflammatory response in neurons includes activation of microglia, astrocytes, resulting in the release of inflammatory mediators such as cytokines and ROS. Microglia play a central role in the cellular response to pathological lesions such as Aβ plaques (368). In sporadic AD, inefficient clearance of Aβ has been identified as a major pathogenic pathway (315, 491). In turn Aβ can attract and activate microglia cells, leading to clustering microglia around Aβ deposit sites in the brain. Microglia also expresses scavenger receptors that mediate adhesion of the microglia to Aβ fibril-coated surfaces, leading to ROS secretion and cell immobilization. Secretion of ROS can result in further neuronal damage and increase in oxidative stress. The increase in oxidative stress, neuroinflammation and Aβ plaques formation around neuronal cells causes cellular dysfunction, and eventual death leading to neurodegeneration (368). The brain is the most active organ, and highly susceptible to oxidative stress due to its high oxygen content and utilization, therefore antioxidants have surfaced as potential therapies for AD (103, 105). CeO_2 has surfaced as a promising candidate, previously being investigated for glioma and ischemic stroke therapies, due to its antioxidant behaviour (105, 106). CeO_2 has unique structural and redox properties, however there are few studies about its potential role as a therapy for neurodegeneration. This motivated the systematic and bibliometric study on CeO_2 literature (Chapter 5), to better understand the characteristics of CeO_2 and its relation to research trends from 1990 - 2020. This study highlighted CeO_2 incredible catalytic and redox properties allowing its exploitation for innumerable environmental/industrial and biomedical applications (105-107). This study highlighted its ability to target cancer cells, and as a therapy for inflammatory diseases acting as efficient ROS scavengers (108, 569, 570). This study also revealed the advanced nanotechnology engineering, like manipulation of CeO_2 nanoparticle additives (e.g., dopants/coating, surface functionalized, core-shell structures, nanocomposites, and hybrid structures). These additives proved to increase efficiency of CeO_2 nanoparticles for a wide range of applications, including the most recent studies highlighting its potential as a therapy for neurodegenerative diseases like AD (106).

The advancements in nanoparticle engineering and the ability to enhance CeO_2 nanoparticles for specific therapies led to the investigation of whether CeO_2 and blue silica doped CeO_2

nanoparticles could delay or reverse the air pollutant magnetite induced AD pathologies (Chapter 6). This study was conducted using two *in vitro* models to represent both the neuronal (SH-SY5Y cells) and microglial (BV-2 cells) cells in the brain, along with the *in vivo* model, double transgenic murine APP/PS1 mice. This study found that both CeO_2 nanoparticles were able to reduce oxidative stress and increase cell viability, after magnetite particle exposure in both *in vitro* models. The BV-2 cells appeared to have increased cell viability compared to the control which was not seen in the SH-SY5Y cells, although the cell viability returned to the same as the control. This suggests that CeO_2 nanoparticles stimulate different reactions on different cell types, or perhaps some cells are more sensitive than others. These results suggest that BV-2 cells are more sensitive to both CeO_2 nanoparticles, particularly the BV-2 cell line, they are promoting cell survival and proliferation. BV-2 cells are microglial cells, and therefore are highly sensitive to any sort of change in homeostasis and are the initial responders in an immune response (571). We suggest that CeO_2 nanoparticles are having the same effect (promoting cell survival and proliferation) on both the SH-SY5Y and BV-2 cells, however the BV-2 cells are more sensitive. Western blot analysis was conducted on the *in vitro* (SH-SY5Y) and *in vivo* models, finding that both CeO_2 nanoparticles, but particularly blue $SiCeO_2$ nanoparticles induced anti-inflammatory effects on various inflammatory transcription factors and downstream cytokines and mediators after magnetite particle exposure. Of interest, both CeO_2 nanoparticles induced an upregulation of BDNF in the *in vitro* (SH-SY5Y) model surpassing that of the control. BDNF is a neurotrophic factor promoting cell survival and proliferation, therefore the increase in cell viability would occur downstream to this activation, further supporting the suggestion that are promoting cell survival and proliferation on both cell types (543). These results combined with the cell viability results in both *in vitro* cell models suggesting that CeO_2 nanoparticles are exhibiting properties promoting cell proliferation perhaps through the upregulation of neurotrophic factors like BDNF which may occur because of a change in glial polarization (from the pro-inflammatory M1 state to anti-inflammatory M2 state) (572, 573). The classical, proinflammatory (M1) macrophage phenotype is associated with the expression of cytotoxic genes (e.g., TNF and IL-6) and is accompanied by impaired phagocytic capacity (315, 491). This would explain the constant activation and upregulation in the cell viability and the decrease in pro-inflammatory cytokines and mediators seen in the western blot results. In summary, the results indicate that CeO_2 nanoparticles are inducing neuroprotective effects when in the presence of magnetite particles. The neuroprotective effects have shown to reduce inflammatory and oxidative stress biomarkers induced by magnetite particles.

CeO_2 nanoparticles are known to be bifunctional in that they exhibit both protective and cytotoxic effects, similar to that of the polarization of microglial and astrocytic cells (108). CeO_2 nanoparticles are known and effective ROS scavengers, however, there are other unknown mechanisms triggering signalling neurotrophic pathways inducing cell survival and proliferation which may be influencing and altering macrophage activation and polarization (from M2 to M1 polarization). A study using microglial BV-2 cells found CeO_2 nanoparticles, delayed microglial growth in S-phase of the cell cycle, in the presence of Aβ protein treatment on the cells (574). This indicates that CeO_2 nanoparticles can mediate the activation and inhibition of microglial cells dependent on its environment, and therefore must be further explored. CeO_2 nanoparticles were found to decrease Aβ species formations, after magnetite particle exposure in both W/T and APP/PS1 mice, suggesting that by targeting both oxidative stress and inflammation Aβ plaque formation is decreased (17, 368). Histological analysis found that blue $SiCeO_2$ nanoparticles delayed neuronal cell loss in the hippocampal Ca1, Ca3 and DG regions in the W/T mice after magnetite particle exposure. Suggesting that blue $SiCeO_2$ nanoparticles were effective in delaying neuronal cell loss despite the constant magnetite particle exposure. This further supports CeO_2 nanoparticles as promoting cell survival and proliferation. Furthermore, CeO_2 and blue $SiCeO_2$ nanoparticles were found to delay the progression of cognitive impairment, after exposure with magnetite particles, however no effect was seen on anxiety and stress or depressive like symptoms. This study demonstrates that CeO_2 and particularly blue $SiCeO_2$ nanoparticles, are potent antioxidant and anti-inflammatory agents, decreasing the pathologies associated with AD as well as delaying cognitive impairment. Therefore, this suggests that silica coated CeO_2 nanoparticles prove to be promising therapies for air pollutant magnetite induced AD pathologies.

The anti-inflammatory and antioxidant characteristics of the $SiCeO_2$ nanoparticles, along with the small size, enhanced enzymatic and mimetic capabilities make these nanoparticles a potential therapy for other neurodegenerative diseases like motor neuron disease, Parkinson's disease and Huntington's disease, all of which oxidative stress and inflammation play a significant role in disease progression (575). Diagnosis of AD usually occurs in patients around 65 years of age, with symptoms of cognitive impairment like the inability to retain new information, memory loss, difficulty in completing familiar tasks, changes in mood, poor

judgment, increased anxiety etc. By the time these symptoms have manifested, the pathological markers of Aβ plaques, NFTs and neuronal death are well underway, which can be confirmed with tests assessing memory and thinking skills, along with MRI detecting amyloid and tau proteins in plasma and cerebral spinal fluid (3, 4, 491, 576). As AD is a degenerative condition which progresses with age, early diagnosis is vital and therefore treatment should start immediately after diagnosis. Due to the degenerative nature of AD a continuous low dose would be recommended similar to current AD therapies, like Donepezil and Rivastigmine which are given daily at 5 mg and 1.5 mg per day respectively, however this needs to be further investigated (576).

7.2 Future Perspectives

The data presented has demonstrated that air pollutant particles, iron, diesel and most damaging, magnetite induce the onset and progression of pathologies associated with AD. Furthermore, this study confirmed that CeO_2 and particularly blue $SiCeO_2$ nanoparticles induced potent antioxidant, anti-inflammatory and neuroprotective properties after magnetite particle exposure. Significantly, CeO_2 and particularly blue $SiCeO_2$ nanoparticles exhibited cell proliferation, neurotrophic and possible control of microglial activation and inhibition. However, based on the findings in the present thesis, many new questions have arisen. Recommendations for future research to enable a better understanding of how air pollutant magnetite particles influence AD and how CeO_2 nanoparticles can be developed for therapeutic approaches in preventing AD are listed below.

What other cells play a role in the development of AD that might be activated by air pollutant magnetite particles? The brain is comprised of the two prominent cells; neurons and glial (microglial and astrocytic) cells that all play a role in the proper functioning of the brain (577). In AD, the dysfunction of these cells can lead to over production of inflammatory mediators and oxidative stress, causing chronic inflammation, and eventually cell. In this dissertation, only neuronal cells (SH-SY5Y) and microglial cells (BV-2) were used, however, studies have found that astrocytic cells also become activated and play a role in the progression of AD. It would therefore be of interest to investigate whether air pollutant magnetite particles can have the same effect on astrocytic cells.

Will a different mouse model of AD also show the adverse effects from air pollutant magnetite particles? There are numerous transgenic murine models that have been extensively used for AD research. The double transgenic APP/PS1 model used in this dissertation, carries two mutations both of which promote the production Aβ plaque development, and therefore do not accurately represent the development of sporadic AD (578). The other hallmark pathology of AD is NFT's consisting of aggregated tau protein, in which mutations have also been implemented in transgenic models with overexpression of human 4R tau mutations promoting the formation of NFTs (e.g., rTg4510 and PS19 are the most commonly used murine models). Contrary to most APP/Aβ transgenic models, and consistent with human clinicopathology, the tau mice exhibit age-dependant neurodegeneration in addition to synaptic and cognitive deficits (579). Thus, exploring the effects of air pollutant MNPs on a different transgenic model would be beneficial.

Are there any gender differences in response to both research studies? The APP/PS1 murine model, used in this dissertation has also been investigated in previous studies, with one focusing on the correlation between pancreatic islet function and AD development. Finding that male mice developed impaired glucose and insulin tolerance faster than females, with Aβ40 and Aβ42 protein levels in the females was significantly higher than that of the males (580). While the gender was considered when the mice were subdivided into treatment groups, the female mice proportionate to the male is different in some groups is different due to their genotype, and therefore it is difficult to determine whether gender had any possible effects due to the vast difference in mice number per group (table 2.4.1, 2.4.2). However, investigation into the potential gender differences would be highly valuable.

Would CeO_2 and blue $SiCeO_2$ nanoparticle treatment unaccompanied by magnetite particles have the same antioxidant and anti-inflammatory effects? Due to the novelty of this study, treatment groups of CeO_2 or blue $SiCeO_2$ nanoparticles alone, were missing and therefore should be investigated in future studies to identify any adverse effects that both CeO_2 nanoparticle treatment may have on the *in vitro* and *in vivo* models. Adding these treatment groups will be significant in identifying whether both CeO_2 or blue $SiCeO_2$ nanoparticles will have a cytotoxic affect or a benign affect and therefore will influence its future use as a biomedicine. Including these treatment groups will also be a determining factor in optimising

the dosage type and amount (e.g., bolus or constant administration) for neurodegenerative diseases, which can then be translated into a clinical setting.

The experimental analysis verified that magnetite particles do indeed induce the pathologies associated with AD, therefore may play a significant role in the onset or progression of sporadic AD. Furthermore, CeO_2 and particularly blue $SiCeO_2$ nanoparticles prove to be promising therapies to counteract the oxidative stress and neuroinflammation that corresponded with the magnetite induced AD pathologies. Importantly, blue $SiCeO_2$ nanoparticles also displayed the potential to mediate microglial activation and inhibition, therefore this must be investigated in future studies. Further research should also continue to delineate the precise mechanism of magnetite particles in the brain and the exact triggering that leads to its detrimental effects. Doing so would provide a greater understanding of the key targets that are necessary in developing a therapy for AD.

References

References

1. Swerdlow, R. H. (2007) Pathogenesis of Alzheimer's disease. *Clinical Interventions in Aging* **2**, 347-359
2. Sosa-Ortiz, A. L., Acosta-Castillo, Isaac, Prince, M.J. (2012) Epidemiology of Dementias and Alzheimer's Disease. *Archives of Medical Research* **43**, 600-608
3. Association, A. s. (2016) 2016 Alzheimer's disease facts and figures. *Alzheimer's and Dementia* **12**, 10
4. Swerdlow, R. H., Khan, S.M. (2004) A "mitochondrial cascade hypothesis" for sporadic Alzheimer's disease. *Medical Hypothesis* **63**, 8-20
5. Dubois, B., Hampel, H., Feldman, H. H., Scheltens, P., Aisen, P., Andrieu, S., Bakardjian, H., Benali, H., Bertram, L., and Blennow, K. (2016) Preclinical Alzheimer's disease: definition, natural history, and diagnostic criteria. *Alzheimer's & Dementia* **12**, 292-323
6. Eckert, A., Schmitt, K., and Götz, J. (2011) Mitochondrial dysfunction-the beginning of the end in Alzheimer's disease? Separate and synergistic modes of tau and amyloid-β toxicity. *Alzheimer's research & therapy* **3**, 1-11
7. Kivipelto, M., Ngandu, T., Fratiglioni, L., Viitanen, M., Kåreholt, I., Winblad, B., Helkala, E. L., Tuomilehto, J., Soininen, H., and Nissinen, A. (2005) Obesity and vascular risk factors at midlife and the risk of dementia and Alzheimer disease. *Arch Neurol* **62**, 1556-1560
8. Zhang, L., Trushin, S., Christensen, T. A., Bachmeier, B. V., Gateno, B., Schroeder, A., Yao, J., Itoh, K., Sesaki, H., Poon, W. W., Gylys, K. H., Patterson, E. R., Parisi, J. E., Diaz Brinton, R., Salisbury, J. L., and Trushina, E. (2016) Altered brain energetics induces mitochondrial fission arrest in Alzheimer's Disease. *Sci Rep* **6**, 18725
9. Piaceri, I., Nacmias, B., and Sorbi, S. (2013) Genetics of familial and sporadic Alzheimer's disease. *Front Biosci (Elite Ed)* **5**, 167-177
10. Tiwari, S., Atluri, V., Kaushik, A., Yndart, A., and Nair, M. (2019) Alzheimer's disease: pathogenesis, diagnostics, and therapeutics. *International journal of nanomedicine* **14**, 5541-5554
11. Karch, C. M., and Goate, A. M. (2015) Alzheimer's Disease Risk Genes and Mechanisms of Disease Pathogenesis. *Biological Psychiatry* **77**, 43-51
12. Du, X., Wang, X., and Geng, M. (2018) Alzheimer's disease hypothesis and related therapies. *Translational neurodegeneration* **7**, 2-2
13. Edwards, F. A. (2019) A Unifying Hypothesis for Alzheimer’s Disease: From Plaques to Neurodegeneration. *Trends in Neurosciences* **42**, 310-322
14. Kametani, F., and Hasegawa, M. (2018) Reconsideration of Amyloid Hypothesis and Tau Hypothesis in Alzheimer's Disease. *Frontiers in Neuroscience* **12**
15. Kang, J., Lemaire, H.-G., Unterbeck, A., Salbaum, J. M., Masters, C. L., Grzeschik, K.-H., Multhaup, G., Beyreuther, K., and Müller-Hill, B. (1987) The precursor of Alzheimer's disease amyloid A4 protein resembles a cell-surface receptor. *Nature* **325**, 733-736
16. Murphy, M. P., and LeVine, H., 3rd. (2010) Alzheimer's disease and the amyloid-beta peptide. *Journal of Alzheimer's disease : JAD* **19**, 311-323
17. Walters, A., Phillips, E., Zheng, R., Biju, M., and Kuruvilla, T. (2016) Evidence for neuroinflammation in Alzheimer's disease. *Progress in Neurology and Psychiatry* **20**, 25-31

18. Morgan, D., Diamond, D. M., Gottschall, P. E., Ugen, K. E., Dickey, C., Hardy, J., Duff, K., Jantzen, P., DiCarlo, G., Wilcock, D., Connor, K., Hatcher, J., Hope, C., Gordon, M., and Arendash, G. W. (2000) A beta peptide vaccination prevents memory loss in an animal model of Alzheimer's disease. *Nature* **408**, 982-985
19. Karelina, T., Demin, O., Jr., Demin, O., Duvvuri, S., and Nicholas, T. (2017) Studying the Progression of Amyloid Pathology and Its Therapy Using Translational Longitudinal Model of Accumulation and Distribution of Amyloid Beta. *CPT: pharmacometrics & systems pharmacology* **6**, 676-685
20. Delabar, J.-M., Goldgaber, D., Lamour, Y., Nicole, A., Huret, J.-L., Grouchy, J. d., Brown, P., Gajdusek, D. C., and Sinet, P.-M. (1987) Amyloid Gene Duplication in Alzheimer's Disease and Karyotypically Normal Down Syndrome. *Science* **235**, 1390-1392
21. Elder, G. A., Gama Sosa, M. A., and De Gasperi, R. (2010) Transgenic mouse models of Alzheimer's disease. *The Mount Sinai journal of medicine, New York* **77**, 69-81
22. Li, H., Liu, C.-C., Zheng, H., and Huang, T. Y. (2018) Amyloid, tau, pathogen infection and antimicrobial protection in Alzheimer's disease –conformist, nonconformist, and realistic prospects for AD pathogenesis. *Translational Neurodegeneration* **7**, 34
23. Violet, M., Chauderlier, A., Delattre, L., Tardivel, M., Chouala, M. S., Sultan, A., Marciniak, E., Humez, S., Binder, L., Kayed, R., Lefebvre, B., Bonnefoy, E., Buée, L., and Galas, M. C. (2015) Prefibrillar Tau oligomers alter the nucleic acid protective function of Tau in hippocampal neurons in vivo. *Neurobiol Dis* **82**, 540-551
24. Silver, I. A., Deas, J., and Erecińska, M. (1997) Ion homeostasis in brain cells: differences in intracellular ion responses to energy limitation between cultured neurons and glial cells. *Neuroscience* **78**, 589-601
25. Lacovich, V., Espindola, S. L., Alloatti, M., Pozo Devoto, V., Cromberg, L. E., Čarná, M. E., Forte, G., Gallo, J.-M., Bruno, L., Stokin, G. B., Avale, M. E., and Falzone, T. L. (2017) Tau Isoforms Imbalance Impairs the Axonal Transport of the Amyloid Precursor Protein in Human Neurons. *The Journal of Neuroscience* **37**, 58-69
26. Joseph, M., Anglada-Huguet, M., Paesler, K., Mandelkow, E., and Mandelkow, E. M. (2017) Anti-aggregant tau mutant promotes neurogenesis. *Mol Neurodegener* **12**, 88
27. Komuro, Y., Xu, G., Bhaskar, K., and Lamb, B. T. (2015) Human tau expression reduces adult neurogenesis in a mouse model of tauopathy. *Neurobiol Aging* **36**, 2034-2042
28. Bolós, M., Llorens-Martín, M., Perea, J. R., Jurado-Arjona, J., Rábano, A., Hernández, F., and Avila, J. (2017) Absence of CX3CR1 impairs the internalization of Tau by microglia. *Mol Neurodegener* **12**, 59
29. Ardura-Fabregat, A., Boddeke, E. W. G. M., Boza-Serrano, A., Brioschi, S., Castro-Gomez, S., Ceyzériat, K., Dansokho, C., Dierkes, T., Gelders, G., Heneka, M. T., Hoeijmakers, L., Hoffmann, A., Iaccarino, L., Jahnert, S., Kuhbandner, K., Landreth, G., Lonnemann, N., Löschmann, P. A., McManus, R. M., Paulus, A., Reemst, K., Sanchez-Caro, J. M., Tiberi, A., Van der Perren, A., Vautheny, A., Venegas, C., Webers, A., Weydt, P., Wijasa, T. S., Xiang, X., and Yang, Y. (2017) Targeting Neuroinflammation to Treat Alzheimer's Disease. *CNS drugs* **31**, 1057-1082
30. Nagele, R. G., D'Andrea, M. R., Lee, H., Venkataraman, V., and Wang, H. Y. (2003) Astrocytes accumulate A beta 42 and give rise to astrocytic amyloid plaques in Alzheimer disease brains. *Brain Res* **971**, 197-209
31. Anand, K. S., and Dhikav, V. (2012) Hippocampus in health and disease: An overview. *Annals of Indian Academy of Neurology* **15**, 239-246

32. Leroy, K., Ando, K., Laporte, V., Dedecker, R., Suain, V., Authelet, M., Héraud, C., Pierrot, N., Yilmaz, Z., Octave, J.-N., and Brion, J.-P. (2012) Lack of Tau Proteins Rescues Neuronal Cell Death and Decreases Amyloidogenic Processing of APP in APP/PS1 Mice. *Am J Pathol* **181**, 1928-1940
33. Telegina, D. V., Suvorov, G. K., Kozhevnikova, O. S., and Kolosova, N. G. (2019) Mechanisms of Neuronal Death in the Cerebral Cortex during Aging and Development of Alzheimer's Disease-Like Pathology in Rats. *Int J Mol Sci* **20**, 5632
34. Lok, K., Zhao, H., Shen, H., Wang, Z., Gao, X., Zhao, W., and Yin, M. (2013) Characterization of the APP/PS1 mouse model of Alzheimer's disease in senescence accelerated background. *Neuroscience Letters* **557**, 84-89
35. Oakley, H., Cole, S. L., Logan, S., Maus, E., Shao, P., Craft, J., Guillozet-Bongaarts, A., Ohno, M., Disterhoft, J., Van Eldik, L., Berry, R., and Vassar, R. (2006) Intraneuronal beta-amyloid aggregates, neurodegeneration, and neuron loss in transgenic mice with five familial Alzheimer's disease mutations: potential factors in amyloid plaque formation. *J Neurosci* **26**, 10129-10140
36. Behl, C. (1999) Alzheimer's disease and oxidative stress: implications for novel therapeutic approaches. *Progress in Neurobiology* **57**, 301-323
37. Harris, M. E., Hensley, K., Butterfield, D. A., Leedle, R. A., and Carney, J. M. (1995) Direct evidence of oxidative injury produced by the Alzheimer's β-Amyloid peptide (1–40) in cultured hippocampal neurons. *Experimental Neurology* **131**, 193-202
38. Hensley, K. (2010) Neuroinflammation in Alzheimer's Disease: Mechanisms,Pathologic Consequences, and Potential for Therapeutic Manipulation. *Journal of Alzheimer's Disease* **21**, 20
39. Ames, B. N., Shigenaga, M. K., and Hagen, T. M. (1993) Oxidants, antioxidants, and the degenerative diseases of aging. *Proceedings of the National Academy of Sciences* **90**, 7915-7922
40. Beckman, J. S., Chen, J., Crow, J. P., and Ye, Y. Z. (1994) Chapter 31 Reactions of nitric oxide, superoxide and peroxynitrite with superoxide dismutase in neurodegeneration. In *Progress in Brain Research* (Seil, F. J., ed) Vol. 103 pp. 371-380, Elsevier
41. Imlay, J. A., Chin, S. M., and Linn, S. (1988) Toxic DNA Damage by Hydrogen Peroxide Through the Fenton Reaction in Vivo and in Vitro. *Science* **240**, 640-642
42. Behl, C., Davis, J., Cole, G. M., and Schubert, D. (1992) Vitamin E protects nerve cells from amyloid βprotein toxicity. *Biochemical and Biophysical Research Communications* **186**, 944-950
43. Calderon-Garciduenas, L., Reynoso-Robles, R., Vargas-Martinez, J., Gomez-Maqueo-Chew, A., Perez-Guille, B., Mukherjee, P. S., Torres-Jardon, R., Perry, G., and Gonzalez-Maciel, A. (2016) Prefrontal white matter pathology in air pollution exposed Mexico City young urbanites and their potential impact on neurovascular unit dysfunction and the development of Alzheimer's disease. *Environ Res* **146**, 404-417
44. Calderón-Garcidueñas, L., Maronpot, R. R., Torres-Jardon, R., Henríquez-Roldán, C., Schoonhoven, R., Acuña-Ayala, H., Villarreal-Calderón, A., Nakamura, J., Fernando, R., Reed, W., Azzarelli, B., and Swenberg, J. A. (2003) DNA damage in nasal and brain tissues of canines exposed to air pollutants is associated with evidence of chronic brain inflammation and neurodegeneration. *Toxicol Pathol* **31**, 524-538
45. Brockmeyer, S., and D'Angiulli, A. (2016) How air pollution alters brain development: the role of neuroinflammation. *Transl Neurosci* **7**, 24-30

46. Moulton, P. V., and Yang, W. (2012) Air pollution, oxidative stress, and Alzheimer's disease. *J Environ Public Health* **2012**, 472751
47. Turner, M. C., Andersen, Z. J., Baccarelli, A., Diver, W. R., Gapstur, S. M., Pope III, C. A., Prada, D., Samet, J., Thurston, G., and Cohen, A. (2020) Outdoor air pollution and cancer: An overview of the current evidence and public health recommendations. *CA: A Cancer Journal for Clinicians* **70**, 460-479
48. Kelly, F. J., and Fussell, J. C. (2015) Air pollution and public health: emerging hazards and improved understanding of risk. *Environmental geochemistry and health* **37**, 631-649
49. Organization, W. H. (2016) Ambient air pollution: A global assessment of exposure and burden of diseases. In *Environmental Exposure* (Communication, I., ed) pp. 19-21, World Health Organization, Avenue Appia 20, CH-1211, Geneva, Switzerland
50. Manisalidis, I., Stavropoulou, E., Stavropoulos, A., and Bezirtzoglou, E. (2020) Environmental and Health Impacts of Air Pollution: A Review. *Front Public Health* **8**, 14-14
51. Eze, I. C., Schaffner, E., Fischer, E., Schikowski, T., Adam, M., Imboden, M., Tsai, M., Carballo, D., von Eckardstein, A., Künzli, N., Schindler, C., and Probst-Hensch, N. (2014) Long-term air pollution exposure and diabetes in a population-based Swiss cohort. *Environ Int* **70**, 95-105
52. Kelishadi, R., and Poursafa, P. (2010) Air pollution and non-respiratory health hazards for children. *Arch Med Sci* **6**, 483-495
53. Stone, V., Johnston, H., and Clift, M. J. (2007) Air pollution, ultrafine and nanoparticle toxicology: cellular and molecular interactions. *IEEE Trans Nanobioscience* **6**, 331-340
54. Mannucci, P. M., and Franchini, M. (2017) Health Effects of Ambient Air Pollution in Developing Countries. *International Journal of Environmental Research and Public Health* **14**, 1048
55. Guo, Y., Zeng, H., Zheng, R., Li, S., Pereira, G., Liu, Q., Chen, W., and Huxley, R. (2017) The burden of lung cancer mortality attributable to fine particles in China. *Science of The Total Environment* **579**, 1460-1466
56. Kankaria, A., Nongkynrih, B., and Gupta, S. K. (2014) Indoor air pollution in India: implications on health and its control. *Indian journal of community medicine : official publication of Indian Association of Preventive & Social Medicine* **39**, 203-207
57. Parajuli, I., Lee, H., and Shrestha, K. R. (2016) Indoor Air Quality and ventilation assessment of rural mountainous households of Nepal. *International Journal of Sustainable Built Environment* **5**, 301-311
58. Dherani, M., Pope, D., Mascarenhas, M., Smith, K. R., Weber, M., and Bruce, N. (2008) Indoor air pollution from unprocessed solid fuel use and pneumonia risk in children aged under five years: a systematic review and meta-analysis. *Bulletin of the World Health Organization* **86**, 390-398C
59. Kassomenos, P. A., Kelessis, A., Petrakakis, M., Zoumakis, N., Christidis, T., and Paschalidou, A. K. (2012) Air quality assessment in a heavily polluted urban Mediterranean environment through air quality indices. *Ecological Indicators* **18**, 259-268
60. Dockery, D. W., Pope, C. A., 3rd, Xu, X., Spengler, J. D., Ware, J. H., Fay, M. E., Ferris, B. G., Jr., and Speizer, F. E. (1993) An association between air pollution and mortality in six U.S. cities. *N Engl J Med* **329**, 1753-1759

61. Jankowska-Kieltyka, M., Roman, A., and Nalepa, I. (2021) The Air We Breathe: Air Pollution as a Prevalent Proinflammatory Stimulus Contributing to Neurodegeneration. *Frontiers in Cellular Neuroscience* **15**
62. Chen, R., Hu, B., Liu, Y., Xu, J., Yang, G., Xu, D., and Chen, C. (2016) Beyond PM2.5: The role of ultrafine particles on adverse health effects of air pollution. *Biochimica et Biophysica Acta (BBA) - General Subjects* **1860**, 2844-2855
63. Kim, H., Kim, W.-H., Kim, Y.-Y., and Park, H.-Y. (2020) Air Pollution and Central Nervous System Disease: A Review of the Impact of Fine Particulate Matter on Neurological Disorders. *Frontiers in Public Health* **8**
64. Andersen, Z. J., Pedersen, M., Weinmayr, G., Stafoggia, M., Galassi, C., Jørgensen, J. T., Sommar, J. N., Forsberg, B., Olsson, D., Oftedal, B., Aasvang, G. M., Schwarze, P., Pyko, A., Pershagen, G., Korek, M., Faire, U. D., Östenson, C.-G., Fratiglioni, L., Eriksen, K. T., Poulsen, A. H., Tjønneland, A., Bräuner, E. V., Peeters, P. H., Bueno-de-Mesquita, B., Jaensch, A., Nagel, G., Lang, A., Wang, M., Tsai, M.-Y., Grioni, S., Marcon, A., Krogh, V., Ricceri, F., Sacerdote, C., Migliore, E., Vermeulen, R., Sokhi, R., Keuken, M., de Hoogh, K., Beelen, R., Vineis, P., Cesaroni, G., Brunekreef, B., Hoek, G., and Raaschou-Nielsen, O. (2017) Long-term exposure to ambient air pollution and incidence of brain tumor: the European Study of Cohorts for Air Pollution Effects (ESCAPE). *Neuro-Oncology* **20**, 420-432
65. Gao, R., Ku, T., Ji, X., Zhang, Y., Li, G., and Sang, N. (2017) Abnormal energy metabolism and tau phosphorylation in the brains of middle-aged mice in response to atmospheric PM2.5 exposure. *Journal of Environmental Sciences* **62**, 145-153
66. Kumar, A., Singh, A., and Ekavali. (2015) A review on Alzheimer's disease pathophysiology and its management: an update. *Pharmacol Rep* **67**, 195-203
67. Sram, R. J., Veleminsky, M., Jr., Veleminsky, M., Sr., and Stejskalová, J. (2017) The impact of air pollution to central nervous system in children and adults. *Neuro Endocrinol Lett* **38**, 389-396
68. Frölich, L., Blum-Degen, D., Bernstein, H. G., Engelsberger, S., Humrich, J., Laufer, S., Muschner, D., Thalheimer, A., Türk, A., Hoyer, S., Zöchling, R., Boissl, K. W., Jellinger, K., and Riederer, P. (1998) Brain insulin and insulin receptors in aging and sporadic Alzheimer's disease. *J Neural Transm (Vienna)* **105**, 423-438
69. Kim, Y. D. L.-M., S.M.; Ali, S.F.; Kleinman, M.T.; Choi, Y.S.; Kim, H. (2014) Effects of ultrafine diesel exhaust particles on oxidative stress generation and dopamine metabolism in PC-12 cells. *Environmental Toxicology and Pharmacology* **37**, 5
70. Harrison, R. M., Rob MacKenzie, A., Xu, H., Alam, M. S., Nikolova, I., Zhong, J., Singh, A., Zeraati-Rezaei, S., Stark, C., Beddows, D. C. S., Liang, Z., Xu, R., and Cai, X. (2018) Diesel exhaust nanoparticles and their behaviour in the atmosphere. *Proceedings of the Royal Society A: Mathematical, Physical and Engineering Sciences* **474**, 20180492
71. Fiebig, M., Wiartalla, A., Holderbaum, B., and Kiesow, S. (2014) Particulate emissions from diesel engines: correlation between engine technology and emissions. *Journal of Occupational Medicine and Toxicology* **9**, 6
72. Levesque, S., Surace, M. J., McDonald, J., and Block, M. L. (2011) Air pollution & the brain: Subchronic diesel exhaust exposure causes neuroinflammation and elevates early markers of neurodegenerative disease. *Journal of neuroinflammation* **8**, 105-105
73. Colasanti, T., Fiorito, S., Alessandri, C., Serafino, A., Andreola, F., Barbati, C., Morello, F., Alfè, M., Di Blasio, G., Gargiulo, V., Vomero, M., Conti, F., and Valesini, G. (2018)

Diesel exhaust particles induce autophagy and citrullination in Normal Human Bronchial Epithelial cells. *Cell Death & Disease* **9**, 1073
74. Li, N. N., A.E. (2006) The cellular impacts of diesel exhaust particles: beyond inflammation and death. *European Respiratory Journal* **27**, 2
75. Ackland, M. L., Zou, L., Freestone, D., van de Waasenburg, S., and Michalczyk, A. A. (2007) Diesel exhaust particulate matter induces multinucleate cells and zinc transporter-dependent apoptosis in human airway cells. *Immunology & Cell Biology* **85**, 617-622
76. Castellani, R. J., Lee, H. G., Zhu, X., Nunomura, A., Perry, G., and Smith, M. A. (2006) Neuropathology of Alzheimer disease: pathognomonic but not pathogenic. *Acta Neuropathol* **111**, 503-509
77. Collingwood, J. F., Mikhaylova, A., Davidson, M., Batich, C., Streit, W.J., Terry, J., Dobson, J. (2005) In situ characterization and mapping of iron compounds in Alzheimer's disease tissue. *Journal of Alzheimer's Disease* **7**, 2
78. Zhao, Z. (2019) Iron and oxidizing species in oxidative stress and Alzheimer's disease. *AGING MEDICINE* **2**, 82-87
79. Brem, F., Hirt, A. M., Winklhofer, M., Frei, K., Yonekawa, Y., Wieser, H.-G., and Dobson, J. (2006) Magnetic iron compounds in the human brain: a comparison of tumour and hippocampal tissue. *Journal of the Royal Society, Interface* **3**, 833-841
80. Yarjanli, Z., Ghaedi, K., Esmaeili, A., Rahgozar, S., and Zarrabi, A. (2017) Iron oxide nanoparticles may damage to the neural tissue through iron accumulation, oxidative stress, and protein aggregation. *BMC Neurosci* **18**, 51-51
81. Dobson, J. (2001) Nanoscale biogenic iron oxides and neurodegenerative disease. *FEBS Letters* **496**, 1-5
82. Pankhurst, Q., Hautot, D., Khan, N., and Dobson, J. (2008) Increased levels of magnetic iron compounds in Alzheimer's disease. *J Alzheimers Dis* **13**, 49-52
83. Maher, B. A., González-Maciel, A., Reynoso-Robles, R., Torres-Jardón, R., and Calderón-Garcidueñas, L. (2020) Iron-rich air pollution nanoparticles: An unrecognised environmental risk factor for myocardial mitochondrial dysfunction and cardiac oxidative stress. *Environmental research* **188**, 109816-109816
84. Kirschvink, J. L., Kobayashi-Kirschvink, A., and Woodford, B. J. (1992) Magnetite biomineralization in the human brain. *Proceedings of the National Academy of Sciences* **89**, 7683
85. Hautot, D., Pankhurst, Q. A., Khan, N., and Dobson, J. (2003) Preliminary evaluation of nanoscale biogenic magnetite in Alzheimer's disease brain tissue. *Proc Biol Sci* **270 Suppl 1**, S62-64
86. Dobson, J. (2001) Nanoscale biogenic iron oxides and neurodegenerative disease. *FEBS Letters* **496**, 5
87. Schipper, H. M. (2012) Neurodegeneration with brain iron accumulation - clinical syndromes and neuroimaging. *Biochim Biophys Acta* **1822**, 350-360
88. Maher, B. A., Ahmed, I. A. M., Karloukovski, V., MacLaren, D. A., Foulds, P. G., Allsop, D., Mann, D. M. A., Torres-Jardón, R., and Calderon-Garciduenas, L. (2016) Magnetite pollution nanoparticles in the human brain. *Proceedings of the National Academy of Sciences* **113**, 10797
89. Shah, R. S., Lee, H.-G., Xiongwei, Z., Perry, G., Smith, M. A., and Castellani, R. J. (2008) Current approaches in the treatment of Alzheimer's disease. *Biomedicine & Pharmacotherapy* **62**, 199-207

90. Melnikova, I. (2007) Therapies for Alzheimer's disease. *Nature Reviews Drug Discovery* **6**, 341-342
91. Nygaard, H. B. (2013) Current and Emerging Therapies for Alzheimer's Disease. *Clinical Therapeutics* **35**, 1480-1489
92. Serrano-Pozo, A., William, C. M., Ferrer, I., Uro-Coste, E., Delisle, M. B., Maurage, C. A., Hock, C., Nitsch, R. M., Masliah, E., Growdon, J. H., Frosch, M. P., and Hyman, B. T. (2010) Beneficial effect of human anti-amyloid-beta active immunization on neurite morphology and tau pathology. *Brain* **133**, 1312-1327
93. Boche, D., Donald, J., Love, S., Harris, S., Neal, J. W., Holmes, C., and Nicoll, J. A. (2010) Reduction of aggregated Tau in neuronal processes but not in the cell bodies after Abeta42 immunisation in Alzheimer's disease. *Acta Neuropathol* **120**, 13-20
94. Panza, F., Solfrizzi, V., Seripa, D., Imbimbo, B. P., Lozupone, M., Santamato, A., Zecca, C., Barulli, M. R., Bellomo, A., Pilotto, A., Daniele, A., Greco, A., and Logroscino, G. (2016) Tau-Centric Targets and Drugs in Clinical Development for the Treatment of Alzheimer's Disease. *Biomed Res Int* **2016**, 3245935
95. Congdon, E. E., and Sigurdsson, E. M. (2018) Tau-targeting therapies for Alzheimer disease. *Nat Rev Neurol* **14**, 399-415
96. Gauthier, S., Feldman, H. H., Schneider, L. S., Wilcock, G. K., Frisoni, G. B., Hardlund, J. H., Moebius, H. J., Bentham, P., Kook, K. A., Wischik, D. J., Schelter, B. O., Davis, C. S., Staff, R. T., Bracoud, L., Shamsi, K., Storey, J. M., Harrington, C. R., and Wischik, C. M. (2016) Efficacy and safety of tau-aggregation inhibitor therapy in patients with mild or moderate Alzheimer's disease: a randomised, controlled, double-blind, parallel-arm, phase 3 trial. *Lancet* **388**, 2873-2884
97. Oberdörster, G., Sharp, Z., Atudorei, V., Elder, A., Gelein, R., Kreyling, W., and Cox, C. (2004) Translocation of Inhaled Ultrafine Particles to the Brain. *Inhalation Toxicology* **16**, 437-445
98. Walker, D. G., Link, J., Lue, L. F., Dalsing-Hernandez, J. E., and Boyes, B. E. (2006) Gene expression changes by amyloid beta peptide-stimulated human postmortem brain microglia identify activation of multiple inflammatory processes. *J Leukoc Biol* **79**, 596-610
99. Elliott, D. E., Li, J., Blum, A. M., Metwali, A., Patel, Y. C., and Weinstock, J. V. (1999) SSTR2A is the dominant somatostatin receptor subtype expressed by inflammatory cells, is widely expressed and directly regulates T cell IFN-gamma release. *Eur J Immunol* **29**, 2454-2463
100. Armani, C., Catalani, E., Balbarini, A., Bagnoli, P., and Cervia, D. (2007) Expression, pharmacology, and functional role of somatostatin receptor subtypes 1 and 2 in human macrophages. *J Leukoc Biol* **81**, 845-855
101. Chowers, Y., Cahalon, L., Lahav, M., Schor, H., Tal, R., Bar-Meir, S., and Levite, M. (2000) Somatostatin through its specific receptor inhibits spontaneous and TNF-alpha- and bacteria-induced IL-8 and IL-1 beta secretion from intestinal epithelial cells. *J Immunol* **165**, 2955-2961
102. Walker, D., and Lue, L.-F. (2007) Anti-inflammatory and immune therapy for Alzheimer's disease: current status and future directions. *Current neuropharmacology* **5**, 232-243
103. Shah, R. S., Lee, H., Xiongwei, Z., Perry, G., Smith, M.A., Castellani, R.J. (2008) Current approaches in the treatment of Alzheimer's disease. *Biomedicien & Pharmacotherapy* **62**, 8

104. Grundman, M. (2000) Vitamin E and Alzheimer disease: the basis for additional clinical trials. *Am J Clin Nutr* **71**, 630s-636s
105. Naz, S., Beach, J., Heckert, B., Tummala, T., Pashchenko, O., Banerjee, T., and Santra, S. (2017) Cerium oxide nanoparticles: a 'radical' approach to neurodegenerative disease treatment. *Nanomedicine (Lond)* **12**, 545-553
106. Celardo, I., Traversa, E., and Ghibelli, L. (2011) Cerium oxide nanoparticles: a promise for applications in therapy. *J Exp Ther Oncol* **9**, 47-51
107. Nelson, B. C., Johnson, M. E., Walker, M. L., Riley, K. R., and Sims, C. M. (2016) Antioxidant Cerium Oxide Nanoparticles in Biology and Medicine. *Antioxidants (Basel)* **5**
108. Xu, C., and Qu, X. (2014) Cerium oxide nanoparticle: a remarkably versatile rare earth nanomaterial for biological applications. *NPG Asia Materials* **6**, e90-e90
109. Ighodaro, O. M., and Akinloye, O. A. (2018) First line defence antioxidants-superoxide dismutase (SOD), catalase (CAT) and glutathione peroxidase (GPX): Their fundamental role in the entire antioxidant defence grid. *Alexandria Journal of Medicine* **54**, 287-293
110. Pelletier, D. A., Suresh, A. K., Holton, G. A., McKeown, C. K., Wang, W., Gu, B., Mortensen, N. P., Allison, D. P., Joy, D. C., Allison, M. R., Brown, S. D., Phelps, T. J., and Doktycz, M. J. (2010) Effects of Engineered Cerium Oxide Nanoparticles on Bacterial Growth and Viability. *Applied and Environmental Microbiology* **76**, 7981-7989
111. Alili, L., Sack, M., Karakoti, A. S., Teuber, S., Puschmann, K., Hirst, S. M., Reilly, C. M., Zanger, K., Stahl, W., Das, S., Seal, S., and Brenneisen, P. (2011) Combined cytotoxic and anti-invasive properties of redox-active nanoparticles in tumor-stroma interactions. *Biomaterials* **32**, 2918-2929
112. Perez, J. M., Asati, A., Nath, S., and Kaittanis, C. (2008) Synthesis of biocompatible dextran-coated nanoceria with pH-dependent antioxidant properties. *Small* **4**, 552-556
113. Ristow, M. (2006) Oxidative metabolism in cancer growth. *Curr Opin Clin Nutr Metab Care* **9**, 339-345
114. Singh, S., Kumar, U., Gittess, D., Sakthivel, T. S., Babu, B., and Seal, S. (2021) Cerium oxide nanomaterial with dual antioxidative scavenging potential: Synthesis and characterization. *J Biomater Appl* **36**, 834-842
115. Mittal, S., and Pandey, A. K. (2014) Cerium Oxide Nanoparticles Induced Toxicity in Human Lung Cells: Role of ROS Mediated DNA Damage and Apoptosis. *BioMed Research International* **2014**, 891934
116. Lin, W., Huang, Y.-w., Zhou, X.-D., and Ma, Y. (2006) Toxicity of Cerium Oxide Nanoparticles in Human Lung Cancer Cells. *International Journal of Toxicology* **25**, 451-457
117. Hirst, S. M., Karakoti, A. S., Tyler, R. D., Sriranganathan, N., Seal, S., and Reilly, C. M. (2009) Anti-inflammatory properties of cerium oxide nanoparticles. *Small* **5**, 2848-2856
118. Ma, J., Mercer, R. R., Barger, M., Schwegler-Berry, D., Cohen, J. M., Demokritou, P., and Castranova, V. (2015) Effects of amorphous silica coating on cerium oxide nanoparticles induced pulmonary responses. *Toxicology and Applied Pharmacology* **288**, 63-73
119. Konduru, N., Jimenez, R., Swami, A., Friend, S., Castranova, V., Demokritou, P., Brain, J., and Molina, R. (2015) Silica coating influences the corona and biokinetics of cerium oxide nanoparticles. *Particle and Fibre Toxicology* **12**

120. Mädler, L., Stark, W. J., and Pratsinis, S. E. (2002) Flame-made Ceria Nanoparticles. *Journal of Materials Research* **17**, 1356-1362
121. Lord, M. S., Jung, M., Teoh, W. Y., Gunawan, C., Vassie, J. A., Amal, R., and Whitelock, J. M. (2012) Cellular uptake and reactive oxygen species modulation of cerium oxide nanoparticles in human monocyte cell line U937. *Biomaterials* **33**, 7915-7924
122. (2019) Research Models, APPswe/PSEN1dE9 (C57BL6). Vol. 2022, Alzforum
123. Carrera, I., Etcheverría, I., Li, Y., Fernández-Novoa, L., Lombardi, V., Vigo, C., Palacios, H. H., Benberin, V. V., Cacabelos, R., and Aliev, G. (2013) Immunocytochemical characterization of Alzheimer disease hallmarks in APP/PS1 transgenic mice treated with a new anti-amyloid-β vaccine. *Biomed Res Int* **2013**, 709145
124. Maia, L. F., Kaeser, S. A., Reichwald, J., Hruscha, M., Martus, P., Staufenbiel, M., and Jucker, M. (2013) Changes in amyloid-β and Tau in the cerebrospinal fluid of transgenic mice overexpressing amyloid precursor protein. *Sci Transl Med* **5**, 194re192
125. Radde, R., Bolmont, T., Kaeser, S. A., Coomaraswamy, J., Lindau, D., Stoltze, L., Calhoun, M. E., Jäggi, F., Wolburg, H., Gengler, S., Haass, C., Ghetti, B., Czech, C., Hölscher, C., Mathews, P. M., and Jucker, M. (2006) Abeta42-driven cerebral amyloidosis in transgenic mice reveals early and robust pathology. *EMBO reports* **7**, 940-946
126. Lee, S., Varvel, N. H., Konerth, M. E., Xu, G., Cardona, A. E., Ransohoff, R. M., and Lamb, B. T. (2010) CX3CR1 deficiency alters microglial activation and reduces beta-amyloid deposition in two Alzheimer's disease mouse models. *Am J Pathol* **177**, 2549-2562
127. Rupp, N. J., Wegenast-Braun, B. M., Radde, R., Calhoun, M. E., and Jucker, M. (2011) Early onset amyloid lesions lead to severe neuritic abnormalities and local, but not global neuron loss in APPPS1 transgenic mice. *Neurobiol Aging* **32**, 2324. e2321-2324. e2326
128. Bittner, T., Burgold, S., Dorostkar, M. M., Fuhrmann, M., Wegenast-Braun, B. M., Schmidt, B., Kretzschmar, H., and Herms, J. (2012) Amyloid plaque formation precedes dendritic spine loss. *Acta Neuropathol* **124**, 797-807
129. Kesavachandran, C., Pangtey, B. S., Bihari, V., Fareed, M., Pathak, M. K., Srivastava, A. K., and Mathur, N. (2013) Particulate matter concentration in ambient air and its effects on lung functions among residents in the National Capital Region, India. *Environ Monit Assess* **185**, 1265-1272
130. Borghi, F., Spinazzè, A., Mandaglio, S., Fanti, G., Campagnolo, D., Rovelli, S., Keller, M., Cattaneo, A., and Cavallo, D. M. (2021) Estimation of the Inhaled Dose of Pollutants in Different Micro-Environments: A Systematic Review of the Literature. *Toxics* **9**, 140
131. Wahle, T., Sofranko, A., Dekkers, S., Miller, M. R., Heusinkveld, H. J., Albrecht, C., Cassee, F. R., and Schins, R. P. F. (2020) Evaluation of neurological effects of cerium dioxide nanoparticles doped with different amounts of zirconium following inhalation exposure in mouse models of Alzheimer's and vascular disease. *Neurochemistry International* **138**, 104755
132. Demokritou, P., Gass, S., Pyrgiotakis, G., Cohen, J. M., Goldsmith, W., McKinney, W., Frazer, D., Ma, J., Schwegler-Berry, D., Brain, J., and Castranova, V. (2013) An in vivo and in vitro toxicological characterisation of realistic nanoscale CeO2 inhalation exposures. *Nanotoxicology* **7**, 1338-1350
133. Schikowski, T., and Altuğ, H. (2020) The role of air pollution in cognitive impairment and decline. *Neurochemistry International* **136**, 104708

134. Liu, Y., Li, Y., Yang, T., Yang, J., Wang, H., and Wu, G. (2016) Acute changes in murine hippocampus and olfactory bulb after nasal instillation of varying size cerium dioxide particles. *Journal of Toxicology and Environmental Health, Part A* **79**, 869-877
135. Fahlström, A., Zeberg, H., and Ulfhake, B. (2012) Changes in behaviors of male C57BL/6J mice across adult life span and effects of dietary restriction. *Age (Dordrecht, Netherlands)* **34**, 1435-1452
136. Lueptow, L. M. (2017) Novel Object Recognition Test for the Investigation of Learning and Memory in Mice. *Journal of visualized experiments : JoVE*, 55718
137. Jew, K., Herr, D., Wong, C., Kennell, A., Morris-Schaffer, K., Oberdörster, G., O'Banion, M. K., Cory-Slechta, D. A., and Elder, A. (2019) Selective memory and behavioral alterations after ambient ultrafine particulate matter exposure in aged 3xTgAD Alzheimer's disease mice. *Particle and Fibre Toxicology* **16**, 45
138. Walf, A. A., and Frye, C. A. (2007) The use of the elevated plus maze as an assay of anxiety-related behavior in rodents. *Nature Protocols* **2**, 322-328
139. Olesen, L. Ø., Bouzinova, E. V., Severino, M., Sivasaravanaparan, M., Hasselstrøm, J. B., Finsen, B., and Wiborg, O. (2016) Behavioural Phenotyping of APPswe/PS1δE9 Mice: Age-Rrelated Changes and Effect of Long-Term Paroxetine Treatment. *PLOS ONE* **11**, e0165144
140. Can, A., Dao, D. T., Terrillion, C. E., Piantadosi, S. C., Bhat, S., and Gould, T. D. (2012) The tail suspension test. *Journal of visualized experiments : JoVE*, e3769-e3769
141. Zhang, X., Tian, Y., Zhang, C., Tian, X., Ross, A. W., Moir, R. D., Sun, H., Tanzi, R. E., Moore, A., and Ran, C. (2015) Near-infrared fluorescence molecular imaging of amyloid beta species and monitoring therapy in animal models of Alzheimer's disease. *Proceedings of the National Academy of Sciences of the United States of America* **112**, 9734-9739
142. Manzine, P. R., Souza, M. D. S., and Cominetti, M. R. (2016) BACE1 levels are increased in plasma of Alzheimer's disease patients compared with matched cognitively healthy controls. *Per Med* **13**, 531-540
143. Vakilian, A., Masoumi, J., Mirzaee, S., and Khorramdelazad, H. (2019) Expression analysis of beta-secretase 1 (BACE1) enzyme in peripheral blood of patients with Alzheimer's disease. *Caspian journal of internal medicine* **10**, 276-280
144. Setti, S. E., Hunsberger, H. C., and Reed, M. N. (2017) Alterations in Hippocampal Activity and Alzheimer's Disease. *Translational issues in psychological science* **3**, 348-356
145. Stephen, J. M., Montaño, R., Donahue, C. H., Adair, J. C., Knoefel, J., Qualls, C., Hart, B., Ranken, D., and Aine, C. J. (2010) Somatosensory responses in normal aging, mild cognitive impairment, and Alzheimer's disease. *Journal of Neural Transmission* **117**, 217-225
146. Benavides-Piccione, R., Regalado-Reyes, M., Fernaud-Espinosa, I., Kastanauskaite, A., Tapia-González, S., León-Espinosa, G., Rojo, C., Insausti, R., Segev, I., and DeFelipe, J. (2019) Differential Structure of Hippocampal CA1 Pyramidal Neurons in the Human and Mouse. *Cerebral Cortex* **30**, 730-752
147. Lee, S.-P., Falangola, M. F., Nixon, R. A., Duff, K., and Helpern, J. A. (2004) Visualization of beta-amyloid plaques in a transgenic mouse model of Alzheimer's disease using MR microscopy without contrast reagents. *Magn Reson Med* **52**, 538-544
148. Takeuchi, A., Irizarry, M. C., Duff, K., Saido, T. C., Hsiao Ashe, K., Hasegawa, M., Mann, D. M., Hyman, B. T., and Iwatsubo, T. (2000) Age-related amyloid beta deposition in

transgenic mice overexpressing both Alzheimer mutant presenilin 1 and amyloid beta precursor protein Swedish mutant is not associated with global neuronal loss. *Am J Pathol* **157**, 331-339
149. Hirsch, C., and Schildknecht, S. (2019) In Vitro Research Reproducibility: Keeping Up High Standards. *Frontiers in Pharmacology* **10**
150. Pavlovska, I., Ramata-Stunda, A., Martinsone, Z., Boroduskis, M., Patetko, L., Martinsone, I., Seile, A., and Vanadzins, I. (2021) In vitro impact preliminary assessment of airborne particulate from metalworking and woodworking industries. *Scientific Reports* **11**, 20181
151. Steenhof, M., Gosens, I., Strak, M., Godri, K. J., Hoek, G., Cassee, F. R., Mudway, I. S., Kelly, F. J., Harrison, R. M., Lebret, E., Brunekreef, B., Janssen, N. A. H., and Pieters, R. H. H. (2011) In vitro toxicity of particulate matter (PM) collected at different sites in the Netherlands is associated with PM composition, size fraction and oxidative potential - the RAPTES project. *Particle and Fibre Toxicology* **8**, 26
152. Forest, V., Leclerc, L., Hochepied, J.-F., Trouvé, A., Sarry, G., and Pourchez, J. (2017) Impact of cerium oxide nanoparticles shape on their in vitro cellular toxicity. *Toxicology in Vitro* **38**, 136-141
153. Lopez-Pascual, A., Urrutia-Sarratea, A., Lorente-Cebrián, S., Martinez, J. A., and González-Muniesa, P. (2019) Cerium Oxide Nanoparticles Regulate Insulin Sensitivity and Oxidative Markers in 3T3-L1 Adipocytes and C2C12 Myotubes. *Oxidative Medicine and Cellular Longevity* **2019**, 2695289
154. Fotakis, G., and Timbrell, J. A. (2006) In vitro cytotoxicity assays: comparison of LDH, neutral red, MTT and protein assay in hepatoma cell lines following exposure to cadmium chloride. *Toxicology letters* **160**, 171-177
155. Costa, L. G., Cole, T. B., Dao, K., Chang, Y.-C., Coburn, J., and Garrick, J. M. (2020) Effects of air pollution on the nervous system and its possible role in neurodevelopmental and neurodegenerative disorders. *Pharmacology & Therapeutics* **210**, 107523
156. Genove, G., DeMarco, U., Xu, H., Goins, W. F., and Ahrens, E. T. (2005) A new transgene reporter for in vivo magnetic resonance imaging. *Nat Med* **11**, 450-454
157. Livak, K. J., and Schmittgen, T. D. (2001) Analysis of relative gene expression data using real-time quantitative PCR and the 2(-Delta Delta C(T)) Method. *Methods* **25**, 402-408
158. Bustin, S. A. (2000) Absolute quantification of mRNA using real-time reverse transcription polymerase chain reaction assays. *J Mol Endocrinol* **25**, 169-193
159. Kostka, J. E., and Nealson, K. H. (1995) Dissolution and reduction of magnetite by bacteria. *Environ Sci Technol* **29**, 2535-2540
160. Su, C. (2017) Environmental implications and applications of engineered nanoscale magnetite and its hybrid nanocomposites: A review of recent literature. *J Hazard Mater* **322**, 48-84
161. Akbarzadeh, A., Samiei, M., and Davaran, S. (2012) Magnetic nanoparticles: preparation, physical properties, and applications in biomedicine. *Nanoscale Research Letters* **7**, 144
162. Gorski, C. A. (2009) Redox behavior of magnetite in the environment: moving towards a semiconductor model. In *Civil and Environmental Engineering* Vol. Philosophy degree in Civil and Environmental Engineering p. 238, The University of Iowa, Iowa
163. Gul, S. K., S.B.; Rehman, I.U.; Khan, M.A.; Khan, M.I. (2019) A Comprehensive Review of Magnetic Nanomaterials Modern Day Theranostics. *Frontiers in Materials* **6**, 15

164. White, A. F., and Peterson, M. L. (1996) Reduction of aqueous transition metal species on the surfaces of Fe(II) -containing oxides. *Geochimica et Cosmochimica Acta* **60**, 3799-3814
165. Kanel, S. R. G., J. M.; Choi, H. (2006) Arsenic(V) Removal from Groundwater Using Nano Scale Zero-Valent Iron as a Colloidal Reactive Barrier Material. *Environmental Science and Technology* **40**, 5
166. Chen, K., He, J., Li, Y., Cai, X., Zhang, K., Liu, T., Hu, Y., Lin, D., Kong, L., and Liu, J. (2017) Removal of cadmium and lead ions from water by sulfonated magnetic nanoparticle adsorbents. *Journal of Colloid and Interface Science* **494**, 307-316
167. Kumari, M., Pittman, C. U., and Mohan, D. (2015) Heavy metals [chromium (VI) and lead (II)] removal from water using mesoporous magnetite (Fe3O4) nanospheres. *Journal of Colloid and Interface Science* **442**, 120-132
168. Ai, L., Zhang, C., and Chen, Z. (2011) Removal of methylene blue from aqueous solution by a solvothermal-synthesized graphene/magnetite composite. *J Hazard Mater* **192**, 1515-1524
169. Deng, R., Lin, D., Zhu, L., Majumdar, S., White, J. C., Gardea-Torresdey, J. L., and Xing, B. (2017) Nanoparticle interactions with co-existing contaminants: joint toxicity, bioaccumulation and risk. *Nanotoxicology* **11**, 591-612
170. Kim, Y. S. R., N. H. A.; Gu, M. B. (2016) Aptamer-based nanobiosensors. *Biosensors and Bioelectronics* **76**, 17
171. Gul, S., Khan, S. B., Rehman, I. U., Khan, M. A., and Khan, M. I. (2019) A Comprehensive Review of Magnetic Nanomaterials Modern Day Theranostics. *Frontiers in Materials* **6**
172. Xie, J., Shen, Z., Anraku, Y., Kataoka, K., and Chen, X. (2019) Nanomaterial-based blood-brain-barrier (BBB) crossing strategies. *Biomaterials* **224**, 119491
173. Zanganeh, S., Hutter, G., Spitler, R., Lenkov, O., Mahmoudi, M., Shaw, A., Pajarinen, J. S., Nejadnik, H., Goodman, S., Moseley, M., Coussens, L. M., and Daldrup-Link, H. E. (2016) Iron oxide nanoparticles inhibit tumour growth by inducing pro-inflammatory macrophage polarization in tumour tissues. *Nat Nanotechnol* **11**, 986-994
174. Flynn, E. R., and Bryant, H. C. (2005) A biomagnetic system for in vivo cancer imaging. *Phys Med Biol* **50**, 1273-1293
175. Lee, G. Y., Qian, W. P., Wang, L., Wang, Y. A., Staley, C. A., Satpathy, M., Nie, S., Mao, H., and Yang, L. (2013) Theranostic nanoparticles with controlled release of gemcitabine for targeted therapy and MRI of pancreatic cancer. *ACS Nano* **7**, 2078-2089
176. Sharma, H. S., Menon, P. K., Lafuente, J. V., Aguilar, Z. P., Wang, Y. A., Muresanu, D. F., Mössler, H., Patnaik, R., and Sharma, A. (2014) The role of functionalized magnetic iron oxide nanoparticles in the central nervous system injury and repair: new potentials for neuroprotection with Cerebrolysin therapy. *J Nanosci Nanotechnol* **14**, 577-595
177. Dilnawaz, F., and Sahoo, S. K. (2015) Therapeutic approaches of magnetic nanoparticles for the central nervous system. *Drug Discov Today* **20**, 1256-1264
178. Gao, H., Pang, Z, Jiang, X. (2013) Targeted delivery of nano-therapeutics for major disorders of the central nervous system. *Pharmaceutical Research* **30**, 13
179. Huang, H. W. S., M. S.; Petruska, A. J.; Pane, S.; Nelson, B. J. (2016) Soft micromachines with programmable motility and morphology. *Nature Communications* **7**, 10
180. Block, M. L., and Calderón-Garcidueñas, L. (2009) Air pollution: mechanisms of neuroinflammation and CNS disease. *Trends in neurosciences* **32**, 506-516

181. Maher, B. A., Ahmed, I. A., Karloukovski, V., MacLaren, D. A., Foulds, P. G., Allsop, D., Mann, D. M., Torres-Jardón, R., and Calderon-Garciduenas, L. (2016) Magnetite pollution nanoparticles in the human brain. *Proceedings of the National Academy of Sciences* **113**, 10797-10801
182. Hitzman, M. W., Oreskes, N., and Einaudi, M. T. (1992) Geological characteristics and tectonic setting of proterozoic iron oxide (Cu U Au REE) deposits. *Precambrian Research* **58**, 241-287
183. Kostka, J. E., Luther, G, W. (1993) Partitioning and speciation of solid phase iron in saltmarsh sediments. *Geochimica et Cosmochimica Acta* **58**, 9
184. Sharp, Z. D. (1990) A laser-based microanalytical method for the in situ determination of oxygen isotope ratios of silicates and oxides. *Geochimica et Cosmochimica Acta* **54**, 1353-1357
185. Yong-fei, Z. (1991) Calculation of oxygen isotope fractionation in metal oxides. *Geochimica et Cosmochimica Acta* **55**, 2299-2307
186. Jung, C. W., and Jacobs, P. (1995) Physical and chemical properties of superparamagnetic iron oxide MR contrast agents: ferumoxides, ferumoxtran, ferumoxsil. *Magn Reson Imaging* **13**, 661-674
187. Meldrum, F., C., Heywood, B, R., Mann, S. (1992) Magnetoferritin: In Vitro Synthesis of a Novel Magnetic Protein. *Science* **257**, 2
188. Chouly, C., Pouliquen, D., Lucet, I., Jeune, J. J., and Jallet, P. (1996) Development of superparamagnetic nanoparticles for MRI: effect of particle size, charge and surface nature on biodistribution. *J Microencapsul* **13**, 245-255
189. Andersen, D. J., Lindsley, D. H., and Davidson, P. M. (1993) QUILF: A pascal program to assess equilibria among Fe Mg Mn Ti oxides, pyroxenes, olivine, and quartz. *Computers & Geosciences* **19**, 1333-1350
190. Cheng, F. Y., Su, C. H., Yang, Y. S., Yeh, C. S., Tsai, C. Y., Wu, C. L., Wu, M. T., and Shieh, D. B. (2005) Characterization of aqueous dispersions of Fe(3)O(4) nanoparticles and their biomedical applications. *Biomaterials* **26**, 729-738
191. Fredrickson, J. K., Zachara, J. M., Kennedy, D. W., Dong, H., Onstott, T. C., Hinman, N. W., and Li, S.-m. (1998) Biogenic iron mineralization accompanying the dissimilatory reduction of hydrous ferric oxide by a groundwater bacterium. *Geochimica et Cosmochimica Acta* **62**, 3239-3257
192. Maher, B. A. (1998) Magnetic properties of modern soils and Quaternary loessic paleosols: paleoclimatic implications. *Palaeogeography, Palaeoclimatology, Palaeoecology* **137**, 25-54
193. Poulton, S. W., and Canfield, D. E. (2005) Development of a sequential extraction procedure for iron: implications for iron partitioning in continentally derived particulates. *Chemical Geology* **214**, 209-221
194. White, Powell, Holland, and Worley. (2000) The effect of TiO2 and Fe2O3 on metapelitic assemblages at greenschist and amphibolite facies conditions: mineral equilibria calculations in the system K2O–FeO–MgO–Al2O3–SiO2–H2O–TiO2–Fe2O3. *Journal of Metamorphic Geology* **18**, 497-511
195. Moskalyk, R. R., and Alfantazi, A. M. (2003) Processing of vanadium: a review. *Minerals Engineering* **16**, 793-805
196. Jones, D. A., Lelyveld, T. P., Mavrofidis, S. D., Kingman, S. W., and Miles, N. J. (2002) Microwave heating applications in environmental engineering—a review. *Resources, Conservation and Recycling* **34**, 75-90

197. Dixit, S., Hering, J.G. (2003) Comparison of Arsenic(V) and Arsenic(III) Sorption onto Iron Oxide Minerals: Implications for Arsenic Mobility. *Environmental Science Technology* **37**, 7
198. Kanel, S. R., Manning, B., Charlet, L., and Choi, H. (2005) Removal of Arsenic(III) from Groundwater by Nanoscale Zero-Valent Iron. *Environmental Science & Technology* **39**, 1291-1298
199. Hu, A., Yee, G. T., and Lin, W. (2005) Magnetically Recoverable Chiral Catalysts Immobilized on Magnetite Nanoparticles for Asymmetric Hydrogenation of Aromatic Ketones. *Journal of the American Chemical Society* **127**, 12486-12487
200. Ohtomo, A., and Hwang, H. Y. (2004) A high-mobility electron gas at the LaAlO3/SrTiO3 heterointerface. *Nature* **427**, 423-426
201. Beydoun, D., Amal, R., Low, G. K. C., and McEvoy, S. (2000) Novel Photocatalyst: Titania-Coated Magnetite. Activity and Photodissolution. *The Journal of Physical Chemistry B* **104**, 4387-4396
202. Sun, S., Zeng, H., Robinson, D. B., Raoux, S., Rice, P. M., Wang, S. X., and Li, G. (2004) Monodisperse MFe2O4 (M = Fe, Co, Mn) Nanoparticles. *Journal of the American Chemical Society* **126**, 273-279
203. Li, J., Zhang, S., Chen, C., Zhao, G., Yang, X., Li, J., and Wang, X. (2012) Removal of Cu(II) and Fulvic Acid by Graphene Oxide Nanosheets Decorated with Fe3O4 Nanoparticles. *ACS Applied Materials & Interfaces* **4**, 4991-5000
204. Tang, S. C. N., and Lo, I. M. C. (2013) Magnetic nanoparticles: Essential factors for sustainable environmental applications. *Water Research* **47**, 2613-2632
205. Xu, L. W., J. (2012) Magnetic Nanoscaled Fe3O4/CeO2 Composite as an Efficient Fenton-Like Heterogeneous Catalyst for Degradation of 4-Chlorophenol. *Environmental Science and Technology* **46**, 8
206. Frost, D. J., and McCammon, C. A. (2008) The Redox State of Earth's Mantle. *Annual Review of Earth and Planetary Sciences* **36**, 389-420
207. Chandra, V., Park, J., Chun, Y., Lee, J. W., Hwang, I.-C., and Kim, K. S. (2010) Water-Dispersible Magnetite-Reduced Graphene Oxide Composites for Arsenic Removal. *ACS Nano* **4**, 3979-3986
208. Hua, M., Zhang, S., Pan, B., Zhang, W., Lv, L., and Zhang, Q. (2012) Heavy metal removal from water/wastewater by nanosized metal oxides: a review. *J Hazard Mater* **211-212**, 317-331
209. Teja, A. S., and Koh, P.-Y. (2009) Synthesis, properties, and applications of magnetic iron oxide nanoparticles. *Progress in Crystal Growth and Characterization of Materials* **55**, 22-45
210. Deo, K. A., Lokhande, G., and Gaharwar, A. K. (2019) Nanostructured Hydrogels for Tissue Engineering and Regenerative Medicine. In *Encyclopedia of Tissue Engineering and Regenerative Medicine* (Reis, R. L., ed) pp. 21-32, Academic Press, Oxford
211. Quesada-González, D., and Merkoçi, A. (2015) Nanoparticle-based lateral flow biosensors. *Biosensors and Bioelectronics* **73**, 47-63
212. Teymourian, H., Salimi, A., and Khezrian, S. (2013) Fe3O4 magnetic nanoparticles/reduced graphene oxide nanosheets as a novel electrochemical and bioeletrochemical sensing platform. *Biosensors and Bioelectronics* **49**, 1-8
213. Lei, C., Han, F., Li, D., Li, W.-C., Sun, Q., Zhang, X.-Q., and Lu, A.-H. (2013) Dopamine as the coating agent and carbon precursor for the fabrication of N-doped carbon coated Fe3O4 composites as superior lithium ion anodes. *Nanoscale* **5**, 1168-1175

214. Mahdavi, M., Ahmad, M. B., Haron, M. J., Namvar, F., Nadi, B., Rahman, M. Z., and Amin, J. (2013) Synthesis, surface modification and characterisation of biocompatible magnetic iron oxide nanoparticles for biomedical applications. *Molecules* **18**, 7533-7548
215. Kolhatkar, A. G., Jamison, A. C., Litvinov, D., Willson, R. C., and Lee, T. R. (2013) Tuning the magnetic properties of nanoparticles. *Int J Mol Sci* **14**, 15977-16009
216. Pereira, C., Pereira, A. M., Fernandes, C., Rocha, M., Mendes, R., Fernández-García, M. P., Guedes, A., Tavares, P. B., Grenèche, J.-M., Araújo, J. P., and Freire, C. (2012) Superparamagnetic MFe2O4 (M = Fe, Co, Mn) Nanoparticles: Tuning the Particle Size and Magnetic Properties through a Novel One-Step Coprecipitation Route. *Chemistry of Materials* **24**, 1496-1504
217. Wang, Z., Lee, S., Koo, K., and Kim, K. (2016) Nanowire-Based Sensors for Biological and Medical Applications. *IEEE Trans Nanobioscience* **15**, 186-199
218. Liu, J., Sun, Z., Deng, Y., Zou, Y., Li, C., Guo, X., Xiong, L., Gao, Y., Li, F., and Zhao, D. (2009) Highly Water-Dispersible Biocompatible Magnetite Particles with Low Cytotoxicity Stabilized by Citrate Groups. *Angewandte Chemie International Edition* **48**, 5875-5879
219. Saslow, W. M. (2002) Chapter 9 - The Magnetism of Magnets. In *Electricity, Magnetism, and Light* (Saslow, W. M., ed) pp. 384-418, Academic Press, San Diego
220. Lee, J. E., Lee, N., Kim, H., Kim, J., Choi, S. H., Kim, J. H., Kim, T., Song, I. C., Park, S. P., Moon, W. K., and Hyeon, T. (2010) Uniform Mesoporous Dye-Doped Silica Nanoparticles Decorated with Multiple Magnetite Nanocrystals for Simultaneous Enhanced Magnetic Resonance Imaging, Fluorescence Imaging, and Drug Delivery. *Journal of the American Chemical Society* **132**, 552-557
221. Zand, Z., Khaki, P. A., Salihi, A., Sharifi, M., Qadir Nanakali, N. M., Alasady, A. A., Aziz, F. M., Shahpasand, K., Hasan, A., and Falahati, M. (2019) Cerium oxide NPs mitigate the amyloid formation of α-synuclein and associated cytotoxicity. *International journal of nanomedicine* **14**, 6989-7000
222. Mahmoudi, M., Sant, S., Wang, B., Laurent, S., and Sen, T. (2011) Superparamagnetic iron oxide nanoparticles (SPIONs): development, surface modification and applications in chemotherapy. *Adv Drug Deliv Rev* **63**, 24-46
223. Morishita, N., Nakagami, H., Morishita, R., Takeda, S., Mishima, F., Terazono, B., Nishijima, S., Kaneda, Y., and Tanaka, N. (2005) Magnetic nanoparticles with surface modification enhanced gene delivery of HVJ-E vector. *Biochem Biophys Res Commun* **334**, 1121-1126
224. Laurent, S., Saei, A. A., Behzadi, S., Panahifar, A., and Mahmoudi, M. (2014) Superparamagnetic iron oxide nanoparticles for delivery of therapeutic agents: opportunities and challenges. *Expert Opin Drug Deliv* **11**, 1449-1470
225. Kumar, C. S. M., F. (2011) Magnetic nanomaterials for hyperthermia-based therapy and controlled drug delivery. *Advanced Drug Delivery Reviews* **63**, 19
226. Martinez-Boubeta, C., Simeonidis, K., Makridis, A., Angelakeris, M., Iglesias, O., Guardia, P., Cabot, A., Yedra, L., Estradé, S., Peiró, F., Saghi, Z., Midgley, P. A., Conde-Leborán, I., Serantes, D., and Baldomir, D. (2013) Learning from Nature to Improve the Heat Generation of Iron-Oxide Nanoparticles for Magnetic Hyperthermia Applications. *Scientific Reports* **3**, 1652
227. Shubayev, V. I., Pisanic, T. R., 2nd, and Jin, S. (2009) Magnetic nanoparticles for theragnostics. *Adv Drug Deliv Rev* **61**, 467-477

228. Wan, Z., and Wang, J. (2017) Degradation of sulfamethazine using Fe3O4-Mn3O4/reduced graphene oxide hybrid as Fenton-like catalyst. *Journal of Hazardous Materials* **324**, 653-664
229. Zhao, D., Gao, X., Wu, C., Xie, R., Feng, S., and Chen, C. (2016) Facile preparation of amino functionalized graphene oxide decorated with Fe3O4 nanoparticles for the adsorption of Cr(VI). *Applied Surface Science* **384**, 1-9
230. Wang, P., Cao, M., Wang, C., Ao, Y., Hou, J., and Qian, J. (2014) Kinetics and thermodynamics of adsorption of methylene blue by a magnetic graphene-carbon nanotube composite. *Applied Surface Science* **290**, 116-124
231. Maleki, A., Hajizadeh, Z., Sharifi, V., and Emdadi, Z. (2019) A green, porous and eco-friendly magnetic geopolymer adsorbent for heavy metals removal from aqueous solutions. *Journal of Cleaner Production* **215**, 1233-1245
232. Liu, Q., Zhong, L.-B., Zhao, Q.-B., Frear, C., and Zheng, Y.-M. (2015) Synthesis of Fe3O4/Polyacrylonitrile Composite Electrospun Nanofiber Mat for Effective Adsorption of Tetracycline. *ACS Applied Materials & Interfaces* **7**, 14573-14583
233. Chen, B., and Kan, H. (2008) Air pollution and population health: a global challenge. *Environmental Health and Preventive Medicine* **13**, 94-101
234. Sun, Y., Ding, C., Cheng, W., and Wang, X. (2014) Simultaneous adsorption and reduction of U(VI) on reduced graphene oxide-supported nanoscale zerovalent iron. *J Hazard Mater* **280**, 399-408
235. Hassandoost, R., Pouran, S. R., Khataee, A., Orooji, Y., and Joo, S. W. (2019) Hierarchically structured ternary heterojunctions based on Ce3+/ Ce4+ modified Fe3O4 nanoparticles anchored onto graphene oxide sheets as magnetic visible-light-active photocatalysts for decontamination of oxytetracycline. *Journal of Hazardous Materials* **376**, 200-211
236. Das, R. S., V. S.; Paumo, H. K.; Bhaumik, M.; Maity, A. (2019) Silver decorated magnetic nanocomposite (Fe3O4@PPy-MAA/Ag) as highly active catalyst towards reduction of 4-nitrophenol and toxic organic dyes. *Applied Catalysis B: Environmental* **244**, 12
237. Guo, X., Du, B., Wei, Q., Yang, J., Hu, L., Yan, L., and Xu, W. (2014) Synthesis of amino functionalized magnetic graphenes composite material and its application to remove Cr(VI), Pb(II), Hg(II), Cd(II) and Ni(II) from contaminated water. *J Hazard Mater* **278**, 211-220
238. Wang, L. H., Y.; Sun, X.; Huang, H.; Lui, P.; Zong, M.; Wang, Y. (2014) Synthesis and microwave absorption enhancement of graphene Fe3O4 SiO2 NiO nanosheet hierarchical structures. *Nanoscale* **2014**
239. Wu, N., Liu, C., Xu, D., Liu, J., Liu, W., Shao, Q., and Guo, Z. (2018) Enhanced Electromagnetic Wave Absorption of Three-Dimensional Porous Fe3O4/C Composite Flowers. *ACS Sustainable Chemistry & Engineering* **6**, 12471-12480
240. Qiao, M., Lei, X., Ma, Y., Tian, L., He, X., Su, K., and Zhang, Q. (2018) Application of yolk–shell Fe3O4@N-doped carbon nanochains as highly effective microwave-absorption material. *Nano Research* **11**, 1500-1519
241. Liu, J., Liang, H., and Wu, H. (2020) Hierarchical flower-like Fe3O4/MoS2 composites for selective broadband electromagnetic wave absorption performance. *Composites Part A: Applied Science and Manufacturing* **130**, 105760
242. Wang, T., Zhang, L., Li, C., Yang, W., Song, T., Tang, C., Meng, Y., Dai, S., Wang, H., Chai, L., and Luo, J. (2015) Synthesis of Core–Shell Magnetic Fe3O4@poly(m-

Phenylenediamine) Particles for Chromium Reduction and Adsorption. *Environmental Science & Technology* **49**, 5654-5662
243. Vu, H. C., Dwivedi, A. D., Le, T. T., Seo, S.-H., Kim, E.-J., and Chang, Y.-S. (2017) Magnetite graphene oxide encapsulated in alginate beads for enhanced adsorption of Cr(VI) and As(V) from aqueous solutions: Role of crosslinking metal cations in pH control. *Chemical Engineering Journal* **307**, 220-229
244. He, X., Liu, X., Li, R., Yang, B., Yu, K., Zeng, M., and Yu, R. (2016) Effects of local structure of Ce(3+) ions on luminescent properties of Y3Al5O12:Ce nanoparticles. *Scientific reports* **6**, 22238-22238
245. Li, N., Huang, G. W., Li, Y. Q., Xiao, H. M., Feng, Q. P., Hu, N., and Fu, S. Y. (2017) Enhanced Microwave Absorption Performance of Coated Carbon Nanotubes by Optimizing the Fe3O4 Nanocoating Structure. *ACS Appl Mater Interfaces* **9**, 2973-2983
246. Jiaolong, L., Hongsheng, L., and Wu, H. (2019) Hierarchical flower-like Fe3O4/MoS2 composites for selective broadband electromagnetic wave absorption performance. *Composites Part A Applied Science and Manufacturing*, 105760
247. Wang, X., Pan, F., Xiang, Z., Zeng, Q., Pei, K., Che, R., and Lu, W. (2020) Magnetic vortex core-shell Fe3O4@C nanorings with enhanced microwave absorption performance. *Carbon* **157**, 130-139
248. Sharma, S., Sahu, B. K., Cao, L., Bindra, P., Kaur, K., Chandel, M., Koratkar, N., Huang, Q., and Shanmugam, V. (2021) Porous nanomaterials: Main vein of agricultural nanotechnology. *Progress in Materials Science* **121**, 100812
249. Zhang, X. J., G.; Liu, W.; Quan, B.; Liang, X.; Shang, C.; Cheng, Y.; Du, Y. (2015) Thermal conversion of an Fe3O4 metal–organic framework: a new method for an efficient Fe–Co/nanoporous carbon microwave absorbing material. *Nanoscale* **7**, 11
250. Cruz Viggi, C., Rossetti, S., Fazi, S., Paiano, P., Majone, M., and Aulenta, F. (2014) Magnetite Particles Triggering a Faster and More Robust Syntrophic Pathway of Methanogenic Propionate Degradation. *Environmental Science & Technology* **48**, 7536-7543
251. Guo, J. S., H.; Liu, H.; Luo, C.; Ren, Y.; Ding, T.; Khan, M.; YOung, D.; Liu, X.; Zhang, X.; Kong, J.; Guo, Z. (2017) Polypyrrole-interface-functionalized nano-magnetite epoxy nanocomposites as electromagnetic wave absorbers with enhanced flame retardancy. *Journal of Materials Chemistry C* **5**, 10
252. Wang, Q., Jiao, L., Du, H., Wang, Y., and Yuan, H. (2014) Fe3O4 nanoparticles grown on graphene as advanced electrode materials for supercapacitors. *Journal of Power Sources* **245**, 101-106
253. Sharif, F., Arjmand, M., Moud, A. A., Sundararaj, U., and Roberts, E. P. L. (2017) Segregated Hybrid Poly(methyl methacrylate)/Graphene/Magnetite Nanocomposites for Electromagnetic Interference Shielding. *ACS Applied Materials & Interfaces* **9**, 14171-14179
254. Bashir, M. R., Bhatti, L., Marin, D., and Nelson, R. C. (2015) Emerging applications for ferumoxytol as a contrast agent in MRI. *J Magn Reson Imaging* **41**, 884-898
255. Li, J., Hu, Y., Yang, J., Wei, P., Sun, W., Shen, M., Zhang, G., and Shi, X. (2015) Hyaluronic acid-modified Fe3O4@Au core/shell nanostars for multimodal imaging and photothermal therapy of tumors. *Biomaterials* **38**, 10-21
256. Das, P., Colombo, M., and Prosperi, D. (2019) Recent advances in magnetic fluid hyperthermia for cancer therapy. *Colloids and Surfaces B: Biointerfaces* **174**, 42-55

257. Gao, S., Lin, H., Zhang, H., Yao, H., Chen, Y., and Shi, J. (2019) Nanocatalytic Tumor Therapy by Biomimetic Dual Inorganic Nanozyme-Catalyzed Cascade Reaction. *Advanced Science* **6**, 1801733
258. Rashid, M., Khan, M. I., Hayat, T., Khan, M. I., and Alsaedi, A. (2019) Entropy generation in flow of ferromagnetic liquid with nonlinear radiation and slip condition. *Journal of Molecular Liquids* **276**, 441-452
259. Revia, R. A., and Zhang, M. (2016) Magnetite nanoparticles for cancer diagnosis, treatment, and treatment monitoring: recent advances. *Materials Today* **19**, 157-168
260. Shen, S., Wang, S., Zheng, R., Zhu, X., Jiang, X., Fu, D., and Yang, W. (2015) Magnetic nanoparticle clusters for photothermal therapy with near-infrared irradiation. *Biomaterials* **39**, 67-74
261. Fan, J. P., M.; Wang, H.; Zheng, H.; Liu, Z.; Li, C.; Wang, X.; Liu, X.; Cheng, S.; Zhang, X. (2019) Engineered Bacterial Bioreactor for Tumor Therapy via Fenton-Like Reaction with Localized H2O2 Generation. *Advanced Materials* **31**
262. Feng, W., Han, X., Wang, R., Gao, X., Hu, P., Yue, W., Chen, Y., and Shi, J. (2019) Nanocatalysts-Augmented and Photothermal-Enhanced Tumor-Specific Sequential Nanocatalytic Therapy in Both NIR-I and NIR-II Biowindows. *Adv Mater* **31**, e1805919
263. Song, J., Lin, L., Yang, Z., Zhu, R., Zhou, Z., Li, Z.-W., Wang, F., Chen, J., Yang, H., and Chen, X. (2019) Self-Assembled Responsive Bilayered Vesicles with Adjustable Oxidative Stress for Enhanced Cancer Imaging and Therapy. *Journal of the American Chemical Society* **141**, 8158-8170
264. Rao, L. C., B.; Bu, L.; Liao, Q.; Guo, S.; Zhao, X.; Dong, W.; Liu, W. (2017) Microfluidic Electroporation-Facilitated Synthesis of Erythrocyte Membrane-Coated Magnetic Nanoparticles for Enhanced Imaging-Guided Cancer Therapy. *ACS Nano* **11**, 9
265. Tietze, R. Z., J.; Unterweger, H.; Lyer, S.; Friedrich, R. P.; Janko, C.; Pottler, M.; Durr, S.; Alexiou, C. (2015) Magnetic nanoparticle-based drug delivery for cancer therapy. *Biochemical and Biophysical Research Communications* **468**, 7
266. Li, X., Wei, J., Aifantis, K. E., Fan, Y., Feng, Q., Cui, F. Z., and Watari, F. (2016) Current investigations into magnetic nanoparticles for biomedical applications. *J Biomed Mater Res A* **104**, 1285-1296
267. Xi, Z., Huang, R., Li, Z., He, N., Wang, T., Su, E., and Deng, Y. (2015) Selection of HBsAg-Specific DNA Aptamers Based on Carboxylated Magnetic Nanoparticles and Their Application in the Rapid and Simple Detection of Hepatitis B Virus Infection. *ACS Applied Materials & Interfaces* **7**, 11215-11223
268. Liu, M., Li, X. Y., Li, J. J., Su, X. M., Wu, Z. Y., Li, P. F., Lei, F. H., Tan, X. C., and Shi, Z. W. (2015) Synthesis of magnetic molecularly imprinted polymers for the selective separation and determination of metronidazole in cosmetic samples. *Anal Bioanal Chem* **407**, 3875-3880
269. Chen, F., Wang, G., Griffin, J. I., Brenneman, B., Banda, N. K., Holers, V. M., Backos, D. S., Wu, L., Moghimi, S. M., and Simberg, D. (2017) Complement proteins bind to nanoparticle protein corona and undergo dynamic exchange in vivo. *Nat Nanotechnol* **12**, 387-393
270. Shuai, C., Yang, W., He, C., Peng, S., Gao, C., Yang, Y., Qi, F., and Feng, P. (2020) A magnetic micro-environment in scaffolds for stimulating bone regeneration. *Materials & Design* **185**, 108275

271. Zhang, Z., Zhang, X., Liu, B., and Liu, J. (2017) Molecular Imprinting on Inorganic Nanozymes for Hundred-fold Enzyme Specificity. *Journal of the American Chemical Society* **139**, 5412-5419
272. Zhang, R., Lu, N., Zhang, J., Yan, R., Li, J., Wang, L., Wang, N., Lv, M., and Zhang, M. (2020) Ultrasensitive aptamer-based protein assays based on one-dimensional core-shell nanozymes. *Biosensors and Bioelectronics* **150**, 111881
273. Arabi, M., Ghaedi, M., and Ostovan, A. (2017) Development of a Lower Toxic Approach Based on Green Synthesis of Water-Compatible Molecularly Imprinted Nanoparticles for the Extraction of Hydrochlorothiazide from Human Urine. *ACS Sustainable Chemistry & Engineering* **5**, 3775-3785
274. Phillips, D. H., and Arlt, V. M. (2009) Genotoxicity: damage to DNA and its consequences. *Exs* **99**, 87-110
275. Sadeghiani, N., Barbosa, L. S., Silva, L. P., Azevedo, R. B., Morais, P. C., and Lacava, Z. G. M. (2005) Genotoxicity and inflammatory investigation in mice treated with magnetite nanoparticles surface coated with polyaspartic acid. *Journal of Magnetism and Magnetic Materials* **289**, 466-468
276. Hwang, D. W., Lee, D. S., and Kim, S. (2012) Gene expression profiles for genotoxic effects of silica-free and silica-coated cobalt ferrite nanoparticles. *J Nucl Med* **53**, 106-112
277. Singh, N., Jenkins, G. J., Nelson, B. C., Marquis, B. J., Maffeis, T. G., Brown, A. P., Williams, P. M., Wright, C. J., and Doak, S. H. (2012) The role of iron redox state in the genotoxicity of ultrafine superparamagnetic iron oxide nanoparticles. *Biomaterials* **33**, 163-170
278. Hong, S. C., Lee, J. H., Lee, J., Kim, H. Y., Park, J. Y., Cho, J., Lee, J., and Han, D. W. (2011) Subtle cytotoxicity and genotoxicity differences in superparamagnetic iron oxide nanoparticles coated with various functional groups. *Int J Nanomedicine* **6**, 3219-3231
279. Magdolenova, Z., Collins, A., Kumar, A., Dhawan, A., Stone, V., and Dusinska, M. (2014) Mechanisms of genotoxicity. A review of in vitro and in vivo studies with engineered nanoparticles. *Nanotoxicology* **8**, 233-278
280. Könczöl, M., Ebeling, S., Goldenberg, E., Treude, F., Gminski, R., Gieré, R., Grobéty, B., Rothen-Rutishauser, B., Merfort, I., and Mersch-Sundermann, V. (2011) Cytotoxicity and Genotoxicity of Size-Fractionated Iron Oxide (Magnetite) in A549 Human Lung Epithelial Cells: Role of ROS, JNK, and NF-κB. *Chemical Research in Toxicology* **24**, 1460-1475
281. Gonet, T., Maher, B. A., and Kukutschová, J. (2021) Source apportionment of magnetite particles in roadside airborne particulate matter. *Science of The Total Environment* **752**, 141828
282. Giere, R. (2016) Magnetite in the human body: Biogenic vs. anthropogenic. *Proc Natl Acad Sci U S A* **113**, 11986-11987
283. Zhang, Q., Lu, D., Wang, D., Yang, X., Zuo, P., Yang, H., Fu, Q., Liu, Q., and Jiang, G. (2020) Separation and Tracing of Anthropogenic Magnetite Nanoparticles in the Urban Atmosphere. *Environmental Science & Technology* **54**, 9274-9284
284. Maher, B. A. (2019) Airborne Magnetite- and Iron-Rich Pollution Nanoparticles: Potential Neurotoxicants and Environmental Risk Factors for Neurodegenerative Disease, Including Alzheimer's Disease. *Journal of Alzheimer's Disease* **71**, 361-375

285. Aksnes, D. W., Langfeldt, L., and Wouters, P. (2019) Citations, Citation Indicators, and Research Quality: An Overview of Basic Concepts and Theories. *SAGE Open* **9**, 2158244019829575
286. Ito, A., Shinkai, M., Honda, H., and Kobayashi, T. (2005) Medical application of functionalized magnetic nanoparticles. *J Biosci Bioeng* **100**, 1-11
287. Sharma, N., Jandaik, S., Singh, T. G., and Kumar, S. (2016) Chapter 14 - Nanoparticles: Boon to mankind and bane to pathogens. In *Nanobiomaterials in Antimicrobial Therapy* (Grumezescu, A. M., ed) pp. 483-509, William Andrew Publishing
288. Sun, C., Lee, J. S. H., and Zhang, M. (2008) Magnetic nanoparticles in MR imaging and drug delivery. *Advanced drug delivery reviews* **60**, 1252-1265
289. Cojocaru, B., Avram, D., Kessler, V., Parvulescu, V., Seisenbaeva, G., and Tiseanu, C. (2017) Nanoscale insights into doping behavior, particle size and surface effects in trivalent metal doped SnO(2). *Scientific reports* **7**, 9598-9598
290. Predescu, A. M., Matei, E., Berbecaru, A. C., Pantilimon, C., Drăgan, C., Vidu, R., Predescu, C., and Kuncser, V. (2018) Synthesis and characterization of dextran-coated iron oxide nanoparticles. *Royal Society open science* **5**, 171525-171525
291. Tassa, C., Shaw, S. Y., and Weissleder, R. (2011) Dextran-coated iron oxide nanoparticles: a versatile platform for targeted molecular imaging, molecular diagnostics, and therapy. *Acc Chem Res* **44**, 842-852
292. Stephen, Z. R., Kievit, F. M., and Zhang, M. (2011) Magnetite Nanoparticles for Medical MR Imaging. *Materials today (Kidlington, England)* **14**, 330-338
293. Harris, L., A., Goff, J, D., Carmichael, A, Y., Riffle, J, S., Harburn, J, J., Pierre, T, G, St., Saunders, M. (2003) Magnetite Nanoparticle Dispersions Stabilized wth Triblock Copolymers. *Chemistry of Materials* **15**, 10
294. Mornet, S., Vasseur, S., Grasset, F., and Duguet, E. (2004) Magnetic nanoparticle design for medical diagnosis and therapy. *Journal of Materials Chemistry* **14**, 2161-2175
295. Mout, R., Moyano, D. F., Rana, S., and Rotello, V. M. (2012) Surface functionalization of nanoparticles for nanomedicine. *Chemical Society reviews* **41**, 2539-2544
296. Pinelli, F., Perale, G., and Rossi, F. (2020) Coating and Functionalization Strategies for Nanogels and Nanoparticles for Selective Drug Delivery. *Gels (Basel, Switzerland)* **6**, 6
297. Liakos, I., Grumezescu, A. M., and Holban, A. M. (2014) Magnetite nanostructures as novel strategies for anti-infectious therapy. *Molecules (Basel, Switzerland)* **19**, 12710-12726
298. Liu, Y., Wang, X., Hussain, M., Lv, M., Dong, X., Wang, T., Xu, X., and Liu, B. (2018) Theranostics Applications of Nanoparticles in Cancer Immunotherapy. *Med Sci (Basel)* **6**
299. Veisi, H., Ghorbani, M., and Hemmati, S. (2019) Sonochemical in situ immobilization of Pd nanoparticles on green tea extract coated Fe(3)O(4) nanoparticles: An efficient and magnetically recyclable nanocatalyst for synthesis of biphenyl compounds under ultrasound irradiations. *Mater Sci Eng C Mater Biol Appl* **98**, 584-593
300. Asmatulu, R., Fakhari, A., Wamocha, H. L., Chu, H. Y., Chen, Y. Y., Eltabey, M. M., Hamdeh, H. H., and Ho, J. C. (2009) Drug-Carrying Magnetic Nanocomposite Particles for Potential Drug Delivery Systems. *Journal of Nanotechnology* **2009**, 238536
301. D'Agostino, C., Chansai, S., Bush, I., Gao, C., Mantle, M. D., Hardacre, C., James, S. L., and Gladden, L. F. (2016) Assessing the effect of reducing agents on the selective

catalytic reduction of NOx over Ag/Al2O3 catalysts. *Catalysis Science & Technology* **6**, 1661-1666
302. Fadeel, B. (2019) Hide and Seek: Nanomaterial Interactions With the Immune System. *Frontiers in immunology* **10**, 133-133
303. Malachowski, T., and Hassel, A. (2020) Engineering nanoparticles to overcome immunological barriers for enhanced drug delivery. *Engineered Regeneration* **1**, 35-50
304. Wang, G., Zhao, D., Li, N., Wang, X., and Ma, Y. (2018) Drug-loaded poly (ε-caprolactone)/Fe3O4 composite microspheres for magnetic resonance imaging and controlled drug delivery. *Journal of Magnetism and Magnetic Materials* **456**, 316-323
305. Zhang, L., Ren, Y., Peng, S., Guo, D., Wen, S., Luo, J., and Xie, G. (2019) Core–shell nanospheres to achieve ultralow friction polymer nanocomposites with superior mechanical properties. *Nanoscale* **11**, 8237-8246
306. Özgür, M. E., Ulu, A., Balcıoğlu, S., Özcan, İ., Köytepe, S., and Ateş, B. (2018) The Toxicity Assessment of Iron Oxide (Fe_3O_4) Nanoparticles on Physical and Biochemical Quality of Rainbow Trout Spermatozoon. *Toxics* **6**, 62
307. Rafieepour, A., Azari, M. R., Peirovi, H., Khodagholi, F., Jaktaji, J. P., Mehrabi, Y., Naserzadeh, P., and Mohammadian, Y. (2019) Investigation of the effect of magnetite iron oxide particles size on cytotoxicity in A549 cell line. *Toxicology and Industrial Health* **35**, 703-713
308. Costa, C., Brandão, F., Bessa, M. J., Costa, S., Valdiglesias, V., Kiliç, G., Fernández-Bertólez, N., Quaresma, P., Pereira, E., Pásaro, E., Laffon, B., and Teixeira, J. P. (2016) In vitro cytotoxicity of superparamagnetic iron oxide nanoparticles on neuronal and glial cells. Evaluation of nanoparticle interference with viability tests. *J Appl Toxicol* **36**, 361-372
309. Ketebo, A. A., Shin, T. H., Jun, M., Lee, G., and Park, S. (2020) Effect of silica-coated magnetic nanoparticles on rigidity sensing of human embryonic kidney cells. *Journal of Nanobiotechnology* **18**, 170
310. Heusinkveld, H. J., Wahle, T., Campbell, A., Westerink, R. H. S., Tran, L., Johnston, H., Stone, V., Cassee, F. R., and Schins, R. P. F. (2016) Neurodegenerative and neurological disorders by small inhaled particles. *Neurotoxicology* **56**, 94-106
311. Bazylinski, D., A., Garratt-Reed, A, J., Frankel, R, B. (1994) Electron Microscopic Studies of Magnetosomes in Magnetotactic Bacteria. *Microscopy Research and Technique* **27**, 12
312. Kirschvink, J., L., Kobayashi-Kirschvink, A., Diaz-Ricci, J, C., Kirschvink, S, J. (1992) Magnetite in Human Tissues: A Mechanism for the Biological Effects of Weak ELF Magnetic Fields. *Bioelectromagnetics Supplement* **1**, 12
313. Levesque, S., Surace, M. J., McDonald, J., and Block, M. L. (2011) Air pollution & the brain: Subchronic diesel exhaust exposure causes neuroinflammation and elevates early markers of neurodegenerative disease. *J Neuroinflammation* **8**, 105
314. Schieber, M., and Chandel, N. S. (2014) ROS function in redox signaling and oxidative stress. *Current biology : CB* **24**, R453-R462
315. Heneka, M. T., Carson, M. J., El Khoury, J., Landreth, G. E., Brosseron, F., Feinstein, D. L., Jacobs, A. H., Wyss-Coray, T., Vitorica, J., Ransohoff, R. M., Herrup, K., Frautschy, S. A., Finsen, B., Brown, G. C., Verkhratsky, A., Yamanaka, K., Koistinaho, J., Latz, E., Halle, A., Petzold, G. C., Town, T., Morgan, D., Shinohara, M. L., Perry, V. H., Holmes, C., Bazan, N. G., Brooks, D. J., Hunot, S., Joseph, B., Deigendesch, N., Garaschuk, O., Boddeke, E., Dinarello, C. A., Breitner, J. C., Cole, G. M., Golenbock, D. T., and Kummer,

M. P. (2015) Neuroinflammation in Alzheimer's disease. *The Lancet. Neurology* **14**, 388-405
316. Chen, X., Guo, C., and Kong, J. (2012) Oxidative stress in neurodegenerative diseases. *Neural regeneration research* **7**, 376
317. Laurent, S., Dutz, S., Häfeli, U. O., and Mahmoudi, M. (2011) Magnetic fluid hyperthermia: Focus on superparamagnetic iron oxide nanoparticles. *Advances in Colloid and Interface Science* **166**, 8-23
318. Kelley, B. J., and Petersen, R. C. (2007) Alzheimer's disease and mild cognitive impairment. *Neurologic clinics* **25**, 577-v
319. Justice, N. J. (2018) The relationship between stress and Alzheimer's disease. *Neurology of Stress* **8**, 3
320. Trinchese, F., Liu, S., Battaglia, F., Walter, S., Mathews, P. M., and Arancio, O. (2004) Progressive age-related development of Alzheimer-like pathology in APP/PS1 mice. *Annals of Neurology* **55**, 801-814
321. Kim, J., and Wessling-Resnick, M. (2014) Iron and mechanisms of emotional behavior. *The Journal of nutritional biochemistry* **25**, 1101-1107
322. Lok, K. H., Zhao, H., Zhang, C., He, N., Shen, H., Wang, Z., Zhao, W., and Yin, M. (2013) Effects of accelerated senescence on learning and memory, locomotion and anxiety-like behavior in APP/PS1 mouse model of Alzheimer's disease. *Journal of the neurological sciences* **335**
323. Padurariu, M., Ciobica, A., Mavroudis, I., Fotiou, D., and Baloyannis, S. (2012) Hippocampal neuronal loss in the CA1 and CA3 areas of Alzheimer's disease patients. *Psychiatr Danub* **24**, 152-158
324. Beauquis, J., Vinuesa, A., Pomilio, C., Pavía, P., Galván, V., and Saravia, F. (2014) Neuronal and glial alterations, increased anxiety, and cognitive impairment before hippocampal amyloid deposition in PDAPP mice, model of Alzheimer's disease. *Hippocampus* **24**, 257-269
325. Chi, H., Chang, H.-Y., and Sang, T.-K. (2018) Neuronal Cell Death Mechanisms in Major Neurodegenerative Diseases. *Int J Mol Sci* **19**, 3082
326. Benice, T. S., Rizk, A., Kohama, S., Pfankuch, T., and Raber, J. (2006) Sex-differences in age-related cognitive decline in C57BL/6J mice associated with increased brain microtubule-associated protein 2 and synaptophysin immunoreactivity. *Neuroscience* **137**, 413-423
327. Adler, D. H., Wisse, L. E. M., Ittyerah, R., Pluta, J. B., Ding, S. L., Xie, L., Wang, J., Kadivar, S., Robinson, J. L., Schuck, T., Trojanowski, J. Q., Grossman, M., Detre, J. A., Elliott, M. A., Toledo, J. B., Liu, W., Pickup, S., Miller, M. I., Das, S. R., Wolk, D. A., and Yushkevich, P. A. (2018) Characterizing the human hippocampus in aging and Alzheimer's disease using a computational atlas derived from ex vivo MRI and histology. *Proc Natl Acad Sci U S A* **115**, 4252-4257
328. Radde, R., Bolmont, T., Kaeser, S. A., Coomaraswamy, J., Lindau, D., Stoltze, L., Calhoun, M. E., Jäggi, F., Wolburg, H., Gengler, S., Haass, C., Ghetti, B., Czech, C., Hölscher, C., Mathews, P. M., and Jucker, M. (2006) Aβ42-driven cerebral amyloidosis in transgenic mice reveals early and robust pathology. *EMBO reports* **7**, 940-946
329. Carrera, I., Etcheverría, I., Li, Y., Fernández-Novoa, L., Lombardi, V., Vigo, C., Palacios, H. H., Benberin, V. V., Cacabelos, R., and Aliev, G. (2013) Immunocytochemical Characterization of Alzheimer Disease Hallmarks in APP/PS1 Transgenic Mice Treated

with a New Anti-Amyloid-β Vaccine. *BioMed Research International* **2013**, 709145
330. Cui, J., Wang, X., Li, X., Wang, X., Zhang, C., Li, W., Zhang, Y., Gu, H., Xie, X., Nan, F., Zhao, J., and Pei, G. (2015) Targeting the γ-/β-secretase interaction reduces β-amyloid generation and ameliorates Alzheimer's disease-related pathogenesis. *Cell Discovery* **1**, 15021
331. O'Brien, R. J., and Wong, P. C. (2011) Amyloid precursor protein processing and Alzheimer's disease. *Annual review of neuroscience* **34**, 185-204
332. Liu, Q., Xie, F., Alvarado-Diaz, A., Smith, M. A., Moreira, P. I., Zhu, X., and Perry, G. (2011) Neurofilamentopathy in neurodegenerative diseases. *The open neurology journal* **5**, 58-62
333. Medeiros, R., Baglietto-Vargas, D., and LaFerla, F. M. (2011) The Role of Tau in Alzheimer's Disease and Related Disorders. *CNS Neuroscience & Therapeutics* **17**, 514-524
334. Hampel, H., Blennow, K., Shaw, L. M., Hoessler, Y. C., Zetterberg, H., and Trojanowski, J. Q. (2010) Total and phosphorylated tau protein as biological markers of Alzheimer's disease. *Experimental Gerontology* **45**, 30-40
335. Agholme, L., Lindström, T., Kågedal, K., Marcusson, J., and Hallbeck, M. (2010) An in vitro model for neuroscience: differentiation of SH-SY5Y cells into cells with morphological and biochemical characteristics of mature neurons. *J Alzheimers Dis* **20**, 1069-1082
336. de Medeiros, L. M., De Bastiani, M. A., Rico, E. P., Schonhofen, P., Pfaffenseller, B., Wollenhaupt-Aguiar, B., Grun, L., Barbé-Tuana, F., Zimmer, E. R., Castro, M. A. A., Parsons, R. B., and Klamt, F. (2019) Cholinergic Differentiation of Human Neuroblastoma SH-SY5Y Cell Line and Its Potential Use as an In vitro Model for Alzheimer's Disease Studies. *Mol Neurobiol* **56**, 7355-7367
337. Nguyen, T., Li, G. E., Chen, H., Cranfield, C. G., McGrath, K. C., and Gorrie, C. A. (2018) Maternal E-Cigarette Exposure Results in Cognitive and Epigenetic Alterations in Offspring in a Mouse Model. *Chem Res Toxicol* **31**, 601-611
338. Picken, M. M., and Herrera, G. A. (2015) Thioflavin T Stain: An Easier and More Sensitive Method for Amyloid Detection. In *Amyloid and Related Disorders: Surgical Pathology and Clinical Correlations* (Picken, M. M., Herrera, G. A., and Dogan, A., eds) pp. 225-227, Springer International Publishing, Cham
339. Bisla, A., Srivastava, N., Rautela, R., Yadav, V., Singh, P., Kumar, A., Ghosh, S. K., Ghosh, S., and Katiyar, R. (2020) Effect of ultra-sonication and peptization on the aqueous phase stability of iron oxide nanoparticles. *Inorganic and Nano-Metal Chemistry* **50**, 1103-1114
340. Nguyen, T., Li, G. E., Chen, H., Cranfield, C. G., McGrath, K. C., and Gorrie, C. A. (2018) Maternal E-Cigarette Exposure Results in Cognitive and Epigenetic Alterations in Offspring in a Mouse Model. *Chemical Research in Toxicology* **31**, 601-611
341. McGrath, K. C., Li, X. H., Whitworth, P. T., Kasz, R., Tan, J. T., McLennan, S. V., Celermajer, D. S., Barter, P. J., Rye, K.-A., and Heather, A. K. (2014) High density lipoproteins improve insulin sensitivity in high-fat diet-fed mice by suppressing hepatic inflammation [S]. *Journal of Lipid Research* **55**, 421-430
342. McGrath, K. C.-Y., Hill, M. D., McRobb, L. S., and Heather, A. K. (2010) The androgen receptor drives the sex-specific expression of vascular cell adhesion molecule-1 in

endothelial cells but not lipid metabolism genes in monocyte-derived macrophages. *Hormone Molecular Biology and Clinical Investigation* **2**, 203-209
343. McGrath, K. C. Y., Li, X.-H., McRobb, L. S., and Heather, A. K. (2015) Inhibitory Effect of a French Maritime Pine Bark Extract-Based Nutritional Supplement on TNF-α-Induced Inflammation and Oxidative Stress in Human Coronary Artery Endothelial Cells. *Evidence-Based Complementary and Alternative Medicine* **2015**, 260530
344. Snow, W. M., and Albensi, B. C. (2016) Neuronal Gene Targets of NF-κB and Their Dysregulation in Alzheimer's Disease. *Frontiers in molecular neuroscience* **9**, 118-118
345. West, M. J., Kawas, C. H., Martin, L. J., and Troncoso, J. C. (2000) The CA1 region of the human hippocampus is a hot spot in Alzheimer's disease. *Ann N Y Acad Sci* **908**, 255-259
346. Teitsdottir, U. D., Jonsdottir, M. K., Lund, S. H., Darreh-Shori, T., Snaedal, J., and Petersen, P. H. (2020) Association of glial and neuronal degeneration markers with Alzheimer's disease cerebrospinal fluid profile and cognitive functions. *Alzheimer's Research & Therapy* **12**, 92
347. Escher, C. M., Sannemann, L., and Jessen, F. (2019) Stress and Alzheimer's disease. *Journal of Neural Transmission* **126**, 1155-1161
348. Ran, K., Yang, J., Nair, A. V., Zhu, B., and Ran, C. (2020) CRANAD-28: A Robust Fluorescent Compound for Visualization of Amyloid Beta Plaques. *Molecules (Basel, Switzerland)* **25**, 863
349. Dyrks, T., Dyrks, E., Masters, C. L., and Beyreuther, K. (1993) Amyloidogenicity of rodent and human beta A4 sequences. *FEBS Lett* **324**, 231-236
350. Kitazawa, M., Medeiros, R., and Laferla, F. M. (2012) Transgenic mouse models of Alzheimer disease: developing a better model as a tool for therapeutic interventions. *Curr Pharm Des* **18**, 1131-1147
351. Vassar, R. (2004) BACE1: the beta-secretase enzyme in Alzheimer's disease. *J Mol Neurosci* **23**, 105-114
352. Schneider, A., Biernat, J., von Bergen, M., Mandelkow, E., and Mandelkow, E. M. (1999) Phosphorylation that detaches tau protein from microtubules (Ser262, Ser214) also protects it against aggregation into Alzheimer paired helical filaments. *Biochemistry* **38**, 3549-3558
353. Wu, H., Wei, S., Huang, Y., Chen, L., Wang, Y., Wu, X., Zhang, Z., Pei, Y., and Wang, D. (2020) Aβ monomer induces phosphorylation of Tau at Ser-214 through β2AR-PKA-JNK signaling pathway. *The FASEB Journal* **34**
354. Vainchtein, I. D., and Molofsky, A. V. (2020) Astrocytes and Microglia: In Sickness and in Health. *Trends Neurosci* **43**, 144-154
355. Wang, W.-Y., Tan, M.-S., Yu, J.-T., and Tan, L. (2015) Role of pro-inflammatory cytokines released from microglia in Alzheimer's disease. *Annals of Translational Medicine* **3**, 7
356. Xiao, K., Liu, C., Tu, Z., Xu, Q., Chen, S., Zhang, Y., Wang, X., Zhang, J., Hu, C.-A. A., and Liu, Y. (2020) Activation of the NFκB and MAPK Signaling Pathways Contributes to the Inflammatory Responses, but Not Cell Injury, in IPEC-1 Cells Challenged with Hydrogen Peroxide. *Oxidative Medicine and Cellular Longevity* **2020**, 5803639
357. Huang, G., Shi, L. Z., and Chi, H. (2009) Regulation of JNK and p38 MAPK in the immune system: signal integration, propagation and termination. *Cytokine* **48**, 161-169

358. Miranda, M., Morici, J. F., Zanoni, M. B., and Bekinschtein, P. (2019) Brain-Derived Neurotrophic Factor: A Key Molecule for Memory in the Healthy and the Pathological Brain. *Frontiers in Cellular Neuroscience* **13**
359. Marlin, S. D., and Rothlein, R. (1998) Intercellular Adhesion Molecules: ICAM-1, ICAM-2 And ICAM-3. In *Encyclopedia of Immunology (Second Edition)* (Delves, P. J., ed) pp. 1409-1412, Elsevier, Oxford
360. Frohman, E. M., Frohman, T. C., Gupta, S., de Fougerolles, A., and van den Noort, S. (1991) Expression of intercellular adhesion molecule 1 (ICAM-1) in Alzheimer's disease. *J Neurol Sci* **106**, 105-111
361. Faria, M. C., Gonçalves, G. S., Rocha, N. P., Moraes, E. N., Bicalho, M. A., Gualberto Cintra, M. T., Jardim de Paula, J., José Ravic de Miranda, L. F., Clayton de Souza Ferreira, A., Teixeira, A. L., Gomes, K. B., Carvalho, M. d. G., and Sousa, L. P. (2014) Increased plasma levels of BDNF and inflammatory markers in Alzheimer's disease. *Journal of Psychiatric Research* **53**, 166-172
362. Angelucci, F., Spalletta, G., di Iulio, F., Ciaramella, A., Salani, F., Colantoni, L., Varsi, A. E., Gianni, W., Sancesario, G., Caltagirone, C., and Bossù, P. (2009) P2-037: Alzheimer's disease (ad) and mild cognitive impairment (mci) patients are characterized by increased bdnf serum levels. *Alzheimer's & Dementia* **5**, P272-P273
363. Laske, C., Stransky, E., Leyhe, T., Eschweiler, G. W., Wittorf, A., Richartz, E., Bartels, M., Buchkremer, G., and Schott, K. (2006) Stage-dependent BDNF serum concentrations in Alzheimer's disease. *Journal of neural transmission (Vienna, Austria : 1996)* **113**, 1217-1224
364. Wennström, M., and Nielsen, H. M. (2012) Cell adhesion molecules in Alzheimer's disease. *Degenerative neurological and neuromuscular disease* **2**, 65-77
365. Takeda, K., Obinata, Y., Konishi, A., Kajiya, M., Matsuda, S., Mizuno, N., Sasaki, S., Fujita, T., and Kurihara, H. (2016) Brain-Derived Neurotrophic Factor Inhibits Intercellular Adhesion Molecule-1 Expression in Interleukin-1[beta]-Treated Endothelial Cells. *Cell Biochemistry and Biophysics* **74**, 399-406
366. Waller, R., Baxter, L., Fillingham, D. J., Coelho, S., Pozo, J. M., Mozumder, M., Frangi, A. F., Ince, P. G., Simpson, J. E., and Highley, J. R. (2019) Iba-1-/CD68+ microglia are a prominent feature of age-associated deep subcortical white matter lesions. *PLOS ONE* **14**, e0210888
367. Ito, D., Tanaka, K., Suzuki, S., Dembo, T., and Fukuuchi, Y. (2001) Enhanced expression of Iba1, ionized calcium-binding adapter molecule 1, after transient focal cerebral ischemia in rat brain. *Stroke* **32**, 1208-1215
368. Agostinho, P., Cunha, R. A., and Oliveira, C. (2010) Neuroinflammation, oxidative stress and the pathogenesis of Alzheimer's disease. *Curr Pharm Des* **16**, 2766-2778
369. Xie, J., Gorlé, N., Vandendriessche, C., Van Imschoot, G., Van Wonterghem, E., Van Cauwenberghe, C., Parthoens, E., Van Hamme, E., Lippens, S., Van Hoecke, L., and Vandenbroucke, R. E. (2021) Low-grade peripheral inflammation affects brain pathology in the AppNL-G-Fmouse model of Alzheimer's disease. *Acta Neuropathologica Communications* **9**, 163
370. Liu, T., Zhang, L., Joo, D., and Sun, S.-C. (2017) NF-κB signaling in inflammation. *Signal Transduction and Targeted Therapy* **2**, 17023
371. Du, Y., Du, Y., Zhang, Y., Huang, Z., Fu, M., Li, J., Pang, Y., Lei, P., Wang, Y. T., Song, W., He, G., and Dong, Z. (2019) MKP-1 reduces Aβ generation and alleviates cognitive

impairments in Alzheimer's disease models. *Signal Transduction and Targeted Therapy* **4**, 58
372. Jones, S. V., and Kounatidis, I. (2017) Nuclear Factor-Kappa B and Alzheimer Disease, Unifying Genetic and Environmental Risk Factors from Cell to Humans. *Frontiers in immunology* **8**, 1805-1805
373. Rajapakse, N. W., and Mattson, D. L. (2009) Role of L-arginine in nitric oxide production in health and hypertension. *Clin Exp Pharmacol Physiol* **36**, 249-255
374. Mander, P., and Brown, G. C. (2004) Nitric oxide, hypoxia and brain inflammation. *Biochem Soc Trans* **32**, 1068-1069
375. Hickey, M. K., Miller, N. C., Haapala, J., Demerath, E. W., Pfister, K. M., Georgieff, M. K., and Gale, C. A. (2021) Infants exposed to antibiotics after birth have altered recognition memory responses at one month of age. *Pediatr Res* **89**, 1500-1507
376. Jiang, H., Jiang, Q., and Feng, J. (2004) Parkin increases dopamine uptake by enhancing the cell surface expression of dopamine transporter. *J Biol Chem* **279**, 54380-54386
377. Nogawa, S., Forster, C., Zhang, F., Nagayama, M., Ross, M. E., and Iadecola, C. (1998) Interaction between inducible nitric oxide synthase and cyclooxygenase-2 after cerebral ischemia. *Proceedings of the National Academy of Sciences* **95**, 10966-10971
378. Nathan, C., and Xie, Q. W. (1994) Regulation of biosynthesis of nitric oxide. *Journal of Biological Chemistry* **269**, 13725-13728
379. Kaltschmidt, B., Linker, R. A., Deng, J., and Kaltschmidt, C. (2002) Cyclooxygenase-2 is a neuronal target gene of NF-κB. *BMC Molecular Biology* **3**, 16
380. Dahle, J. T., and Arai, Y. (2015) Environmental geochemistry of cerium: applications and toxicology of cerium oxide nanoparticles. *International journal of environmental research and public health* **12**, 1253-1278
381. Kuchibhatla, S. V. N. T., Karakoti, A. S., Vasdekis, A. E., Windisch, C. F., Jr., Seal, S., Thevuthasan, S., and Baer, D. R. (2019) An unexpected phase transformation of ceria nanoparticles in aqueous media. *Journal of materials research* **34**, 465-473
382. Krenzke, P. T., and Davidson, J. H. (2015) On the Efficiency of Solar H2 and CO Production via the Thermochemical Cerium Oxide Redox Cycle: The Option of Inert-Swept Reduction. *Energy & Fuels* **29**, 1045-1054
383. Lashtabeg, A., and Skinner, S. J. (2006) Solid oxide fuel cells—a challenge for materials chemists? *Journal of Materials Chemistry* **16**, 3161-3170
384. Corma, A., Atienzar, P., García, H., and Chane-Ching, J. Y. (2004) Hierarchically mesostructured doped CeO2 with potential for solar-cell use. *Nat Mater* **3**, 394-397
385. Rui, Y., Zhang, P., Zhang, Y., Ma, Y., He, X., Gui, X., Li, Y., Zhang, J., Zheng, L., Chu, S., Guo, Z., Chai, Z., Zhao, Y., and Zhang, Z. (2015) Transformation of ceria nanoparticles in cucumber plants is influenced by phosphate. *Environmental Pollution* **198**, 8-14
386. Karakoti, A. S., Kuchibhatla, S. V. N. T., Babu, K. S., and Seal, S. (2007) Direct Synthesis of Nanoceria in Aqueous Polyhydroxyl Solutions. *The Journal of Physical Chemistry C* **111**, 17232-17240
387. Murray, E. P., Tsai, T., and Barnett, S. A. (1999) A direct-methane fuel cell with a ceria-based anode. *Nature* **400**, 649
388. Dhall, A., and Self, W. (2018) Cerium Oxide Nanoparticles: A Brief Review of Their Synthesis Methods and Biomedical Applications. *Antioxidants (Basel, Switzerland)* **7**, 97
389. Pourkhalili, N., Hosseini, A., Nili-Ahmadabadi, A., Hassani, S., Pakzad, M., Baeeri, M., Mohammadirad, A., and Abdollahi, M. (2011) Biochemical and cellular evidence of the

benefit of a combination of cerium oxide nanoparticles and selenium to diabetic rats. *World J Diabetes* **2**, 204-210
390. Pešić, M., Podolski-Renić, A., Stojković, S., Matović, B., Zmejkoski, D., Kojić, V., Bogdanović, G., Pavićević, A., Mojović, M., Savić, A., Milenković, I., Kalauzi, A., and Radotić, K. (2015) Anti-cancer effects of cerium oxide nanoparticles and its intracellular redox activity. *Chem Biol Interact* **232**, 85-93
391. Reichel, M. P. W., L.C.; Ellis, J.T. (2020) Research into Neospora caninum—What Have We Learnt in the Last Thirty Years? *Pathogens* **9**, 17
392. Eguchi, K., Setoguchi, T., Inoue, T., and Arai, H. (1992) Electrical properties of ceria-based oxides and their application to solid oxide fuel cells. *Solid State Ionics* **52**, 165-172
393. Conesa, J. (1995) Computer modeling of surfaces and defects on cerium dioxide. *Surface Science* **339**, 337-352
394. Trovarelli, A. (1996) Catalytic Properties of Ceria and CeO2-Containing Materials. *Catalysis Reviews* **38**, 439-520
395. Yashima, M., Arashi, H., Kakihana, M., and Yoshimura, M. (1994) Raman Scattering Study of Cubic–Tetragonal Phase Transition in Zr1−xCexO2 Solid Solution. *Journal of the American Ceramic Society* **77**, 1067-1071
396. Malhotra, B. D., and Ali, M. A. (2018) Chapter 5 - Nanocomposite Materials: Biomolecular Devices. In *Nanomaterials for Biosensors* (Malhotra, B. D., and Ali, M. A., eds) pp. 145-159, William Andrew Publishing
397. El Morabet, R. (2019) Effects of Outdoor Air Pollution on Human Health. In *Encyclopedia of Environmental Health (Second Edition)* (Nriagu, J., ed) pp. 278-286, Elsevier, Oxford
398. Kharton, V. V., Figueiredo, F. M., Navarro, L., Naumovich, E. N., Kovalevsky, A. V., Yaremchenko, A. A., Viskup, A. P., Carneiro, A., Marques, F. M. B., and Frade, J. R. (2001) Ceria-based materials for solid oxide fuel cells. *Journal of Materials Science* **36**, 1105-1117
399. Campbell, C. T., and Peden, C. H. F. (2005) Oxygen Vacancies and Catalysis on Ceria Surfaces. *Science* **309**, 713
400. Steele, B. C. H. (2000) Appraisal of Ce1−yGdyO2−y/2 electrolytes for IT-SOFC operation at 500°C. *Solid State Ionics* **129**, 95-110
401. Li, Y., Fu, Q., and Flytzani-Stephanopoulos, M. (2000) Low-temperature water-gas shift reaction over Cu- and Ni-loaded cerium oxide catalysts. *Applied Catalysis B: Environmental* **27**, 179-191
402. Hori, C. E., Permana, H., Ng, K. Y. S., Brenner, A., More, K., Rahmoeller, K. M., and Belton, D. (1998) Thermal stability of oxygen storage properties in a mixed CeO2-ZrO2 system. *Applied Catalysis B: Environmental* **16**, 105-117
403. Zaki, M. I., Hasan, M. A., Al-Sagheer, F. A., and Pasupulety, L. (2001) In situ FTIR spectra of pyridine adsorbed on SiO2–Al2O3, TiO2, ZrO2 and CeO2: general considerations for the identification of acid sites on surfaces of finely divided metal oxides. *Colloids and Surfaces A: Physicochemical and Engineering Aspects* **190**, 261-274
404. Trovarelli, A., de Leitenburg, C., Boaro, M., and Dolcetti, G. (1999) The utilization of ceria in industrial catalysis. *Catalysis Today* **50**, 353-367
405. Tuller, H. L. (2000) Ionic conduction in nanocrystalline materials. *Solid State Ionics* **131**, 143-157

406. Abad, A., Concepción, P., Corma, A., and García, H. (2005) A collaborative effect between gold and a support induces the selective oxidation of alcohols. *Angew Chem Int Ed Engl* **44**, 4066-4069
407. Kundakovic, L., and Flytzani-Stephanopoulos, M. (1998) Reduction characteristics of copper oxide in cerium and zirconium oxide systems. *Applied Catalysis A: General* **171**, 13-29
408. Wang, S., and Lu, G. Q. (1998) Role of CeO2 in Ni/CeO2–Al2O3 catalysts for carbon dioxide reforming of methane. *Applied Catalysis B: Environmental* **19**, 267-277
409. Hilaire, S., Wang, X., Luo, T., Gorte, R. J., and Wagner, J. (2001) A comparative study of water-gas-shift reaction over ceria supported metallic catalysts. *Applied Catalysis A: General* **215**, 271-278
410. Fu, Q., Weber, A., and Flytzani-Stephanopoulos, M. (2001) Nanostructured Au–CeO2 Catalysts for Low-Temperature Water–Gas Shift. *Catalysis Letters* **77**, 87-95
411. Rosenzweig, A. C. (2015) Biochemistry: Breaking methane. *Nature* **518**, 309-310
412. Ta, N., Liu, J., Chenna, S., Crozier, P. A., Li, Y., Chen, A., and Shen, W. (2012) Stabilized Gold Nanoparticles on Ceria Nanorods by Strong Interfacial Anchoring. *Journal of the American Chemical Society* **134**, 20585-20588
413. Han, Z.-K., Zhang, L., Liu, M., Ganduglia-Pirovano, M. V., and Gao, Y. (2019) The Structure of Oxygen Vacancies in the Near-Surface of Reduced CeO2 (111) Under Strain. *Frontiers in Chemistry* **7**
414. Mai, H. X., Sun, L. D., Zhang, Y. W., Si, R., Feng, W., Zhang, H. P., Liu, H. C., and Yan, C. H. (2005) Shape-selective synthesis and oxygen storage behavior of ceria nanopolyhedra, nanorods, and nanocubes. *J Phys Chem B* **109**, 24380-24385
415. Skorodumova, N. V., Simak, S. I., Lundqvist, B. I., Abrikosov, I. A., and Johansson, B. (2002) Quantum origin of the oxygen storage capability of ceria. *Phys Rev Lett* **89**, 166601
416. Zhou, K., Wang, X., Sun, X., Peng, Q., and Li, Y. (2005) Enhanced catalytic activity of ceria nanorods from well-defined reactive crystal planes. *Journal of Catalysis* **229**, 206-212
417. Limbach, L. K., Li, Y., Grass, R. N., Brunner, T. J., Hintermann, M. A., Muller, M., Gunther, D., and Stark, W. J. (2005) Oxide nanoparticle uptake in human lung fibroblasts: effects of particle size, agglomeration, and diffusion at low concentrations. *Environ Sci Technol* **39**, 9370-9376
418. Tarnuzzer, R. W., Colon, J., Patil, S., and Seal, S. (2005) Vacancy engineered ceria nanostructures for protection from radiation-induced cellular damage. *Nano Lett* **5**, 2573-2577
419. Chen, D., Ran, R., Zhang, K., Wang, J., and Shao, Z. (2009) Intermediate-temperature electrochemical performance of a polycrystalline PrBaCo2O5+δ cathode on samarium-doped ceria electrolyte. *Journal of Power Sources* **188**, 96-105
420. Sharma, S., and Pollet, B. G. (2012) Support materials for PEMFC and DMFC electrocatalysts—A review. *Journal of Power Sources* **208**, 96-119
421. Andersson, D. A., Simak, S. I., Skorodumova, N. V., Abrikosov, I. A., and Johansson, B. (2006) Optimization of ionic conductivity in doped ceria. *Proceedings of the National Academy of Sciences of the United States of America* **103**, 3518-3521
422. Chuayboon, S., Abanades, S., and Rodat, S. (2019) Syngas production via solar-driven chemical looping methane reforming from redox cycling of ceria porous foam in a volumetric solar reactor. *Chemical Engineering Journal* **356**, 756-770

423. Bruix, A., Rodriguez, J. A., Ramírez, P. J., Senanayake, S. D., Evans, J., Park, J. B., Stacchiola, D., Liu, P., Hrbek, J., and Illas, F. (2012) A new type of strong metal-support interaction and the production of H2 through the transformation of water on Pt/CeO2(111) and Pt/CeO(x)/TiO2(110) catalysts. *J Am Chem Soc* **134**, 8968-8974
424. Ratnasamy, C., and Wagner, J. P. (2009) Water Gas Shift Catalysis. *Catalysis Reviews* **51**, 325-440
425. Farmer, J. A., and Campbell, C. T. (2010) Ceria Maintains Smaller Metal Catalyst Particles by Strong Metal-Support Bonding. *Science* **329**, 933
426. Wang, X., Rodriguez, J. A., Hanson, J. C., Gamarra, D., Martínez-Arias, A., and Fernández-García, M. (2006) In Situ Studies of the Active Sites for the Water Gas Shift Reaction over Cu−CeO2 Catalysts: Complex Interaction between Metallic Copper and Oxygen Vacancies of Ceria. *The Journal of Physical Chemistry B* **110**, 428-434
427. Sharma, S., Hu, Z., Zhang, P., McFarland, E. W., and Metiu, H. (2011) CO2 methanation on Ru-doped ceria. *Journal of Catalysis* **278**, 297-309
428. Wu, Z., Jin, R., Wang, H., and Liu, Y. (2009) Effect of ceria doping on SO2 resistance of Mn/TiO2 for selective catalytic reduction of NO with NH3 at low temperature. *Catalysis Communications* **10**, 935-939
429. Roy, T., Sahani, S., and Chandra Sharma, Y. (2020) Study on kinetics-thermodynamics and environmental parameter of biodiesel production from waste cooking oil and castor oil using potassium modified ceria oxide catalyst. *Journal of Cleaner Production* **247**, 119166
430. Shapovalov, V., and Metiu, H. (2007) Catalysis by doped oxides: CO oxidation by AuxCe1−xO2. *Journal of Catalysis* **245**, 205-214
431. Camellone, M. F., and Fabris, S. (2009) Reaction Mechanisms for the CO Oxidation on Au/CeO2 Catalysts: Activity of Substitutional Au3+/Au+ Cations and Deactivation of Supported Au+ Adatoms. *Journal of the American Chemical Society* **131**, 10473-10483
432. Aneggi, E., Boaro, M., Leitenburg, C. d., Dolcetti, G., and Trovarelli, A. (2006) Insights into the redox properties of ceria-based oxides and their implications in catalysis. *Journal of Alloys and Compounds* **408-412**, 1096-1102
433. Vivier, L., and Duprez, D. (2010) Ceria-based solid catalysts for organic chemistry. *ChemSusChem* **3**, 654-678
434. Tana, Zhang, M., Li, J., Li, H., Li, Y., and Shen, W. (2009) Morphology-dependent redox and catalytic properties of CeO2 nanostructures: Nanowires, nanorods and nanoparticles. *Catalysis Today* **148**, 179-183
435. Gorte, R. J. (2010) Ceria in catalysis: From automotive applications to the water–gas shift reaction. *AIChE Journal* **56**, 1126-1135
436. Zhong, L.-S., Hu, J.-S., Cao, A.-M., Liu, Q., Song, W.-G., and Wan, L.-J. (2007) 3D Flowerlike Ceria Micro/Nanocomposite Structure and Its Application for Water Treatment and CO Removal. *Chemistry of Materials* **19**, 1648-1655
437. Lanone, S., Rogerieux, F., Geys, J., Dupont, A., Maillot-Marechal, E., Boczkowski, J., Lacroix, G., and Hoet, P. (2009) Comparative toxicity of 24 manufactured nanoparticles in human alveolar epithelial and macrophage cell lines. *Particle and fibre toxicology* **6**, 14-14
438. Lykaki, M., Pachatouridou, E., Carabineiro, S. A. C., Iliopoulou, E., Andriopoulou, C., Kallithrakas-Kontos, N., Boghosian, S., and Konsolakis, M. (2018) Ceria nanoparticles shape effects on the structural defects and surface chemistry: Implications in CO oxidation by Cu/CeO2 catalysts. *Applied Catalysis B: Environmental* **230**, 18-28

439. Pagliari, F., Mandoli, C., Forte, G., Magnani, E., Pagliari, S., Nardone, G., Licoccia, S., Minieri, M., Di Nardo, P., and Traversa, E. (2012) Cerium Oxide Nanoparticles Protect Cardiac Progenitor Cells from Oxidative Stress. *ACS Nano* **6**, 3767-3775
440. Ornatska, M., Sharpe, E., Andreescu, D., and Andreescu, S. (2011) Paper Bioassay Based on Ceria Nanoparticles as Colorimetric Probes. *Analytical Chemistry* **83**, 4273-4280
441. Das, M., Patil, S., Bhargava, N., Kang, J.-F., Riedel, L. M., Seal, S., and Hickman, J. J. (2007) Auto-catalytic ceria nanoparticles offer neuroprotection to adult rat spinal cord neurons. *Biomaterials* **28**, 1918-1925
442. Korsvik, C., Patil, S., Seal, S., and Self, W. T. (2007) Superoxide dismutase mimetic properties exhibited by vacancy engineered ceria nanoparticles. *Chem Commun (Camb)*, 1056-1058
443. Carofiglio, M., Barui, S., Cauda, V., and Laurenti, M. (2020) Doped Zinc Oxide Nanoparticles: Synthesis, Characterization and Potential Use in Nanomedicine. *Applied Sciences* **10**, 5194
444. Asati, A., Santra, S., Kaittanis, C., and Perez, J. M. (2010) Surface-Charge-Dependent Cell Localization and Cytotoxicity of Cerium Oxide Nanoparticles. *ACS Nano* **4**, 5321-5331
445. Asati, A., Santra, S., Kaittanis, C., Nath, S., and Perez, J. M. (2009) Oxidase-like activity of polymer-coated cerium oxide nanoparticles. *Angew Chem Int Ed Engl* **48**, 2308-2312
446. Kim, C. K., Kim, T., Choi, I.-Y., Soh, M., Kim, D., Kim, Y.-J., Jang, H., Yang, H.-S., Kim, J. Y., Park, H.-K., Park, S. P., Park, S., Yu, T., Yoon, B.-W., Lee, S.-H., and Hyeon, T. (2012) Ceria Nanoparticles that can Protect against Ischemic Stroke. *Angewandte Chemie International Edition* **51**, 11039-11043
447. Li, Y., He, X., Yin, J.-J., Ma, Y., Zhang, P., Li, J., Ding, Y., Zhang, J., Zhao, Y., Chai, Z., and Zhang, Z. (2015) Acquired Superoxide-Scavenging Ability of Ceria Nanoparticles. *Angewandte Chemie International Edition* **54**, 1832-1835
448. Schubert, D., Dargusch, R., Raitano, J., and Chan, S. W. (2006) Cerium and yttrium oxide nanoparticles are neuroprotective. *Biochem Biophys Res Commun* **342**, 86-91
449. Park, E.-J., Choi, J., Park, Y.-K., and Park, K. (2008) Oxidative stress induced by cerium oxide nanoparticles in cultured BEAS-2B cells. *Toxicology* **245**, 90-100
450. Zhang, P., Ma, Y., Zhang, Z., He, X., Zhang, J., Guo, Z., Tai, R., Zhao, Y., and Chai, Z. (2012) Biotransformation of Ceria Nanoparticles in Cucumber Plants. *ACS Nano* **6**, 9943-9950
451. Ali, D., Alarifi, S., Alkahtani, S., AlKahtane, A. A., and Almalik, A. (2015) Cerium Oxide Nanoparticles Induce Oxidative Stress and Genotoxicity in Human Skin Melanoma Cells. *Cell Biochem Biophys* **71**, 1643-1651
452. Kunwar, D., Zhou, S., DeLaRiva, A., Peterson, E. J., Xiong, H., Pereira-Hernández, X. I., Purdy, S. C., ter Veen, R., Brongersma, H. H., Miller, J. T., Hashiguchi, H., Kovarik, L., Lin, S., Guo, H., Wang, Y., and Datye, A. K. (2019) Stabilizing High Metal Loadings of Thermally Stable Platinum Single Atoms on an Industrial Catalyst Support. *ACS Catalysis* **9**, 3978-3990
453. Pastor-Pérez, L., Patel, V., Le Saché, E., and Reina, T. R. (2020) CO2 methanation in the presence of methane: Catalysts design and effect of methane concentration in the reaction mixture. *Journal of the Energy Institute* **93**, 415-424

454. Ding, Y., Wu, Q., Lin, B., Guo, Y., Guo, Y., Wang, Y., Wang, L., and Zhan, W. (2020) Superior catalytic activity of a Pd catalyst in methane combustion by fine-tuning the phase of ceria-zirconia support. *Applied Catalysis B: Environmental* **266**, 118631
455. Maria Magdalane, C., Kaviyarasu, K., Matinise, N., Mayedwa, N., Mongwaketsi, N., Letsholathebe, D., Mola, G. T., AbdullahAl-Dhabi, N., Arasu, M. V., Henini, M., Kennedy, J., Maaza, M., and Jeyaraj, B. (2018) Evaluation on La2O3 garlanded ceria heterostructured binary metal oxide nanoplates for UV/ visible light induced removal of organic dye from urban wastewater. *South African Journal of Chemical Engineering* **26**, 49-60
456. Jones, J., Xiong, H., DeLaRiva, A. T., Peterson, E. J., Pham, H., Challa, S. R., Qi, G., Oh, S., Wiebenga, M. H., Pereira Hernández, X. I., Wang, Y., and Datye, A. K. (2016) Thermally stable single-atom platinum-on-ceria catalysts via atom trapping. *Science* **353**, 150-154
457. Das, S., Ashok, J., Bian, Z., Dewangan, N., Wai, M. H., Du, Y., Borgna, A., Hidajat, K., and Kawi, S. (2018) Silica–Ceria sandwiched Ni core–shell catalyst for low temperature dry reforming of biogas: Coke resistance and mechanistic insights. *Applied Catalysis B: Environmental* **230**, 220-236
458. Liu, Q., Yang, Y., Lv, X., Ding, Y., Zhang, Y., Jing, J., and Xu, C. (2017) One-step synthesis of uniform nanoparticles of porphyrin functionalized ceria with promising peroxidase mimetics for H2O2 and glucose colorimetric detection. *Sensors and Actuators B: Chemical* **240**, 726-734
459. Sun, L., Ding, Y., Jiang, Y., and Liu, Q. (2017) Montmorillonite-loaded ceria nanocomposites with superior peroxidase-like activity for rapid colorimetric detection of H2O2. *Sensors and Actuators B: Chemical* **239**, 848-856
460. Atif, M., Iqbal, S., Fakhar-E-Alam, M., Ismail, M., Mansoor, Q., Mughal, L., Aziz, M. H., Hanif, A., and Farooq, W. A. (2019) Manganese-Doped Cerium Oxide Nanocomposite Induced Photodynamic Therapy in MCF-7 Cancer Cells and Antibacterial Activity. *BioMed Research International* **2019**, 7156828
461. Yu, H., Jin, F., Liu, D., Shu, G., Wang, X., Qi, J., Sun, M., Yang, P., Jiang, S., Ying, X., and Du, Y. (2020) ROS-responsive nano-drug delivery system combining mitochondria-targeting ceria nanoparticles with atorvastatin for acute kidney injury. *Theranostics* **10**, 2342-2357
462. He, L., Huang, G., Liu, H., Sang, C., Liu, X., and Chen, T. (2020) Highly bioactive zeolitic imidazolate framework-8–capped nanotherapeutics for efficient reversal of reperfusion-induced injury in ischemic stroke. *Science Advances* **6**, eaay9751
463. Kwon, H. J., Cha, M.-Y., Kim, D., Kim, D. K., Soh, M., Shin, K., Hyeon, T., and Mook-Jung, I. (2016) Mitochondria-Targeting Ceria Nanoparticles as Antioxidants for Alzheimer's Disease. *ACS Nano* **10**, 2860-2870
464. Ebrahimi, P., Kumar, A., and Khraisheh, M. (2020) A review of recent advances in water-gas shift catalysis for hydrogen production. *Emergent Materials* **3**, 881-917
465. Crabtree, G. W., and Dresselhaus, M. S. (2008) The Hydrogen Fuel Alternative. *MRS Bulletin* **33**, 421-428
466. Nyoka, M., Choonara, Y. E., Kumar, P., Kondiah, P. P. D., and Pillay, V. (2020) Synthesis of Cerium Oxide Nanoparticles Using Various Methods: Implications for Biomedical Applications. *Nanomaterials* **10**, 242
467. Li, M., Liu, Z., Hu, Y., Wang, M., and Li, H. (2008) Effect of doping elements on catalytic performance of CeO2-ZrO2 solid solutions. *Journal of Rare Earths* **26**, 357-361

468. Mousavi-Kamazani, M., and Azizi, F. (2019) Facile sonochemical synthesis of Cu doped CeO2 nanostructures as a novel dual-functional photocatalytic adsorbent. *Ultrasonics Sonochemistry* **58**, 104695
469. Mužina, K., Kurajica, S., Dražić, G., Guggenberger, P., and Matijašić, G. (2021) True doping levels in hydrothermally derived copper-doped ceria. *Journal of Nanoparticle Research* **23**, 149
470. Sharma, P. K., and Pandey, O. P. (2022) Enhanced photocatalytic activity with metal ion doping and co-doping in CeO2 nanoparticles. *Solid State Sciences* **126**, 106846
471. Walkey, C., Das, S., Seal, S., Erlichman, J., Heckman, K., Ghibelli, L., Traversa, E., McGinnis, J. F., and Self, W. T. (2015) Catalytic Properties and Biomedical Applications of Cerium Oxide Nanoparticles. *Environ Sci Nano* **2**, 33-53
472. Nourmohammadi, E., Khoshdel-sarkarizi, H., Nedaeinia, R., Darroudi, M., and Kazemi Oskuee, R. (2020) Cerium oxide nanoparticles: A promising tool for the treatment of fibrosarcoma in-vivo. *Materials Science and Engineering: C* **109**, 110533
473. Alpaslan, E., Yazici, H., H. Golshan, N., Ziemer, K., and Webster, T. (2015) Dextran Coated Cerium Oxide Nanoparticles For Inhibiting Bone Cancer Cell Functions. pp. 187-196
474. Valdeperez, D., Wang, T., Eußner, J. P., Weinert, B., Hao, J., Parak, W. J., Dehnen, S., and Pelaz, B. (2017) Polymer-coated nanoparticles: Carrier platforms for hydrophobic water- and air-sensitive metallo-organic compounds. *Pharmacological Research* **117**, 261-266
475. Bagheri, S., Khalil, M., and Muhd Julkapli, N. (2020) Cerium (IV) oxide nanocomposites: Catalytic properties and industrial application. *Journal of Rare Earths* **39**
476. Fu, Q., Deng, W., Saltsburg, H., and Flytzani-Stephanopoulos, M. (2005) Activity and stability of low-content gold–cerium oxide catalysts for the water–gas shift reaction. *Applied Catalysis B: Environmental* **56**, 57-68
477. Alpaslan, E., Yazici, H., Golshan, N. H., Ziemer, K. S., and Webster, T. J. (2015) pH-Dependent Activity of Dextran-Coated Cerium Oxide Nanoparticles on Prohibiting Osteosarcoma Cell Proliferation. *ACS Biomaterials Science & Engineering* **1**, 1096-1103
478. Datta, A., Mishra, S., Manna, K., Saha, K. D., Mukherjee, S., and Roy, S. (2020) Pro-Oxidant Therapeutic Activities of Cerium Oxide Nanoparticles in Colorectal Carcinoma Cells. *ACS Omega* **5**, 9714-9723
479. Alpaslan, E., Geilich, B. M., Yazici, H., and Webster, T. J. (2017) pH-Controlled Cerium Oxide Nanoparticle Inhibition of Both Gram-Positive and Gram-Negative Bacteria Growth. *Scientific Reports* **7**, 45859
480. Chelombitko, M. A. (2018) Role of Reactive Oxygen Species in Inflammation: A Minireview. *Moscow University Biological Sciences Bulletin* **73**, 199-202
481. Dewberry, L. K., Zgheib, C., Hilton, S. A., Seal, S., Newsom, J., Krebs, M. D., Hu, J., Xu, J., and Liechty, K. W. (2019) Cerium Oxide Nanoparticle-miR146a Decreases Inflammation in a Murine Dextran Sodium Sulfate Colitis Model. *Journal of the American College of Surgeons* **229**, S91
482. Chai, W. F., and Tang, K. S. (2021) Protective potential of cerium oxide nanoparticles in diabetes mellitus. *J Trace Elem Med Biol* **66**, 126742
483. Wei, F., Neal, C. J., Sakthivel, T. S., Kean, T., Seal, S., and Coathup, M. J. (2021) Multi-functional cerium oxide nanoparticles regulate inflammation and enhance osteogenesis. *Materials Science and Engineering: C* **124**, 112041

484. Jan, A., Shin, J., Ahn, J., Yang, S., Yoon, K. J., Son, J.-W., Kim, H., Lee, J.-H., and Ji, H.-I. (2019) Promotion of Pt/CeO2 catalyst by hydrogen treatment for low-temperature CO oxidation. *RSC Advances* **9**, 27002-27012
485. Muravev, V., Spezzati, G., Su, Y.-Q., Parastaev, A., Chiang, F.-K., Longo, A., Escudero, C., Kosinov, N., and Hensen, E. J. M. (2021) Interface dynamics of Pd–CeO2 single-atom catalysts during CO oxidation. *Nature Catalysis* **4**, 469-478
486. Sack, Z., Bader, and Brenneisen, P. (2017) Cerium Oxide Nanoparticles as Novel Tool in Glioma Treatment: An In vitro Study. *Journal of Nanomedicine & Nanotechnology* **8**
487. Naz, S., Beach, J., Heckert, B., Tummala, T., Pashchenko, O., Banerjee, T., and Santra, S. (2017) Cerium oxide nanoparticles: a 'radical' approach to neurodegenerative disease treatment. *Nanomedicine* **12**, 545-553
488. Ali, D., Alarifi, S., Alkahtani, S., AlKahtane, A. A., and Almalik, A. (2015) Cerium Oxide Nanoparticles Induce Oxidative Stress and Genotoxicity in Human Skin Melanoma Cells. *Cell Biochemistry and Biophysics* **71**, 1643-1651
489. Gunawan, C., Lord, M. S., Lovell, E., Wong, R. J., Jung, M. S., Oscar, D., Mann, R., and Amal, R. (2019) Oxygen-Vacancy Engineering of Cerium-Oxide Nanoparticles for Antioxidant Activity. *ACS Omega* **4**, 9473-9479
490. Gella, A., and Durany, N. (2009) Oxidative stress in Alzheimer disease. *Cell adhesion & migration* **3**, 88-93
491. Heneka, M. T., Carson, M. J., El Khoury, J., Landreth, G. E., Brosseron, F., Feinstein, D. L., Jacobs, A. H., Wyss-Coray, T., Vitorica, J., and Ransohoff, R. M. (2015) Neuroinflammation in Alzheimer's disease. *The Lancet Neurology* **14**, 388-405
492. D'Angelo, B., Santucci, S., Benedetti, E., Di Loreto, S., Phani, A., Falone, S., Amicarelli, F., Cerù, M., and Cimini, A. (2009) Cerium Oxide Nanoparticles Trigger Neuronal Survival in a Human Alzheimer Disease Model By Modulating BDNF Pathway. *Current Nanoscience* **5**, 167-176
493. Siposova, K., Huntosova, V., Shlapa, Y., Lenkavska, L., Macajova, M., Belous, A., and Musatov, A. (2019) Advances in the Study of Cerium Oxide Nanoparticles: New Insights into Antiamyloidogenic Activity. *ACS Applied Bio Materials* **2**, 1884-1896
494. Kumari, M., Singh, S. P., Chinde, S., Rahman, M. F., Mahboob, M., and Grover, P. (2014) Toxicity Study of Cerium Oxide Nanoparticles in Human Neuroblastoma Cells. *International Journal of Toxicology* **33**, 86-97
495. Niu, J., Azfer, A., Rogers, L. M., Wang, X., and Kolattukudy, P. E. (2007) Cardioprotective effects of cerium oxide nanoparticles in a transgenic murine model of cardiomyopathy. *Cardiovasc Res* **73**, 549-559
496. Wong, W. (2020) Economic burden of Alzheimer disease and managed care considerations. *Am J Manag Care* **26**, S177-s183
497. Tini, G., Scagliola, R., Monacelli, F., La Malfa, G., Porto, I., Brunelli, C., and Rosa, G. M. (2020) Alzheimer's Disease and Cardiovascular Disease: A Particular Association. *Cardiology research and practice* **2020**, 2617970-2617970
498. Juginović, A., Vuković, M., Aranza, I., and Biloš, V. (2021) Health impacts of air pollution exposure from 1990 to 2019 in 43 European countries. *Scientific Reports* **11**, 22516
499. Hullmann, M., Albrecht, C., Berlo, D., Gerlofs-Nijland, M., Wahle, T., Boots, A., Krutmann, J., Cassee, F., Bayer, T., and Schins, R. (2017) Diesel engine exhaust accelerates plaque formation in a mouse model of Alzheimer's disease. *Particle and Fibre Toxicology* **14**, 35

500. Ajmani, G. S., Suh, H. H., and Pinto, J. M. (2016) Effects of Ambient Air Pollution Exposure on Olfaction: A Review. *Environmental health perspectives* **124**, 1683-1693
501. Elder, A., Gelein, R., Silva, V., Feikert, T., Opanashuk, L., Carter, J., Potter, R., Maynard, A., Ito, Y., Finkelstein, J., and Oberdörster, G. (2006) Translocation of inhaled ultrafine manganese oxide particles to the central nervous system. *Environ Health Perspect* **114**, 1172-1178
502. Haghani, A., Johnson, R., Safi, N., Zhang, H., Thorwald, M., Mousavi, A., Woodward, N. C., Shirmohammadi, F., Coussa, V., Wise, J. P., Forman, H. J., Sioutas, C., Allayee, H., Morgan, T. E., and Finch, C. E. (2020) Toxicity of urban air pollution particulate matter in developing and adult mouse brain: Comparison of total and filter-eluted nanoparticles. *Environment International* **136**, 105510
503. Aragon, M. J., Topper, L., Tyler, C. R., Sanchez, B., Zychowski, K., Young, T., Herbert, G., Hall, P., Erdely, A., Eye, T., Bishop, L., Saunders, S. A., Muldoon, P. P., Ottens, A. K., and Campen, M. J. (2017) Serum-borne bioactivity caused by pulmonary multiwalled carbon nanotubes induces neuroinflammation via blood–brain barrier impairment. *Proceedings of the National Academy of Sciences* **114**, E1968
504. Snezhkina, A. V., Kudryavtseva, A. V., Kardymon, O. L., Savvateeva, M. V., Melnikova, N. V., Krasnov, G. S., and Dmitriev, A. A. (2019) ROS generation and antioxidant defense systems in normal and malignant cells. *Oxidative medicine and cellular longevity* **2019**
505. Salim, S. (2017) Oxidative Stress and the Central Nervous System. *The Journal of pharmacology and experimental therapeutics* **360**, 201-205
506. Serebrovska, Z., Swanson, R. J., Portnichenko, V., Shysh, A., Pavlovich, S., Tumanovska, L., Dorovskych, A., Lysenko, V., Tertykh, V., Bolbukh, Y., and Dosenko, V. (2017) Anti-inflammatory and antioxidant effect of cerium dioxide nanoparticles immobilized on the surface of silica nanoparticles in rat experimental pneumonia. *Biomedicine & Pharmacotherapy* **92**, 69-77
507. Corsi, F., Caputo, F., Traversa, E., and Ghibelli, L. (2018) Not Only Redox: The Multifaceted Activity of Cerium Oxide Nanoparticles in Cancer Prevention and Therapy. *Frontiers in oncology* **8**, 309-309
508. Wang, J., Luo, B., Li, X., Lu, W., Yang, J., Hu, Y., Huang, P., and Wen, S. (2017) Inhibition of cancer growth in vitro and in vivo by a novel ROS-modulating agent with ability to eliminate stem-like cancer cells. *Cell Death Dis* **8**, e2887
509. Rajeshkumar, S., and Naik, P. (2018) Synthesis and biomedical applications of Cerium oxide nanoparticles – A Review. *Biotechnology Reports* **17**, 1-5
510. Nanda, H. S. (2016) Surface modification of promising cerium oxide nanoparticles for nanomedicine applications. *RSC Advances* **6**, 111889-111894
511. El Morabet, R. (2018) Effects of Outdoor Air Pollution on Human Health. In *Reference Module in Earth Systems and Environmental Sciences*, Elsevier
512. Bellardita, M., Fiorenza, R., Palmisano, L., and Scirè, S. (2020) 4 - Photocatalytic and photothermocatalytic applications of cerium oxide-based materials. In *Cerium Oxide (CeO_2): Synthesis, Properties and Applications* (Scirè, S., and Palmisano, L., eds) pp. 109-167, Elsevier
513. Yang, H., Li, X., Wang, Y., Mu, M., Li, X., and Kou, G. (2016) Experimental investigation into the oxidation reactivity and nanostructure of particulate matter from diesel engine fuelled with diesel/polyoxymethylene dimethyl ethers blends. *Scientific Reports* **6**, 37611

514. Lighty, J. S., Veranth, J. M., and Sarofim, A. F. (2000) Combustion aerosols: factors governing their size and composition and implications to human health. *J Air Waste Manag Assoc* **50**, 1565-1618; discussion 1619-1522
515. Xicoy, H., Wieringa, B., and Martens, G. J. M. (2017) The SH-SY5Y cell line in Parkinson's disease research: a systematic review. *Molecular Neurodegeneration* **12**, 10
516. Wilcock, D. M. (2012) A Changing Perspective on the Role of Neuroinflammation in Alzheimer's Disease. *International Journal of Alzheimer’s Disease* **2012**, 495243
517. Calcerrada, P., Peluffo, G., and Radi, R. (2011) Nitric oxide-derived oxidants with a focus on peroxynitrite: molecular targets, cellular responses and therapeutic implications. *Curr Pharm Des* **17**, 3905-3932
518. Stephen Inbaraj, B., and Chen, B. H. (2020) An overview on recent in vivo biological application of cerium oxide nanoparticles. *Asian J Pharm Sci* **15**, 558-575
519. Li, H., Xia, P., Pan, S., Qi, Z., Fu, C., Yu, Z., Kong, W., Chang, Y., Wang, K., Wu, D., and Yang, X. (2020) The Advances of Ceria Nanoparticles for Biomedical Applications in Orthopaedics. *Int J Nanomedicine* **15**, 7199-7214
520. Pandur, E., Varga, E., Tamási, K., Pap, R., Nagy, J., and Sipos, K. (2018) Effect of Inflammatory Mediators Lipopolysaccharide and Lipoteichoic Acid on Iron Metabolism of Differentiated SH-SY5Y Cells Alters in the Presence of BV-2 Microglia. *Int J Mol Sci* **20**, 17
521. Dowding, J., Song, W., Bossy, K., Karakoti, A., Kumar, A., Kim, A., Bossy, B., Seal, S., Ellisman, M., Perkins, G., Self, W., and Bossy-Wetzel, E. (2014) Cerium oxide nanoparticles protect against Aβ-induced mitochondrial fragmentation and neuronal cell death. *Cell death and differentiation* **21**
522. Patel, P., Kansara, K., Singh, R., Shukla, R. K., Singh, S., Dhawan, A., and Kumar, A. (2018) Cellular internalization and antioxidant activity of cerium oxide nanoparticles in human monocytic leukemia cells. *International journal of nanomedicine* **13**, 39-41
523. Zhao, Y., Xu, Q., Xu, W., Wang, D., Tan, J., Zhu, C., and Tan, X. (2016) Probing the molecular mechanism of cerium oxide nanoparticles in protecting against the neuronal cytotoxicity of Aβ1–42 with copper ions†. *Metallomics* **8**, 644-647
524. Fischer, R., and Maier, O. (2015) Interrelation of oxidative stress and inflammation in neurodegenerative disease: role of TNF. *Oxidative medicine and cellular longevity* **2015**
525. Chen, L., Deng, H., Cui, H., Fang, J., Zuo, Z., Deng, J., Li, Y., Wang, X., and Zhao, L. (2017) Inflammatory responses and inflammation-associated diseases in organs. *Oncotarget* **9**, 7204-7218
526. Zarubin, T., and Han, J. (2005) Activation and signaling of the p38 MAP kinase pathway. *Cell Research* **15**, 11-18
527. Saha, R. N., Jana, M., and Pahan, K. (2007) MAPK p38 regulates transcriptional activity of NF-kappaB in primary human astrocytes via acetylation of p65. *Journal of immunology (Baltimore, Md. : 1950)* **179**, 7101-7109
528. Liu, T., Zhang, L., Joo, D., and Sun, S.-C. (2017) NF-κB signaling in inflammation. *Signal transduction and targeted therapy* **2**, 17023
529. Reber, L., Vermeulen, L., Haegeman, G., and Frossard, N. (2009) Ser276 Phosphorylation of NF-kB p65 by MSK1 Controls SCF Expression in Inflammation. *PLOS ONE* **4**, e4393

530. Selvaraj, V., Nepal, N., Rogers, S., Manne, N. D. P. K., Arvapalli, R., Rice, K. M., Asano, S., Fankenhanel, E., Ma, J. Y., Shokuhfar, T., Maheshwari, M., and Blough, E. R. (2015) Lipopolysaccharide induced MAP kinase activation in RAW 264.7 cells attenuated by cerium oxide nanoparticles. *Data in Brief* **4**, 96-99
531. Cheng, G., Guo, W., Han, L., Chen, E., Kong, L., Wang, L., Ai, W., Song, N., Li, H., and Chen, H. (2013) Cerium oxide nanoparticles induce cytotoxicity in human hepatoma SMMC-7721 cells via oxidative stress and the activation of MAPK signaling pathways. *Toxicol In Vitro* **27**, 1082-1088
532. Del Turco, S., Ciofani, G., Cappello, V., Navarra, T., Caselli, C., Gemmi, M., Mattoli, V., and Basta, G. (2013) Anti-inflammatory and antioxidant effects of cerium oxide nanoparticles in human endothelial cells. *European Heart Journal* **34**, P4174-P4174
533. Selvaraj, V., Manne, N., Arvapalli, R., Rice, K., Nandyala, G., Fankhanel, E., and Blough, E. (2015) Effect of cerium oxide nanoparticles on sepsis induced mortality and NF-B signaling in cultured macrophages. *Nanomedicine (London, England)* **10**, 1275-1288
534. Müller, N. (2019) The Role of Intercellular Adhesion Molecule-1 in the Pathogenesis of Psychiatric Disorders. *Frontiers in Pharmacology* **10**
535. van de Stolpe, A., and van der Saag, P. T. (1996) Intercellular adhesion molecule-1. *J Mol Med (Berl)* **74**, 13-33
536. Lockyer, J. M., Colladay, J. S., Alperin-Lea, W. L., Hammond, T., and Buda, A. J. (1998) Inhibition of nuclear factor-kappaB-mediated adhesion molecule expression in human endothelial cells. *Circ Res* **82**, 314-320
537. Gliga, A. R., Edoff, K., Caputo, F., Källman, T., Blom, H., Karlsson, H. L., Ghibelli, L., Traversa, E., Ceccatelli, S., and Fadeel, B. (2017) Cerium oxide nanoparticles inhibit differentiation of neural stem cells. *Scientific Reports* **7**, 9284
538. Chang, R., Knox, J., Chang, J., Derbedrossian, A., Vasilevko, V., Cribbs, D., Boado, R. J., Pardridge, W. M., and Sumbria, R. K. (2017) Blood–Brain Barrier Penetrating Biologic TNF-α Inhibitor for Alzheimer's Disease. *Molecular Pharmaceutics* **14**, 2340-2349
539. Tang, G., Yue, Z., Talloczy, Z., Hagemann, T., Cho, W., Messing, A., Sulzer, D. L., and Goldman, J. E. (2008) Autophagy induced by Alexander disease-mutant GFAP accumulation is regulated by p38/MAPK and mTOR signaling pathways. *Human Molecular Genetics* **17**, 1540-1555
540. Cimini, A., D'Angelo, B., Das, S., Gentile, R., Benedetti, E., Singh, V., Monaco, A. M., Santucci, S., and Seal, S. (2012) Antibody-conjugated PEGylated cerium oxide nanoparticles for specific targeting of Aβ aggregates modulate neuronal survival pathways. *Acta Biomaterialia* **8**, 2056-2067
541. Bathina, S., and Das, U. N. (2015) Brain-derived neurotrophic factor and its clinical implications. *Archives of medical science : AMS* **11**, 1164-1178
542. Bai, L., Zhang, S., Zhou, X., Li, Y., and Bai, J. (2019) Brain-derived neurotrophic factor induces thioredoxin-1 expression through TrkB/Akt/CREB pathway in SH-SY5Y cells. *Biochimie* **160**, 55-60
543. Yasutake, C., Kuroda, K., Yanagawa, T., Okamura, T., and Yoneda, H. (2006) Serum BDNF, TNF-α and IL-1β levels in dementia patients. *European Archives of Psychiatry and Clinical Neuroscience* **256**, 402-406
544. Phillips, H. S., Hains, J. M., Armanini, M., Laramee, G. R., Johnson, S. A., and Winslow, J. W. (1991) BDNF mRNA is decreased in the hippocampus of individuals with Alzheimer's disease. *Neuron* **7**, 695-702

545. Dowding, J. M., Song, W., Bossy, K., Karakoti, A., Kumar, A., Kim, A., Bossy, B., Seal, S., Ellisman, M. H., Perkins, G., Self, W. T., and Bossy-Wetzel, E. (2014) Cerium oxide nanoparticles protect against Aβ-induced mitochondrial fragmentation and neuronal cell death. *Cell Death Differ* **21**, 1622-1632
546. Hsieh, H. L., and Yang, C. M. (2013) Role of redox signaling in neuroinflammation and neurodegenerative diseases. *Biomed Res Int* **2013**, 484613
547. DiSabato, D. J., Quan, N., and Godbout, J. P. (2016) Neuroinflammation: the devil is in the details. *Journal of neurochemistry* **139 Suppl 2**, 136-153
548. Walker, K. A. (2018) Inflammation and neurodegeneration: chronicity matters. *Aging* **11**, 3-4
549. Ismail, R., Parbo, P., Madsen, L. S., Hansen, A. K., Hansen, K. V., Schaldemose, J. L., Kjeldsen, P. L., Stokholm, M. G., Gottrup, H., Eskildsen, S. F., and Brooks, D. J. (2020) The relationships between neuroinflammation, beta-amyloid and tau deposition in Alzheimer's disease: a longitudinal PET study. *Journal of Neuroinflammation* **17**, 151
550. Bellistri, E., Aguilar, J., Brotons-Mas, J. R., Foffani, G., and de la Prida, L. M. (2013) Basic properties of somatosensory-evoked responses in the dorsal hippocampus of the rat. *The Journal of physiology* **591**, 2667-2686
551. Teller, S., Tahirbegi, I. B., Mir, M., Samitier, J., and Soriano, J. (2015) Magnetite-Amyloid-β deteriorates activity and functional organization in an in vitro model for Alzheimer's disease. *Scientific Reports* **5**, 17261
552. Vorhees, C. V., and Williams, M. T. (2014) Assessing spatial learning and memory in rodents. *ILAR journal* **55**, 310-332
553. Sadowski, M., Pankiewicz, J., Scholtzova, H., Ji, Y., Quartermain, D., Jensen, C. H., Duff, K., Nixon, R. A., Gruen, R. J., and Wisniewski, T. (2004) Amyloid-β Deposition Is Associated with Decreased Hippocampal Glucose Metabolism and Spatial Memory Impairment in APP/PS1 Mice. *Journal of Neuropathology & Experimental Neurology* **63**, 418-428
554. Robinson, J. L., Molina-Porcel, L., Corrada, M. M., Raible, K., Lee, E. B., Lee, V. M. Y., Kawas, C. H., and Trojanowski, J. Q. (2014) Perforant path synaptic loss correlates with cognitive impairment and Alzheimer's disease in the oldest-old. *Brain : a journal of neurology* **137**, 2578-2587
555. Vyas, Y., Montgomery, J. M., and Cheyne, J. E. (2020) Hippocampal Deficits in Amyloid-β-Related Rodent Models of Alzheimer's Disease. *Frontiers in Neuroscience* **14**
556. Zhang, R., Xue, G., Wang, S., Zhang, L., Shi, C., and Xie, X. (2012) Novel object recognition as a facile behavior test for evaluating drug effects in AβPP/PS1 Alzheimer's disease mouse model. *J Alzheimers Dis* **31**, 801-812
557. Vorhees, C. V., and Williams, M. T. (2006) Morris water maze: procedures for assessing spatial and related forms of learning and memory. *Nature protocols* **1**, 848-858
558. Samaey, C., Schreurs, A., Stroobants, S., and Balschun, D. (2019) Early Cognitive and Behavioral Deficits in Mouse Models for Tauopathy and Alzheimer's Disease. *Frontiers in aging neuroscience* **11**, 335-335
559. Filali, M., Lalonde, R., and Rivest, S. (2011) Anomalies in social behaviors and exploratory activities in an APPswe/PS1 mouse model of Alzheimer's disease. *Physiol Behav* **104**, 880-885
560. Justice, N. J. (2018) The relationship between stress and Alzheimer's disease. *Neurobiology of stress* **8**, 127-133

561. Ouanes, S., and Popp, J. (2019) High Cortisol and the Risk of Dementia and Alzheimer's Disease: A Review of the Literature. *Frontiers in aging neuroscience* **11**, 43-43
562. Wu, C., Zhang, H., Zhang, J., Zhang, H., Zeng, Y., Fang, S., Li, P., Zhang, Y., Lin, X., Wang, L., Xue, Y., and Guan, M. (2019) Increased oxidative stress, inflammation and fibrosis in perirenal adipose tissue of patients with cortisol-producing adenoma. *Adipocyte* **8**, 347-356
563. Zavvari, F., Nahavandi, A., and Shahbazi, A. (2020) Neuroprotective effects of cerium oxide nanoparticles on experimental stress-induced depression in male rats. *Journal of Chemical Neuroanatomy* **106**, 101799
564. Fiordelisi, A., Piscitelli, P., Trimarco, B., Coscioni, E., Iaccarino, G., and Sorriento, D. (2017) The mechanisms of air pollution and particulate matter in cardiovascular diseases. *Heart Fail Rev* **22**, 337-347
565. Wong, I. C. K., Ng, Y.-K., and Lui, V. W. Y. (2014) Cancers of the lung, head and neck on the rise: perspectives on the genotoxicity of air pollution. *Chinese journal of cancer* **33**, 476-480
566. Su, C. (2017) Environmental implications and applications of engineered nanoscale magnetite and its hybrid nanocomposites: A review of recent literature. *Journal of Hazardous Materials* **322**, 48-84
567. Kim, Y., and Roh, Y. (2019) Environmental Application of Biogenic Magnetite Nanoparticles to Remediate Chromium(III/VI)-Contaminated Water. *Minerals* **9**, 260
568. Kiliç, G., Costa, C., Fernández-Bertólez, N., Pásaro, E., Teixeira, J. P., Laffon, B., and Valdiglesias, V. (2016) In vitro toxicity evaluation of silica-coated iron oxide nanoparticles in human SHSY5Y neuronal cells. *Toxicology Research* **5**, 235-247
569. Wason, M. S., Lu, H., Yu, L., Lahiri, S. K., Mukherjee, D., Shen, C., Das, S., Seal, S., and Zhao, J. (2018) Cerium Oxide Nanoparticles Sensitize Pancreatic Cancer to Radiation Therapy through Oxidative Activation of the JNK Apoptotic Pathway. *Cancers* **10**, 303
570. Wason, M. S., and Zhao, J. (2013) Cerium oxide nanoparticles: potential applications for cancer and other diseases. *Am J Transl Res* **5**, 126-131
571. Henn, A., Lund, S., Hedtjärn, M., Schrattenholz, A., Pörzgen, P., and Leist, M. (2009) The suitability of BV2 cells as alternative model system for primary microglia cultures or for animal experiments examining brain inflammation. *Altex* **26**, 83-94
572. Orecchioni, M., Ghosheh, Y., Pramod, A. B., and Ley, K. (2019) Macrophage Polarization: Different Gene Signatures in M1(LPS+) vs. Classically and M2(LPS–) vs. Alternatively Activated Macrophages. *Frontiers in Immunology* **10**
573. Chávez-Galán, L., Olleros, M. L., Vesin, D., and Garcia, I. (2015) Much More than M1 and M2 Macrophages, There are also CD169+ and TCR+ Macrophages. *Frontiers in Immunology* **6**
574. Sikorska, K., Grądzka, I., Sochanowicz, B., Presz, A., Męczyńska-Wielgosz, S., Brzóska, K., and Kruszewski, M. K. (2020) Diminished amyloid-β uptake by mouse microglia upon treatment with quantum dots, silver or cerium oxide nanoparticles: Nanoparticles and amyloid-β uptake by microglia. *Hum Exp Toxicol* **39**, 147-158
575. Gitler, A. D., Dhillon, P., and Shorter, J. (2017) Neurodegenerative disease: models, mechanisms, and a new hope. *Dis Model Mech* **10**, 499-502
576. Cummings, J. L., Frank, J. C., Cherry, D., Kohatsu, N. D., Kemp, B., Hewett, L., and Mittman, B. (2002) Guidelines for managing Alzheimer's disease: Part II. Treatment. *Am Fam Physician* **65**, 2525-2534

577. Sochocka, M., Diniz, B. S., and Leszek, J. (2017) Inflammatory Response in the CNS: Friend or Foe? *Molecular neurobiology* **54**, 8071-8089
578. Zeng, Y.-Q., Wang, Y.-J., and Zhou, X.-F. (2014) Effects of (-)Epicatechin on the Pathology of APP/PS1 Transgenic Mice. *Frontiers in neurology* **5**, 69-69
579. Jankowsky, J. L., and Zheng, H. (2017) Practical considerations for choosing a mouse model of Alzheimer's disease. *Molecular Neurodegeneration* **12**, 89
580. Li, X., Feng, Y., Wu, W., Zhao, J., Fu, C., Li, Y., Ding, Y., Wu, B., Gong, Y., Yang, G., and Zhou, X. (2016) Sex differences between APPswePS1dE9 mice in A-beta accumulation and pancreatic islet function during the development of Alzheimer's disease. *Laboratory Animals* **50**, 275-285

Appendices

Appendix 1: Western blot images for *in vivo* study 1

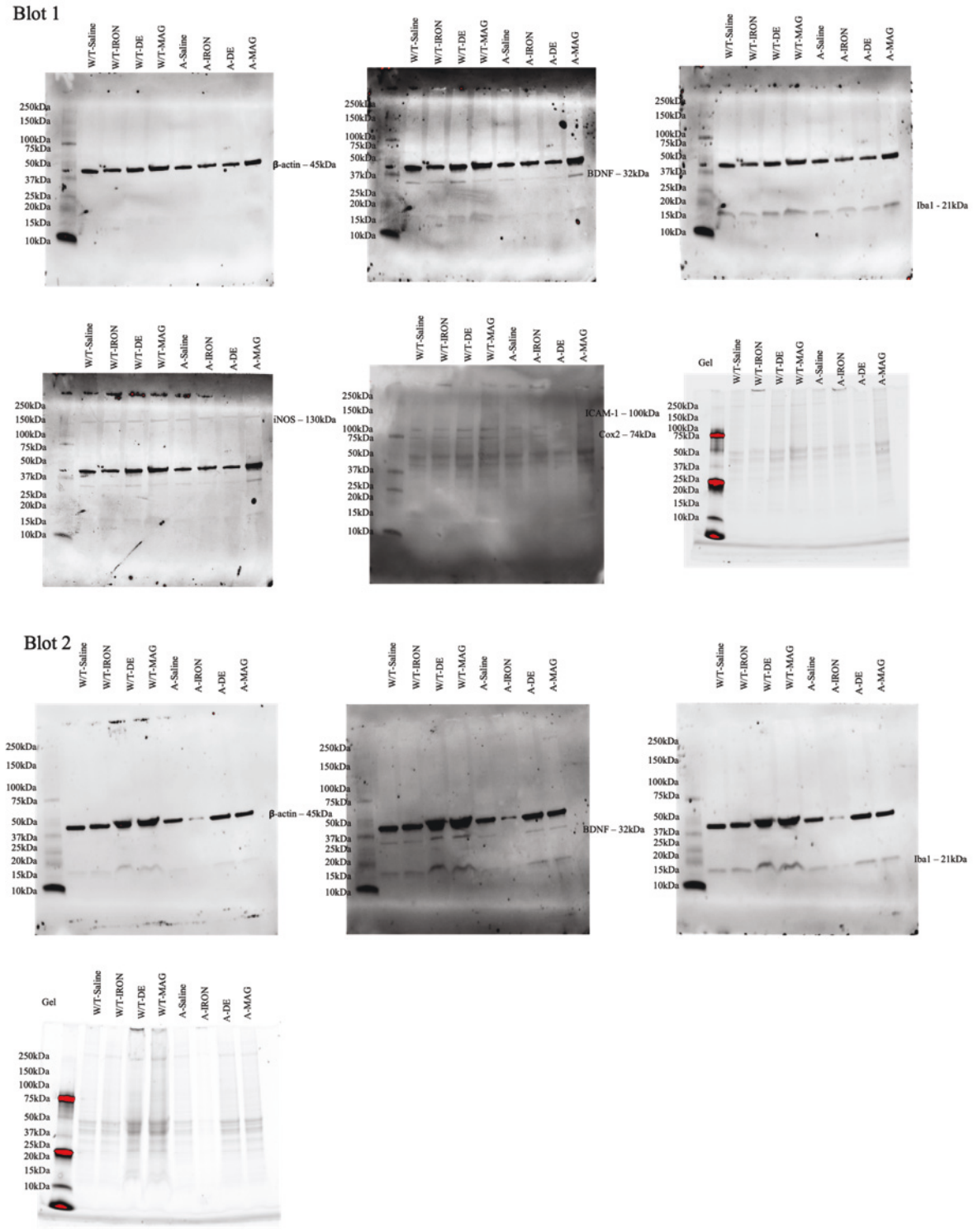

Blot 3

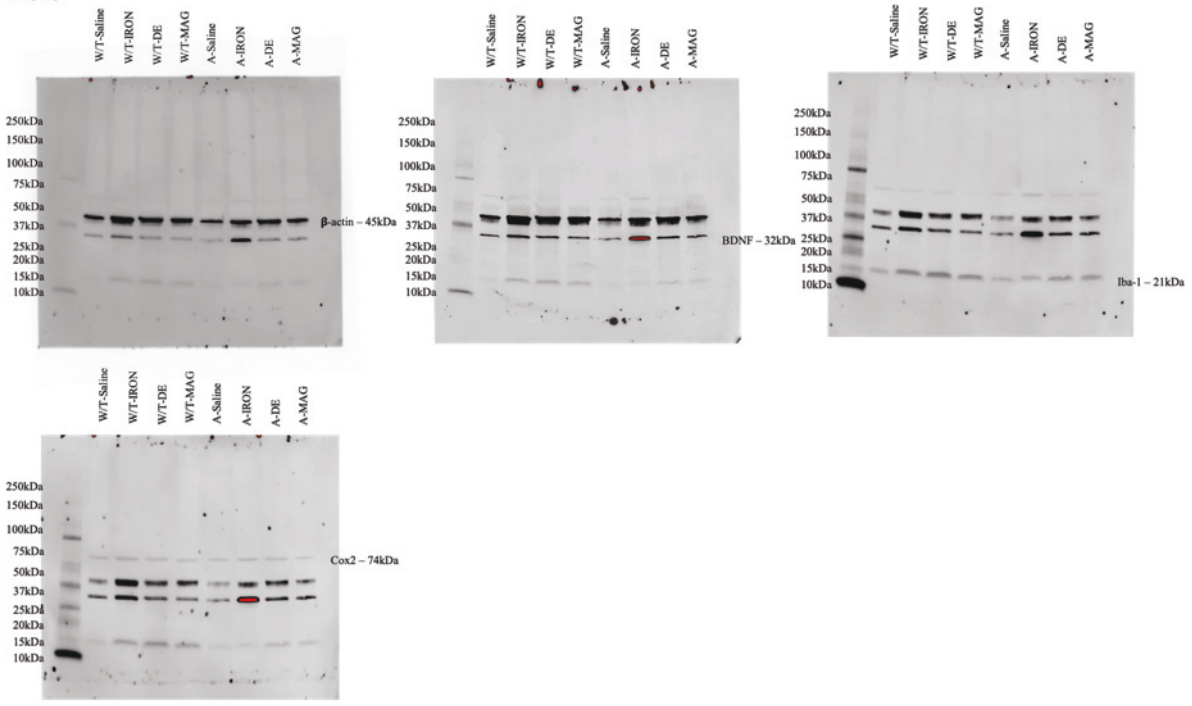
W/T-Saline
W/T-IRON
W/T-DE
W/T-MAG
A-Saline
A-IRON
A-DE
A-MAG
250kDa
150kDa
100kDa
75kDa
50kDa
37kDa
25kDa
20kDa
15kDa
10kDa
β-actin – 45kDa
BDNF – 32kDa
Iba-1 – 21kDa
Cox2 – 74kDa

Blot 4

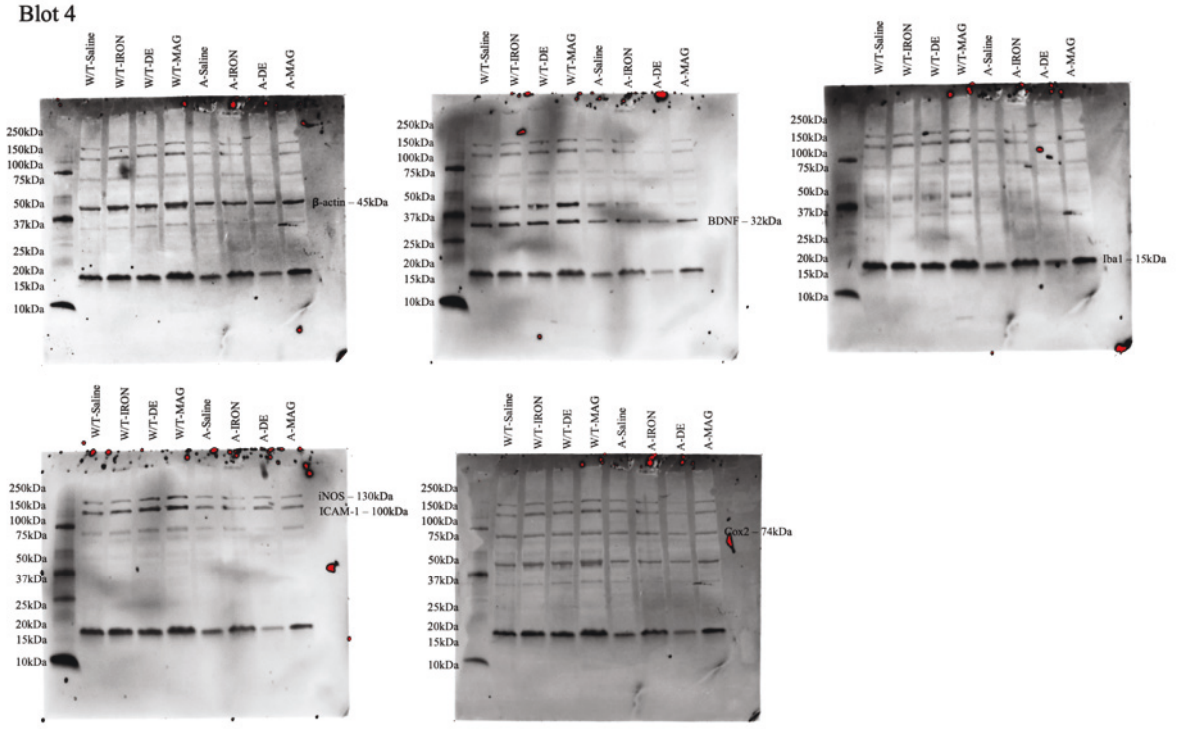
W/T-Saline
W/T-IRON
W/T-DE
W/T-MAG
A-Saline
A-IRON
A-DE
A-MAG
250kDa
150kDa
100kDa
75kDa
50kDa
37kDa
25kDa
20kDa
15kDa
10kDa
β-actin – 45kDa
BDNF – 32kDa
Iba1 – 15kDa
iNOS – 130kDa
ICAM-1 – 100kDa
Cox2 – 74kDa

Blot 5

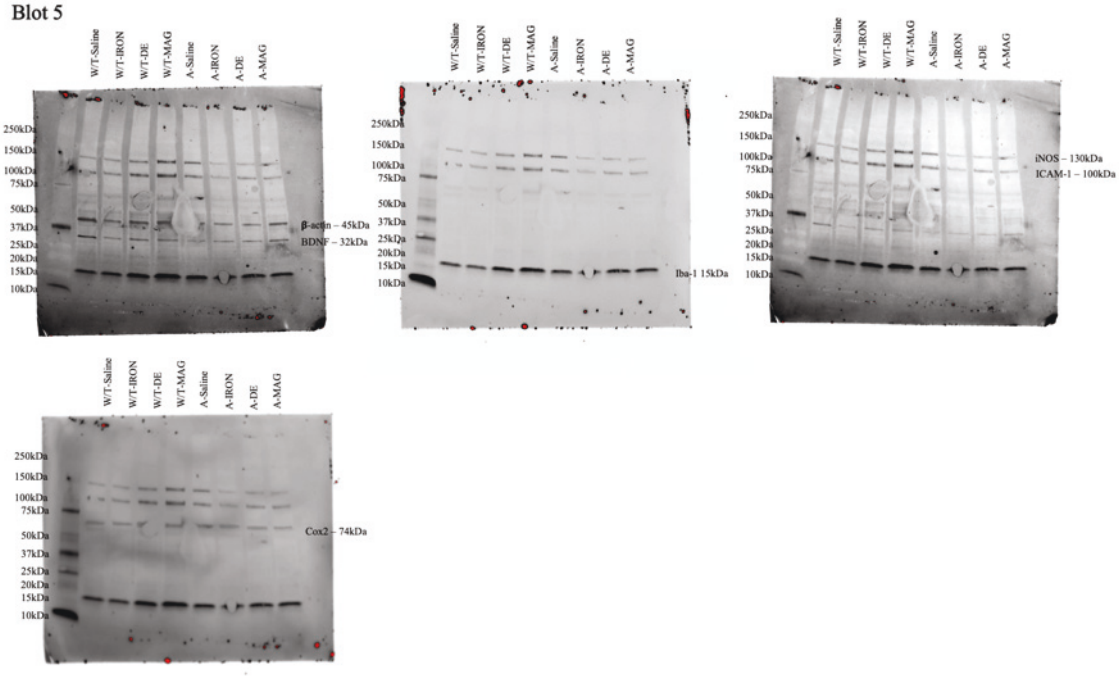
W/T-Saline
W/T-IRON
W/T-DE
W/T-MAG
A-Saline
A-IRON
A-DE
A-MAG
250kDa
150kDa
100kDa
75kDa
50kDa
37kDa
25kDa
20kDa
15kDa
10kDa
β-actin – 45kDa
BDNF – 32kDa
Iba-1 15kDa
iNOS – 130kDa
ICAM-1 – 100kDa
Cox2 – 74kDa

Blot 6

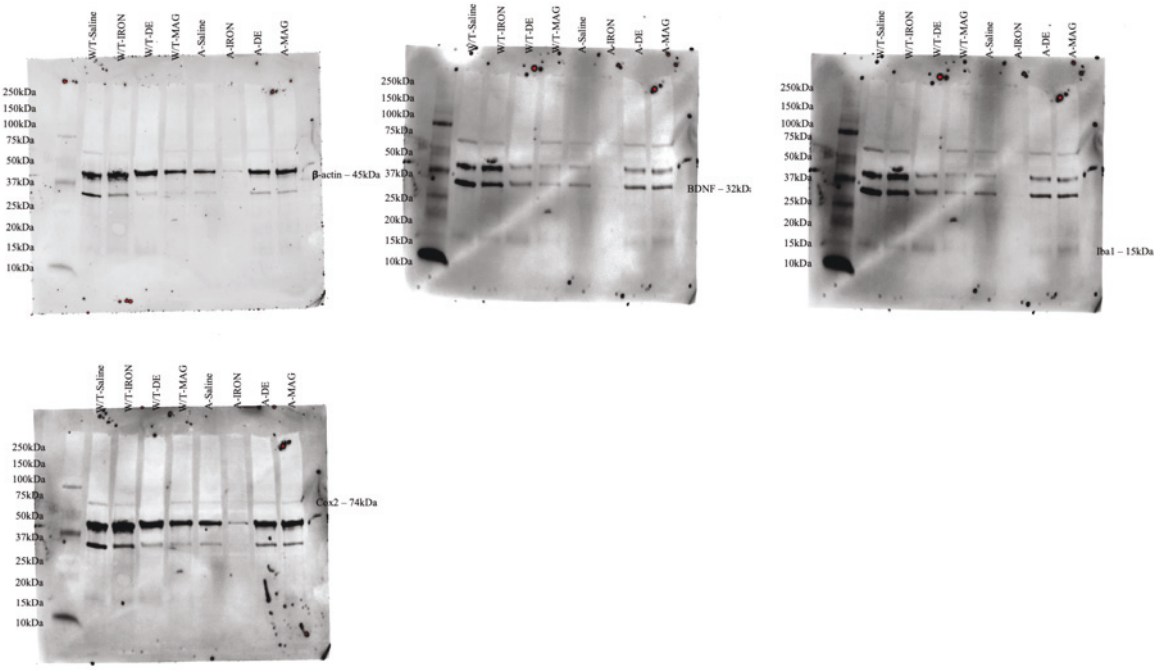
W/T-Saline
W/T-IRON
W/T-DE
W/T-MAG
A-Saline
A-IRON
A-DE
A-MAG
250kDa
150kDa
100kDa
75kDa
50kDa
37kDa
25kDa
20kDa
15kDa
10kDa
β-actin – 45kDa
BDNF – 32kDa
Iba1 – 15kDa
Cox2 – 74kDa

Blot 7

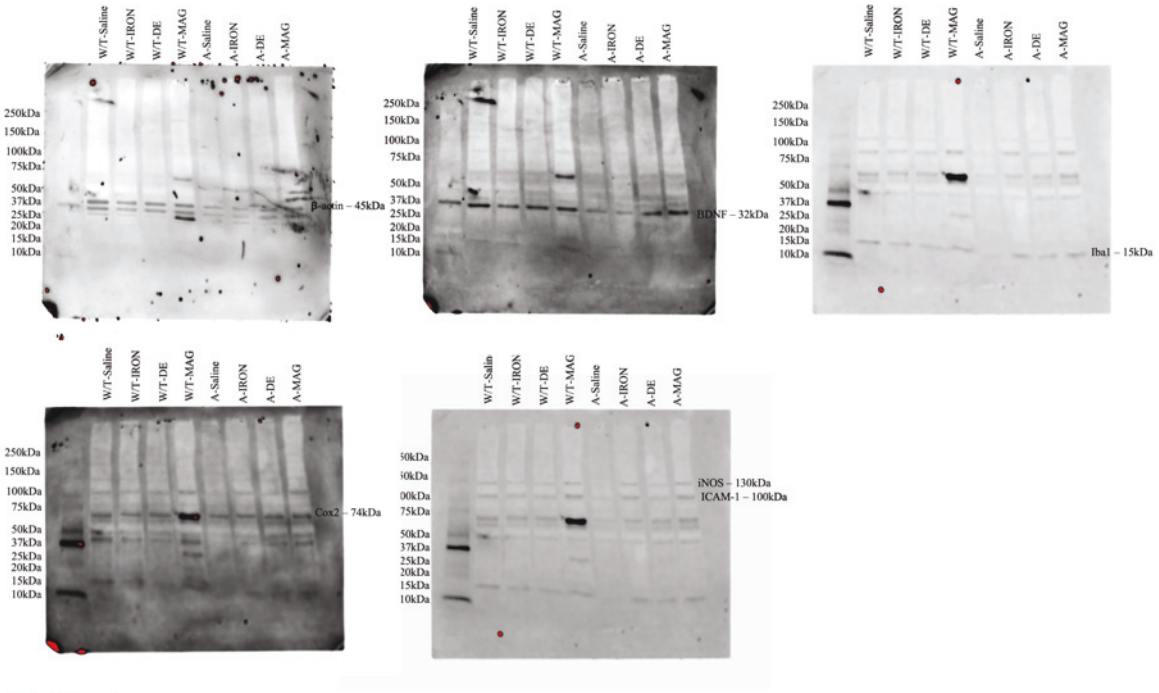
W/T-Saline
W/T-IRON
W/T-DE
W/T-MAG
A-Saline
A-IRON
A-DE
A-MAG
250kDa
150kDa
100kDa
75kDa
50kDa
37kDa
25kDa
20kDa
15kDa
10kDa
β-actin – 45kDa
BDNF – 32kDa
Iba1 – 15kDa
Cox2 – 74kDa
iNOS – 130kDa
ICAM-1 – 100kDa

Blot 8

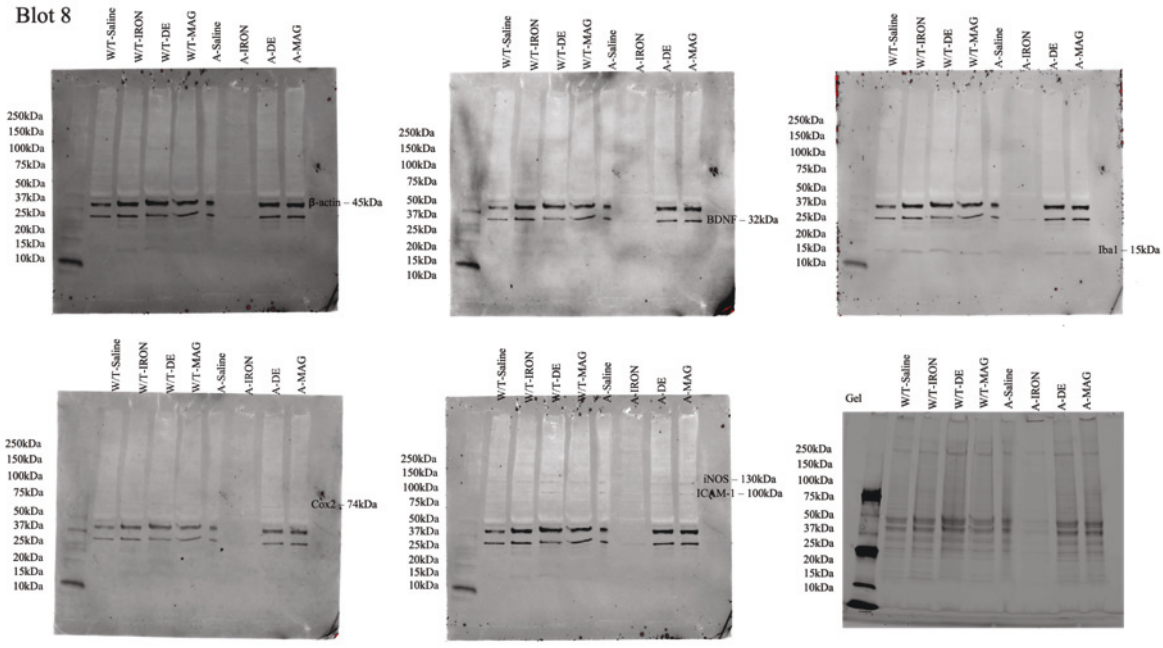
W/T-Saline
W/T-IRON
W/T-DE
W/T-MAG
A-Saline
A-IRON
A-DE
A-MAG
250kDa
150kDa
100kDa
75kDa
50kDa
37kDa
25kDa
20kDa
15kDa
10kDa
β-actin – 45kDa
BDNF – 32kDa
Iba1 – 15kDa
Cox2 – 74kDa
iNOS – 130kDa
ICAM-1 – 100kDa
Gel

Appendix 2: Western blot images for *in vitro* study 1

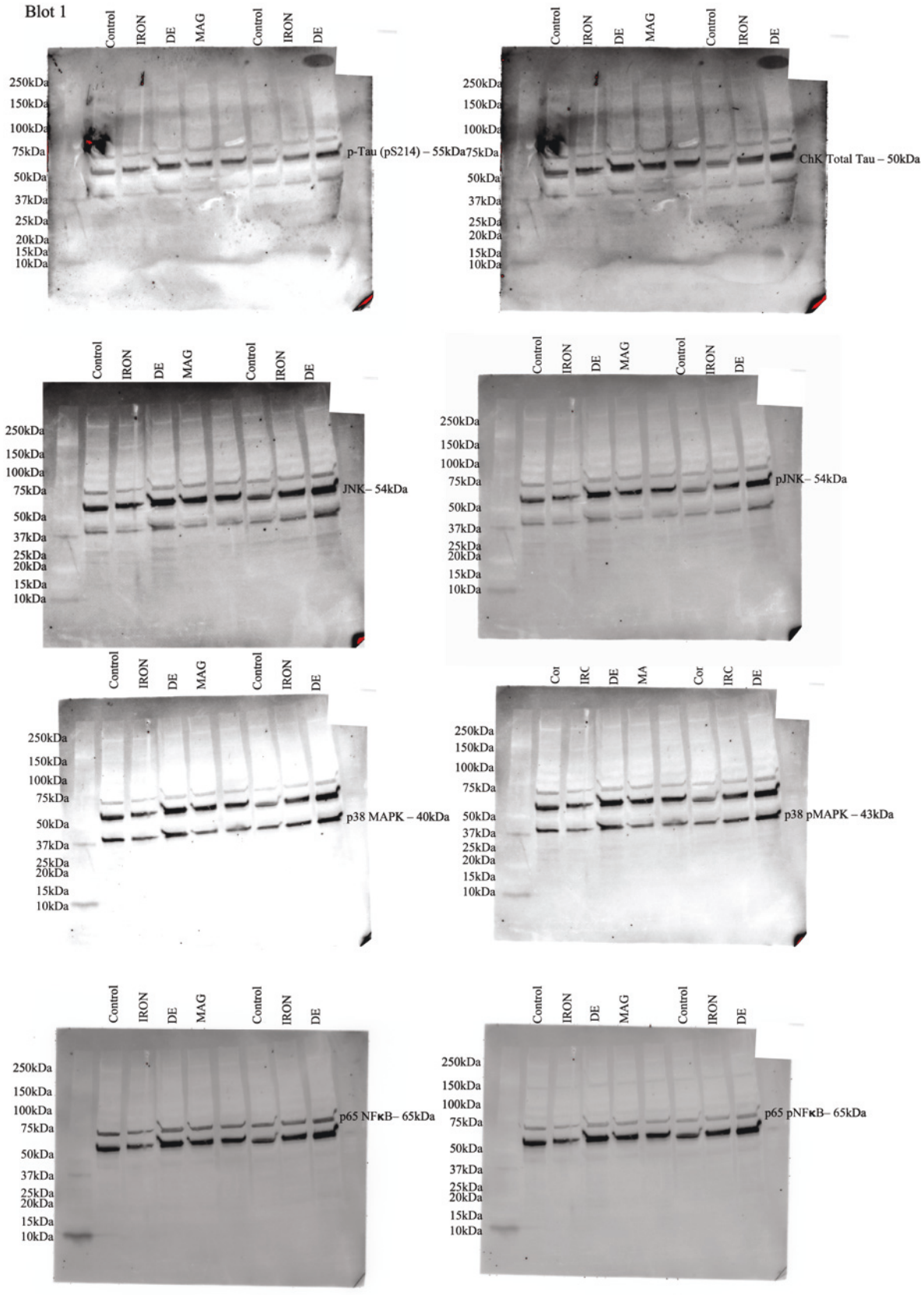

Blot 2

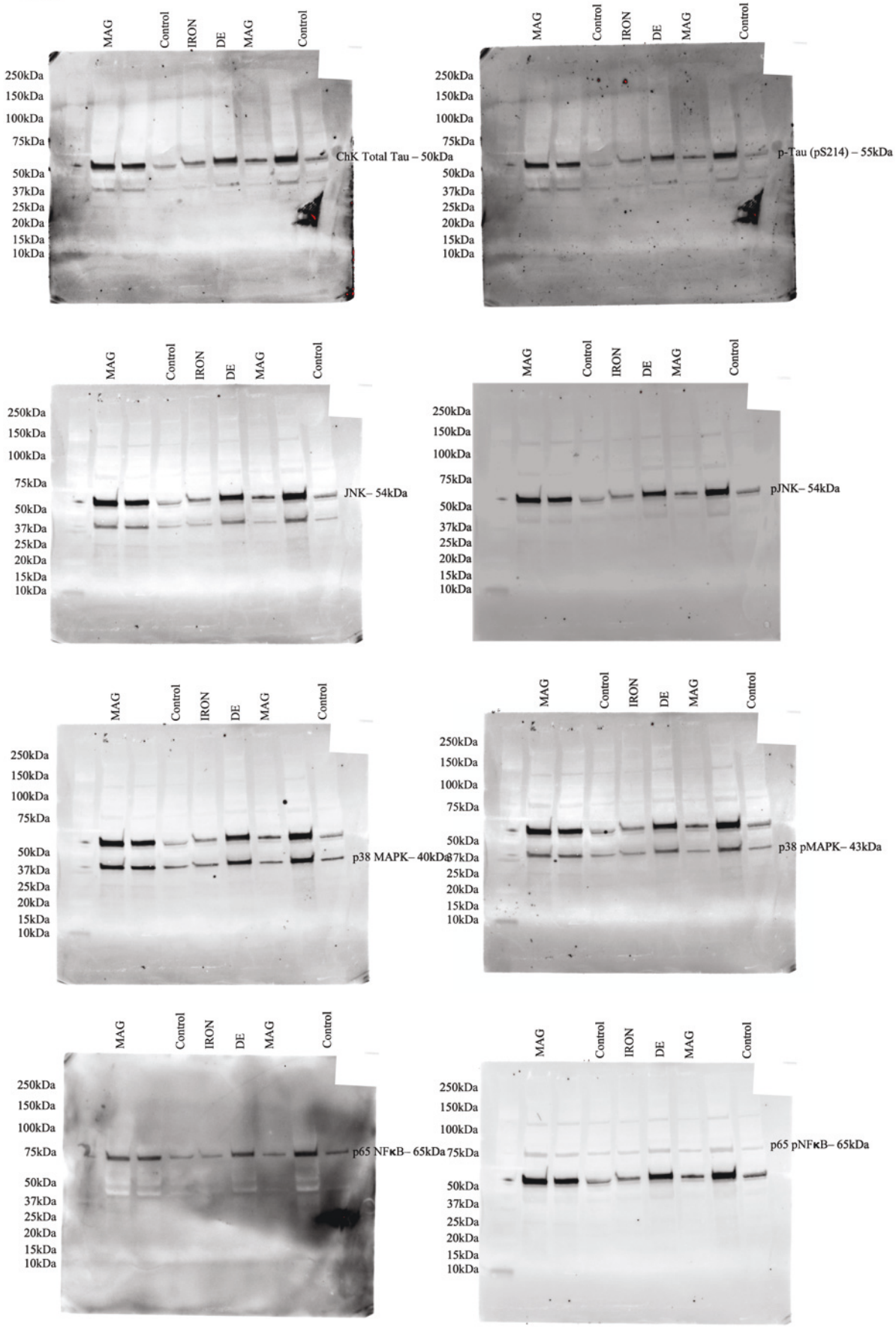
MAG
Control
IRON
DE
MAG
Control
250kDa
150kDa
100kDa
75kDa
50kDa
37kDa
25kDa
20kDa
15kDa
10kDa
ChK Total Tau – 50kDa
p-Tau (pS214) – 55kDa
JNK– 54kDa
pJNK– 54kDa
p38 MAPK– 40kDa
p38 pMAPK– 43kDa
p65 NFκB– 65kDa
p65 pNFκB– 65kDa

Blot 3

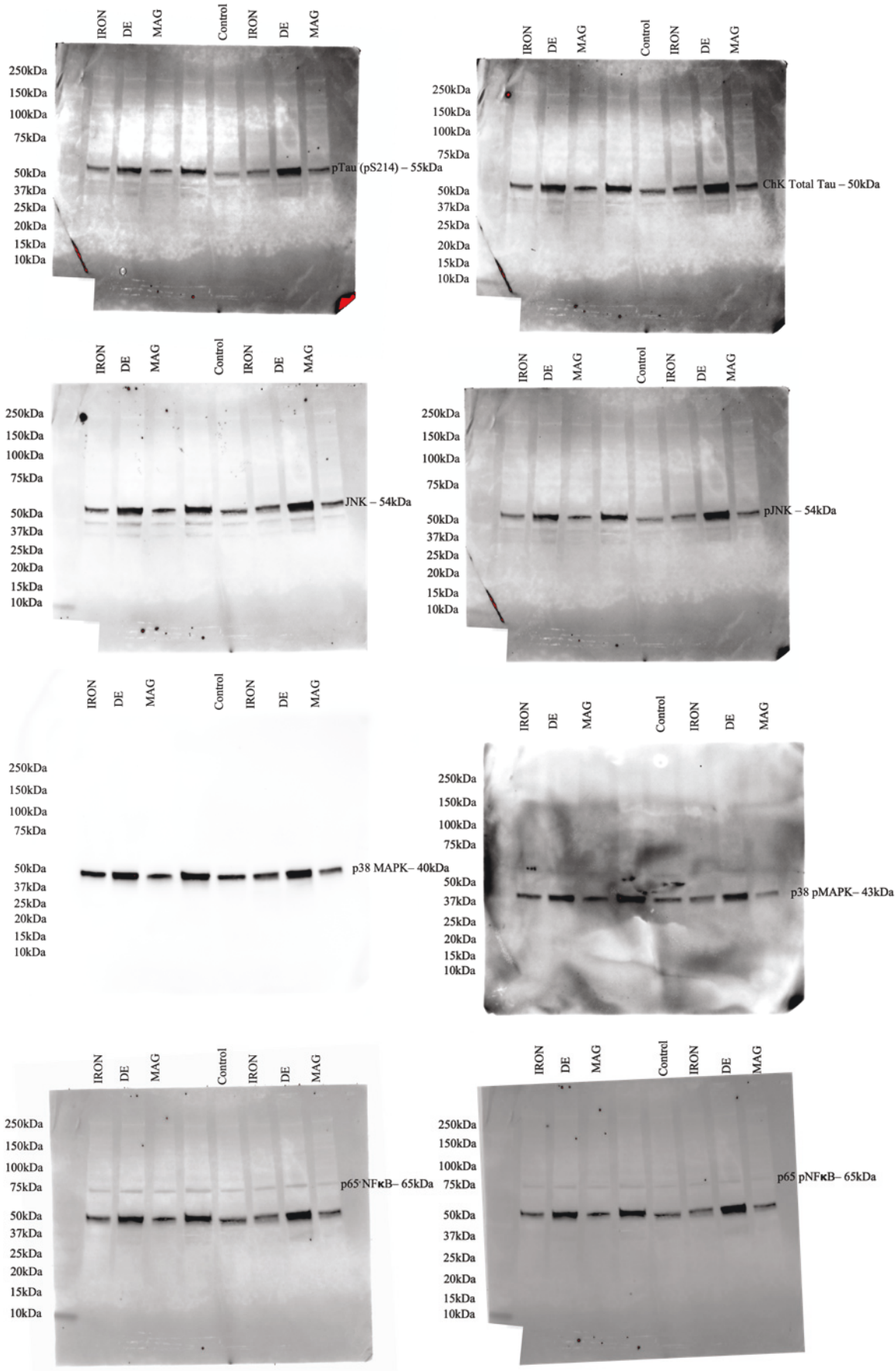
IRON
DE
MAG
Control
IRON
DE
MAG
250kDa
150kDa
100kDa
75kDa
50kDa
37kDa
25kDa
20kDa
15kDa
10kDa
pTau (pS214) – 55kDa
ChK Total Tau – 50kDa
JNK – 54kDa
pJNK – 54kDa
p38 MAPK– 40kDa
p38 pMAPK– 43kDa
p65 NFκB– 65kDa
p65 pNFκB– 65kDa

Blot 4

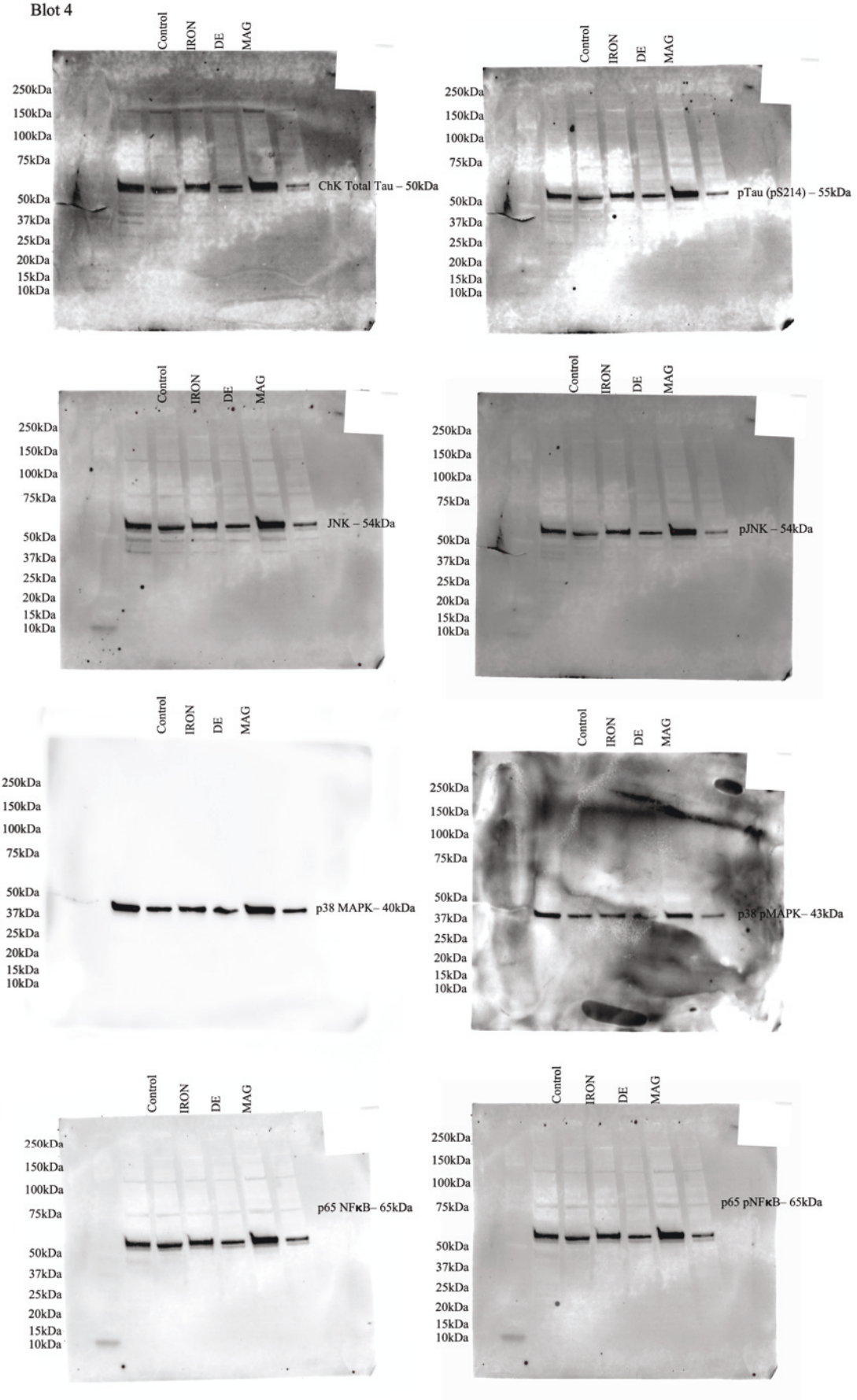
Control
IRON
DE
MAG
250kDa
150kDa
100kDa
75kDa
50kDa
37kDa
25kDa
20kDa
15kDa
10kDa
ChK Total Tau – 50kDa
pTau (pS214) – 55kDa
JNK – 54kDa
pJNK – 54kDa
p38 MAPK– 40kDa
p38 pMAPK– 43kDa
p65 NFκB– 65kDa
p65 pNFκB– 65kDa

Appendix 3: Western blot images for *in vivo* study 2

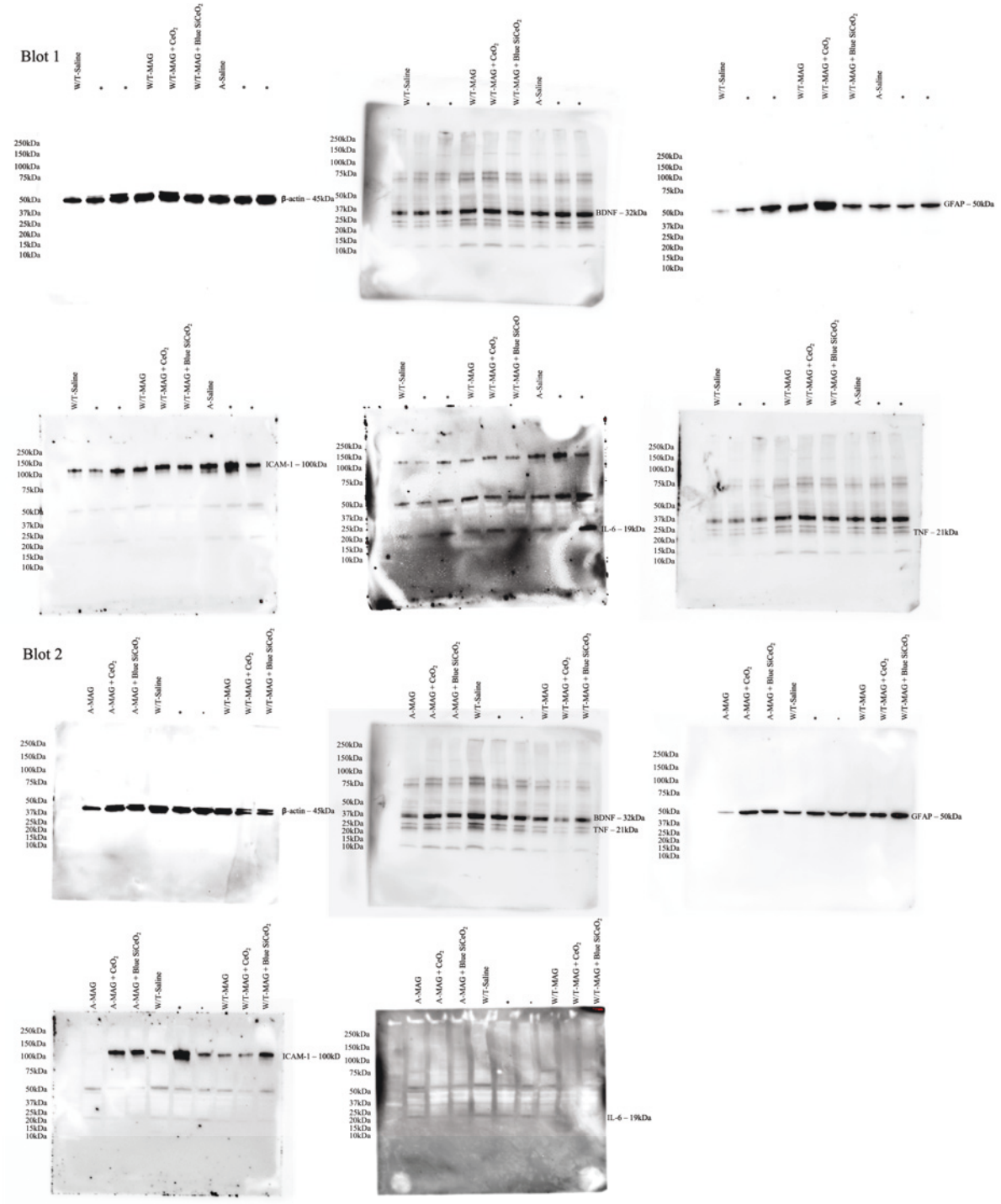

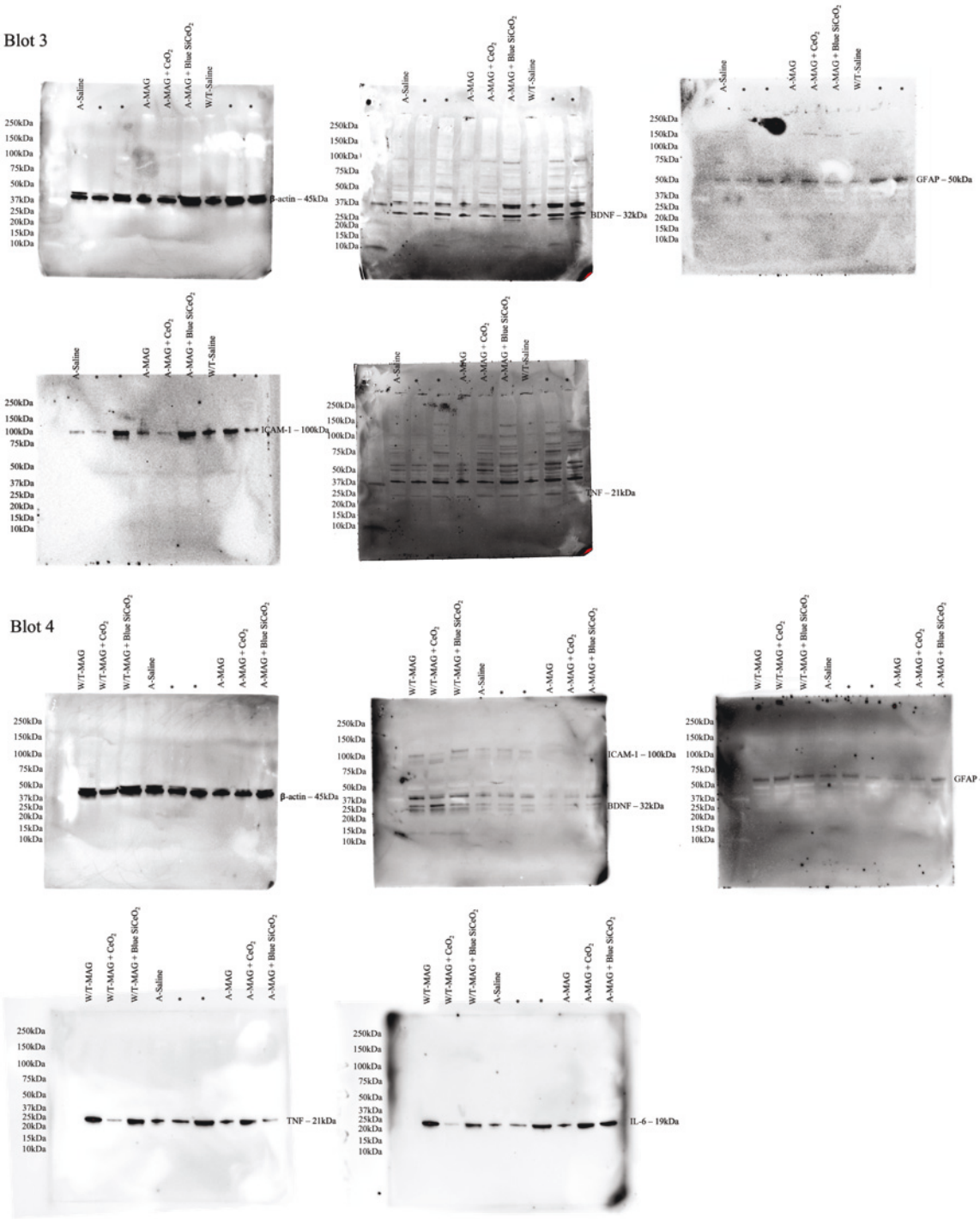
Blot 3
A-Saline
A-MAG
A-MAG + CeO2
A-MAG + Blue SiCeO2
W/T-Saline
250kDa
150kDa
100kDa
75kDa
50kDa
37kDa
25kDa
20kDa
15kDa
10kDa
β-actin – 45kDa
BDNF – 32kDa
GFAP – 50kDa
ICAM-1 – 100kDa
TNF – 21kDa
Blot 4
W/T-MAG
W/T-MAG + CeO2
W/T-MAG + Blue SiCeO2
A-Saline
A-MAG
A-MAG + CeO2
A-MAG + Blue SiCeO2
β-actin – 45kDa
ICAM-1 – 100kDa
BDNF – 32kDa
GFAP – 50kDa
TNF – 21kDa
IL-6 – 19kDa

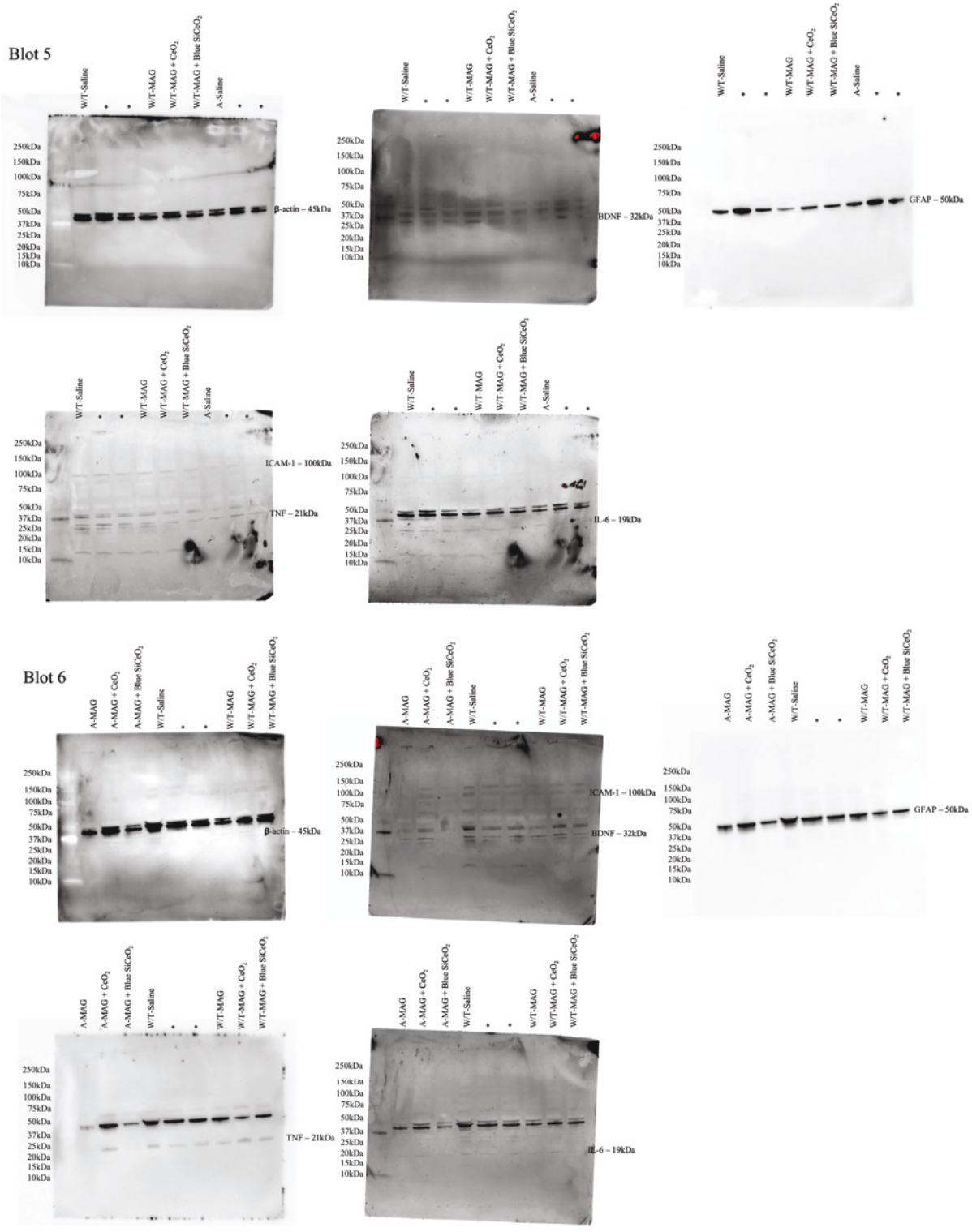
Blot 5
W/T-Saline
W/T-MAG
W/T-MAG + CeO2
W/T-MAG + Blue SiCeO2
A-Saline
250kDa
150kDa
100kDa
75kDa
50kDa
37kDa
25kDa
20kDa
15kDa
10kDa
β-actin – 45kDa
BDNF – 32kDa
GFAP – 50kDa
ICAM-1 – 100kDa
TNF – 21kDa
IL-6 – 19kDa
Blot 6
A-MAG
A-MAG + CeO2
A-MAG + Blue SiCeO2
W/T-Saline
W/T-MAG
W/T-MAG + CeO2
W/T-MAG + Blue SiCeO2
β-actin – 45kDa
ICAM-1 – 100kDa
BDNF – 32kDa
GFAP – 50kDa
TNF – 21kDa
IL-6 – 19kDa

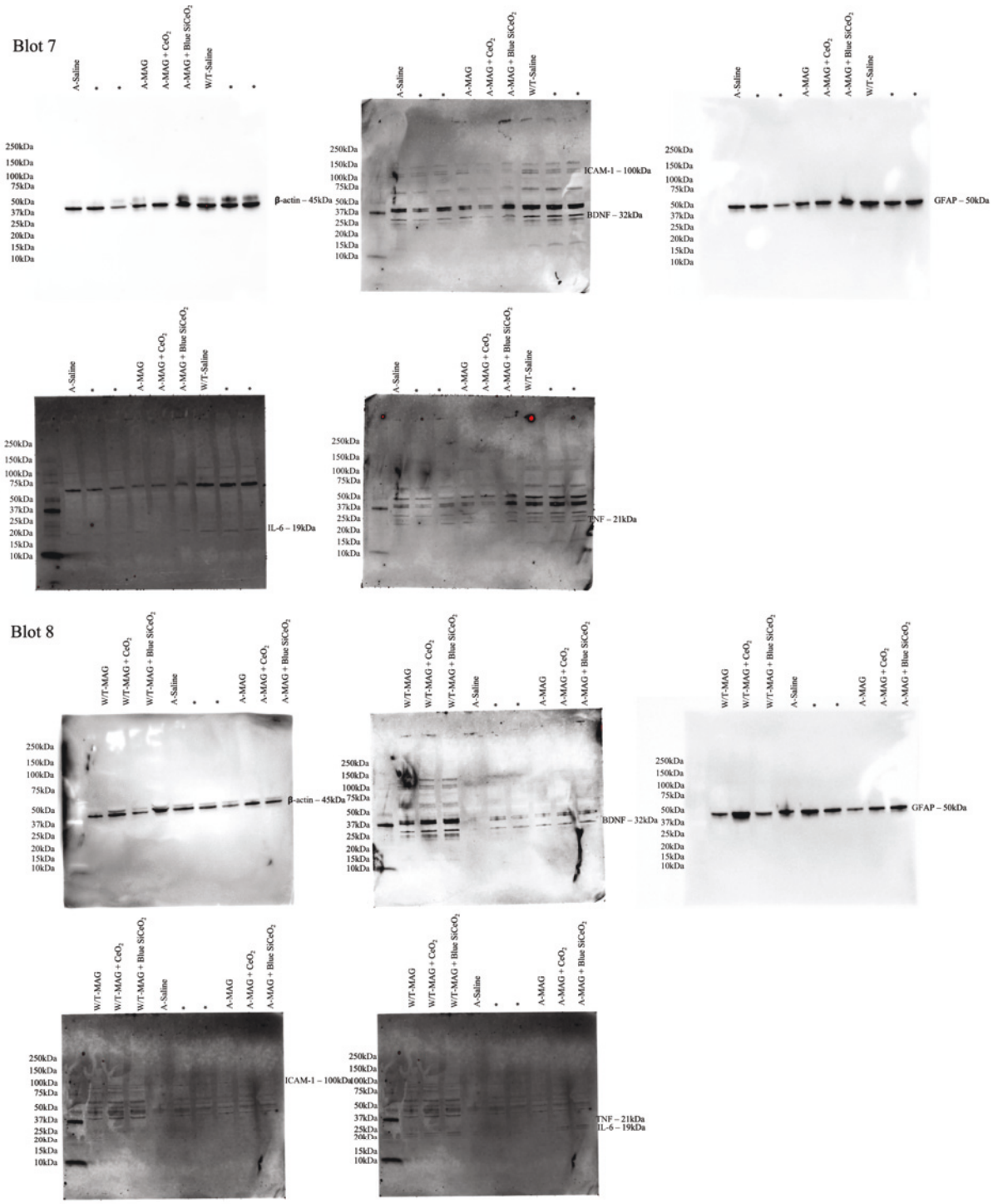
Blot 7
A-Saline
A-MAG
A-MAG + CeO2
A-MAG + Blue SiCeO2
W/T-Saline
250kDa
150kDa
100kDa
75kDa
50kDa
37kDa
25kDa
20kDa
15kDa
10kDa
β-actin – 45kDa
ICAM-1 – 100kDa
BDNF – 32kDa
GFAP – 50kDa
IL-6 – 19kDa
TNF – 21kDa
Blot 8
W/T-MAG
W/T-MAG + CeO2
W/T-MAG + Blue SiCeO2
A-Saline
A-MAG
A-MAG + CeO2
A-MAG + Blue SiCeO2
β-actin – 45kDa
BDNF – 32kDa
GFAP – 50kDa
ICAM-1 – 100kDa
TNF – 21kDa
IL-6 – 19kDa

Appendix 4: Western blot images for *in vitro* study 2

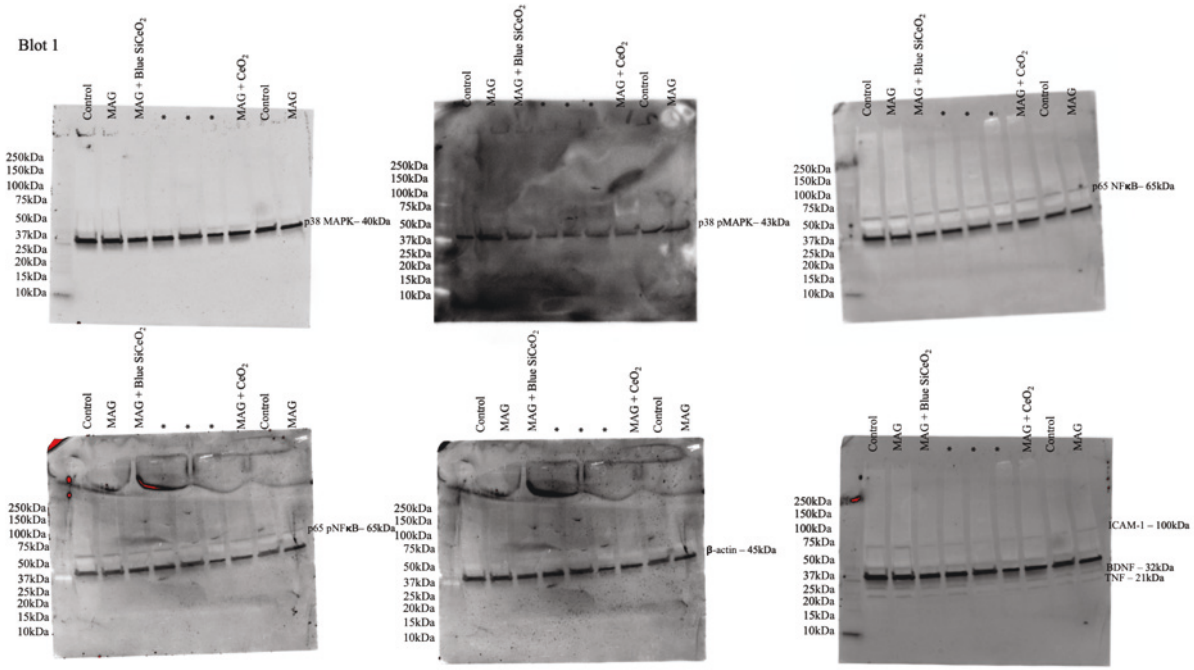

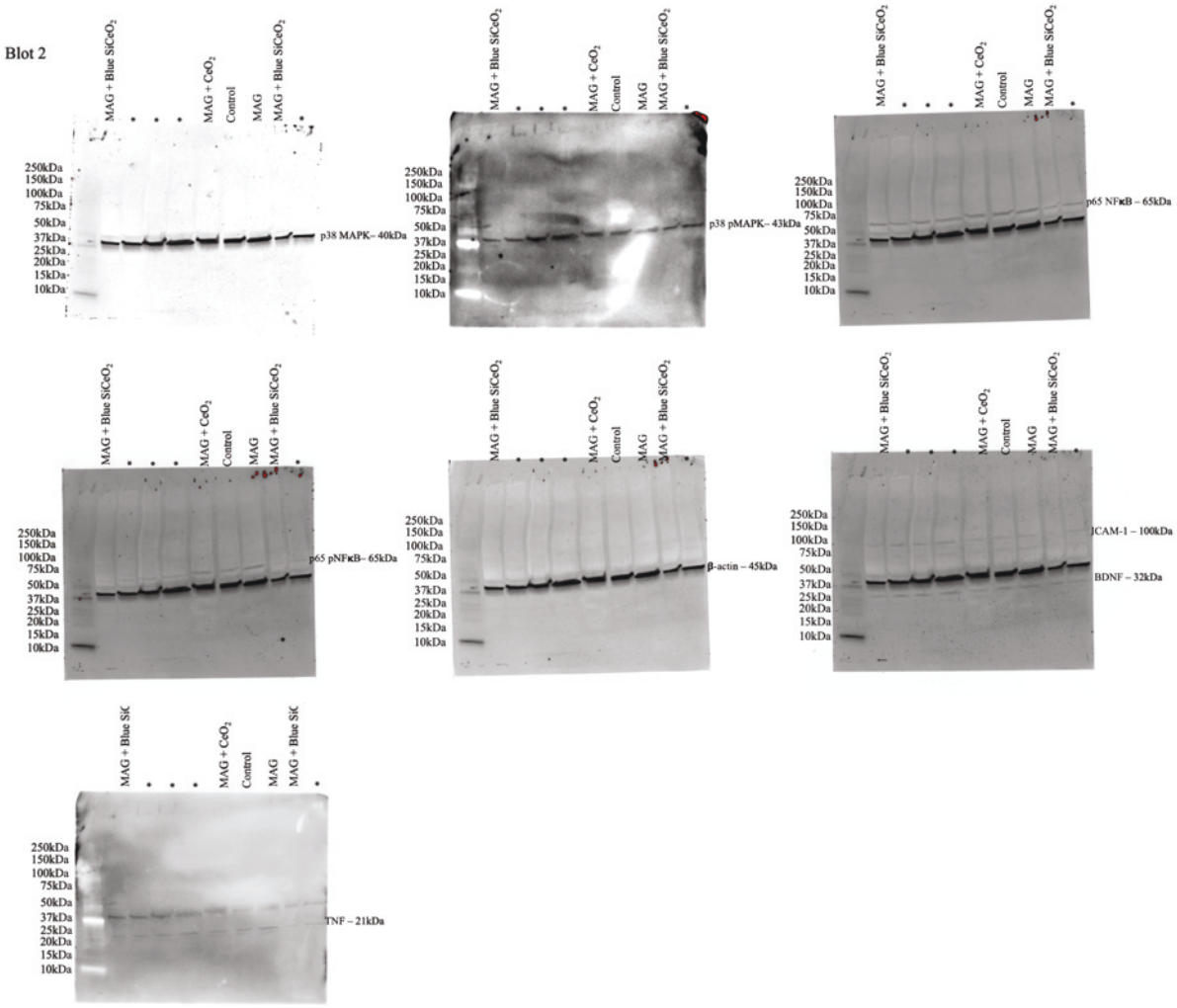
Blot 2
MAG + Blue SiCeO2
MAG + CeO2
Control
MAG
MAG + Blue SiCeO2
250kDa
150kDa
100kDa
75kDa
50kDa
37kDa
25kDa
20kDa
15kDa
10kDa
p38 MAPK– 40kDa
p38 pMAPK– 43kDa
p65 NFκB – 65kDa
p65 pNFκB– 65kDa
β-actin – 45kDa
ICAM-1 – 100kDa
BDNF – 32kDa
MAG + Blue SiC
TNF – 21kDa

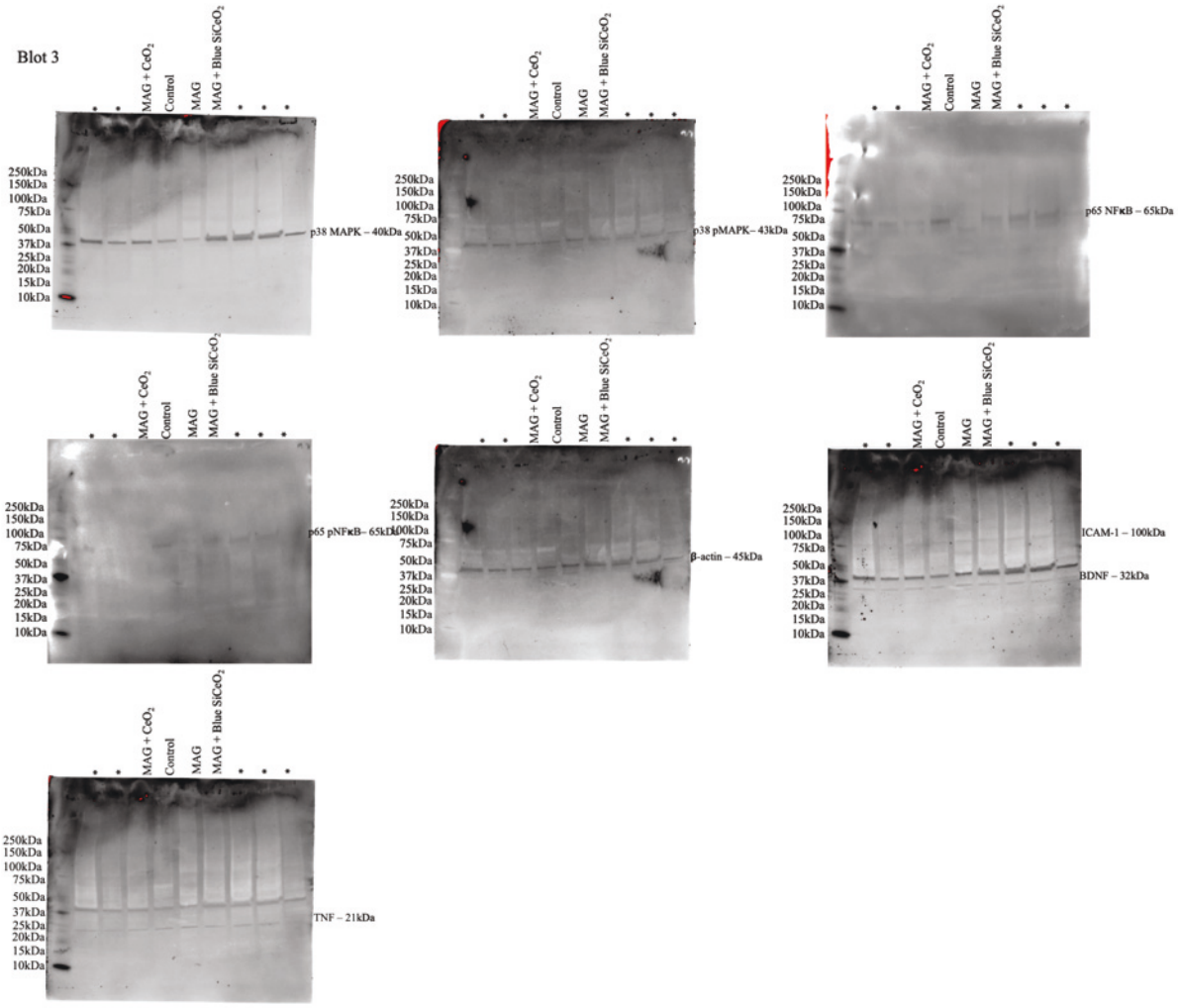
Blot 3
MAG + CeO2
Control
MAG
MAG + Blue SiCeO2
250kDa
150kDa
100kDa
75kDa
50kDa
37kDa
25kDa
20kDa
15kDa
10kDa
p38 MAPK – 40kDa
p38 pMAPK– 43kDa
p65 NFκB – 65kDa
p65 pNFκB– 65kDa
β-actin – 45kDa
ICAM-1 – 100kDa
BDNF – 32kDa
TNF – 21kDa

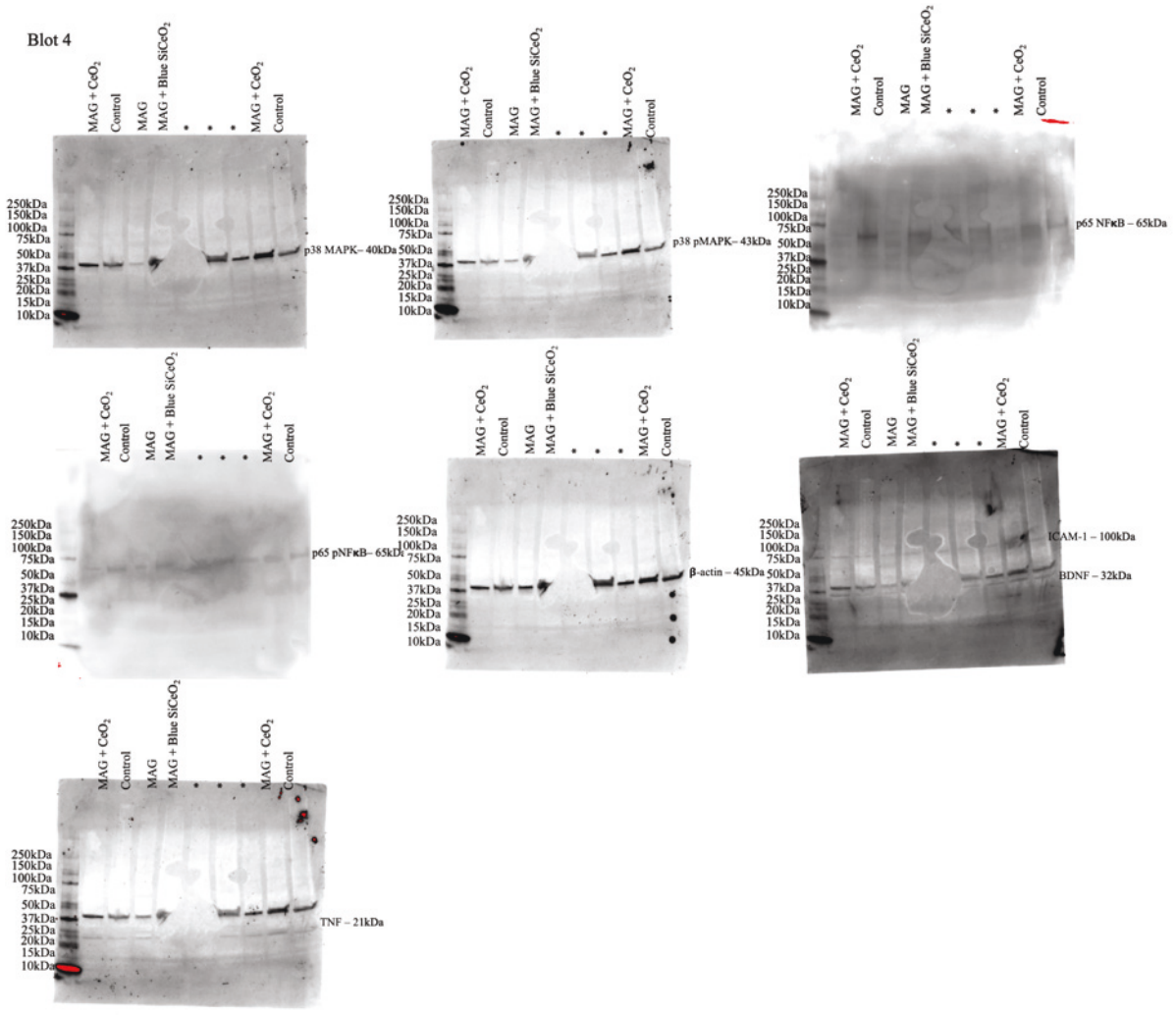
Blot 4
MAG + CeO2
Control
MAG
MAG + Blue SiCeO2
250kDa
150kDa
100kDa
75kDa
50kDa
37kDa
25kDa
20kDa
15kDa
10kDa
p38 MAPK– 40kDa
p38 pMAPK– 43kDa
p65 NFκB – 65kDa
p65 pNFκB– 65kDa
β-actin – 45kDa
ICAM-1 – 100kDa
BDNF – 32kDa
TNF – 21kDa

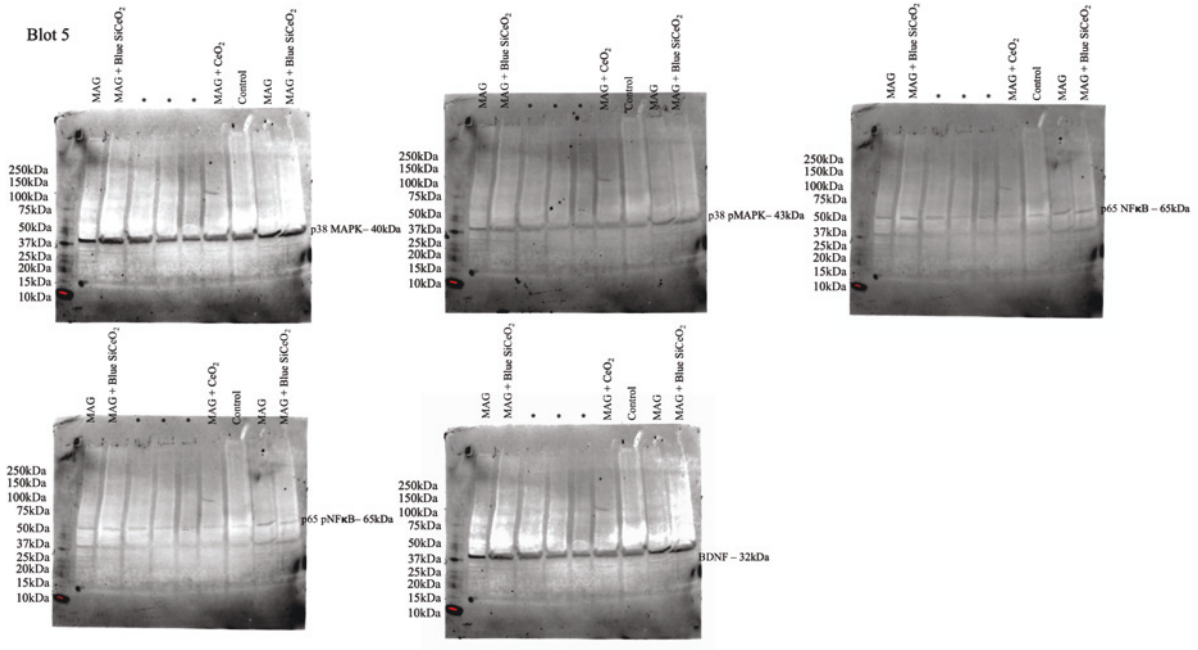
Blot 5
MAG
MAG + Blue SiCeO2
MAG + CeO2
Control
250kDa
150kDa
100kDa
75kDa
50kDa
37kDa
25kDa
20kDa
15kDa
10kDa
p38 MAPK– 40kDa
p38 pMAPK– 43kDa
p65 NFκB – 65kDa
p65 pNFκB– 65kDa
BDNF – 32kDa

Appendix 5: Systematic and Bibliometric Analysis of Magnetite Nanoparticles and Their Application in (Biomedical) Research

RESEARCH ARTICLE

Global Challenges

www.global-challenges.com

Systematic and Bibliometric Analysis of Magnetite Nanoparticles and Their Applications in (Biomedical) Research

Charlotte L. Fleming, Mojtaba Golzan, Cindy Gunawan, and Kristine C. McGrath**

Recent reports show air pollutant magnetite nanoparticles (MNPs) in the brains of people with Alzheimer's disease (AD). Considering various field applications of MNPs because of developments in nanotechnology, the aim of this study is to identify major trends and data gaps in research on magnetite to allow for relevant environmental and health risk assessment. Herein, a bibliometric and systematic analysis of the published magnetite literature (n = 31 567) between 1990 to 2020 is completed. Following appraisal, publications (n = 244) are grouped into four time periods with the main research theme identified for each as 1990–1997 "oxides," 1998–2005 "ferric oxide," 2006–2013 "pathology," and 2014–2020 "animal model." Magnetite formation and catalytic activity dominate the first two time periods, with the last two focusing on the exploitation of nanoparticle engineering. Japan and China have the highest number of citations for articles published. Longitudinal analysis indicates that magnetite research for the past 30 years shifted from environmental and industrial applications, to biomedical and its potential toxic effects. Therefore, whilst this study presents the research profile of different countries, the development in research on MNPs, it also reveals that further studies on the effects of MNPs on human health is much needed.

C. L. Fleming, K. C. McGrath
School of Life Sciences
Faculty of Science
University of Technology Sydney
Sydney, NSW 2008, Australia
E-mail: Kristine.McGrath@uts.edu.au
M. Golzan
Vision Science Group
Graduate School of Health
University of Technology Sydney
Sydney, NSW 2008, Australia
C. Gunawan
Australian Institute for Microbiology and Infection
University of Technology Sydney
Sydney, NSW 2008, Australia
E-mail: Cindy.Gunawan@uts.edu.au

The ORCID identification number(s) for the author(s) of this article can be found under https://doi.org/10.1002/gch2.202200009.

DOI: 10.1002/gch2.202200009

1. Introduction

Magnetite is an iron oxide (Fe_3O_4) rock mineral occurring naturally on Earth. Magnetite belongs to the spinel crystallizing group of minerals, with the formula $FeFe_2O_4$.[1] In the natural environment, magnetite is found in the form of igneous (basic rocks, basalts) and sedimentary rocks (banded iron formations, beach sands) formed via different ways, usually, the reaction between ferric iron mats and ferrous iron anaerobically.[2] Magnetite can readily react with oxygen to produce hematite (Fe_2O_3) where it can be used to determine oxygen concentrations in rocks, due to the changes in the atmospheric oxygen content.[3] Magnetite exhibits ferrimagnetism where dipole forces align in the same direction, permitting active magnetization to occur. This property of magnetite is influenced by size of the particles and is essential for the reconstruction of tectonics plates on the Earth's crust.[3,4] Overall, magnetite is a unique iron oxide compound that is it extremely versatile due to its magnetic, structural, and redox characteristics.[5]

Material and life scientists have shown particular interest in substances at nano-scale, referred to as nanomaterials or nanoparticles.[6] Iron oxide magnetic nanoparticles or magnetite nanoparticles (MNPs) have become the focus for studies across various fields, including industrial, environmental, and biomedical applications of the nanoparticles. MNPs have been used extensively due to the fundamental properties of MNPs in the closely packed cubic lattice structure with the iron ions located at interstices between the oxygen ions, in either the tetrahedral or octahedral sites. The crystal structure of magnetite allows the movement from one ion to another (transitioning of valence states), exhibiting high conductivity, high catalytic performance, and regenerative abilities exhibiting ferromagnetic or superparamagnetic properties, which means that the external magnetic field can magnetize the particles to a paramagnetic (weakly attracted to magnets) but with much larger magnetic susceptibility.[4] MNPs can be chemically synthesized and is relatively cheap to manufacture on a large scale, thus it is abundantly available.[7] The pliability of synthetic MNPs has allowed them to be used in various environmental, industrial, and biomedical applications. For example, MNPs have been previously

used to remove chromium, zinc, lead, arsenic, palladium, copper, and chloroform from polluted water and soil.[8–12] In industries, MNPs (combined with carbon) have been shown to improve sodium and lithium battery life, improve rechargeable device efficiency, aid in the advancements of solar cells and biofuels due to thermal and catalytic properties.[7,13] In biomedical applications, superparamagnetic synthetic MNPs coated with organic materials has been shown to increase its stability and biocompatibility making it a safe and efficient biomedicine.[6,14] For example, in magnetic resonance imaging (MRI), MNPs have been used as a contrasting agent for tumor diagnosis, and hypothermia-based cancer therapies and for inflammatory diseases.[15–20] The various applications of synthetic MNPs show their versatility, with manufacturer's exploiting the remarkable properties that they possess, which have been improved in many applications through the advancements in nanoparticle engineering and manufacturing.[21,22]

Whilst magnetite research over the last 30 years has yielded progress in our understanding of the properties of magnetite, and the ways in which we can exploit its properties for various uses, there are aspects of MNPs which are unknown, which include the way in which they are harmful to human health.[23] For example, a study by Maher et al. has shown that air pollutant-externally-derived MNPs have been found in abundance in the brains of people suffering from Alzheimer's disease (AD).[24] The aim of this study therefore is to conduct a bibliometric analysis of the literature over the past three decades on MNPs related research and highlight future research needs.

2. Experimental Section

2.1. Topic Modelling

The database, Pubmed (https://pubmed.ncbi.nlm.nih.gov/), was used to search the term "magnetite" (938 publications). The publications that were within the years 1990–2020 and either a research or review articles were exported (PMID list file). They were then imported into the Sciome Workbench for Interactive Computer-Facilitated Text-mining (SWIFT) review software (https://www.sciome.com/swift-review/) where the articles were segregated based on keywords, then organized into topic models of magnetite research, and ranked in order from most to least prevalent topics. To enlarge the search range, other databases were used as a source of bibliographic data.

2.2. Bibliometric Analysis

The bibliographic data collected from a "magnetite" search including title, abstract, and all citations (accessed on 14th December 2020) for the period 1990–2020, was exported from the Web of Science Core Collection (WoS) database (txt. file). Duplicates identified were removed before all data were imported into the VOSviewer software (www.vosviewer.com). A bibliographic analysis was performed based on co-occurrence of authors keywords in the paper title (11 949 keywords), using full counting, with a minimum of 20 occurrences in the dataset specified (134 keywords).

2.3. Longitudinal Study

To undertake a review of the literature for the research on "magnetite" over the past three decades, the bibliometric data present in Scopus (which included authors key words) for the topic "magnetite" (accessed on 14th December 2020) was obtained. This data (31 567 publications) was imported into Science Mapping Analysis Software Tool (SciMAT) (https://sci2s.ugr.es/scimat/) for analyses; singular and plural version of the same words were grouped. The publications were arbitrarily assigned to four time periods (1990–1997, 1998–2005, 2006–2013, 2014–2021) so that changes over this chronological period could be analyzed, using the workflow described (**Figure 1**). Normalization was performed using the analysis function focusing on words and specifically authors keywords, with a frequency reduction minimum of 10, a co-occurrence matrix, the edge value reduction of 8, normalization of association strength, simple algorithm centers, and core mapper, with quality measuring h-index and the longitudinal analysis with an evolution map (using Jaccard's Index) and an overlapping map (using Inclusion Index). Important motor-themes were identified by their location in the upper-right hand quadrant of the strategic diagram generated by SciMAT software.

2.4. Systematic Review of Literature

A systematic review of the total available English language peer-reviewed literature on magnetite in a Scopus database (date accessed on 14th December 2020) was carried out on the four main themes (e.g., magnetite AND oxides, 1990–1997) identified in SciMAT. Publications were restricted to the relevant time period related to the motor theme. The publications found were assessed according to the field citation ratio (FCR) for all time periods. A total of 244 publications were included in this analysis. A value for the FCR of greater than 6 (as a proxy indicating peer-acknowledged quality) was used to justify inclusion of a publication in this study. Reviews, editorials, and short communication were excluded from further analysis.

2.5. Author Network and Citation Bursts

Co-authorship networks were constructed in VOSviewer software using the same dataset from the WoS database (new format, RIS file), from the search on "magnetite" (accessed on 14th December 2020). The data was imported into the VOSviewer software, where a bibliographic database search was completed, for co-authorship using full counting method, finding a total of 46 800 authors. The authors were further refined by a minimum of 14 documents and 20 citations per authors (used to as inclusion criteria for peer-acknowledged quality, h-index) resulting in 80 authors meeting this threshold. The authors affiliations and number of citations, along with the affiliated countries were recorded, and the percentage of citations per country were calculated to determine the frequency of "magnetite" research around the world. The percentage of citations per country was calculated and ordered by most to least.

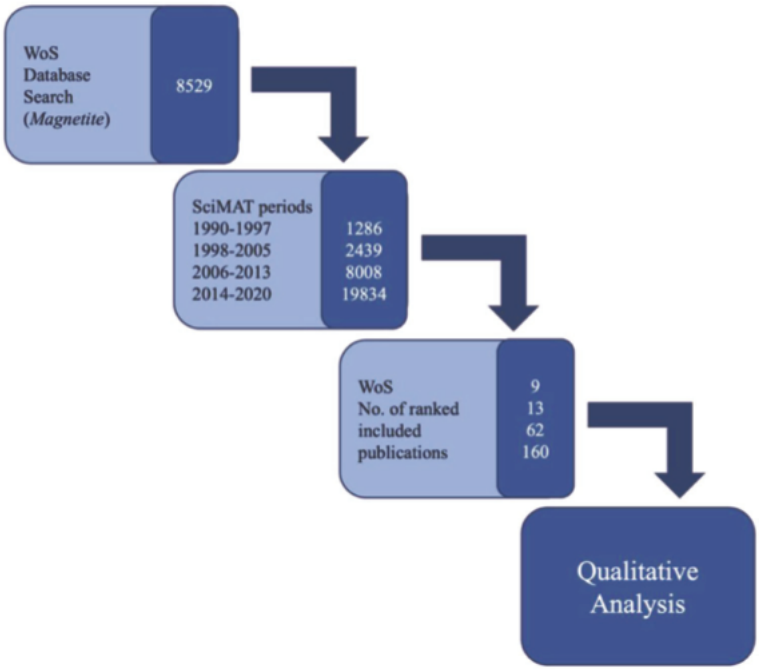

Figure 1. Graphical depiction of the systematic and bibliometric literature review process of the Web of Science (WoS) database (numbers represent the number of papers analyzed at that step).

3. Results

The term "magnetite" was searched in three different databases for scientific literature. A large difference in the number of publications was returned between each database, as seen in **Table 1**. However, the trend for all searches was similar, with the term "magnetite" producing the highest number of publications for all databases. Scopus database returned the highest number (31 567 publications) of publications for all search terms compared to both WoS (8529 publications) and PubMed (938 publications). With the search term of "magnetite AND pathology" returning the smallest number of publications within the Scopus (2121 publications) and WoS (20 publications) database.

Table 1. Summary of the number of papers identified in searches of different databases in the years 1990–2020. Databases Web of Science (WoS), PubMed, and Scopus were accessed on 14th December 2020 and covered the article, title, abstract, and keywords.

Search terms	PubMed	WoS	Scopus
Magnetite	938	8529	31 567
(Magnetite) AND nanoparticle	741	1034	19 007
(Magnetite) AND pollution	22	58	4132
(Magnetite) AND pathology	222	20	2121

3.1. Topic Modelling

The dataset extracted on the PubMed database, from the search term "magnetite" was imported into the SWIFT review software for topic modelling. The articles were triaged based on keywords, categorized into topic models, and organized in ranking order. SWIFT review returned 100 topic models with an overview of the top 19 presented in **Figure 2**. **Table 2** presents the top 19 topic models and includes a summary description of each topic formulated to provide a theme for each model identified (based on the topic model in the review by Reichel et al. 2020).[21] Most of the topics identified are associated with the magnetic properties and applications of MNPs with the latter mostly focusing on advanced imaging techniques. This search was completed to identify the main research themes of MNPs studies conducted from 1990 to 2020, and to identify the main focus and applications of their use.

3.2. Bibliographic Analysis

To examine the growth of literature in research associated with magnetite, the WoS database was used with the search term "magnetite" in the years 1990–2020, yielding 8529 publications. To create a visualization of the co-occurrence of all keyword terms, the extracted dataset (title, abstract, and authors keywords) was

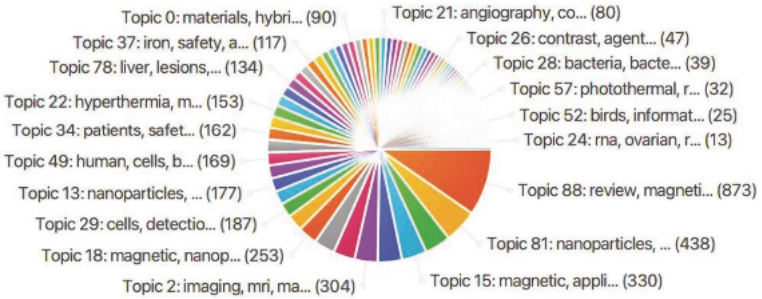

Figure 2. Topic models generated from PubMed dataset (938 publications) by SWIFT review software, using the search term "magnetite." This search was refined to clinical trials, meta-analysis, review, and systematic review articles. Accessed on 14th December 2020.

imported into VOSviewer Software (Universiteit Leiden, Leiden, Netherlands, Version 1.6.15). The main characteristics obtained from an analysis of the co-occurrence of keywords included the frequency and proximity of similar words. The keywords were refined by a minimum of 20 occurrences, resulting in 134 keywords which were organized by VOSviewer into six main clusters, seen in **Table 3**. The main clusters have been organized to provide an overview of the main research that was carried out on "magnetite" from 1990 to 2020. Key discoveries within each cluster were identified with a lay description, seen in Table 3 and in a network visualization map, segregated by colors in **Figure 3**. Cluster 1 (red) is focused on the biomedical applications of MNPs as a drug delivery system in cancer therapies and nanomedicine. Two of the clusters are closely linked to the magnetite formation and methodology used for research purposes (cluster 2 and 4; green and yellow respectively). Cluster 3 (blue) focuses on the

Table 2. Top 19 topic models generated from PubMed dataset (938 publications) by SWIFT review software, using the search term "magnetite." This search was refined to clinical trials, meta-analysis, review, and systematic review articles. The topics have been ordered by number of publications contributing to the topic model in descending order, with topic words and themes established. Accessed on 14th December 2020.

Topic number	Topic words	Number of publications contributing to topic model	Theme of topic model
88	Magnetic, applications, nanoparticles, review, recent, properties, biomedical, advances	873	Biomedical advances
81	Nanoparticles, clinical, applications diagnostics, therapeutics	438	Clinical applications
35	Magnetic, MNPs, biomedical, synthesis, properties, surface, imaging	340	Magnetic imaging properties
15	Iron, oxide, ultrasmall, MRI, superparamagnetic, contrast, imaging	330	Superparamagnetic property as contrast agent
27	Future, research, review, current, function, perspectives	319	Current research
2	Imaging, magnetic, resonance, function, probes, vivo, sensitivity	304	MRI use as contrast agent
23	Iron, oxide, nanoparticles, SPIONs, properties, applications, surface	285	Surface structure and properties
90	Size, magnetite, properties, synthesis, control distribution, specific, range	275	Formation and synthesis
18	Field, separation, particles, fields, external, application, surface, area, magnetic, nanoparticles	253	Conducting properties
3	Drug delivery, targeting, release, targeted, systems, anticancer, nanocarriers	217	Targeted drug delivery
29	Cells, detection, cancer targeting, early, specific, advanced, molecules, tumor, approach	187	Targeted cancer therapy
67	Studies, higher, data, larger, medical, form obtained, initial	178	Research analysis of magnetite
13	Clinical, agent, delivery, magnetic, therapy, gene, potential	177	Gene therapy agent
93	Agents, contrast, imaging, clinical media, tissue, extracellular	172	Clinical use to improve methodology
49	Human, cells, body, in vitro, external, material, found, toxicity, effect, tissues	169	Toxicity of MNPs to human cells
63	Nanoparticles, biological, inorganic, chemical, surface biomolecules, metal additives	169	Surface-functionalized nanoparticles
34	Patients, safety, clinical, adverse, efficacy, event, injection, phase, safe, received	162	Clinical trials for biomedical applications
87	Dose, time, injection, effects, subjects, healthy, volunteers	154	Clinical trials for biomedical applications
22	Hypothermia, magnetic, treatment, cancer, therapy, heat	153	Hyperthermia-based cancer therapy

Table 3. Summary of word clusters identified using VOSviewer and the WoS dataset obtained using a search for the term "magnetite." The network analysis from 8529 publications from 1990 to 2020. The clusters are represented in a visualization map (refer to Figure 3). Accessed on 14th December 2020.

Cluster	Lay/Description	Keywords
1 (red)	Cancer-based therapies	Cancer, contrast agents, design, drug-delivery, efficiency, ferrofluid, functionalization, hyperthermia, in-vitro, magnetite nanoparticles, MRI, release, shape, size, superparamagnetic, therapy, toxicity
2 (green)	Formation, structure, and properties	Behavior, biomineralization, carbon steel, concrete, corrosion, deposition, Fe2O3, hydrogen, kinetics, magnetotactic bacteria, magnetosome formation, microstructure, minerals, Mossbauer spectroscopy, oxidation, phase, surface
3 (blue)	Surface and morphological alterations	Antibacterial activity, chitosan, cytotoxicity, decomposition, gold, graphene, green synthesis, mechanical-properties, microspheres, nanocomposite, nanoparticle, performance, shell, silica
4 (yellow)	Synthesis, magnetic, and physical characteristics. Visualization methods	Conductivity, films, goethite, hematite, hydrothermal synthesis, maghemite, magnetic properties, magnetization, mechanism, Mossbauer, nanostructures, oxide, spectroscopy, system, temperature, transformation, transition, XPS spectra
5 (purple)	Environmental remediator properties and targets	Acid, adsorption, aqueous-solution, catalyst, copper, efficient, heavy-metal ions, humic acid, nanomaterials, nanotechnology, oxides, pH recovery, removal, stability, wastewater
6 (aqua)	Nanoparticle additives, and property characteristics	Carbon, nanotubes, dye, enhancement, graphene oxide, impact, interspecies electron-transfer, ions, methane production, reduction, separation, silver nanoparticles

antibacterial activity, morphology, and composition of MNPs whilst cluster 5 (purple) highlights the chemical adsorbent properties of magnetite in terms of environmental remediation. Cluster 6 (aqua) reveals MNPs additives (e.g., nanocomposites, core–shell, doped, and surface functionalized) for biomedical purposes. This analysis identified nanoparticle engineering enhancements and specific fields using nanotechnology (e.g., as biomedical therapies) which are further investigated.

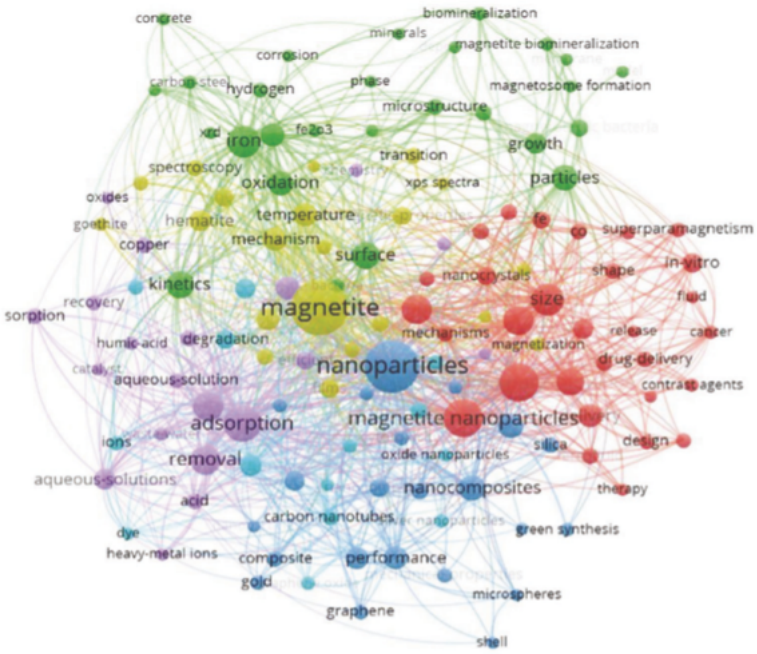

Figure 3. Network visualization map showing six color-coded clusters produced using VOSviewer and the Web of Science (WoS) dataset, with the search "magnetite." The network map shows analysis of 8529 publications from 1990 to 2020. The colors represent the clusters of keywords displayed referred to in Table 3. Accessed on 14th December 2020.

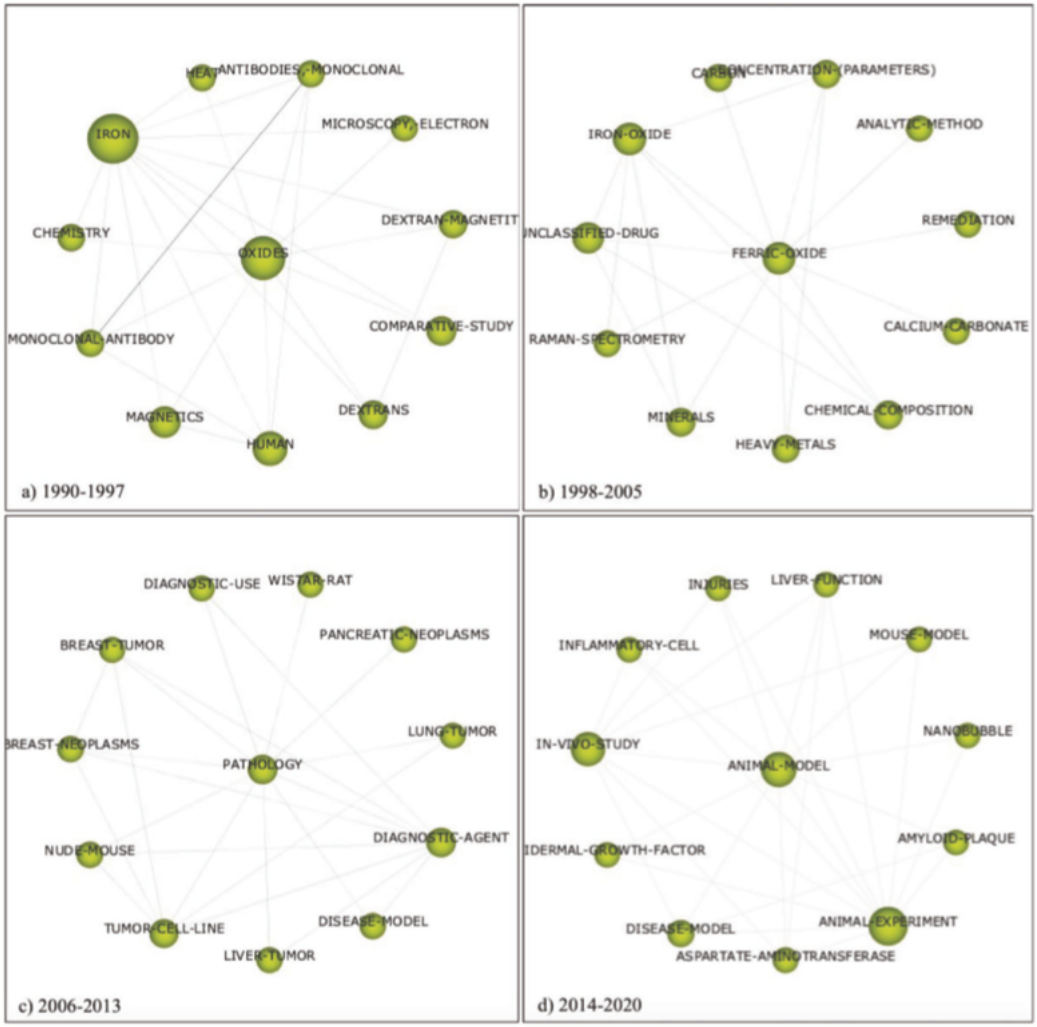

Figure 4. Main themes that emerged in magnetite-related publications extracted from the Scopus database (31 567 publications), over four time periods using SciMAT: a) 1990–1997 (1286 publications); b) 1998–2005 (2439 publications); c) 2006–2013 (8008 publications), and d) 2014–2021 (19 834 publications). The figure shows the links between the keywords within the four major themes identified for each time-period. Accessed on 14th December 2020.

3.3. SciMAT

Scientific research on magnetite has changed significantly over the last three decades, with studies initially investigating the thermal and oxidative properties of MNPs, then shifting focus onto the biomedical applications as a drug delivery and diagnostic agent, eventually looking into the effects of MNPs on the central nervous system, as seen in **Figure 4**. This shift is reflected in the longitudinal study performed using the SciMAT software with the Scopus database (31 567 publications). Between 1990 and 1997 (1286 publications) the term "oxides" is associated with terms like "magnetics," "dextran," and "heat," indicating an additive of dextran coating of MNPs, with electron microscopy appearing as a common technology for sedimentary formation analysis of MNPs.[21] In the period of 1998–2005 (2439 publications) the term "ferric oxide" emerged as the main theme that is associated with words such as "remediation," "unclassified drug," and "carbon." In this period, Raman spectroscopy was a common technology used for soil analysis and chemical composition for remediation

purposes. Of note in this period, studies were beginning to investigate the potential of MNPs as experimental drug delivery agents.

During 2006–2013 (8008 publications) the term "pathology" associated with "diagnostic use" emerged as the major theme. In line with this theme, high-frequency keywords including "tumor" and "diagnostic-agent" were present, with various animal models mentioned ("Wistar rats" and "nude mice") along with tumor cell lines, being used for experimental studies. In 2014–2021 (19 834 publications), analysis showed "animal model" as the main theme in association with terms like "inflammatory cell," "liver function," and "amyloid-plaque" for studies of this period, suggesting that research focused on the role of MNPs in inflammatory and neurodegenerative diseases. The trajectory of MNPs research, initially focuses on the formation and characteristics of doped MNPs, as an anti-cancer agent, eventually leading to the in vivo and in vitro experiments highlighting the potential toxicity and role in neurodegenerative diseases.

3.4. Systematic Review of Literature

The systematic literature analysis, on the Scopus database was completed to provide an analysis of literature from each theme established in the SciMAT search. This yielded a total of 244 scientific publications, refined by a citation ratio of greater than 6 (peer-acknowledged quality threshold). The first time period (1990–1997) produced 9 publications ("oxides"), the second (1998–2005) produced 13 publications ("ferric oxide"), the third time period (2006–2013) produced 62 publications ("pathology"), and the last time period (2014–2020) produced the most with 160 publications ("animal model"), seen in **Figure 5**.

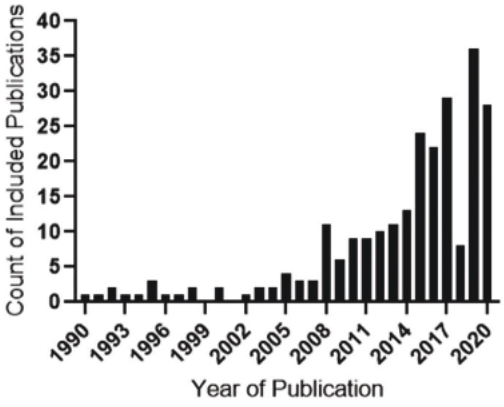

Figure 5. Frequency histogram of 244 publications derived from a systematic search of magnetite literature, conducted in the Scopus database for the search term "magnetite" AND oxides/ferric oxide/pathology/animal model, showing a peak publication between 2015 and 2020. The year 2019 demonstrated the highest number of publications. Accessed on 14th December 2020.

3.4.1. Time Period 1990–1997 (Magnetite and Oxides)

This period yielded nine publications extracted from the literature search with four publications that focused on magnetite formation in sediment and its ability to leach chemical pollutants from soil and groundwater.[25–28] One publication studied magnetite as an oxidizing agent to better understand the reactivity of crystalline iron minerals in marine sediment formation.[26] Two publications focused on magnetite isotope characteristics in sediment for geothermometers to measure temperature in deep sea deposits.[27,28] Three publications focused on the biomedical application of MNPs coated with polypeptide, polyoxymethylene-polypropylene copolymers, ferumoxides, ferumoxtran, or ferumoxsil (dextran coated, dextran covered, or siloxane coated, respectively) found to be superior for MRI contrasting and cell labelling compared to bare superparamagnetic MNPs (SPIONs).[29–31] Last, two publications highlighted the chemical properties and mechanisms of magnetite transitioning between valence states.[26,32] The range of research on magnetite in this period covered many fields with the majority focused on naturally forming magnetite and the mechanistic properties that magnetite particle possess. This period also highlighted the use of coated MNPs as a biomedicine, which are all continued in the successive time periods.

3.4.2. Time Period 1998–2005 (Magnetite and Ferric Oxide)

A total of 13 publications were included in this time period, with some overlapping themes to the previous period; MNPs for environmental remediation and as a contrasting agent for MRI.[33] Five publications highlighted formation, regenerative abilities, and abundance of magnetite in soil, with two studies investigating whether there is a link between the decrease in anerobic respiration, and another study focusing on magnetic properties in soil relating to future environmental change.[34–38] Three publications highlighted environmental remediation studies using of MNPs with hydroxide coatings to extract arsenic and other heavy metals from soil, assessing the effects of particle size, surface texture, and morphology.[39–41] Three publications studied the valence electron transfer mechanism in MNPs coated with various organic compounds and its potential application to have increased regenerative abilities and improved catalytic capacity to increase battery charge.[42–44] Two publications focused on MNPs and its potential as a biomedicine with one study adding bipolar surfactants to the high temperature synthesis reaction resulting in transition from hydrophobic to hydrophilic nanoparticles, increasing dispersibility for biomagnetic applications (e.g., MRI).[45] The second study used surface-functionalized MNPs with hydrophilic organic molecules (e.g., tetramethylammonium hydroxide [$N(CH_3)_4OH$]) and reported enhanced MRI contrasting effects, increase cell viability in in vitro models (monkey kidney Cos-7 cells) and whole human blood samples. The surface modified/functionalized MNPs led to increased dispersion of the nanoparticles, enhancing contrasting abilities.[33] While most of the publications in this period focused on the characterization

and physicochemical biological effects of MNPs in soil and as an environmental remediator, the advancements in the design and engineering of the nanoparticles for biomedical purposes were also significant, the latter being the main theme of research in the next period.

3.4.3. Time Period 2006–2013 (Magnetite and Pathology)

A total of 62 publications were included in this time period, with overlapping themes from the previous period where MNPs were investigated in removing contaminated waste in soil, as MRI contrasting agents and improvements battery life. The studies on the use of MNPs for environmental remediation increased substantially in this period (19 publications) targeting the removal of methylene blue, copper, chromium, arsenic, and chlorophenol as waste contaminants from water and soil.[46–51] These MNPs were coated with various materials (e.g., methylene blue) or as nanocomposites (various compounds incorporated into a matrix of standard materials; ceria/MNPs, graphene oxide/MNPs, and reduced graphene oxide/MNPs) and investigated the nanosheet structure for enhanced catalytic activity to degrade contaminants in soil.[11,47,48,50,52,53]

Three publications referred to MNPs and their role as a biosensor in a variety of biomedical, environmental, and industrial applications. One study utilized MNPs as a colorimetric biosensor, and proved to be extremely sensitive, detecting allergies, toxins in water, and chronic diseases.[54] The second, highlighted graphene oxide/MNPs nanocomposites, found to have improved dispersibility, compared to bare MNPs, thereby increasing electrocatalytic properties, indicating promise for energy.[55] Last, a study used dopamine-coated MNPs, being found to improve electrochemical efficiency and in turn, increasing lithium battery life.[56]

Most of the publications in this period described the biomedical applications of MNPs (31 publications). Many studies (16 publications) focused on improving the design and manufacturing of MNPs so they are more effective in vivo.[52] This was achieved by increasing the surface-to-volume ratio of MNPs and specifically SPIONs, which alter the magnetic property (e.g., as the size decrease, the magnetic anisotropy energy decreases; anisotropy is the energy that keeps the magnetic particles in a certain orientation) of MNPs.[57,58] Studies investigating the morphology of MNPs demonstrated that more compact nano-cubes have less oxygen vacancies and are more stable, compared to more oxygen vacancies, less stable, and less compact nanorods and nanowires.[52,59,60] There is limited evidence to suggest superior morphology, however the most widely used is nano-cubes and nanospheres, with one study suggested that nanowires were extremely effective hyperthermia-based cancer therapy.[57,58] The composition of MNPs is the most commonly cited parameter, which is dependent on the synthesis method (e.g., gas phase, liquid phase, microemulsion, sol-gel, facile and solvothermal, and thermal decomposition), nature of the dopant (e.g., magnetic or non-magnetic), which can affect the stability, dispersibility, coercivity (resistance of a material to changes in magnetization), and functionality of the nanoparticles.[52,61,62] The composition is highly specific for the purpose of the nanoparticles (e.g., core–shell design also impacts the characteristics of MNPs, enhancing biocompatibility) providing another avenue for maximizing coercivity, and therefore biocompatibility.[58,63] Other biomedical applications of MNPs are more specialized, with one publication focusing on surface-functionalized MNPs with protamine sulfate, which gives a cationic surface charge on the magnetic particles, enhancing the transfection efficiency in an in vitro (mouse pLG2 liver cells) and in vivo (BALB/c mice, liver) model based on HVJ-E technology, finding that surface modifications can enhance gene transfer (via magnetic targeting) and potentially overcome gene therapy. Two publications investigated SPIONs, dextran coated (found to increase nanoparticle presence in blood circulation), mesoporous silica, (for controlled drug delivery, isolation of genomic and plasmid DNA), amorphous silica (isolation of biomolecules, drug delivery), and polyethylene glycol[64] as a nanowire (drug delivery agent, targeting drug resistant cancer cells).[60,63,65,66] Coating the MNPs with polymer-like materials (e.g., dextran and PEG) increases the targeting efficiency of SPIONs, showing these coating materials as a potential transport carrier across the blood–brain barrier (BBB).[65] Three publications were found to focus on hyperthermia-based therapies and drug delivery applications, with one publication highlighting core–shell MNPs (used for chemotherapy, radiation, and immunotherapy) and magnetic microcapsules (used for hyperthermia and drug delivery), finding that the latter was highly specific and also remained in circulation for a longer time.[67] Similarly, another publication focuses on the potential for multi-functional modalities of hyperthermia and drug delivery having magnetite as the nanoparticle core with a polymer shell, as a nanocomposite, with targeting agents on the surface. This MNP design allowed for more controlled drug release, increased loading and greater stability of MNPs.[68] Another publication found that nano-cubic iron oxide particles designed specifically for hyperthermia-based therapy demonstrated superior magnetic heating efficiency as the cubic form particles were able to retain heat more readily than other particle shapes of similar size.[69]

One publication reviewed the macrophage recognition to evade the immune response, however also identified the cytotoxic effects of MNPs in vivo (nude mice), finding that oxidative stress was increased, regardless of the composition and even mild exposures of MNPs. The observed toxicity was found to be size-dependent, and if small enough would escape phagocytosis, and lie within macrophages, promoting oxidative stress and reactive oxygen species (ROS) mediated activator protein 1(AP-1) and nuclear factor kappa B (NFκB) activation.[70] This indicates the gaps in knowledge of MNPs as a biomedicine, which is further explored in the following period.

The research on MNPs in this period, provided insight into the physical changes of MNPs, and the physicochemical characteristics of the nanoparticles for specific environmental, biomedical, and industrial application. The various advances in doping, coating and adjusting the size, morphology, and composition in this period was extensive, however the use of nanocomposites prevailed as the most common and effective nanostructure in this period. Combining these manipulations is seen in the later years of this period, which is followed through in the next.

3.4.4. Time Period 2014–2020 (Magnetite and Animal Model): Environmental, Industrial, and Biomedical Applications

This period yielded the highest number of publications (160 publications) making up more than 50% of all included publications in the final literature appraisal. The period also saw the highest number of publications (36 publications) from a single year (2019). The broad themes for this period are again on the environmental and industrial applications, with significant focus on the biomedical applications as well as toxicological studies of air pollutant MNPs. Many studies (nine publications) in this period described the synthesis process, characterization, and engineering of MNPs in nanocomposites.

Publications focusing on the environmental applications of MNPs was the most extensive (76 publications). Research (24 publications) highlighted the ability of graphene oxide, cerium oxide, graphene carbon, silver, silica, carbon, and polymer like/MNPs nanocomposites ability to efficiently adsorb heavy metals (e.g., chromium, lead, copper, caladium, mercury, arsenic, uranium, and nickel), aromatic compounds (e.g., phenazopyridine, tetracycline, and sulfamethazine) and toxic dyes (e.g., methylene blue, organic dyes from polluted waste water, and sediment).[71–80] Microwave adsorption using nanocomposites was also extensively studied (seven publications) with graphene, carbon, yolk–shell, and molybdenum disulfide/MNPs nanocomposites.[81–83] All these nanocomposites have proven to be highly efficient due to the added activated oxygen sites exposed on the surface of these nanocomposites which readily form stable chelates with heavy metal ions and adsorb microwaves.[72,81,84] Other publications (five publications) focused on MNPs with a core–shell of poly(m-phenylenediamine), manganese, and graphene oxide to adsorb/remove pollutants (chromium, cationic dyes, lead, copper, and arsenic) from wastewater.[71,76,85,86] These publications investigated different types of MNPs configuration including nanospheres, nanofibers, nanosheets, nanotubes, nanoflowers, and nanoring, and textured surface for their distinct capacities to remove pollutant moieties.[81,82,84,87–90] The nanosphere structure has been most widely used for this purpose, however nanosheets, nanoflower-like and nanoring structures are highly efficient adsorbers as more surface area increases active sites. Similarly, the more porous a surface the more adsorptive.[81,82,88,90–92]

Many of the advances used for environmental applications of MNPs are also used for industrial applications focusing on renewable energy, with one publication using the catalytic nature of MNPs to increase methanogenic propionate degradation for renewable energy production.[93] Nanocomposites are also widely used in this field with graphene oxide, sodium potassium, and graphene aerogel combined with MNPs for enhanced electrochemical conductivity and supercapacitor performance (for efficient energy storage and usage).[94–96] Other studies used MNPs nanocomposites with lithium–sulfur (enhanced electrical conductivity, improved battery life in lithium ion batteries) and polymethyl methacrylate- functionalized MNPs (found to be flame retardant and be efficient electromagnetic wave adsorbents) as the structure enabled greater dispersion, and recyclable ability.[94]

The biomedical applications of MNPs in this period are extensive, with subtopics reappearing in this period like contrasting agents, applications for therapy in cancer and drug delivery agents. MNPs as a contrasting agent in this period, focused on SPIONs, with one study using a small SPION agents (coated with carbohydrates), ferumoxide, which can be taken up by macrophages and the reticuloendothelial system to image lymph nodes and certain tumors for MRI imaging up to 11 months after injection.[97] Other studies have tested core–shell SPIONS coated with amino-functionalized octahedral carboxylate shells, further functionalized with PEG. This modification increased sensitivity, low toxicity, good biocompatibility, and degradability both in vitro (KB cells – human epithelial carcinoma cells) and in vivo (BALB/C mice bearing KB tumors) making it a promising MRI contrasting agent.[21,98] Last, hyaluronic acid-modified MNPs/Gold (core/shell) nanostars were investigated in in vitro (U87MG cells) and in vivo (BALB/c nude mice) models as an imaging and photothermal therapy of tumors, finding that the nanoparticles are water dispersible, colloidally stable, and biocompatible and therefore have great potential as a contrasting agent.[99]

The use of MNPs as cancer treatments and drug delivery agents are extensively investigated in this period. Many studies (ten publications) highlighted the use of MNPs in various forms (magnetite fluid, hyaluronic acid-modified magnetite gold core/shell, coated with PEG, as ferumoxytol and SPIONs), which accumulate in and around the tumor effectively killing the cancer cells.[21,99–103] The photothermal nature (Fenton reaction) of MNPs initiate the production of ROS and the application of heat which work to kill cancer cells have been seen in in vitro (A549 cells and MMTV-PrMT-derived mammary carcinoma cells) and in vivo (female FVB/N mice) models as well as early mammary cancers and cancer metastases in the liver and lungs.[16,104–106] These studies found that the biocompatibility and physiological stability was improved, along with faster clearance enhanced permeability.[101,107,108] Other publications used mesoporous silica (further functionalized with PEG) and gold, polymer-like shell loaded with doxorubicin that enhanced MNPs photothermal efficiency in killing cancer cells.[5,109,110] Using MNPs as a diagnostic testing tool have been studied with immobilized surface antigen Hepatitis B on the surface of carbon-coated MNPs for better detection of Hepatitis B in serum and protein for diagnostic use.[111]

Other biomedical applications of note in this period focus on the immune response, bone regeneration, and diagnostic testing methods. One publication uses MNPs' surface functionalized with oleic acid to form a complex that is able to diagnose egg allergies.[112] Another study uses dextran-coated SPIONs core–shell nano-worms incubated in human serum, to aid the in removal of proteins which may trigger an immune response to allergies, offering sight into safer nanomedicines for human subjects.[113] MNPs have also been used for bone regeneration studies, using porous poly-lactide/polyglycolic acid (PLLA/PGA)/MNPs nanocomposite to stimulate bone regeneration, tested on in vitro (MG63 cells) and in vivo (New Zealand white rabbits) models, finding that the bone tissue formation was significantly accelerated, along with increase cell proliferation and differentiation.[114] Of particular interest is the synthesis of molecularly imprinted magnetite nanozymes, with one publication finding that it can improve specificity, activity, and mimic peroxidase-like activity as a drug delivery method, and another

study using a nanozyme MNPs/carbon core–shell nanocomposite, in the form a nanowires, for an assay to enhance signal amplification, and detection of platelet-derived growth factor, in human serum samples in order to replace more costly.[115,116] Another study used PEG-coated MNPs, for the detection of hydrochlorothiazide (anti-hypertensive agent) from human urine as a low cost, water compatible, and environmentally friendly method.[117] It is apparent that advances in nanoparticle engineering and their exploitation of the physicochemical characteristics in conjunction with many other compounds for customized biological functions, has driven the significant progress of MNPs biomedical research in this period.

The advancements of nanoparticle engineering in this period are clear, with the extensive use of surface-functionalized, coated, nanocomposite or a combination of these structural components. The biomedical applications of MNPs in this period are of particular interest, showing improvements in drug delivery, and cancer therapies, but also incorporating MNPs in a wide range of diagnostic testing methods, along with aiding and evading the immune response (e.g., allergies and antimicrobial resistance).

3.4.5. Time Period 2014–2020 (Magnetite and Animal Model): Toxicity

In relevance to the in vivo studies, toxicity publications (two publications) also surfaced in this period, describing the potential impact of MNPs use on human health. As the extensive use of MNPs in various fields is established, the studies show that nanoparticles including MNPs, may be toxic in many fields that use them. With publications finding the potential genotoxic (toxic to DNA) effects of MNPs with various coatings; polyaspartic acid (bone marrow cells), silica oxide (Hep3B cells), dextran (MCL5 human lymphoblastoid cell line), and bare MNPs (L-929 murine fibroblasts).[118–122] Of concern is bioaccumulation, biodistribution, and toxicity of various nanoparticles showing damage to cell membranes by increasing permeability, inducing cytotoxicity, and in the environment, inhibiting photosynthesis.[12,123] Scholarly research has also investigated the long-term repercussions of MNPs, those originating from anthropogenic sources, in neurodegenerative diseases. Ultrafine air pollutant MNPs have been previously implicated in cardiovascular diseases and neurodegenerative diseases (i.e., AD), as particles smaller than ≈200 nm can enter the heart via the circulatory system, and the brain via the olfactory nerve through the BBB.[124,125] One publication detected presence of MNPs in the brains of AD patients, deducing that the nanoparticles were inhaled air pollutants with distinct spherical morphology and smooth surface texture unlike those of biological origins (from iron metabolisms) with octahedral morphology.[21] Excess magnetite in the brain causes toxicity, increasing oxidative stress, and ROS, found to be near amyloid-beta (Aβ) fibrils in the AD brain.[24,125–128] The toxicity studies highlighted the extensive use of MNPs in a variety of fields and their impact on human health, which is consistent with the recent evidence that air pollutant MNPs have been implicated in various diseases, including neurodegeneration (i.e. AD).

Table 4. Top 13 countries with the highest percentage of citations (minimum 20) and publications (minimum 14) of authors, grouped by country affiliations and in descending order. Extrapolated from the dataset obtained from the Web of Science (WoS) database using the term "magnetite" in the years 1990–2020. Accessed on 14th December, 2020.

Rank	Country of affiliation	Number of citations	% Citations
1	Japan	8331	22%
2	China	7826	21%
3	Germany	4704	13%
4	USA	4064	11%
5	Iran	2279	6%
6	France	1685	5%
7	Romania	1337	4%
8	Brazil	1091	3%
9	Singapore	821	2%
10	UK	752	2%
11	Hungry	530	1%
12	Korea	492	1%
13	Spain	472	1%

3.5. Author Network and Countries with Most Citations For "Magnetite" Research

Over the past 30 years, the direction of research into magnetite has been influenced by the catalytic and kinetic properties of magnetite, which has enabled the extensive application in the environmental, industrial, and biomedical fields, due to the advancements in technologies to direct the research through its manipulation for specific applications across various fields. To evaluate the authors involved in the advancements of magnetite research, an author network was established using VOSviewer software with the dataset obtained from the search "magnetite" in the years 1990–2020 from the WoS database (8529 publications). A bibliographic analysis for co-authorship (full counting method) refining authors with a minimum of 14 documents and 20 citations per author (used to as inclusion criteria for peer-acknowledged quality, h-index) resulted in 80 authors meeting this threshold.[129] Figure S1, Supporting Information, represents these authors in an overlay visualization network providing the years in which these authors have published. The author's affiliations and number of citations were recorded and the percentage of citations per country was calculated and ordered by most to least citations (**Table 4**).[130] The top 13 countries were established, showing the highest number of citations from Japan (22%), followed closely by China (21%), suggesting that these countries have led the world in magnetite research over the past 30 years. Other countries like Germany (13%), USA (11%), Iran (6%), France (5%), Romania (4%), Brazil (3%), Singapore, United Kingdom (2%), Spain, Hungary, and Republic of Korea (1%) have also contributed to magnetite research over the past 30 years.

4. Discussion

This systematic literature analysis revealed that scholarly studies on "magnetite" have been increasing worldwide with

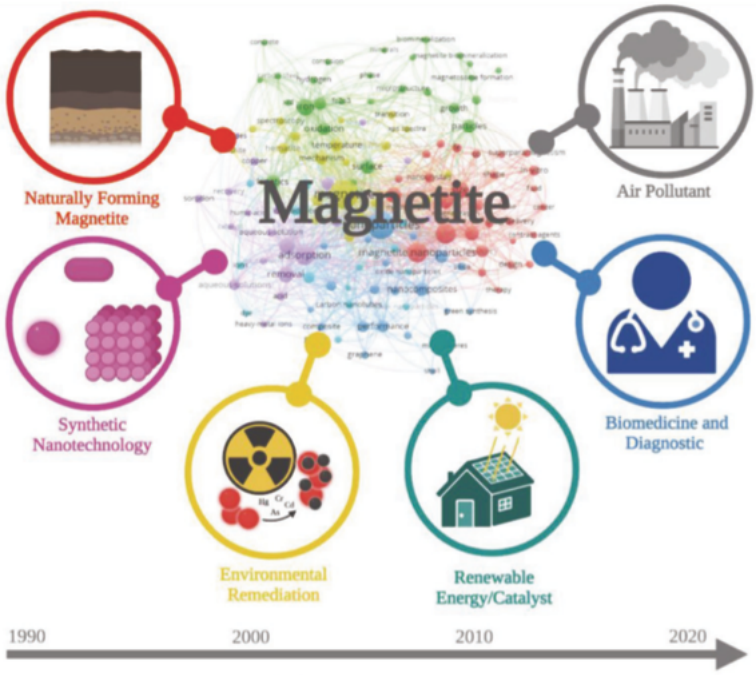

Figure 6. Timeline showing research on magnetite nanoparticle shifting from 1990 to 2020.

the highest percentage of publications originating from Japan and China. The results show that research on "magnetite" have shifted over the last 30 years (**Figure 6**), from initially focusing on the formation of naturally occurring magnetite, into the synthetic development and manipulation of nanoparticles for various environmental, industrial, and biomedical applications. Ultimately, to the advancements in biomedical applications which uncover the potential toxicity of MNPs and air pollutant MNPs being implicated in various diseases including neurodegeneration and AD.[24,126,131] Progress in MNP engineering has allowed applications in environmental remediation, batteries and solar cell, diagnostic and cancer therapy applications through tuning of the nanoparticles size, shape, and surface components, as well as, equally important, the development of MNPs core–shell, nanocomposite, and hybrid nanostructures.

The VOSviewer software was used to analyze literature and identify clusters, highlighting magnetite research which focused on the kinetic and catalytic properties of MNPs, the adsorptive abilities, and remediation targets as an environmental tool and the biomedical applications of MNPs (largely cancer-based therapies highlighting the surface and morphological alterations). The literature analysis using SciMAT software established themes for each time period; the first time period from 1990 to 1997 identified magnetite AND oxides, with environmental remediation and biomedical applications of MNPs as the main themes. The environmental studies in this period mainly described magnetite distribution in soil, its crystalline reactivity structure and its ability to adsorb contaminants (e.g., arsenic).[25–27] The biomedical applications of MNPs in this period are most interesting, with most publications referring to doped/coated MNPs. Doping is a widely used method for modifying the nanoparticles to enhance their electrical, optical, and biological activities.[132,133] Doping provides more stability to the nanoparticle structure, as the dopant increases the hydrophilicity of the nanoparticle, therefore increasing dispersibility and in turn reducing cytotoxicity, thus improving biocompatibility.[134] There are various synthesis methods, and parameters (e.g., temperature, dipping time, and nature of surfactant) that affect the coating thickness, and therefore the overall size of the nanomaterial. For example, increasing concentration of silica (i.e., thicker coating) allows greater dispersion of nanoparticles and enhanced MRI contrasting performance with the use of an external magnetic field.[65] Organic compounds, including surfactants and polymers represent a good choice for coating MNPs. In particular, coating with dextran, a complex branched polysaccharide polymer chain unit of various lengths (from 1 000 000 000 Da), has surfaced as advantageous with its biodegradable and water-soluble properties further enhancing MNP biocompatibility.[135] Coating with dextran 1) prevented nanoparticle agglomeration and toxicity of magnetic particles and 2) increased dispersibility and rapid clearing by macrophages from the blood, liver, spleen, and lymph nodes, compared to bare MNPs.[29,136] Dextran is unique as it allows magnetite's magnetic structure to be extremely strong at the surface where

strong magnetic disorder is usually occurs.[135] Doping/coating of MNPs is observed to be extremely useful finding that there is reduced cytotoxicity, and consequently improving the potential application for diagnostic and therapeutic purposes, which is further investigated in later time periods.[137]

The studies in the second period (1998–2005) focus primarily on the environmental and biomedical applications of MNPs, particularly focusing on the engineered surface chemistry. Both fields further explore the effects of coated MNPs, with adjustments to the surface (surface functionalization/modification) and morphology of the nanostructures. The environmental application of hydroxide-coated MNPs indicated that the cubic spinel structure of MNPs (a cubic lattice structure, whereby Fe (III) ions occupy the tetrahedral and octahedral sites) renders the nanoparticles more hydrophilic and therefore, dispersing relatively easily in aqueous biological systems, enhancing the adsorptive properties. This is consistent with a hydrophilic polymer (polyethylene oxide)-coated MNP study, in which the adsorption of heavy metals was improved due to the increased dispersion rate in solution.[138] The biomedical applications exploring surface modification/functionalization in this period is extensive, specifically referring to the surface chemistry (i.e., increasing, decreasing, or neutralizing the surface charge) which strongly influences the properties of the system (e.g., polymers, small molecules, surfactants, dendrimers, and biomolecules).[139–141] This occurs through the treatment of nanoparticles with specific agents, and is extremely valuable in enhancing cellular utilization, cellular uptake, decreased toxicity, improved binding capacity, enabling selectivity and specificity, with longer retention time, or non-interactions (for evading the immune response) depending on its specific function.[139,140] Polymer surface-functionalized NPs are extremely versatile, with the hydrophilic coating allowing increased circulation time. One study used dextran-coated cross-linked (altering the charge to be more positive) surface-modified MNPs, which reduced drug concentrations at non-target sites, due to increased dispersibility, overall resulting in fewer drug side effects.[141] Another study used surface modification of MNPs with antibiotics, revealing that they could bind to bacterial cell walls, altering the cell wall integrity, due to its positive charge, demonstrating effective antimicrobial abilities. This was found to improve the antimicrobial inhibition against the pathogenic bacteria *Escherichia coli*, *Staphylococcus aureus*, and *Pseudomonas aeruginosa*.[140,142] Like doping or coated additives, surface modification/functionalized, also increases biocompatibility by altering the surface charge, and the nanoparticles can disperse more easily, and evade the immune response, due to the biocompatible additives on the surface, increasing reactive sites and for biomolecule attachments. This is further examined in later time periods, targeting the immune system, transportation of modulating agents, and as potential vaccines.[143]

In the 2006–2013 period, studies on MNPs focused on various morphological additives, particularly the use of nanocomposites due to the small size, increased dispersibility, enhanced adsorption, and solar energy function for environmental and industrial applications.[54] Nanocomposites are nanoparticles incorporated into a matrix, displaying improvements in thermal stability, increased surface defects, chemical resistance, and improved electrical conductivity.[47] For example, graphene oxide/MNP and polymers/MNP nanocomposites were found to have increased adsorptive capabilities of heavy metals and aromatic compounds, due to the increased surface area (increased surface defects) of this matrix structure.[79,81,144] The biomedical applications of MNPs, was the major research theme in this period, with MNP nanocomposites also being considerably investigated. The use of nanocomposites have been found to be superior to doped/coated nanoparticles, as they behave more similarly to superparamagnetic nanomaterials, with a study displaying that polymer-like (PLGA)/MNP nanocomposites are more effective tumor targeting MRI contrasting agents compared to dextran-coated MNPs of similar size.[145] Another study using mesoporous dye-doped silica MNP nanocomposites, loaded with doxorubicin (potent anti-cancer drug), found an improvement in MRI contrasting and tumor targeting abilities, whilst also being able to induce targeted cancer cell death.[63] The combination of adding various nanoparticles into a nanocomposite structure, offers unique properties that are suggested to arise from the interactions of these materials in the matrix. This further proves the advancements in nanotechnology engineering with improved thermal stability, dispersibility, and increased surface exposure, thereby improving compatibility as a biomedicine, which is further explored in the successive time-period, targeting the immune system, transportation of modulating agents, but also as potential vaccines.[143]

The most recent 2014–2020 period showed a shift in MNPs research with less proportion of publications dedicated on environmental remediation, and a clear surge in industrial and biomedical applications. MNP nanocomposite structures are again explored in this period, however there is a trend in studies focusing on the advancement in combining two or more additives (e.g., coating/doping, core–shell, and surface modification/functionalized) into nanocomposite matrix, termed "hybrid." The nanocomposite hybrid was investigated for industrial applications with one study, using lithium–sulfur-coated MNP nanocomposites, surface functionalized with carbon, finding that the catalytic activity excelled due to the increased surface defects, enhancing recovery rate, thereby increasing battery life.[146] In addition to focusing on the nanocomposite structure, the biomedical applications of MNPs in this time period, also focus on the MNP hybrid nanocomposites as more efficient contrasting agents for MRI and drug delivery agents for cancer therapies (e.g., hyaluronic acid-modified gold/MNPs nanocomposites) but extending further into the biomedical field by advancing the engineering of nano systems to overcome immunological barriers.[99] The immune system responds to nanoparticles triggered through mechanisms that recognize surface molecules, peptides, or foreign materials, modulating an immune response based on the size, morphology, surface characteristics, and charge of the nanostructure. Therefore, evading the immune response relies on several properties of nanotechnological engineering, for example, reducing nanostructure size, adjusting morphology to a more biocompatible shape (i.e., nanosphere compared to nanocubes), and adding surface additives that increase the circulation time and overall biocompatibility.[147] The manufacturing additives that can be applied to MNPs nanocomposites amplify the "stealth" ability, increasing circulation time, by which point they can provide active and specific targeting in the

body.[148] One study found that poly(caprolactone)-coated MNPs loaded with doxorubicin hydrochloride, further surface functionalized with Arg–Gly–Asp enzymes, behaved like SPION nanocomposite microspheres, enhancing circulation time, whilst also exhibiting a quick magnetic response, advantageous for controlled drug release at tumor target site.[149] This further confirms MNP nanocomposite hybrids as promising cancer and immune-modulatory therapies. The development of nanotechnology in the past three decades, has discovered the study of nanoparticle additives and most recently nanocomposite hybrids appear to fulfil the growing needs of multifunctional materials, being extremely versatile, with the most increased dispersion and retention rate, as well as the binding force and wear of the nanostructure.[150]

Toward the final years of the 2014–2020 period, several research inquiries reported potential toxic effects of MNPs, being implicated with the environmental and biomedical applications. For example, the use of MNPs for environmental remediation used in wastewater and sediment treatment has led to extensive run off leading to an accumulation in aquatic environments. This accumulation leads to ROS/reactive nitric species (RNS) production, causing damage to exposed organisms, stimulating delays of hatching, damage in cell wall and outer membranes, and depletion of oxygen exchange and hypoxia to an in vitro model (rainbow trout spermatozoon).[151] For biomedical applications, the cytotoxic effect of MNPs were tested using in vivo and in vitro models showing activation of AP-1 and NFκB pathways that subsequently results in increased oxidative stress and induced apoptosis regardless of dosage or composition.[70,152] MNPs coated with oleic acid and silica, were found to exhibit cytotoxicity in in vitro models (human neuroblastoma SH-SY5Y and glioblastoma A172 cells) through a decrease in cell viability.[153] Similarly, MNPs coated with silica and polymer-like materials for the purpose of cell labelling and hyperthermia treatments were also found to permeate cells, accumulating and causing cellular dysfunction.[154] While these studies show the disadvantages of MNPs, the cytotoxic effects were shown to be dose dependent, with one study finding that MNPs cause toxicity to an in vitro model A549 cell line only at concentrations of greater than 50 $\mu g\ mL^{-1}$ and that silica-coated MNPs caused cellular dysfunction by impairing cellular adhesion properties at 0.1 $\mu g\ \mu L^{-1}$.[152,154] Therefore, establishing a safe and effective dose of MNPs as a biomedicine should be more closely investigated to prevent adverse side effects.

Toxicity studies also focused on the biological effects of air pollutant MNPs, more specifically on their potential links with the progression of neurodegenerative diseases like Parkinson's disease and AD.[3,155] Biogenic magnetite can be found in a wide range of organisms from bacteria to animals, including humans.[156] Physiologically biogenic magnetite has been found to aid in the biological metabolism of iron.[20,157] Interestingly, Maher and colleagues showed that anthropogenic (synthetic) MNPs can be found in abundance in the brains of people suffering from AD, distinguished by differences in their morphology to biogenic MNPs.[21] MNPs, like other air pollutant particulate matter, is formed through frictional pressure at high temperatures. It is therefore no surprise that MNPs can be found in abundance in automotive diesel exhaust, grinding of trains on railway lines, welding factories, petroleum exhaust, and coal emission.[158] Due to the formation process of these air pollutant MNP (<200 nm), they can migrate into the central nervous system via the nasal canal and olfactory bulb.[155] Inhaled air pollutant nanoparticles in the brain tissues are thought to trigger ROS/RNS production, leading to oxidative stress.[159–161] This increase in oxidative stress, is believed to further contribute to chronic inflammation, and consequently increase Aβ fibril formation found near Aβ plaques in AD, however, this is not confirmed. Therefore, consequent future studies should focus on understanding the effects of air pollutant MNPs in neurodegenerative diseases including AD.

5. Conclusion

In summary, the scholarly research on magnetite over the last three decades has generated knowledge of how the characteristics of MNPs affect the nanoparticle physical, catalytic, and biological activities, and in turn, how the knowledge is being used to guide the engineering of the nanoparticles for specific environmental, industrial, and biological applications.[106] For the latter, being the most explored applications of MNPs, the tuning of the nanoparticle characteristics is also aimed to optimize biocompatibility, more specifically, for less aggregation, lower toxicity as well as enhancing cellular targeting and uptake, for use in disease diagnostic and therapy.[162] Optimizing the engineering of NPs for biomedical applications has proven difficult, with the ability of the NPs to remain in circulation to achieve a desired goal, and on the other hand remaining too long in circulation causing toxicity, is a balance that has yet to be perfected. Future applications of MNPs in the biomedical field should focus on adjusting the size and morphology of the nanostructure, the "stealth" mechanism to evade the immune response which makes them an effective therapy or detection of human diseases. Considering the increasing evidence on the roles of air-pollutant MNPs and the onset and progression of neurodegenerative diseases, the next phase of research should also focus on elucidating the exact mechanisms of the nanoparticle-induced stress, including activation of inflammatory markers, while also focusing on epidemiology studies to determine any correlation between highly polluted sites and disease prevalence.

Supporting Information

Supporting Information is available from the Wiley Online Library or from the author.

Acknowledgements

C.G. and K.C.M. share senior authorship. The authors would like to acknowledge the use of BioRender.com for the creation of Figure 6. This research was supported by Australian Government Research Training Program Scholarship.

Conflict of Interest

The authors declare no conflict of interest.

Data Availability Statement

The data that supports the findings of this study are available within the article itself.

Keywords

applications, bibliometrics, composition, magnetite, nanoparticles, reviews

Received: February 10, 2022
Revised: August 9, 2022
Published online:

[1] B. Dubois, H. Hampel, H. H. Feldman, P. Scheltens, P. Aisen, S. Andrieu, H. Bakardjian, H. Benali, L. Bertram, K. Blennow, *Alzheimer's Dementia* **2016**, *12*, 292.
[2] J. E. Kostka, K. H. Nealson, *Environ. Sci. Technol.* **1995**, *29*, 2535.
[3] C. Su, *J. Hazard. Mater.* **2017**, *322*, 48.
[4] A. Akbarzadeh, M. Samiei, S. Davaran, *Nanoscale Res. Lett.* **2012**, *7*, 144.
[5] C. A. Gorski, *Ph.D. Redox Behavior of Magnetite in the Environment: Moving Towards a Semiconductor Model*, The University of Iowa **2009**, p. 238.
[6] S. Gul, S. B. Khan, I. U. Rehman, M. A. Khan, M. I. Khan, *Front. Mater.* **2019**, *6*, 15.
[7] A. F. White, M. L. Peterson, *Geochim. Cosmochim. Acta* **1996**, *60*, 3799.
[8] S. R. Kanel, J.-M. Grenèche, H. Choi, *Environ. Sci. Technol.* **2006**, *40*, 5.
[9] K. Chen, J. He, Y. Li, X. Cai, K. Zhang, T. Liu, Y. Hu, D. Lin, L. Kong, J. Liu, *J. Colloid Interface Sci.* **2017**, *494*, 307.
[10] M. Kumari, C. U. Pittman, D. Mohan, *J. Colloid Interface Sci.* **2015**, *442*, 120.
[11] L. Ai, C. Zhang, Z. Chen, *J. Hazard. Mater.* **2011**, *192*, 1515.
[12] R. Deng, D. Lin, L. Zhu, S. Majumdar, J. C. White, J. L. Gardea-Torresdey, B. Xing, *Nanotoxicology* **2017**, *11*, 591.
[13] Y. S. Kim, N. H. A. Raston, M. B. Gu, *Biosens. Bioelectron.* **2016**, *76*, 17.
[14] S. Gul, S. B. Khan, I. U. Rehman, M. A. Khan, M. I. Khan, *Front. Mater.* **2019**, *6*, 179.
[15] J. Xie, Z. Shen, Y. Anraku, K. Kataoka, X. Chen, *Biomaterials* **2019**, *224*, 119491.
[16] S. Zanganeh, G. Hutter, R. Spitler, O. Lenkov, M. Mahmoudi, A. Shaw, J. S. Pajarinen, H. Nejadnik, S. Goodman, M. Moseley, L. M. Coussens, H. E. Daldrup-Link, *Nat. Nanotechnol.* **2016**, *11*, 986.
[17] E. R. Flynn, H. C. Bryant, *Phys. Med. Biol.* **2005**, *50*, 1273.
[18] G. Y. Lee, W. P. Qian, L. Wang, Y. A. Wang, C. A. Staley, M. Satpathy, S. Nie, H. Mao, L. Yang, *ACS Nano* **2013**, *7*, 2078.
[19] H. S. Sharma, P. K. Menon, J. V. Lafuente, Z. P. Aguilar, Y. A. Wang, D. F. Muresanu, H. Mössler, R. Patnaik, A. Sharma, *J. Nanosci. Nanotechnol.* **2014**, *14*, 577.
[20] F. Dilnawaz, S. K. Sahoo, *Drug Discovery Today* **2015**, *20*, 1256.
[21] H. Gao, Z. Pang, X. Jiang, *Pharm. Res.* **2013**, *30*, 13.
[22] H.-W. Huang, M. S. Sakar, A. J. Petruska, S. Pane, B. J. Nelson, *Nat. Commun.* **2016**, *7*, 10.
[23] M. L. Block, L. Calderón-Garcidueñas, *Trends Neurosci.* **2009**, *32*, 506.
[24] B. A. Maher, I. A. Ahmed, V. Karloukovski, D. A. MacLaren, P. G. Foulds, D. Allsop, D. M. Mann, R. Torres-Jardón, L. Calderon-Garciduenas, *Proc. Natl. Acad. Sci. USA* **2016**, *113*, 10797.
[25] M. W. Hitzman, N. Oreskes, M. T. Einaudi, *Precambrian Res.* **1992**, *58*, 241.
[26] J. E. Kostka, G. W. Luther, *Geochim. Cosmochim. Acta* **1993**, *58*, 9.
[27] Z. D. Sharp, *Geochim. Cosmochim. Acta* **1990**, *54*, 1353.
[28] Z. Yong-fei, *Geochim. Cosmochim. Acta* **1991**, *55*, 2299.
[29] C. W. Jung, P. Jacobs, *Magn. Reson. Imaging* **1995**, *13*, 661.
[30] F. C. Meldrum, B. R. Heywood, S. Mann, *Science* **1992**, *257*, 2.
[31] C. Chouly, D. Pouliquen, I. Lucet, J. J. Jeune, P. Jallet, *J. Microencapsulation* **1996**, *13*, 245.
[32] D. J. Andersen, D. H. Lindsley, P. M. Q. Davidson, *Comput. Geosci.* **1993**, *19*, 1333.
[33] F. Y. Cheng, C. H. Su, Y. S. Yang, C. S. Yeh, C. Y. Tsai, C. L. Wu, M. T. Wu, D. B. Shieh, *Biomaterials* **2005**, *26*, 729.
[34] J. K. Fredrickson, J. M. Zachara, D. W. Kennedy, H. Dong, T. C. Onstott, N. W. Hinman, S.-m. Li, *Geochim. Cosmochim. Acta* **1998**, *62*, 3239.
[35] B. A. Maher, *Palaeogeogr., Palaeoclimatol., Palaeoecol.* **1998**, *137*, 25.
[36] S. W. Poulton, D. E. Canfield, *Chem. Geol.* **2005**, *214*, 209.
[37] R. W. White, R. Powell, T. J. B. Holland, B. A. Worley, *J. Metamorph. Geol.* **2000**, *18*, 497.
[38] R. R. Moskalyk, A. M. Alfantazi, *Miner. Eng.* **2003**, *16*, 793.
[39] D. A. Jones, T. P. Lelyveld, S. D. Mavrofidis, S. W. Kingman, N. J. Miles, *Conserv. Recycl.* **2002**, *34*, 75.
[40] S. Dixit, J. G. Hering, *Environ. Sci. Technol.* **2003**, *37*, 7.
[41] S. R. Kanel, B. Manning, L. Charlet, H. Choi, *Environ. Sci. Technol.* **2005**, *39*, 1291.
[42] A. Hu, G. T. Yee, W. Lin, *J. Am. Chem. Soc.* **2005**, *127*, 12486.
[43] A. Ohtomo, H. Y. Hwang, *Nature* **2004**, *427*, 423.
[44] D. Beydoun, R. Amal, G. K. C. Low, S. McEvoy, *J. Phys. Chem. B* **2000**, *104*, 4387.
[45] S. Sun, H. Zeng, D. B. Robinson, S. Raoux, P. M. Rice, S. X. Wang, G. Li, *J. Am. Chem. Soc.* **2004**, *126*, 273.
[46] J. Li, S. Zhang, C. Chen, G. Zhao, X. Yang, J. Li, X. Wang, *ACS Appl. Mater. Interfaces* **2012**, *4*, 4991.
[47] S. C. N. Tang, I. M. C. Lo, *Water Res.* **2013**, *47*, 2613.
[48] L. Xu, J. Wang, *Environ. Sci. Technol.* **2012**, *46*, 8.
[49] D. J. Frost, C. A. McCammon, *Annu. Rev. Earth Planet. Sci.* **2008**, *36*, 389.
[50] V. Chandra, J. Park, Y. Chun, J. W. Lee, I.-C. Hwang, K. S. Kim, *ACS Nano* **2010**, *4*, 3979.
[51] M. Hua, S. Zhang, B. Pan, W. Zhang, L. Lv, Q. Zhang, *J. Hazard. Mater.* **2012**, *211–212*, 317.
[52] A. S. Teja, P.-Y. Koh, *Prog. Cryst. Growth Charact. Mater.* **2009**, *55*, 22.
[53] K. A. Deo, G. Lokhande, A. K. Gaharwar, in *Encyclopedia of Tissue Engineering and Regenerative Medicine* (Ed: R. L. Reis), Academic Press, Oxford **2019**, pp. 21–32.
[54] D. Quesada-González, A. Merkoçi, *Biosens. Bioelectron.* **2015**, *73*, 47.
[55] H. Teymourian, A. Salimi, S. Khezrian, *Biosens. Bioelectron.* **2013**, *49*, 1.
[56] C. Lei, F. Han, D. Li, W.-C. Li, Q. Sun, X.-Q. Zhang, A.-H. Lu, *Nanoscale* **2013**, *5*, 1168.
[57] M. Mahdavi, M. B. Ahmad, M. J. Haron, F. Namvar, B. Nadi, M. Z. Rahman, J. Amin, *Molecules* **2013**, *18*, 7533.
[58] A. G. Kolhatkar, A. C. Jamison, D. Litvinov, R. C. Willson, T. R. Lee, *Int. J. Mol. Sci.* **2013**, *14*, 15977.
[59] C. Pereira, A. M. Pereira, C. Fernandes, M. Rocha, R. Mendes, M. P. Fernández-García, A. Guedes, P. B. Tavares, J.-M. Grenèche, J. P. Araújo, C. Freire, *Chem. Mater.* **2012**, *24*, 1496.
[60] Z. Wang, S. Lee, K. Koo, K. Kim, *IEEE Trans. NanoBioscience* **2016**, *15*, 186.
[61] J. Liu, Z. Sun, Y. Deng, Y. Zou, C. Li, X. Guo, L. Xiong, Y. Gao, F. Li, D. Zhao, *Angew. Chem., Int. Ed.* **2009**, *48*, 5875.
[62] W. M. Saslow, in *Electricity, Magnetism, and Light* (Ed: W. M. Saslow), Academic Press, San Diego **2002**, pp. 384–418.
[63] J. E. Lee, N. Lee, H. Kim, J. Kim, S. H. Choi, J. H. Kim, T. Kim, I. C. Song, S. P. Park, W. K. Moon, T. Hyeon, *J. Am. Chem. Soc.* **2010**, *132*, 552.
[64] Z. Zand, P. A. Khaki, A. Salihi, M. Sharifi, N. M. Q. Nanakali, A. A. Alasady, F. M. Aziz, K. Shahpasand, A. Hasan, M. Falahati, *Int. J. Nanomed.* **2019**, *14*, 6989.
[65] M. Mahmoudi, S. Sant, B. Wang, S. Laurent, T. Sen, *Adv. Drug Delivery Rev.* **2011**, *63*, 24.

[66] N. Morishita, H. Nakagami, R. Morishita, S. Takeda, F. Mishima, B. Terazono, S. Nishijima, Y. Kaneda, N. Tanaka, *Biochem. Biophys. Res. Commun.* **2005**, *334*, 1121.
[67] S. Laurent, A. A. Saei, S. Behzadi, A. Panahifar, M. Mahmoudi, *Expert Opin. Drug Delivery* **2014**, *11*, 1449.
[68] C. S. S. R. Kumar, F. Mohammad, *Adv. Drug Delivery Rev.* **2011**, *63*, 19.
[69] C. Martinez-Boubeta, K. Simeonidis, A. Makridis, M. Angelakeris, O. Iglesias, P. Guardia, A. Cabot, L. Yedra, S. Estradé, F. Peiró, Z. Saghi, P. A. Midgley, I. Conde-Leborán, D. Serantes, D. Baldomir, *Sci. Rep.* **2013**, *3*, 1652.
[70] V. I. Shubayev, T. R. Pisanic2nd , S. Jin, *Adv. Drug Delivery Rev.* **2009**, *61*, 467.
[71] Z. Wan, J. Wang, *J. Hazard. Mater.* **2017**, *324*, 653.
[72] D. Zhao, X. Gao, C. Wu, R. Xie, S. Feng, C. Chen, *Appl. Surf. Sci.* **2016**, *384*, 1.
[73] P. Wang, M. Cao, C. Wang, Y. Ao, J. Hou, J. Qian, *Appl. Surf. Sci.* **2014**, *290*, 116.
[74] A. Maleki, Z. Hajizadeh, V. Sharifi, Z. Emdadi, *J. Cleaner Prod.* **2019**, *215*, 1233.
[75] Q. Liu, L.-B. Zhong, Q.-B. Zhao, C. Frear, Y.-M. Zheng, *ACS Appl. Mater. Interfaces* **2015**, *7*, 14573.
[76] B. Chen, H. Kan, *Environ. Health Prev. Med.* **2008**, *13*, 94.
[77] Y. Sun, C. Ding, W. Cheng, X. Wang, *J. Hazard. Mater.* **2014**, *280*, 399.
[78] R. Hassandoost, S. R. Pouran, A. Khataee, Y. Orooji, S. W. Joo, *J. Hazard. Mater.* **2019**, *376*, 200.
[79] R. Das, V. S. Sypu, H. K. Paumo, M. Bhaumik, A. Maity, *Appl. Catal., B* **2019**, *244*, 12.
[80] X. Guo, B. Du, Q. Wei, J. Yang, L. Hu, L. Yan, W. Xu, *J. Hazard. Mater.* **2014**, *278*, 211.
[81] L. Wang, Y. Huang, X. Sun, H. Huang, P. Lui, M. Zong, Y. Wang, *Nanoscale* **2014**, *6*, 3157.
[82] N. Wu, C. Liu, D. Xu, J. Liu, W. Liu, Q. Shao, Z. Guo, *ACS Sustainable Chem. Eng.* **2018**, *6*, 12471.
[83] M. Qiao, X. Lei, Y. Ma, L. Tian, X. He, K. Su, Q. Zhang, *Nano Res.* **2018**, *11*, 1500.
[84] J. Liu, H. Liang, H. Wu, *Composites, Part A* **2020**, *130*, 105760.
[85] T. Wang, L. Zhang, C. Li, W. Yang, T. Song, C. Tang, Y. Meng, S. Dai, H. Wang, L. Chai, J. Luo, *Environ. Sci. Technol.* **2015**, *49*, 5654.
[86] H. C. Vu, A. D. Dwivedi, T. T. Le, S.-H. Seo, E.-J. Kim, Y.-S. Chang, *Chem. Eng. J.* **2017**, *307*, 220.
[87] X. He, X. Liu, R. Li, B. Yang, K. Yu, M. Zeng, R. Yu, *Sci. Rep.* **2016**, *6*, 22238.
[88] N. Li, G. W. Huang, Y. Q. Li, H. M. Xiao, Q. P. Feng, N. Hu, S. Y. Fu, *ACS Appl. Mater. Interfaces* **2017**, *9*, 2973.
[89] L. Jiaolong, L. Hongsheng, H. Wu, *Composites, Part A* **2019**, *130*, 105760.
[90] X. Wang, F. Pan, Z. Xiang, Q. Zeng, K. Pei, R. Che, W. Lu, *Carbon* **2020**, *157*, 130.
[91] S. Sharma, B. K. Sahu, L. Cao, P. Bindra, K. Kaur, M. Chandel, N. Koratkar, Q. Huang, V. Shanmugam, *Prog. Mater. Sci.* **2021**, *121*, 100812.
[92] X. Zhang, G. Ji, W. Liu, B. Quan, X. Liang, C. Shang, Y. Cheng, Y. Du, *Nanoscale* **2015**, *7*, 11.
[93] C. C. Viggi, S. Rossetti, S. Fazi, P. Paiano, M. Majone, F. Aulenta, *Environ. Sci. Technol.* **2014**, *48*, 7536.
[94] J. Guo, S. Song, H. Liu, C. Luo, Y. Ren, T. Ding, M. Khan, D. YOung, X. Liu, X. Zhang, J. Kong, Z. Guo, *J. Mater. Chem. C* **2017**, *5*, 10.
[95] Q. Wang, L. Jiao, H. Du, Y. Wang, H. Yuan, *J. Power Sources* **2014**, *245*, 101.
[96] F. Sharif, M. Arjmand, A. A. Moud, U. Sundararaj, E. P. L. Roberts, *ACS Appl. Mater. Interfaces* **2017**, *9*, 14171.
[97] M. R. Bashir, L. Bhatti, D. Marin, R. C. Nelson, *J. Magn. Reson. Imaging* **2015**, *41*, 884.
[98] Y. Liu, Y. Li, T. Yang, J. Yang, H. Wang, G. Wu, *J. Toxicol. Environ. Health, Part A* **2016**, *79*, 869.
[99] J. Li, Y. Hu, J. Yang, P. Wei, W. Sun, M. Shen, G. Zhang, X. Shi, *Biomaterials* **2015**, *38*, 10.
[100] P. Das, M. Colombo, D. Prosperi, *Colloids Surf., B* **2019**, *174*, 42.
[101] S. Gao, H. Lin, H. Zhang, H. Yao, Y. Chen, J. Shi, *Adv. Sci.* **2019**, *6*, 1801733.
[102] M. Rashid, M. I. Khan, T. Hayat, M. I. Khan, A. Alsaedi, *J. Mol. Liq.* **2019**, *276*, 441.
[103] R. A. Revia, M. Zhang, *Mater. Today* **2016**, *19*, 157.
[104] S. Shen, S. Wang, R. Zheng, X. Zhu, X. Jiang, D. Fu, W. Yang, *Biomaterials* **2015**, *39*, 67.
[105] J.-X. Fan, M.-Y. Peng, H. Wang, H. Zheng, Z. Liu, C. Li, X. Wang, X. Liu, S. Cheng, X. Zhang, *Adv. Mater.* **2019**, *31*, 1808278.
[106] W. Feng, X. Han, R. Wang, X. Gao, P. Hu, W. Yue, Y. Chen, J. Shi, *Adv. Mater.* **2019**, *31*, 1805919.
[107] J. Song, L. Lin, Z. Yang, R. Zhu, Z. Zhou, Z.-W. Li, F. Wang, J. Chen, H. Yang, X. Chen, *J. Am. Chem. Soc.* **2019**, *141*, 8158.
[108] L. Rao, B. Cai, L. Bu, Q. Liao, S. Guo, X. Zhao, W. Dong, W. Liu, *ACS Nano* **2017**, *11*, 9.
[109] R. Tietze, J. Zaloga, H. Unterweger, S. Lyer, R. P. Friedrich, C. Janko, M. Pottler, S. Durr, C. Alexiou, *Biochem. Biophys. Res. Commun.* **2015**, *468*, 7.
[110] X. Li, J. Wei, K. E. Aifantis, Y. Fan, Q. Feng, F. Z. Cui, F. Watari, *J. Biomed. Mater. Res., Part A* **2016**, *104*, 1285.
[111] Z. Xi, R. Huang, Z. Li, N. He, T. Wang, E. Su, Y. Deng, *ACS Appl. Mater. Interfaces* **2015**, *7*, 11215.
[112] M. Liu, X. Y. Li, J. J. Li, X. M. Su, Z. Y. Wu, P. F. Li, F. H. Lei, X. C. Tan, Z. W. Shi, *Anal. Bioanal. Chem.* **2015**, *407*, 3875.
[113] F. Chen, G. Wang, J. I. Griffin, B. Brenneman, N. K. Banda, V. M. Holers, D. S. Backos, L. Wu, S. M. Moghimi, D. Simberg, *Nat. Nanotechnol.* **2017**, *12*, 387.
[114] C. Shuai, W. Yang, C. He, S. Peng, C. Gao, Y. Yang, F. Qi, P. Feng, *Mater. Des.* **2020**, *185*, 108275.
[115] Z. Zhang, X. Zhang, B. Liu, J. Liu, *J. Am. Chem. Soc.* **2017**, *139*, 5412.
[116] R. Zhang, N. Lu, J. Zhang, R. Yan, J. Li, L. Wang, N. Wang, M. Lv, M. Zhang, *Biosens. Bioelectron.* **2020**, *150*, 111881.
[117] M. Arabi, M. Ghaedi, A. Ostovan, *ACS Sustainable Chem. Eng.* **2017**, *5*, 3775.
[118] D. H. Phillips, V. M. Arlt, in *Molecular, Clinical and Environmental Toxicology*, Vol. *99* (Ed: A. Luch), Birkhäuser, Basel **2009**, pp. 87–110.
[119] N. Sadeghiani, L. S. Barbosa, L. P. Silva, R. B. Azevedo, P. C. Morais, Z. G. M. Lacava, *J. Magn. Magn. Mater.* **2005**, *289*, 466.
[120] D. W. Hwang, D. S. Lee, S. Kim, *J. Nucl. Med.* **2012**, *53*, 106.
[121] N. Singh, G. J. Jenkins, B. C. Nelson, B. J. Marquis, T. G. Maffeis, A. P. Brown, P. M. Williams, C. J. Wright, S. H. Doak, *Biomaterials* **2012**, *33*, 163.
[122] S. C. Hong, J. H. Lee, J. Lee, H. Y. Kim, J. Y. Park, J. Cho, J. Lee, D. W. Han, *Int. J. Nanomed.* **2011**, *6*, 3219.
[123] Z. Magdolenova, A. Collins, A. Kumar, A. Dhawan, V. Stone, M. Dusinska, *Nanotoxicology* **2014**, *8*, 233.
[124] M. Könczöl, S. Ebeling, E. Goldenberg, F. Treude, R. Gminski, R. Gieré, B. Grobéty, B. Rothen-Rutishauser, I. Merfort, V. Mersch-Sundermann, *Chem. Res. Toxicol.* **2011**, *24*, 1460.
[125] T. Gonet, B. A. Maher, J. Kukutschová, *Sci. Total Environ.* **2021**, *752*, 141828.
[126] R. Giere, *Proc. Natl. Acad. Sci. USA* **2016**, *113*, 11986.
[127] Q. Zhang, D. Lu, D. Wang, X. Yang, P. Zuo, H. Yang, Q. Fu, Q. Liu, G. Jiang, *Environ. Sci. Technol.* **2020**, *54*, 9274.
[128] B. A. Maher, *J. Alzheimer's Dis.* **2019**, *71*, 361.
[129] D. W. Aksnes, L. Langfeldt, P. C. Wouters, *SAGE Open* **2019**, *9*, 2158244019829575.
[130] N. J. Abuid, K. M. Gattás-Asfura, D. J. LaShoto, A. M. Poulos, C. L. Stabler, in *Nanoparticles for Biomedical Applications* (Eds: E. J. Chung, L. Leon, C. Rinaldi), Elsevier, New York **2020**, pp. 283–301.

[131] A. Ito, M. Shinkai, H. Honda, T. Kobayashi, *J. Biosci. Bioeng.* **2005**, *100*, 1.
[132] N. Sharma, S. Jandaik, T. G. Singh, S. Kumar, in *Nanobiomaterials in Antimicrobial Therapy* (Ed: A. M. Grumezescu), William Andrew Publishing, Norwich NY, USA **2016**, pp. 483–509.
[133] C. Sun, J. S. H. Lee, M. Zhang, *Adv. Drug Delivery Rev.* **2008**, *60*, 1252.
[134] B. Cojocaru, D. Avram, V. Kessler, V. Parvulescu, G. Seisenbaeva, C. Tiseanu, *Sci. Rep.* **2017**, *7*, 9598.
[135] A. M. Predescu, E. Matei, A. C. Berbecaru, C. Pantilimon, C. Drăgan, R. Vidu, C. Predescu, V. Kuncser, *R. Soc. Open Sci.* **2018**, *5*, 171525.
[136] C. Tassa, S. Y. Shaw, R. Weissleder, *Acc. Chem. Res.* **2011**, *44*, 842.
[137] Z. R. Stephen, F. M. Kievit, M. Zhang, *Mater. Today* **2011**, *14*, 330.
[138] L. A. Harris, J. D. Goff, A. Y. Carmichael, J. S. Riffle, J. J. Harburn, T. G. St. Pierre, M. Saunders, *Chem. Mater.* **2003**, *15*, 10.
[139] S. Mornet, S. Vasseur, F. Grasset, E. Duguet, *J. Mater. Chem.* **2004**, *14*, 2161.
[140] R. Mout, D. F. Moyano, S. Rana, V. M. Rotello, *Chem. Soc. Rev.* **2012**, *41*, 2539.
[141] F. Pinelli, G. Perale, F. Rossi, *Gels* **2020**, *6*, 6.
[142] I. Liakos, A. M. Grumezescu, A. M. Holban, *Molecules* **2014**, *19*, 12710.
[143] Y. Liu, X. Wang, M. Hussain, M. Lv, X. Dong, T. Wang, X. Xu, B. Liu, *Med. Sci.* **2018**, *6*, 100.
[144] H. Veisi, M. Ghorbani, S. Hemmati, *Mater. Sci. Eng., C* **2019**, *98*, 584.
[145] R. Asmatulu, A. Fakhari, H. L. Wamocha, H. Y. Chu, Y. Y. Chen, M. M. Eltabey, H. H. Hamdeh, J. C. Ho, *J. Nanotechnol.* **2009**, *2009*, 238536.
[146] C. D'Agostino, S. Chansai, I. Bush, C. Gao, M. D. Mantle, C. Hardacre, S. L. James, L. F. Gladden, *Catal. Sci. Technol.* **2016**, *6*, 1661.
[147] B. Fadeel, *Front. Immunol.* **2019**, *10*, 133.
[148] T. Malachowski, A. Hassel, *Eng. Regener.* **2020**, *1*, 35.
[149] G. Wang, D. Zhao, N. Li, X. Wang, Y. Ma, *J. Magn. Magn. Mater.* **2018**, *456*, 316.
[150] L. Zhang, Y. Ren, S. Peng, D. Guo, S. Wen, J. Luo, G. Xie, *Nanoscale* **2019**, *11*, 8237.
[151] M. E. Özgür, A. Ulu, S. Balcıoğlu, İ. Özcan, S. Köytepe, B. Ateş, *Toxics* **2018**, *6*, 62.
[152] A. Rafieepour, M. R. Azari, H. Peirovi, F. Khodagholi, J. P. Jaktaji, Y. Mehrabi, P. Naserzadeh, Y. Mohammadian, *Toxicol. Ind. Health* **2019**, *35*, 703.
[153] C. Costa, F. Brandão, M. J. Bessa, S. Costa, V. Valdiglesias, G. Kiliç, N. Fernández-Bertólez, P. Quaresma, E. Pereira, E. Pásaro, B. Laffon, J. P. Teixeira, *J. Appl. Toxicol.* **2016**, *36*, 361.
[154] A. A. Ketebo, T. H. Shin, M. Jun, G. Lee, S. Park, *J. Nanobiotechnol.* **2020**, *18*, 170.
[155] H. J. Heusinkveld, T. Wahle, A. Campbell, R. H. S. Westerink, L. Tran, H. Johnston, V. Stone, F. R. Cassee, R. P. F. Schins, *Neurotoxicology* **2016**, *56*, 94.
[156] D. A. Bazylinski, A.-J. Garratt-Reed, R. B. Frankel, *Microsc. Res. Tech.* **1994**, *27*, 389.
[157] J. L. Kirschvink, A. Kobayashi-Kirschvink, J. C. Diaz-Ricci, S. J. Kirschvink, *Bioelectromagnetics* **1992**, *Suppl 1*, 101.
[158] S. Levesque, M. J. Surace, J. McDonald, M. L. Block, *J. Neuroinflammation* **2011**, *8*, 105.
[159] M. Schieber, N. S. Chandel, *Curr. Biol.* **2014**, *24*, R453.
[160] M. T. Heneka, M. J. Carson, J. El Khoury, G. E. Landreth, F. Brosseron, D. L. Feinstein, A. H. Jacobs, T. Wyss-Coray, J. Vitorica, R. M. Ransohoff, K. Herrup, S. A. Frautschy, B. Finsen, G. C. Brown, A. Verkhratsky, K. Yamanaka, J. Koistinaho, E. Latz, A. Halle, G. C. Petzold, T. Town, D. Morgan, M. L. Shinohara, V. H. Perry, C. Holmes, N. G. Bazan, D. J. Brooks, S. Hunot, B. Joseph, N. Deigendesch, et al., *Lancet Neurol.* **2015**, *14*, 388.
[161] X. Chen, C. Guo, J. Kong, *Neural Regener. Res.* **2012**, *7*, 376.
[162] S. Laurent, S. Dutz, U. O. Häfeli, M. Mahmoudi, *Adv. Colloid Interface Sci.* **2011**, *166*, 8.